NASA CR-
144507

REMOTELY SENSING WHEAT MATURATION WITH RADAR

Remote Sensing Laboratory
RSL Technical Report 177-5

Thomas F. Bush
Fawwaz T. Ulaby

May, 1975

Sponsored by:

NATIONAL AERONAUTICS AND SPACE ADMINISTRATION
Lyndon B. Johnson Space Center
Houston, Texas 77058

CONTRACT NAS 9-10261

THE UNIVERSITY OF KANSAS CENTER FOR RESEARCH, INC.
2291 Irving Hill Drive—Campus West Lawrence, Kansas 66045

THE UNIVERSITY OF KANSAS SPACE TECHNOLOGY CENTER
Raymond Nichols Hall CENTER FOR RESEARCH, INC.
2291 Irving Hill Drive—Campus West Lawrence, Kansas 66045
Telephone:

REMOTELY SENSING WHEAT MATURATION WITH RADAR

Remote Sensing Laboratory
RSL Technical Report 177-55

Thomas F. Bush

Fawwaz T. Ulaby

May, 1975

Sponsored by:

NATIONAL AERONAUTICS AND SPACE ADMINISTRATION
Lyndon B. Johnson Space Center
Houston, Texas. 77058
CONTRACT NAS 9-10201

TABLE OF CONTENTS

LIST OF FIGURES

ABSTRACT

An experiment was conducted during the late spring of 1974 to study the scattering properties of wheat in the 8-18 GHz band as a function of frequency, polarization, incidence angle and crop maturity. Supporting ground truth was collected at the time of measurement. The data indicates that σ^o, the radar backscattering coefficient, is sensitive to both radar system parameters and crop characteristics particularly at incidence angles near nadir. Linear regression analyses of σ^o (dB) on both time and plant moisture content result in rather good correlation, as high as 0.9, with the slope of these regression lines being 0.55 dB/day and -0.275 dB/% plant moisture at 9.4 GHz at nadir. Furthermore, by calculating the average time rate of change of σ^o (real units) it is found that σ^o undergoes rapid variations shortly before and after the wheat is harvested. Both of these analyses suggest methods for estimating wheat maturity and for monitoring the progress of harvest.

1.0 INTRODUCTION

For many years the problem of feeding the worlds expanding population has concerned both the government and civilian populace. As an aid in managing our food resources certain remote sensing techniques have been implemented. At the present time most of the civilian global sensors operate in the visible or infrared portion of the electromagnetic spectrum. While these sensors have displayed many capabilities, their use is limited to cloud free weather conditions. In studies other than remote sensing of cropland this dependence on clear weather may be tolerable, but for dynamic targets like agricultural crops the dependence on cloud free conditions is in most cases intolerable. Because it is nearly weather independent, radar is being investigated as a sensor for agricultural land-use mapping.

Earlier papers [1-8] have dealt with the backscattering properties of certain agricultural targets as a function of both radar parameters and target characteristics in hopes of using σ^o, the radar scattering coefficient, as a target identifier and as an aid in estimating pertinent target properties. For a discussion of the relationship between target properties, system parameters and the measured backscatter the reader is referred to Ulaby [3].

Nearly 2.15 million hectares of the world's cultivated land (representing about 16%) are planted in wheat [9]. Radar studies of wheat, however, do not seem to represent a proportionate part of the domestic research in the remote sensing of croplands. During the late spring of 1974 (May 21 through June 25) an experiment was conducted to study the backscattering properties of wheat as a function of system parameters and target properties. This report presents the results of the experiment which indicate a promising future for monitoring wheat growth with radar.

2.0 MEASUREMENT PROCEDURE

2.1 The MAS 8-18

The radar used in this study, the MAS 8-18 (Microwave Active Spectrometer, 8-18 GHz), is a modified version of the mobile truck-mounted spectrometer described by Bush and Ulaby [10]. The modifications include minor antenna changes, improved

IF filtering and the use of isolators for reflection reduction. All modifications were made to provide an increased signal to noise ratio. Major system parameters remained unchanged with the exception of an increase in RF signal bandwidth from 400 MHz to 800 MHz. Table 1 presents the pertinent system parameters.

2.2 Data Collection

Backscattering measurements were made during the period of May 21 through July 25, 1974. Data was collected for both the like polarized (HH and VV) configurations at angles ranging from 0° (nadir) to 70° in 10° increments. These measurements were made at 11 frequencies in the 8-18 GHz range of the instrument.

Because of its FM character, the system inherently provided fading reduction by averaging in the frequency domain [11-14]. However, due to its limited resolution cell size it was felt that spatial averaging was also necessary. Thus, an average of 17 spatially independent measurements were made at 0° with the number of spatial measurements decreasing to 12 at 70°. The criterion for reducing the number of spatial measurements made at the larger angles was based on the fact that with a panchromatic system, return power variance decreases with incidence angle [12-14].

The amount of variance reduction provided by frequency averaging is a direct function of target extent (measured radially from the antenna). Target extent, however, is not necessarily the physical extent of the target but may be reduced by the range resolution of the system or by the skin depth of the target. In the case of wheat it is not possible, as will be discussed later, to experimentally estimate the degree to which penetration occurs. For lack of this type of information the following approach was taken to estimate depth of penetration.

The dielectric properties of several vegetation types have been measured as a function of plant moisture content by Carlson [15] at X-band. His results indicate that vegetation with 40% moisture content, (the average wheat moisture over the observation period) has a relative complex dielectric constant of approximately $\epsilon_w = 12.5 - j5.0$. A wheat field however is a mixture of dielectrics (air and vegetation) so that the effective dielectric constant of the mixture is less than that of wheat alone. Ground measurements show that the volume of wheat occupying

TABLE 1.

MAS 8-18 System Specifications

Type	FM-CW
Modulating Waveform	Triangular
Frequency Range	8-18 GHz
FM sweep: Δf	800 MHz
Transmitter Power	10 dBm (10 mW)
Intermediate Frequency	50 kHz
IF Bandwidth	10.0 kHz
Antennas	
Height above ground	26 m
Reflector diameter	61 cm
Feeds	Cavity backed, log-periodic
Polarization	Horizontal transmit-Horizontal receive (HH)
	Vertical transmit-Vertical receive (VV)
Incidence Angle Range	0°(nadir)-80°
Calibration:	
Internal	Delay Line
External	Luneberg Lens

$1.0\ m^3$ of free space is approximately $0.1\ m^3$. Thus as a very crude approximation the average effective dielectric constant of the wheat-free space mixture was taken to be

$$\epsilon_{eff} = 0.1\epsilon_w + 0.9$$

$$= 2.15 - j0.5$$

where ϵ_w is the relative dielectric constant of wheat and the relative dielectric constant of free space is taken as 1.0. Making use of ϵ_{eff}, the average skin depth of the target was calculated to be 2.17 cm at 13.0 GHz, the center of the 8-18 GHz band. Knowing the skin depth and the range resolution of the system it is possible to estimate the frequency spacing between two independent samples of the radar return [12] according to the equation:

$$\Delta f_d = \frac{150}{D}\ \text{MHz}$$

where D is the target extent measured radially from the radar antenna. By dividing the system RF bandwidth, 800 MHz, by Δf_d, the decorrelation bandwidth, it is possible to determine the number of independent samples, N, averaged by the system each time a measurement was made. Multiplying N by the number of spatially independent measurements provides the total number of independent samples of the radar return after averaging. Table 2 presents 90% confidence intervals for the backscattering coefficient σ^o calculated using this approach.

3.0 GROUND TRUTH

Although described by Cihlar [16], the method of collecting and processing the ground truth presented herein will be reviewed. Soil moisture, plant moisture, plant height and precipitation data are presented in Figure 1.

3.1 Soil Moisture

To determine the effects of soil moisture on σ^o, six soil samples were taken from the wheat field while scattering measurements were made. Their locations are shown in Figure 2. Locations 1 approximately correspond to scattering measurements

TABLE 2.

Number of Spatially Discrete Measurements with 90% Confidence Intervals of σ^{o}(db) of Wheat

Incidence Angle	Number of Spatially Independent Measurements	90% Confidence Intervals (dB)
0°	17	+1.8
		-2.0
10°	16	+1.8
		-2.0
20°	15	+1.1
		-1.3
30°	14	+.93
		-1.1
40°	13	+0.774
		-0.774
50°	12	+0.622
		-0.622
60°	12	+0.457
		-0.457
70°	12	+0.403
		-0.403

made at 0°, 10° and 20°, locations 2 correspond to 30°, 40° and 50° while locations 3 correspond to 60° and 70°. At each location samples were taken at various depths (0-1 cm, 1-2 cm, 2-5 cm, 5-9 cm and 9-15 cm) to determine the soil moisture profile. Because of skin depth considerations [4] only the data from the top two centimeters were used in analysis. These 0-2 centimeter values were then averaged for each pair of locations. To convert from percent moisture by weight to moisture by volume, bulk density measurements were also taken. All soil moisture data presented herein are on a volumetric basis having units of gm/cm^3. It should be noted that the measurement period (May 21-June 25) was characterized by a high mean soil moisture (0.317 gm/cm^3) with extreme values being 0.40 gm/cm^3 and 0.20 gm/cm^3.

3.2 Plant Moisture

As with soils, the water content of vegetation has a direct influence on its dielectric properties [15]. For this reason it was necessary to collect such data. During each measurement period, wheat samples were obtained and processed to determine the plant moisture content on a wet weight basis, a measure of the fraction of plant weight consisting of water. While it is recognized that the effects of moisture on the dielectric properties of both soil and vegetation will be influenced by the manner in which it is chemically bound with the plant or soil molecules, such data is not generally available. Thus, the plant moisture on a wet weight basis will be used in the discussions of the data presented.

Of particular interest is the range of variation in plant moisture during the measurement period. From Figure 1, we see that the plant moisture curve, while monotonically decreasing an average of 1.66% per day, had two regions during which the plant moisture remained somewhat constant with time (May 21-31 and June 6-12). The second "plateau" in the plant moisture curve may have been caused by the heavy precipitation recorded during the noted period.

Perhaps of more importance is the ripening process, the mechanism responsible for this consistent decrease in plant moisture. Although decreasing plant moisture is one measurable consequence of the ripening of the wheat, there are certainly other changes occurring which may not be readily measured. Thus we should bear in mind that while consistently decreasing plant moisture may be indicative of the maturation process, there are certainly other physiological and morphological processes occurring.

4.0 DISCUSSION OF RESULTS

Because of the quantity of multi-dimensional data gathered during the course of the experiment it is not at this time possible to discuss all of it. Rather, only a representative portion will be presented in the body of this report with the remainder of the data made available in the appendices.

4.1 Temporal Variations of σ^o

σ^o, the radar scattering coefficient, is generally a function of the geometric and dielectric properties of the target of interest. Any variation of these target properties will normally be reflected as a change in σ^o. Thus, if radar is to be useful as a tool in estimating crop maturity it must somehow respond with a reasonable degree of sensitivity to the geometrical and electrical variations a plant undergoes during its maturation process. Among the geometric changes in wheat may be variations in plant height, leaf structure and the appearance of the wheat head. The most obvious dielectric variation is that of changing plant moisture which is quite dramatic in the case of wheat during the final month of its maturity. Thus, while it is recognized that the variations we may observe in σ^o are a function of crop characteristics, we should also bear in mind that these plant characteristics are in turn dependent on the passage of time. Therefore, this first section on temporal variations of σ^o will serve, among other purposes, to introduce the reader to the general trends in the variations of the scattering data.

Figures 3a through 3d present the variations of σ^o with time at an incidence angle of 0^o for four frequencies, 8.6, 9.4, 13.0 and 17.0 GHz. The abscissa identifies the date on which each data set was recorded. Figure 3e presents the results of a linear regression analysis of σ^o_H and σ^o_V on time with the number of days after May 21 being the independent variable. Shown are the estimated correlation coefficients, r^t_H and r^t_V, and the slopes of the regression lines M^t_H and M^t_V, (having units of dB/day). The abscissa scale is frequency in GHz. It should be noted that all regression analyses presented in this report exclude the data set taken on June25 since it was taken after harvest.

As a general observation it is immediately apparent that the radar is responding to the physiological and morphological changes which occurred during the final month of ripening of the wheat. At 8.6 and 9.4 GHz σ^o_H and σ^o_V both show an almost linear variation with time. At 13.0 and 17.0 GHz however this linear response is not quite as

apparent although data at these higher frequencies still exhibit a dependence on the passage of time. Figure 3e presents a more complete and quantifiable representation of these trends. We note that, r^t_H and r^t_V, the estimated correlation coefficients of σ^o_H and σ^o_V on time show a decreasing trend with frequency from approximately 0.95 at 8.6 GHz to about 0.85 at 17.0 GHz. This is in agreement with our earlier, more general observation, that the "linearity" of the variations of σ^o with time undergo a certain amount of degradation as frequency is increased. Certainly, however, r^t_H and r^t_V remain quite high across the 8-18 GHz band.

Of equal importance to r^t_H and r^t_V are M^t_H and M^t_V. These values represent the slope of the regression lines and may be interpreted as a measure of the sensitivity of σ^o to the passage of time. Obviously a very high correlation coefficient is useless in a practical sense if the sensitivity of σ^o to temporal changes is small. The response of of M^t_H and M^t_V to frequency (Figure 3e) shows a very interesting phenomenon near 9.4 GHz. At this frequency M^t behaves in a somewhat "resonant" manner with M^t_V being more pronounced than M^t_H. This suggests that at 9.4 GHz there exists a certain characteristic or combination of wheat characteristics to which the radar is particularly sensitive. Whether these characteristics are of a molecular or geometric nature is not known but it certainly appears to merit a considerable amount of future thought and investigation. At frequencies above 11.8 GHz the curves depicting M^t_H and M^t_V appear to be practically frequency and polarization independent.

Aside from the "resonant" phenomenon occurring at 9.4 GHz, the general increasing trend of σ^o is also quite difficult to explain adequately. If the regression lines exhibited a negative slope it would be possible to argue that the phenomenon observed is due to a decreasing moisture content and thus, decreasing dielectric constant of the target. Since the slope is positive, such an explanation can be discarded. A decreasing dielectric constant does, however, imply decreasing attenuation within the vegetation canopy. This decrease in attenuation within the vegetation canopy would then allow the radar to "see" more of the generally wet underlying soil causing an increasing σ^o. Although this may be a partial explanation of the phenomenon it does not seem to be entirely consistent with the observed data or with the approximated skin depth (section 2.2). Consider, for example, the increase in σ^o_V by about 1.8 dB between June 12 and June 17 during which the soil moisture decreased from 0.35 to 0.18 which clearly indicates no response to soil moisture variations. Furthermore, it does not seem likely that either the "resonance" phenomenon, or polarization dependence at 9.4 GHz would result from soil conditions alone. Also, the difference in

M'_H and M'_V indicates a preferred target geometry. Visual inspection of the soil surface indicates none while the wheat itself does. The wheat was sown in rows spaced 25 cm apart such that at 0^o incidence the wheat rows were oriented parallel to the E field of a horizontally polarized signal (see Figure 4a). At a ground range of 5.3 meters (corresponding approximately to 10^o incidence) the direction of the wheat rows changed by 90^o such that the row - E field orientation was similar to that shown in Figure 4b. At incidence angles greater than 10^o the rows were perpendicular to the E field of a horizontally polarized signal (Figure 4c).

Figures 5a-e present data collected in a manner identical to that presented in Figures 3a-e except the incidence angle is now 30^o. It is immediately obvious that this data contrasts sharply with the data collected at nadir. We begin by noting the lack of any peaking in the M^t (Figure 5e) curves although it does appear that M^t_V and M^t_H trade roles with M^t_H being generally higher than M^t_V. Perhaps more striking, however, is the response of the correlation coefficients r^t_H and r^t_V. At 8.6 GHz we note that r^t_H indicates nearly no consistent trends of σ^o_H with time although r^t_V has a value of 0.675. However, a small increase in frequency to 9.4 GHz causes r^t_H to increase to 0.65 while r^t_V remains nearly constant. This again suggests that the choice of frequency in a rather small band around 9.4 GHz may be critical in studying the temporal variations of the scattering properties of wheat. As we further increase frequency to values above 9.4 GHz we note a marked separation in r^t_H and r^t_V with r^t_H being consistently higher. This is in contrast to the 0^o correlation coefficients which showed practically no polarization dependence at frequencies higher than 11.8 GHz.

Again it is very difficult to even qualitatively explain this behavior adequately although it should be restated that the row - $\bar{E}$ field orientation has now, at 30^o, changed from that of the 0^o data. Let us, however, reconsider the argument that the radar is responding to changes in plant attenuation. As a rough estimate of the amount of loss expected through the wheat we might use the measured value of de Loor [17] whose data indicate that approximately 12.5 dB total attenuation should be expected at 9.3 GHz. If we are to expect this much loss at 9.3 GHz certainly the loss will increase with frequency (assuming the dielectric constant of wheat does not vary drastically with frequency) with a resulting decrease in sensitivity. Although the sensitivity factor

M^t is less at 30° than at 0° we see practically no dependence of M^t on frequency above 11.0 GHz. These data also seem consistent with data presented by Lundien [18] who measured wheat at X-band for various plant heights. His data indicate a large degree of plant canopy attenuation at 0°. For a 8.9 cm stand of wheat he measured a scattering coefficient of 1.9 dB in contrast to -15.6 dB for a 73.7 cm stand. Soil moisture ranged from 15.2 to 27.7 per cent by weight. A study of wheat at other frequencies prompted his statement that "this (data) suggests that the Ka-, X- and C-band results could be used to measure vegetation parameters (height, thickness, moisture content, etc.) and that P-band frequencies may still be used for soil interrogation directly or with simple correcting factors." His statement implies that plant attenuation at higher frequencies results in a masking of underlying soil effects.

Figures 6a-e and 7a-e present the variations of σ^o with time along with linear regression results for 50° and 70° data. At both angles we note that neither r^t_H, r^t_V or M^t_H, M^t_V show much frequency dependence although there still seems to be some polarization dependence. This can be observed by the relative values of the correlation curves at 50° and 70°. At 50° we can see that r^t_H is consistently highe while at 70° they are generally close to one another across the 8-18 GHz band.

Again it can be argued that at 50° and 70° we expect a considerable amount of signal attenuation through the canopy simply due to increased path length. Thus if we are indeed effectively measuring variations in path loss we expect a marked reductior in the absolute values of the M^t curves. Although we do observe a small decrease in M^t_H and M^t_V as the incidence angle increases from 50° to 70° it is certainly not as great as one might expect, even at the upper end of the frequency band. Another possible mechanism responsible for the general increasing trend of σ^o with time is that of changing target geometry as the plants matured. A discussion of this mechanism will be deferred, however, to a later section.

4.2 Rate of Change of σ^o

In the preceding section it was noted that the ability to monitor the ripening process of wheat was greatly influenced by the choice of radar parameters; namely frequency, polarization and incidence angle. In this section a second approach to monitoring wheat growth will be discussed. While this approach appears to be less sensitive to system parameters it is not intended to replace that of section 4.1 but rather to complement the earlier observations.

As noted in section 3.2, the rate of change of plant moisture (one indicator of wheat maturity) did not remain constant throughout the observation period. Rather, the plant moisture sometimes remained nearly constant while at other times is decreased rapidly within a few days. Thus the question may be raised as to how the rate of change of σ^o varied during the observation period.

To answer this question the following procedure was followed. For each two consecutive data sets the average rate of change of σ^o between those sets was calculated. To increase the sensitivity of these calculations all values of σ^o were converted from dB to real values. Thus as an example the rate of change of σ^o between May 21 and Mav 27 was calculated as follows. At 9.4 GHz, 0°, HH polarization

$$S_H = \frac{\sigma^o_{H_2} - \sigma^o_{H_1}}{6 \text{ days}} = -0.04/\text{day}$$

Some results of this analysis are shown below in Figures 8a-8l. Different ordinate scales were used in these figures (8a-8l) so that the relative variations of S can be seen more clearly. The abscissa values represent the date midway between the dates on which the two data sets of interest were taken. For example the value plotted as point May 24 represents the slopes of the line between sets taken on May 22 and May 27. To conserve space, only a representative set of curves is shown. Three frequencies and four angles were chosen; 9.4, 13.0 and 17.0 GHz and 0°, 10°, 20° and 30° respectively. These curves seem representative of all frequencies from 8-18 GHz and all angles from 0° to 30°. They are not necessarily representative of all data at angles greater than 30° although the trends observed between 0° and 30° usually persisted to 40° or 50°.

Figures 8a-d present S curves at 9.4 GHz. At 0° (Figure 8a) we note that S shows a consistent, slow increase between May 24 and June 11. Points at June 14, 19 and 23 however depart from this behavior. Of particular interest are June 19 and 23, for these represent the rate of change of σ^o shortly before and shortly after harvest. Before harvest (June 19) S increases sharply from its value on June 14 while S decreases even more markedly after harvest (June 23). It is also noted that these changes in S are greater for vertical polarization. Similar trends are observed at 10°, 20° and 30° (Figures 8b-d) although S_H shows a sharper increase at 20° on June 19 than S_V.

This effect is much more apparent in the 13.0 GHz data (Figures 8e-h), particularly at 0° incidence. From this figure it is seen that the variation of σ° from day to day was apparently quite small until it was ready for harvest. During the days shortly prior to harvest, σ° shows an extreme dependence on the passage of time, particularly σ°_V. The effect of harvest can again be clearly seen in these figures. It is noted that this trend is not quite as dramatic at angles away from nadir (10°, 20° and 30°) although the trend is still clearly discernable.

Data at 17 GHz (Figures 8i-l) again exhibit similar trends. In general, data at all frequencies from 8-18 GHz and at angles between 0° and 30° indicate that the variations of S_V are much more pronounced than S_H before and after harvest. Thus, it appears if wheat fields are monitored by radar on a regular basis, that the time rate of change of σ° will show a sharp increase prior to harvest followed by a sharp decrease immediately after harvest.

If this is indeed the case, this type of analysis may prove to be an effective means for 1) estimating the proper time of wheat harvest and 2) following the progress of harvest. If harvest progress can be monitored then the problem of properly distributing fuel supplies for harvesting machinery and properly distributing truck and rail transportation for the harvested grain can be reduced considerably.

Another appealing aspect of this method of interpretation is that this method is independent of absolute levels of σ°. Thus it would not be necessary to calibrate (on an absolute scale) any of the existing uncalibrated imaging systems presently in operation nor would it be necessary to have a high degree of confidence in the absolute calibration of a calibrated system if such a system is used.

4.3 Variations of σ° With Plant Moisture

In section 4.1 we considered two possible causes of the increasing trend of σ° with time. The first consideration was that the changes in plant water content (and thus dielectric constant) are directly responsible for the variations in σ°. This argument has been discarded since σ° increases as plant moisture decreases which does not seem at all plausible. The second consideration is that σ° is increasing as the radar signals are better able to penetrate the vegetation canopy as the plant moisture decreases. This argument has not yet been discarded although apparent inconsistencies have been discussed.

Variations of σ° with plant moisture seem to provide additional information. The reader should bear in mind that the variables, time and plant moisture, are by no means independent as can be seen from Figure 1. A consideration of plant moisture as a variable can however, provide some insight into the phenomena being observed.

Consider first Figures 9a-d where σ° has been plotted versus plant moisture for an incidence angle of 0° at four frequencies, 8.6, 9.4, 13.0 and 17.0 GHz. Again the data set taken after harvest has been excluded from all regression analysis although the point is shown with the rest of the data. Figure 9e presents results of a linear regression analysis of σ° on plant moisture. It is interesting to compare the correlation coefficients obtained by regressing σ° on plant moisture to those obtained by regressing σ° on time. Comparing Figures 9e and 3e we see that $|r^{p}| \geq |r^{t}|$ as a general rule. This is certainly not surprising since the passage of time does not necessarily imply that the wheat is maturing whereas consistently decreasing plant moisture usually does imply a maturing crop. It should be noted, however, that the trends of r^{t} and r^{p}, M^{t} and M^{p} with frequency are very comparable at 0° which again implies a strong dependence of plant moisture on time.

Again after harvest, (plant moisture = 11%), σ° shows an interesting trend as noted in section 4.2. We can see that at 0°, σ° is generally lower after harvest than before harvest even though the plant moisture decreased by only an insignificant amount. This implies that this consistent variation of σ° is probably not due to changes in plant moisture but rather to the dramatic change in vegetation geometry caused by the harvest. Since harvesting wheat, and thus altering plant geometry, is manifested as a change in σ°, we should certainly consider the normal morphological changes the wheat undergoes during its ripening stages. Certainly these variations will not be as rapid and gross as those caused by harvest but they bear consideration. We begin by noting (Figure 1) that from June 6 through June 12 neither plant nor soil moisture varied to a significant degree. Plant moisture varied only 3.5 units (around 50%) while soil moisture varied 0.02 gm/cm^{3}. Thus, for all practical purposes we can consider both plant and soil moisture constant during this time. Since the electrical properties of the target were fairly constant over this period, a change in σ° would probably imply a change in plant geometry. At 0° (Figure 9a-d), data at the four frequencies under consideration all show variations in this region. The 9.4 GHz data, however, is the only frequency where a consistent increase in σ° is noted during the period from June 6 through June 12, the period where plant and soil moisture were fairly constant. Similarly at large angles of incidence

(Figures 10-12) a general trend for σ^o to increase during the June 6-12 period is noted. Thus it may be the case that these variations are due to a changing plant configuration. Certainly the most obvious geometrical change that occurred during the observation period was the appearance of the wheat heads as the plant went from a stage of vegetation growth to the reproductive stage. Of particular note is the fact that the heads appear at the tops of the plants where they are most "visible" to the scatterometer. These heads continue to develop until harvest. A second effect that may occur is the withering process the leaves undergo as they lose moisture. Since geometry plays a significant role in determining the scattering properties of a particular target, this effect should also be considered. Furthermore, the reader should bear in mind that even though the linear regressions of σ^o on plant moisture alone yielded reasonable correlations it is not necessarily plant moisture to which the radar is directly responding. This was discussed earlier in section 3.2 where it was noted that although consistently decreasing plant moisture can be indicative of a ripening crop it is only one of a host of processes simultaneously occurring during maturation. Changes in plant morphology should certainly be included as one of these processes although it is more difficult to quantify than plant moisture.

4.4 A Further Regression Analysis of σ^o on Plant Moisture

The customary choice of dB units to express σ^o, is usually for convenience since σ^o in real units can often vary by one or more orders of magnitude between nadir and large angles of incidence. Because plant moisture seems to be an adequate descriptor of plant maturity and because of the difficulty in quantifying plant geometry, an empirical model has been constructed describing σ^o (real units) purely in terms of plant moisture. Our discussion in the previous section indicated that linear regression analysis of σ^o (dB) on plant moisture generally provided quite satisfactory results. Hence, it was decided to express the dependence of σ^o (real units) on plant moisture in the form of an exponential:

$$\hat{\sigma}^o = A \exp (B \cdot M_p) \qquad \text{[real units]}$$

where A and B are constants (for a given frequency-angle-polarization combination) and M_p is plant moisture in % by wet weight. Using the measured σ^o (real units) and M_p values, an exponential regression equation was generated for each combination of sensor parameters. Again because of space considerations, only a portion of the results of this analysis will be shown.

In Figure 13 the measured data is compared to the regression curves at 8.6 GHz for 0°, 30°, 50° and 70°. At 0° we note that B, the coefficient of M_p, has approximately the same value for both polarizations, whereas at the other incidence angles B_V is always larger (in magnitude) than B_H implying that σ°_V is more sensitive to M_p variations than σ°_H.

Similar observations can be made at other frequencies as illustrated in Figures 14, 15 and 16 corresponding to 9.4, 13.3 and 17.0 GHz, respectively. Based on a subjective judgment of the "goodness of fit" of the generated exponential curves, there does appear to be an exponential trend relating σ° to M_p.

4.5 σ° Dependence on Soil Moisture

Figures 17, 18 and 19 present the variations of σ° versus soil moisture measurements corresponding to the particular angle shown (see section 3.1). Only 0° through 20° data are shown because it is felt that this is where the sensitivity of σ° to soil moisture would be maximum. The apparent lack of dependence of σ° on soil moisture seen in these figures is not surprising in light of previous discussions which cast doubt on the ability of radar to penetrate 96 cm of wheat in the 8-18 GHz band. Note that even over this somewhat limited range of soil moistures (approximately 0.20 to 0.40 gms/cm^3) there are variations in σ° from about -1.7 dB to 10.0 dB at 0°, 8.6 GHz, indicating that a mechanism other than the direct influence of soil moisture may be responsible for the variations shown. While it is true that the attenuation of the signal introduced by the plant canopy is varying with time it is expected that it would vary in a consistent monotonic fashion as the plant moisture varied. In other words the attenuation would insert monotonic bias in any data used to extract soil moisture information. Attempts were made to extract such a bias with no definitive results obtained. The lack of a wide range of soil moisture variations hindered the analysis to a significant degree.

4.6 Spectral Response of σ°

Again because of the quantity of data collected only a general discussion of the spectral properties of wheat will be presented. Figures 20 through 23 present spectral curves of wheat between 8 GHz and 18 GHz. Four representative data sets were chosen

for presentation. The first set of curves, Figures 20a through 20d represent data taken on May 21 and are plotted at angles of 0°, 30°, 50° and 70°. As previously noted there seems to be a preferred target orientation as σ^o_V tends to be, on the average, lower than σ^o_H at 0°. We can also note a somewhat greater frequency dependence near 9.4 GHz where a noticeable minimum occurs in the response. Simiarly we note a frequency an polarization dependence at 30°(Figure 20b) although the polarization effects become more pronounced. There is, however, a small tendency for σ^o_V to increase to values somewhat greater than those of σ^o_H near 13.8 GHz after being significantly lower at 8.6 GHz. This is particularly noticeable at 50° where σ^o_H and σ^o_V do not vary much on an absolute basis but definitely exhibit the crossing effect near 12.5 GHz. Finally at 70° we note that σ^o_V, while sometimes practically equal to σ^o_H, is generally a small amount greater than σ^o_H. Thus, as a general observation it seems that as frequency and angle increase σ^o_H and σ^o_V tend to approach, cross and finally separate with σ^o_V being higher than σ^o_H at 70°.

Data taken more than two weeks further into the maturation of the wheat is presented in Figure 21. At zero degrees we note a somewhat constant response of σ^o to frequency although around 13.8,GHz σ^o_H exhibits a pronounced minimum. At 30°, (Figure 21b) a sensitivity of σ^o to frequency near the lower frequencies is noted with σ^o_V being 5.6 dB lower than σ^o_H at 9.4 GHz. With increasing frequency however σ^o_H and σ^o_V tend to approach one another. At 50° (Figure 21c) the same effect is noticeable to a somewhat lesser degree and at 70° σ^o_V is always greater than σ^o_H (Figure 21d).

Figures 22 and 23 present data taken on June 12 and June 21; June 21 being the final data collected before harvest. These data exhibit responses different from one another and different from the previous two shown. At 0° for example the June 12 data, (Figure 22a) shows a marked tendency for σ^o_H to decrease from 4.4 dB to 0.70 dB as we scan from 8.6 GHz to 17.0 GHz. σ^o_V has a nearly identical response. The June 21, 0° data (Figure 23a) on the other hand, shows practically no consistent decreasing trends although there are small undulations within the band. At 30° a completely different trend is noted; that being an increasing σ^o for the June 21 data with a relatively constant σ^o for the June 12 data. Note also that the earlier set exhibits significant polarization differences while the latter shows very little. The response at 50° and 60° is quite similar to the 30° data in both cases with the earlier data somewhat constant relative to the increasing trend in the June 21 data.

4.7 Angular Variations of σ^o

Figures 24-26 show the May 21, June 6, 12 and 21 data plotted versus incidence angle at three frequencies (8.6, 13.0, 17.0 GHz) for both polarizations. Although it is merely the same data discussed earlier, this viewpoint can be quite helpful.

We can first note that at the larger angles, the difference in the shapes of the σ_H^o and σ_V^o curves is quite pronounced. At all three frequencies, σ_H^o continues to decrease with angle while σ_V^o has a tendency to increase near the 60^o-70^o region. This increase in the vertically polarized scattering coefficient can perhaps be explained by a consideration of the wheat geometry. Roughly speaking, wheat is a long, cylindrically shaped plant which may be modeled as a dipole. If this model is basically correc then we would expect the coupling between the incident E field vector and the vertical array of dipole wheat plants to increase with incidence angle. In other words, the projection of the E field vector onto the wheat stem will increase with angle resulting in increased currents in the wheat and thus increased reradiation by the plants.

A second observation which should be noted is the tendency for the curves shown in Figures 24 through 26 to crowd one another in the ranges between 10^o and 30^o and between 60^o and 70^o. This is particularly noticeable at 13.0 and 17.0 GHz. At angles other than those mentioned above the values of σ^o seem to be a bit more distinguishable implying a greater sensitivity of σ^o to target characteristics.

This is shown more clearly in Figures 27a and 27b where the linear regression results discussed in sections 4.1 and 4.3 are now plotted versus incidence angle, θ, instead of frequency. Curves are plotted, for three frequencies, 8.6, 13.0, 17.0 GHz, and both polarizations. Because of the dependence of plant moisture on time, these two figures contain basically the same information and nearly identical trends. Consider Figure 27a. At 0^o we see that both M_H^t and M_V^t are maximum. The tendency is then to decrease to a minimum in the 10^o-30^o region, increase to local maximum at 40^o and then to decrease to a minimum at 70^o. This is particularly true for the horizontally polarized, 8.6 GHz, data. For the vertical case we again see a tendency towards a maximum at 40^o but in general the sensitivity factor, M_V, is relatively constant when compared with M_H. Again this is shown in the curves showing the angular response of σ^o where we note a tendency toward greater separation in the σ_V^o curves at high angles compared to the separation of the σ_H^o curves at corresponding angles. On the basis of this data, this phenomenon suggests that if an imaging radar is to be used for the observation of wheat fields, it should work either quite near nadir or in the 40^o region of incidence angles with vertically polarized antennas.

5.0 CONCLUDING REMARKS

An experiment was conducted to measure the scattering coefficient of wheat during the final month of its growing season. Measurements were made at eleven frequencies in the 8-18 GHz band at angles from 0° to 70° from nadir. Results indicate that σ^o is quite dependent on the physiological and morphological processes occurring during the measurement period with σ^o often showing an increase of more than 10.0 dB as the wheat ripened. Particularly notable were variations of σ^o with frequency and polarization.

Because of many unanswered questions it is felt that further studies should include two additional measurements. The first measurement would be an estimate of plant attenuation either by a dielectric analysis of the wheat or by an in situ measurement of the crop attenuation itself. The second measurement would be some sort of quantifiable study of the wheat morphology. Both studies would be made on a regular basis at the time of the scattering measurements.

Throughout the discussion of the data presented herein it was noted that the greater majority of information was obtained from data taken at, or very near nadir. Investigations of the ability of active microwave sensors to estimate soil moisture also indicate that incidence angles near nadir are optimum [2,4,5,6] (although at lower microwave frequencies). This is unfortunate in view of the fact that the state of the art operational side-looking imaging radars perform poorest at nadir due to resolution considerations. A recent investigation by Larson et al., however, indicates "that a microwave hologram imaging radar is realizable for use on an aircraft or space vehicle" [19]. Furthermore it is noted that the best incidence angle for optimum operation of a microwave hologram radar is near nadir. In light of the potential for radar to remotely sense croplands such a system is very appealing.

REFERENCES

1. Ulaby, F. T. and R. K. Moore, "Radar Spectral Measurements of Vegetation, Proceedings 1973 ASP-ACSM Joint Fall Convention, Orlando, Florida, October, 1973.

2. Ulaby, F. T., "Radar Measurement of Soil Moisture Content," IEEE Trans. on Antennas and Propagation, vol. AP-22, no. 2, March, 1974.

3. Ulaby, F. T., "Radar Response to Vegetation," IEEE Trans. on Antennas and Propagation, vol. AP-23, no. 1, January, 1975.

4. Ulaby, F. T., J. Cihlar and R. K. Moore, "Active Microwave Measurement of Soil Water Content," Remote Sensing of Environment, vol. 3, pp. 185-203, 1974.

5. Ulaby, F. T., "Vegetation and Soil Backscatter Over the 4-18 GHz Region," Proceedings of the URSI Specialist Meeting, September, 1974, Bern, Switzerland.

6. Ulaby, F. T., T. F. Bush and P. P. Batlivala, "Radar Response to Vegetation II: 8-18 GHz Band," accepted for publication in IEEE Trans. on Antennas and Propagation, September, 1975.

7. de Loor, G. P., "Radar Ground Returns Part III: Further Measurements on the Radar Backscatter of Vegetation and Soils," Physics Laboratory TNO, Report No. PHL-974-05, The Hague, The Netherlands, March, 1974.

8. de Loor, G. P. and A. A. Jurriens, "The Radar Backscatter of Vegetation," AGARD Conf. Proc. No. 90 on Propagation Limitations of Remote Sensing, NATO, 1971.

9. Food and Agriculture Organization of the United Nations, 1972, 1972 FAO Production Yearbook, Rome.

10. Bush, T. F. and F. T. Ulaby, "8-18 GHz Radar Spectrometer," University of Kansas Center for Research, Inc., CRES Technical Report 177-43, Lawrence, Kansas, September, 1973.

11. Birkemeir, W. P. and N. D. Wallace, "Radar Tracking Accuracy Improvement by Means of Pulse to Pulse Frequency Modulation," IEEE Trans. on Communications and Electronics, pp. 571-575, January, 1963.

12. Bush, T. F. and F. T. Ulaby, "Fading Characteristics of Radar Backscatter from Selected Agricultural Targets," CRES Technical Report 177-48, University of Kansas Center for Research, Inc., Lawrence, Kansas, December, 1973.

13. Ray, H. K., "Improving Radar Range and Angle Detection with Frequency Agility," Microwave Journal, pp. 63-68, May, 1966.

14. Waite, W. P., Broad-Spectrum Electromagnetic Backscatter," CRES Technical Report 133-17, University of Kansas Center for Research, Inc., Lawrence, Kansas, August, 1970.

15. Carlson, N. L., "Dielectric Constant of Vegetation at 8.5 GHz," Ohio State University, Electro Science Lab., Tech. Report 1903-5, 1967.

16. Cihlar, J., "Ground Data Acquisition Procedure for Microwave (MAPS) Measurements," CRES Technical Memorandum 177-42, University of Kansas Center for Research, Inc., Lawrence, Kansas, July, 1973.

17. de Loor, G. P., "Measurement of Radar Ground Returns," Proceedings of the URSI Specialist Meeting, Bern, Switzerland, September 23-26, 1974.

18. Lundien, J. R., "Terrain Analysis by Electromagnetic Means," Technical Report No. 3-693, Report 2, U. S. Army Engineer Waterways Experiment Station, Vicksburg, Mississippi, p. 55, 1966.

19. Larson, R. W., R. W. Bayma, J. E. Ferris, M. B. Evans, J. S. Zelenka and H. W. Doss, "Investigation of Microwave Hologram Techniques for Application to Earth Resources," Proceedings Fifth Symposium on Remote Sensing of Environment, University of Michigan, Ann Arbor, pp. 1521-1569, April, 1974.

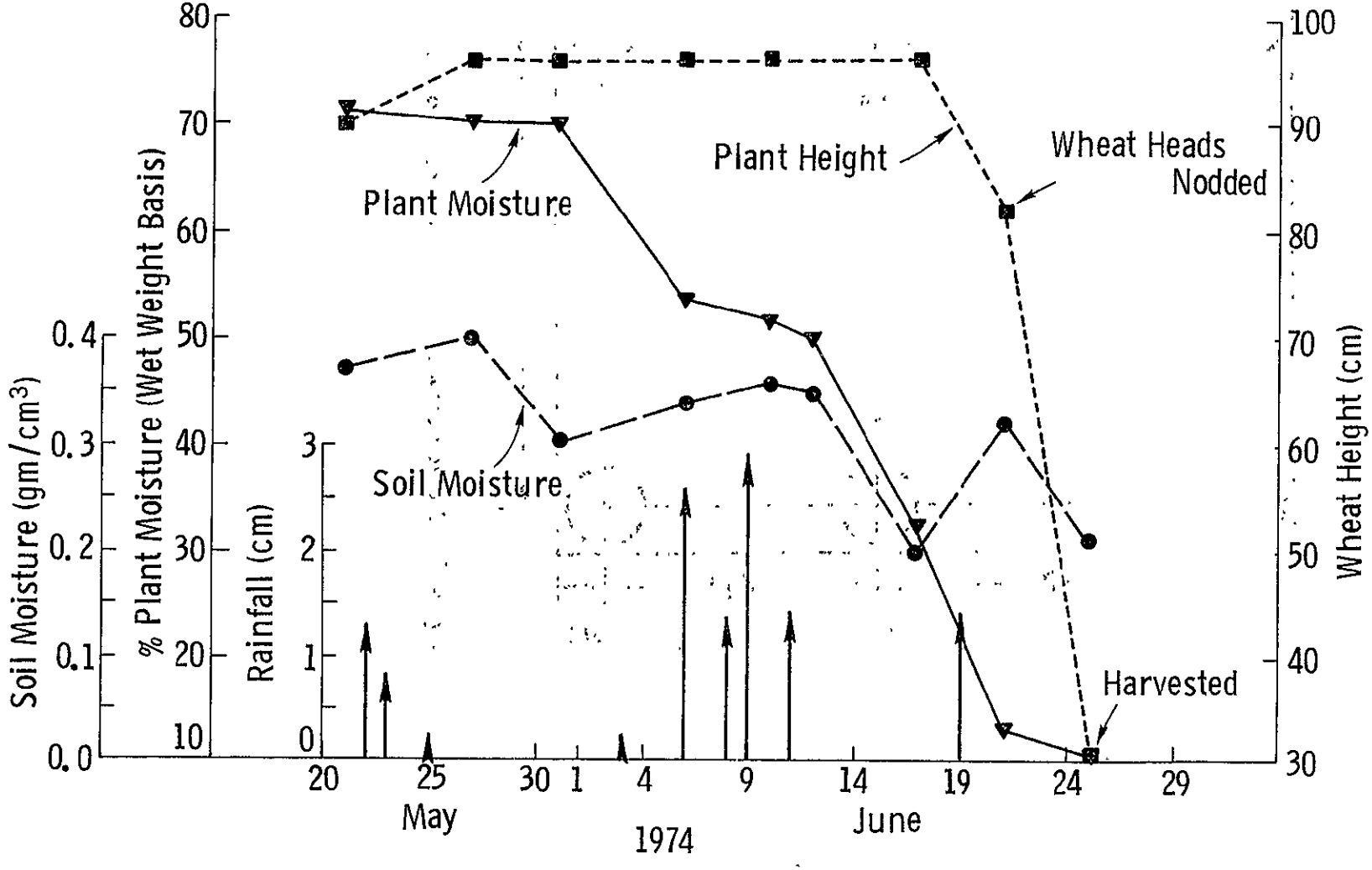

Figure 1. Record of soil moisture, plant moisture, plant height and precipitation during the observation period.

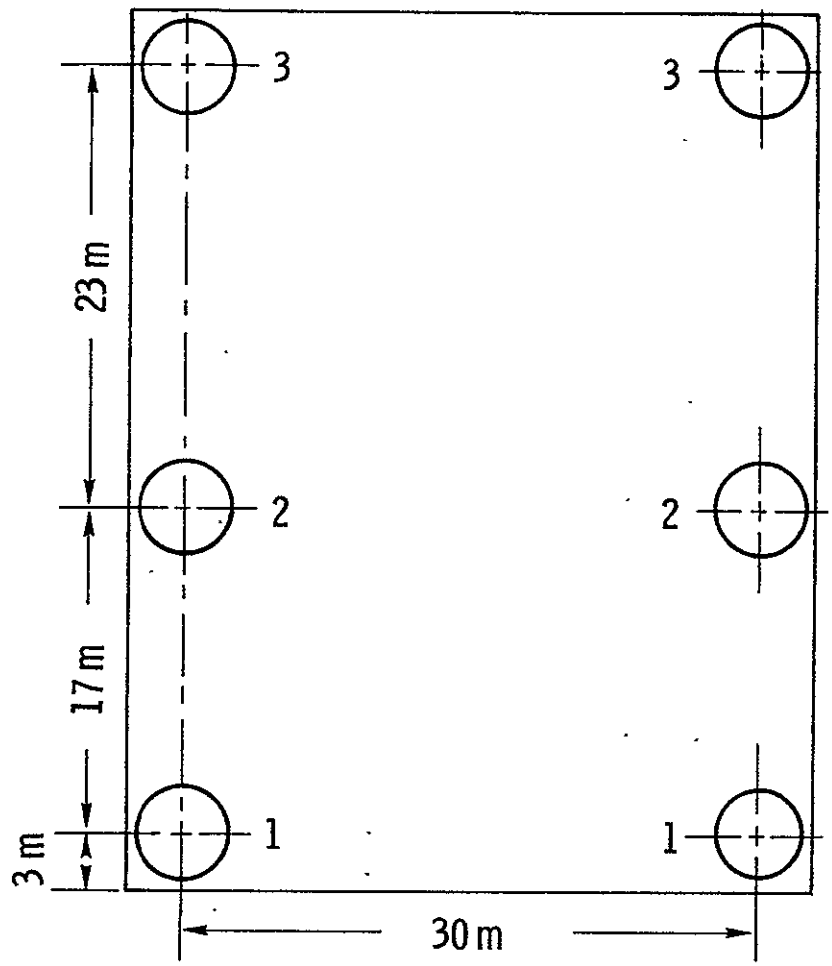

Figure 2. Diagram showing field locations of soil samples.

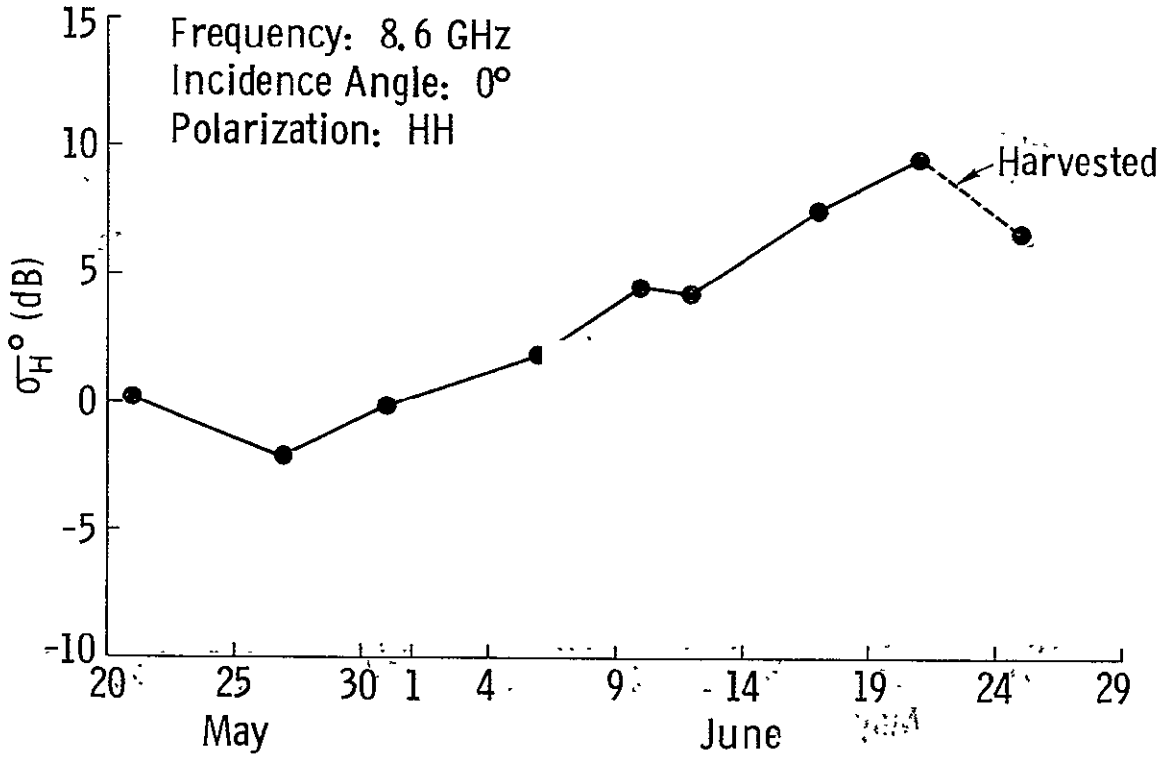

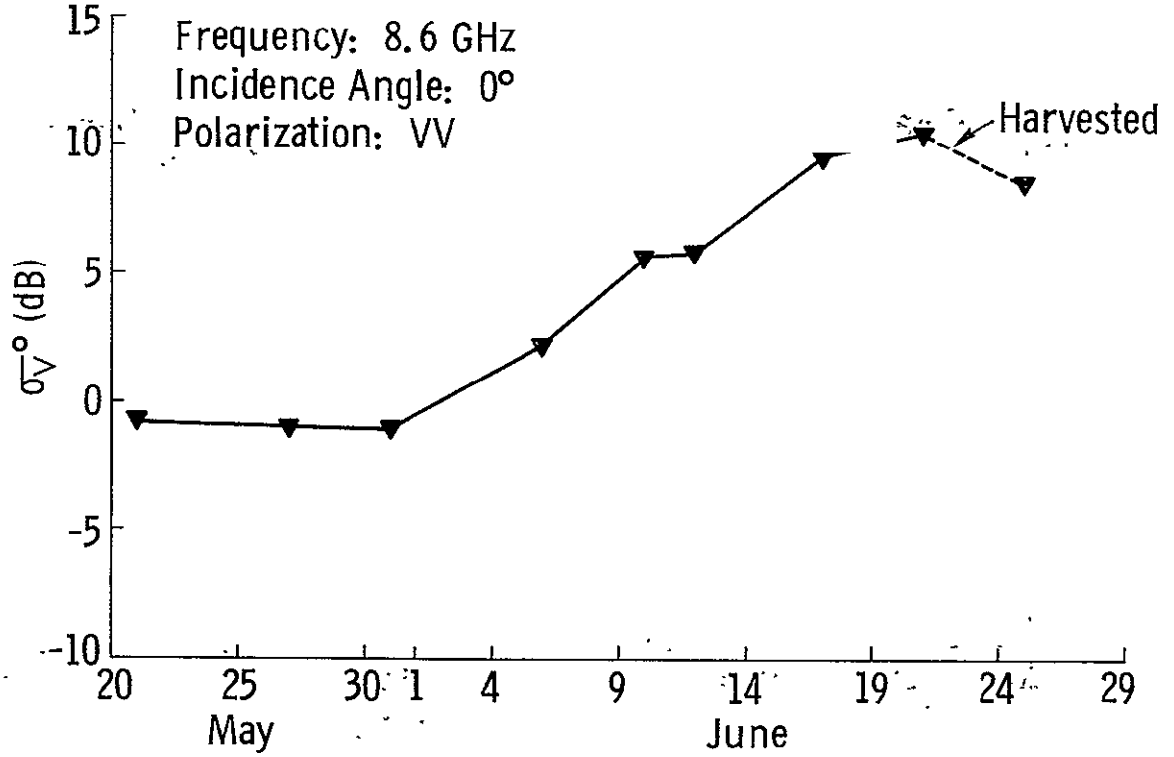

Figure 3a. Temporal variations of σ_H° (dB) and σ_V° (dB) as measured at 0°, 8.6 GHz.

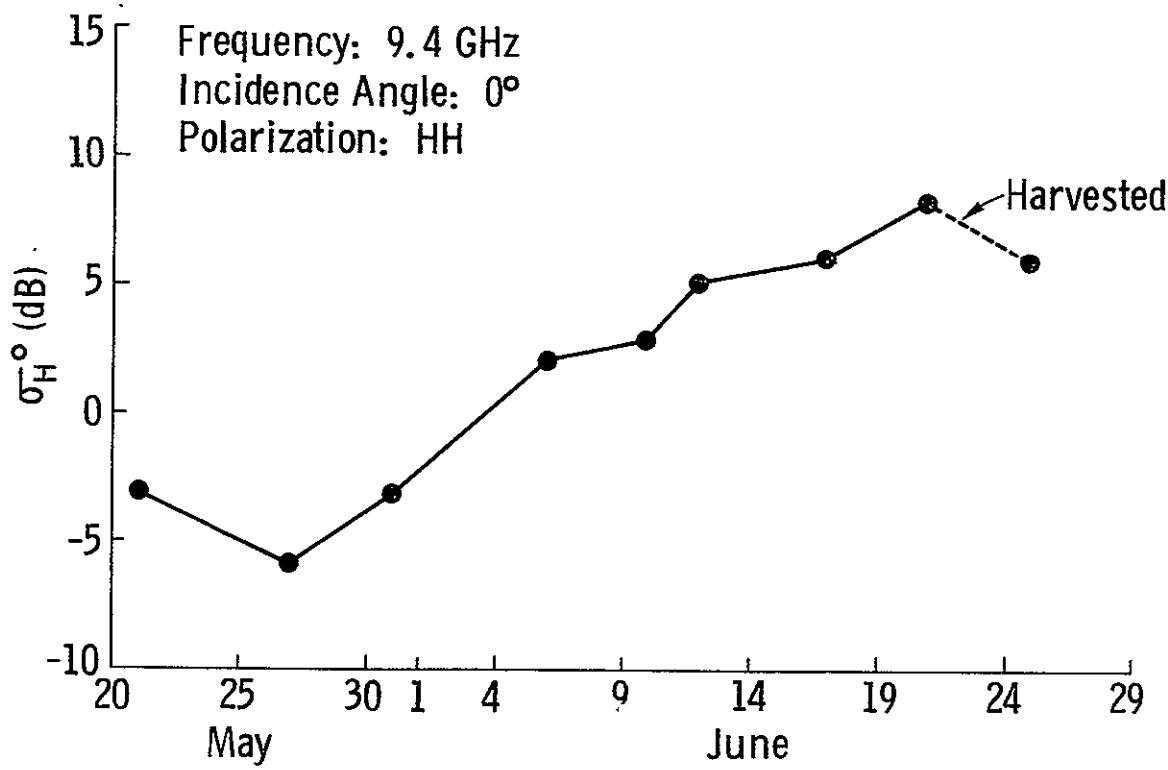

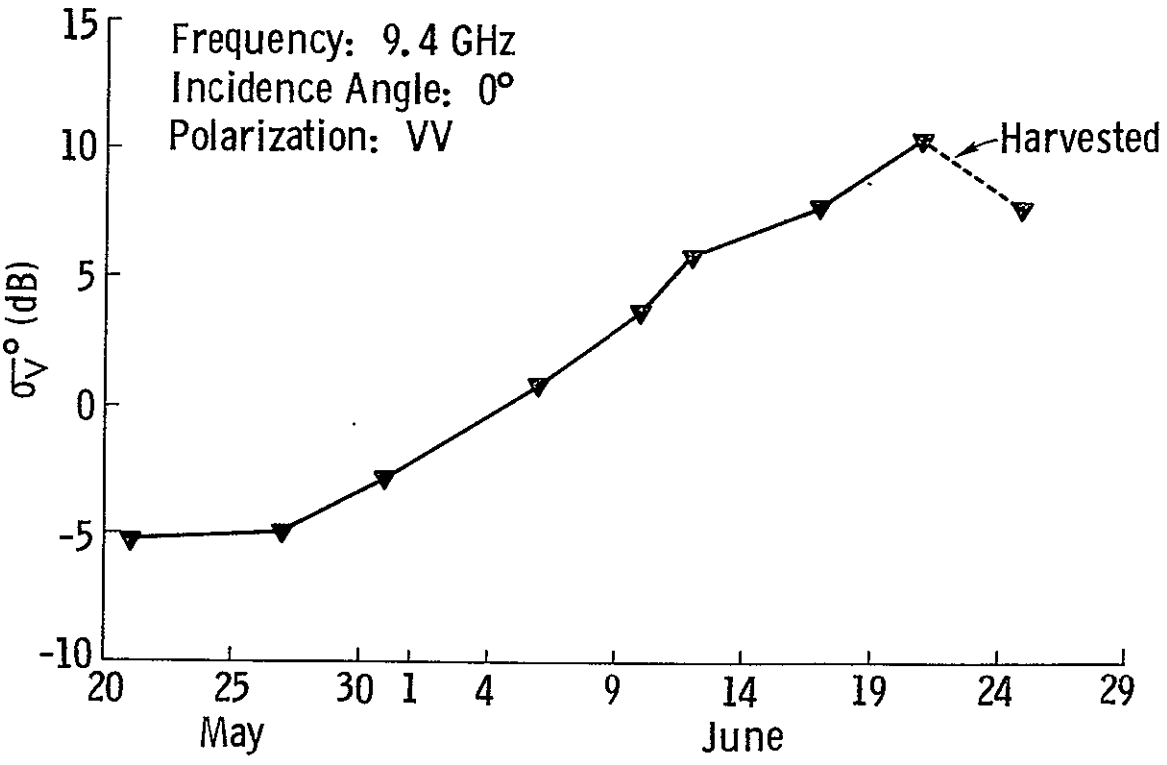

Figure 3b. Temporal variations of σ_H° (dB) and σ_V° (dB) as measured at 0°, 9.4 GHz.

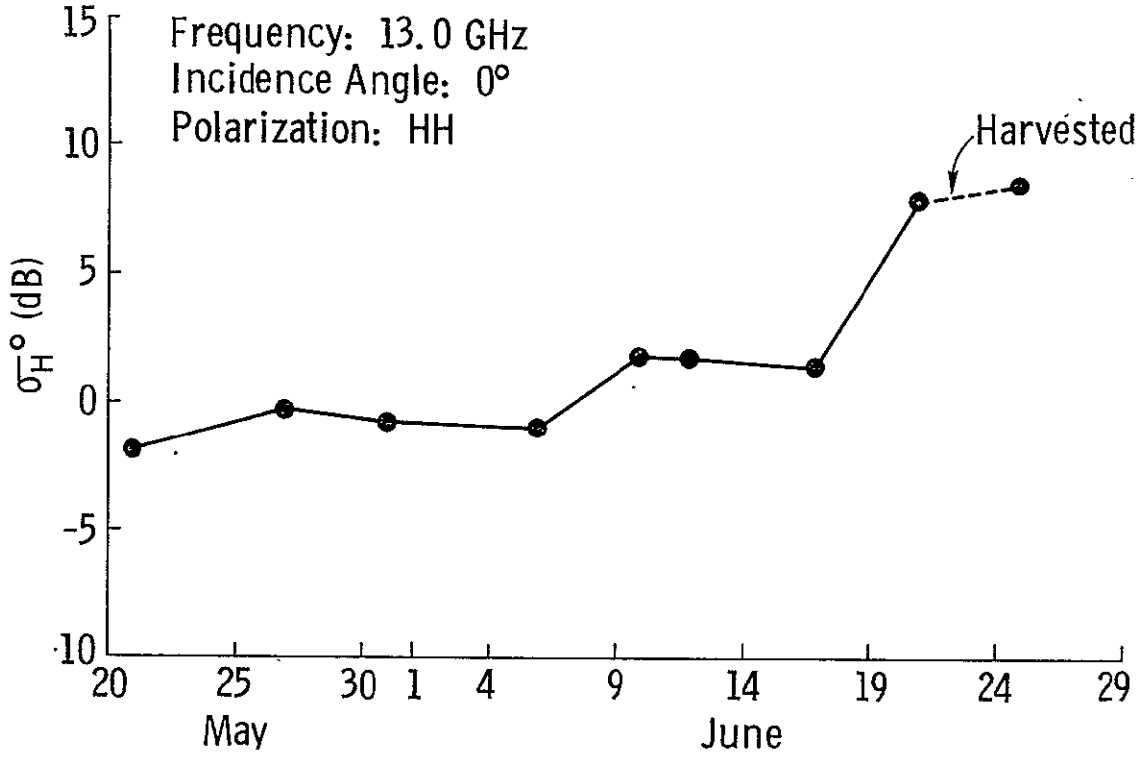

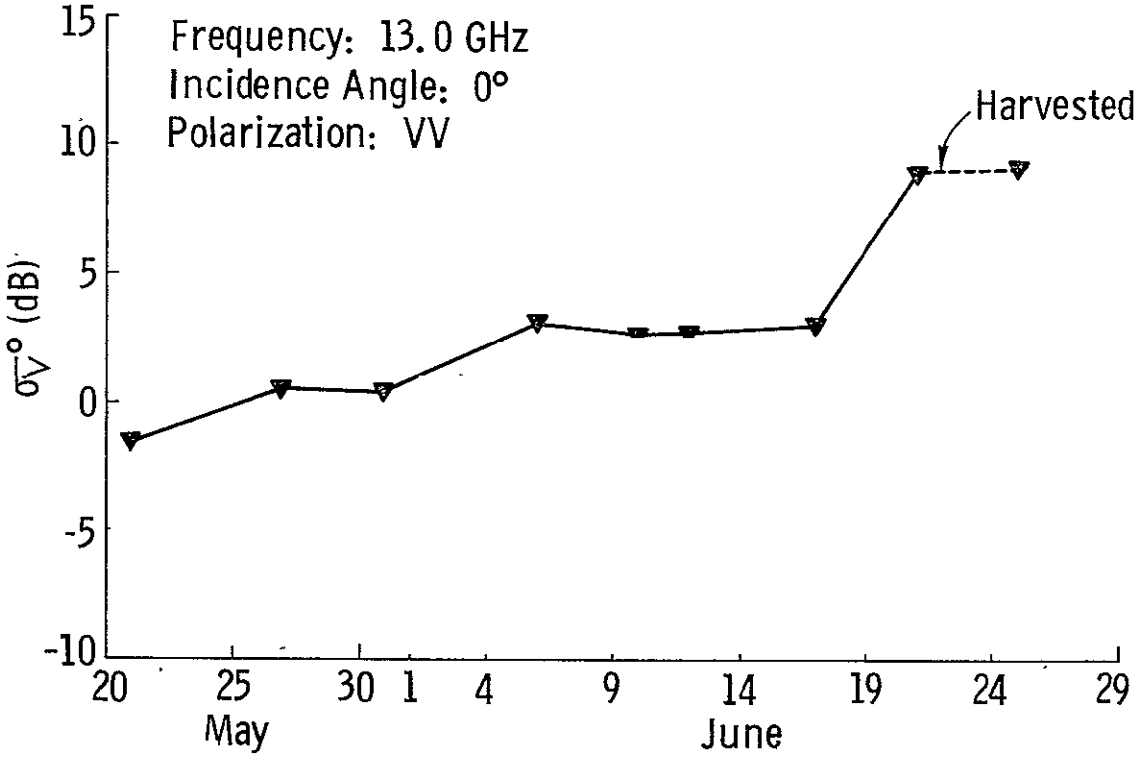

Figure 3c. Temporal variations of σ_H° (dB) and σ_V° (dB) as measured at 0°, 13.0 GHz.

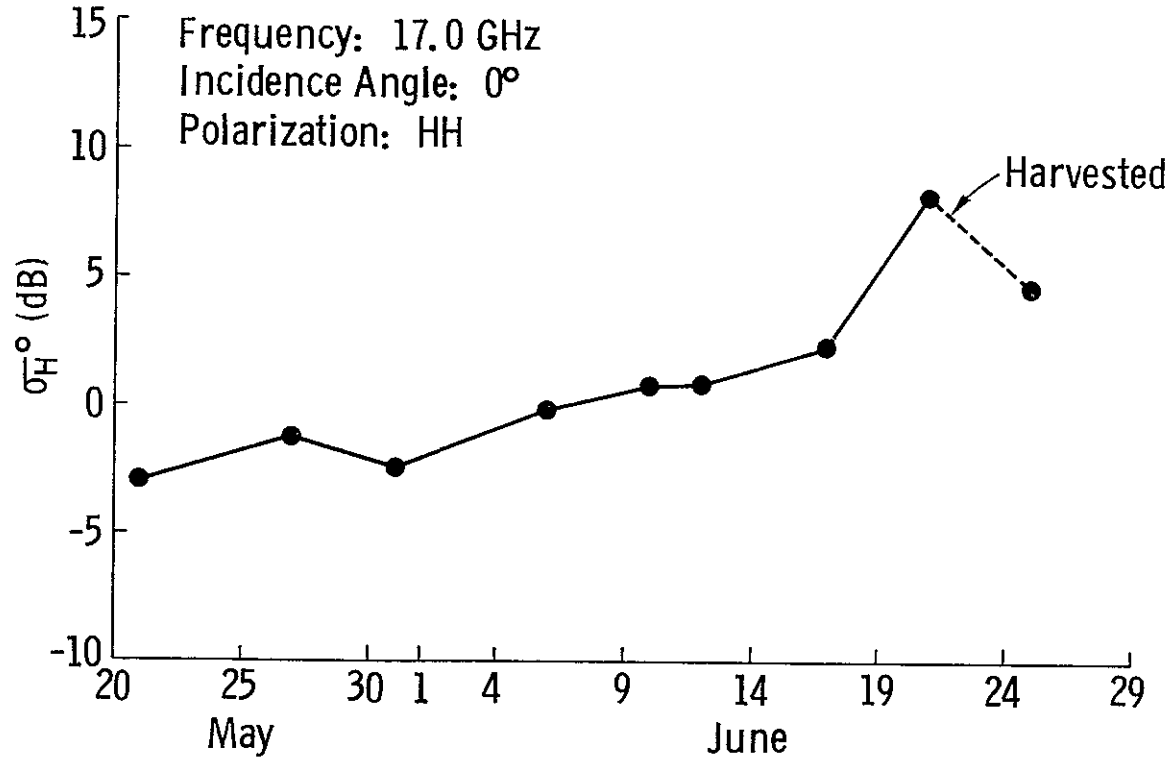

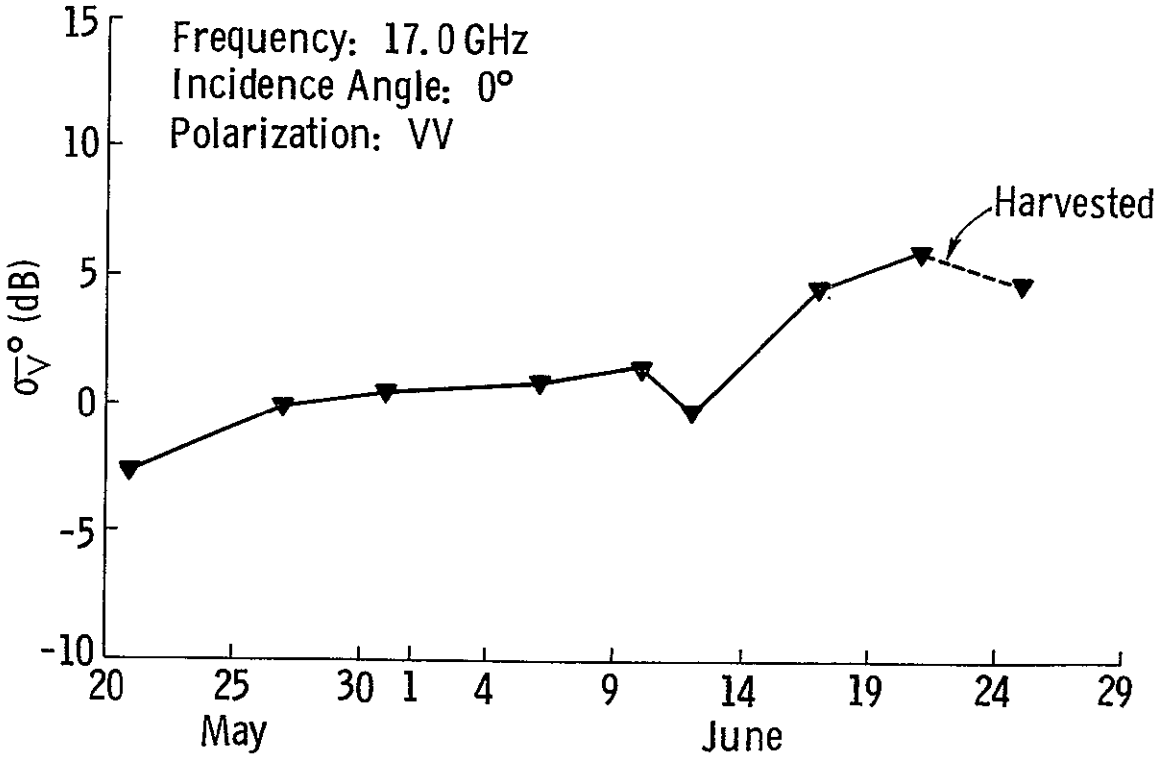

Figure 3d. Temporal variations of σ_H° (dB) and σ_V° (dB) as measured at 0°, 17.0 GHz.

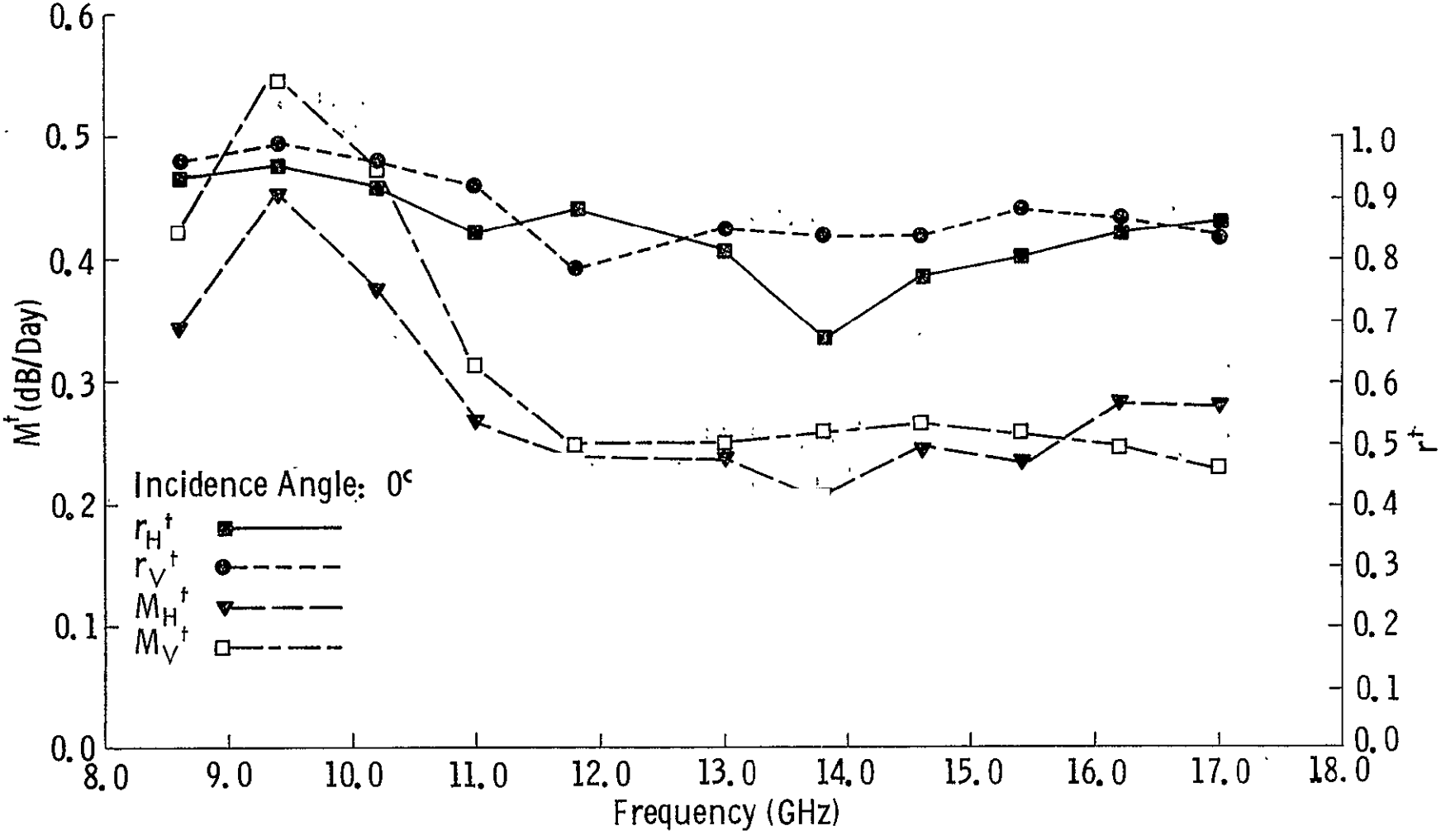

Figure 3e. Variations of $M_H{}^t$, $M_V{}^t$, $r_H{}^t$, and $r_V{}^t$ with frequency. $M_H{}^t$, $M_V{}^t$, $r_H{}^t$, and $r_V{}^t$ are the slopes (dB/day) and estimated correlation coefficients respectively, obtained by a linear regression of σ^o (dB) on time (days). The incidence angle is 0^o.

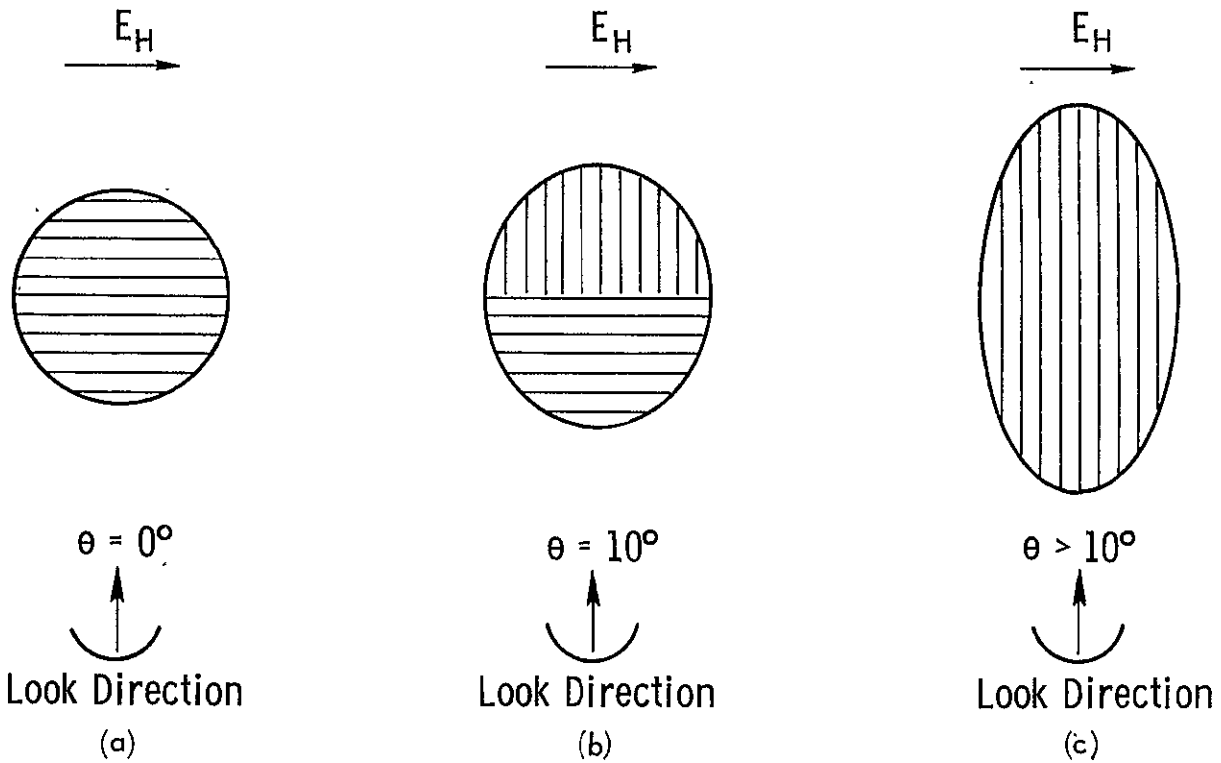

Figure 4. Diagram indicating the relationship between the electric field of a horizontally polarized signal and the wheat row direction for various incidence angles. Note the change of row direction which occurred at a range corresponding to an incidence angle of 10°.

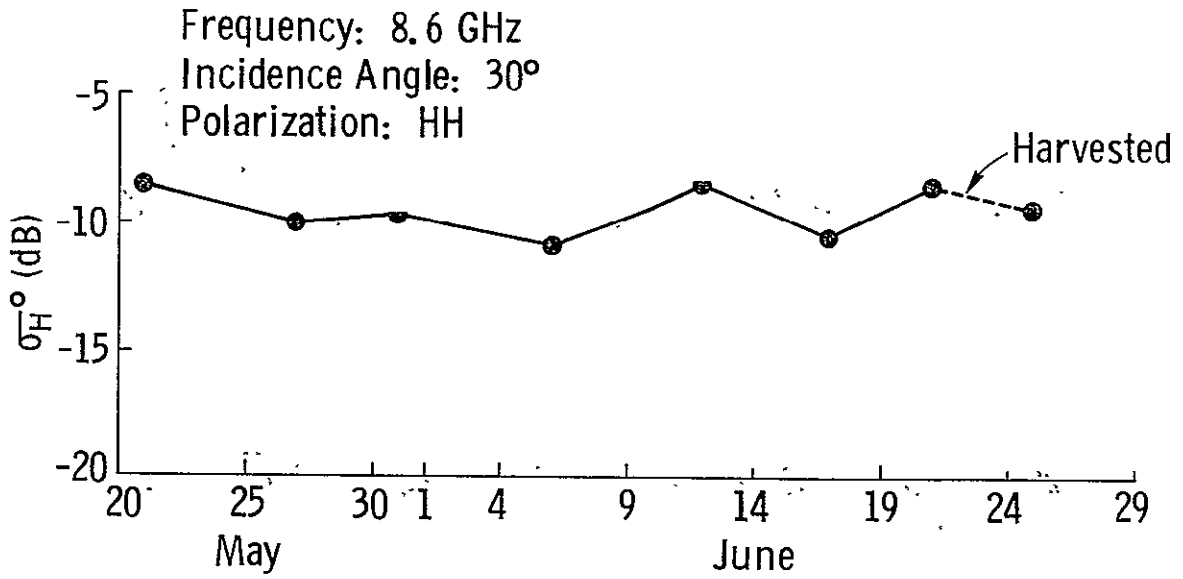

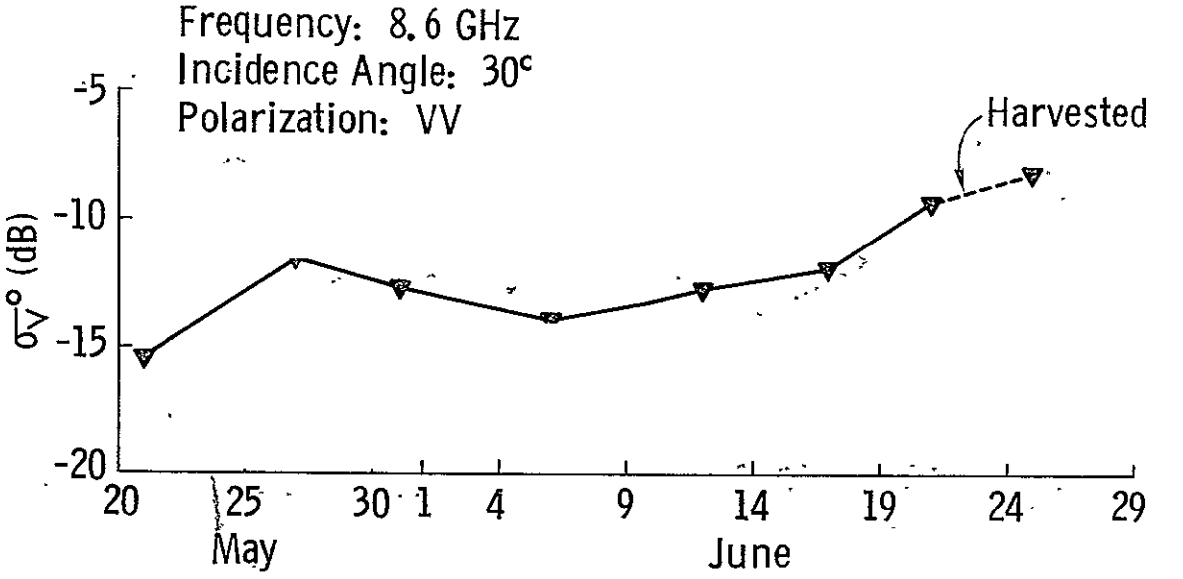

Figure 5a. Temporal variations of σ_H° (dB) and σ_V° (dB) as measured at 30°, 8.6 GHz.

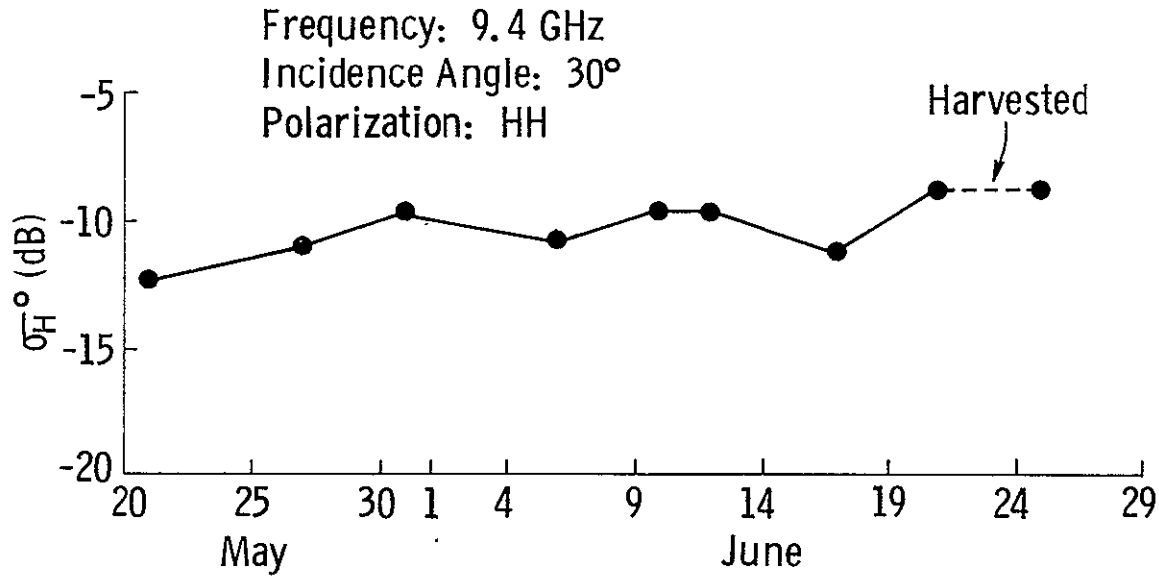

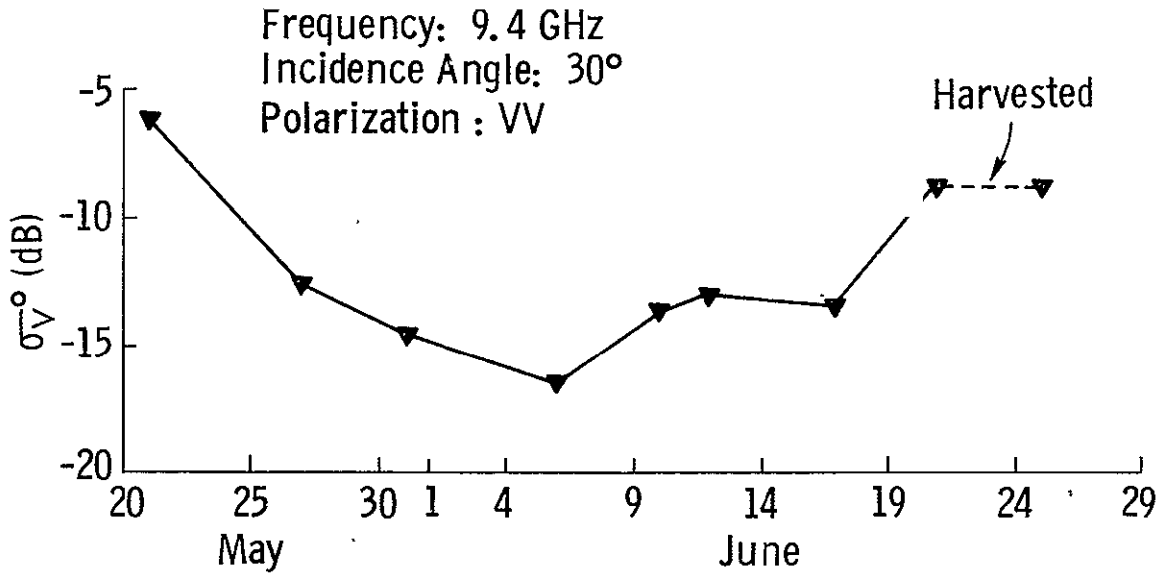

Figure 5b. Temporal variations of $\overline{\sigma_H}^\circ$ (dB) and $\overline{\sigma_V}^\circ$ (dB) as measured at 30°, 9.4 GHz.

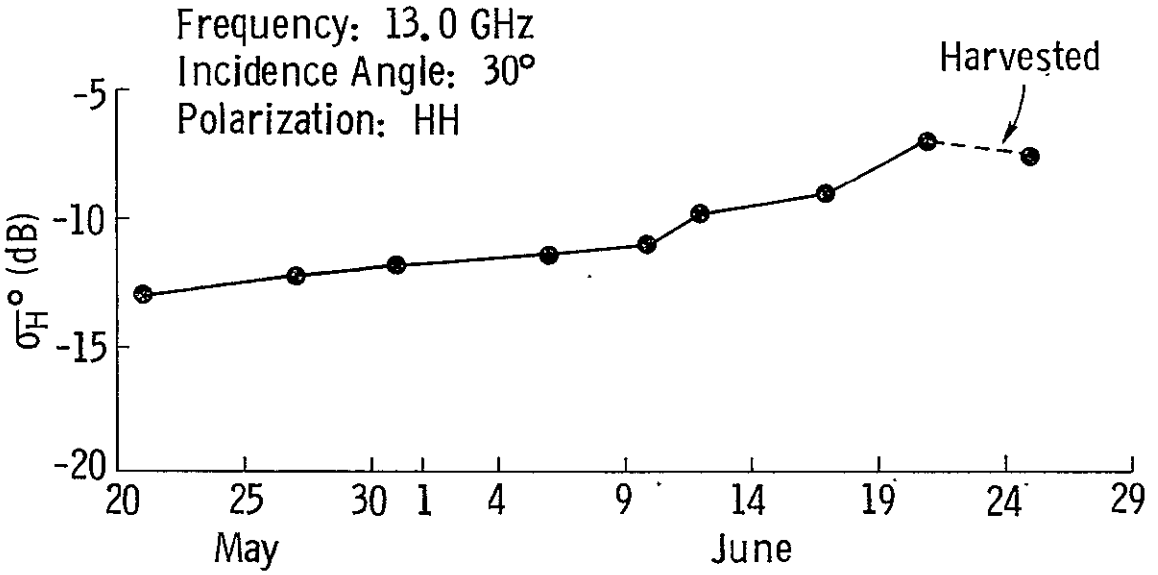

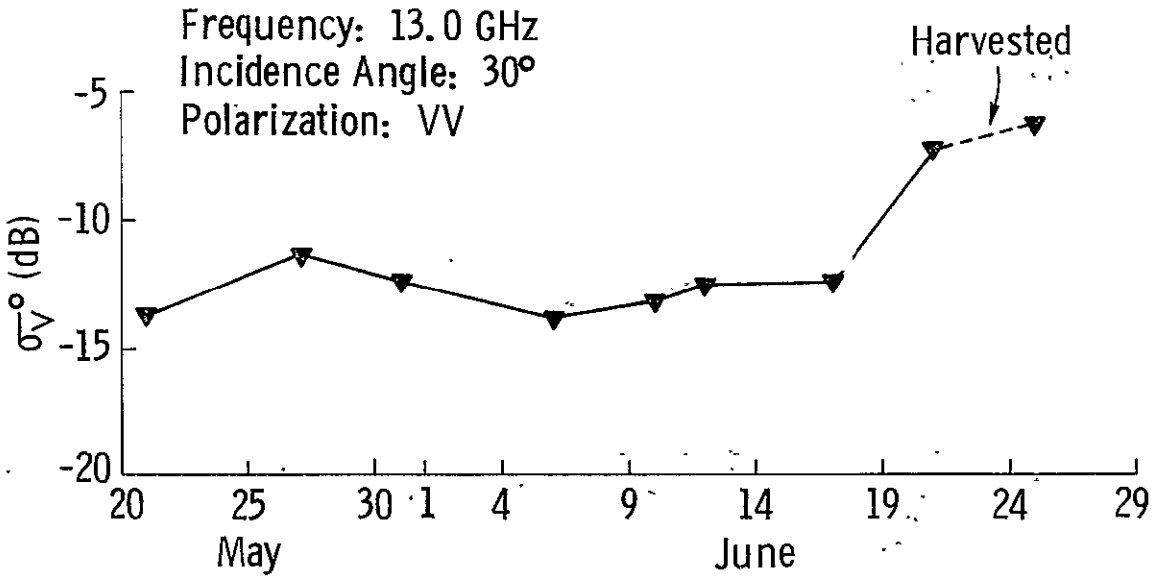

Figure 5c. Temporal variations of $\overline{\sigma_H}^\circ$ (dB) and $\overline{\sigma_V}^\circ$ (dB) as measured at 30°, 13.0 GHz.

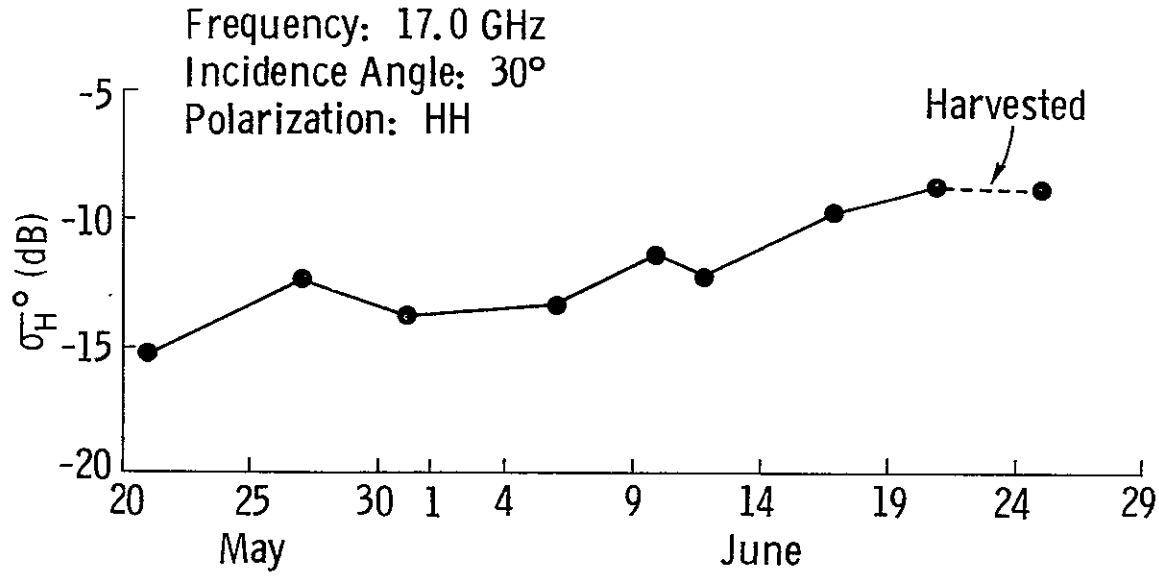

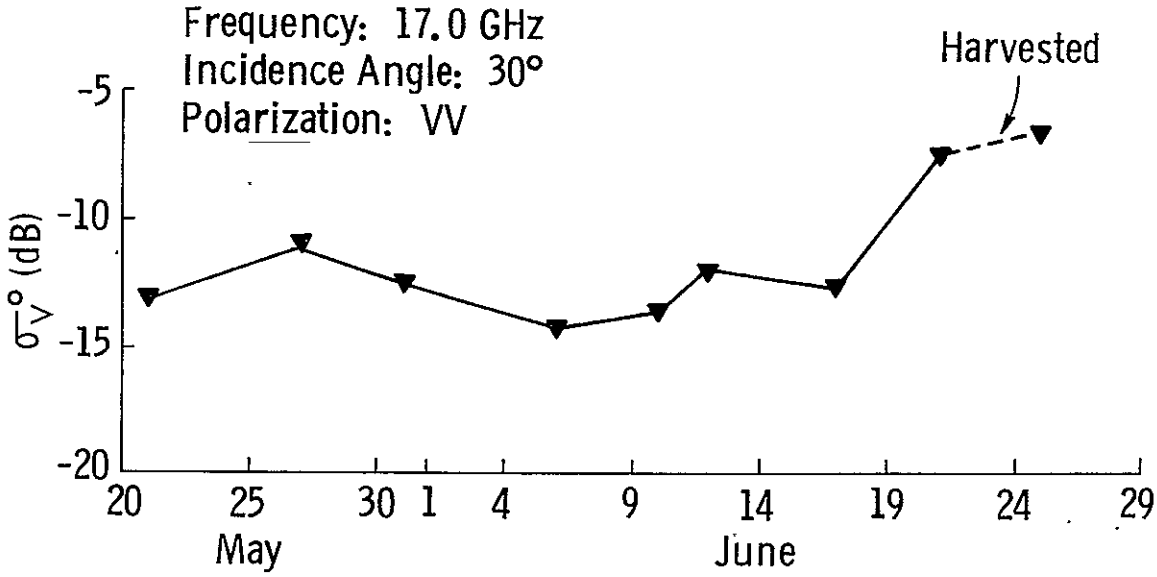

Figure 5d. Temporal variations of σ_H° (dB) and σ_V° (dB) as measured at 30°, 17.0 GHz.

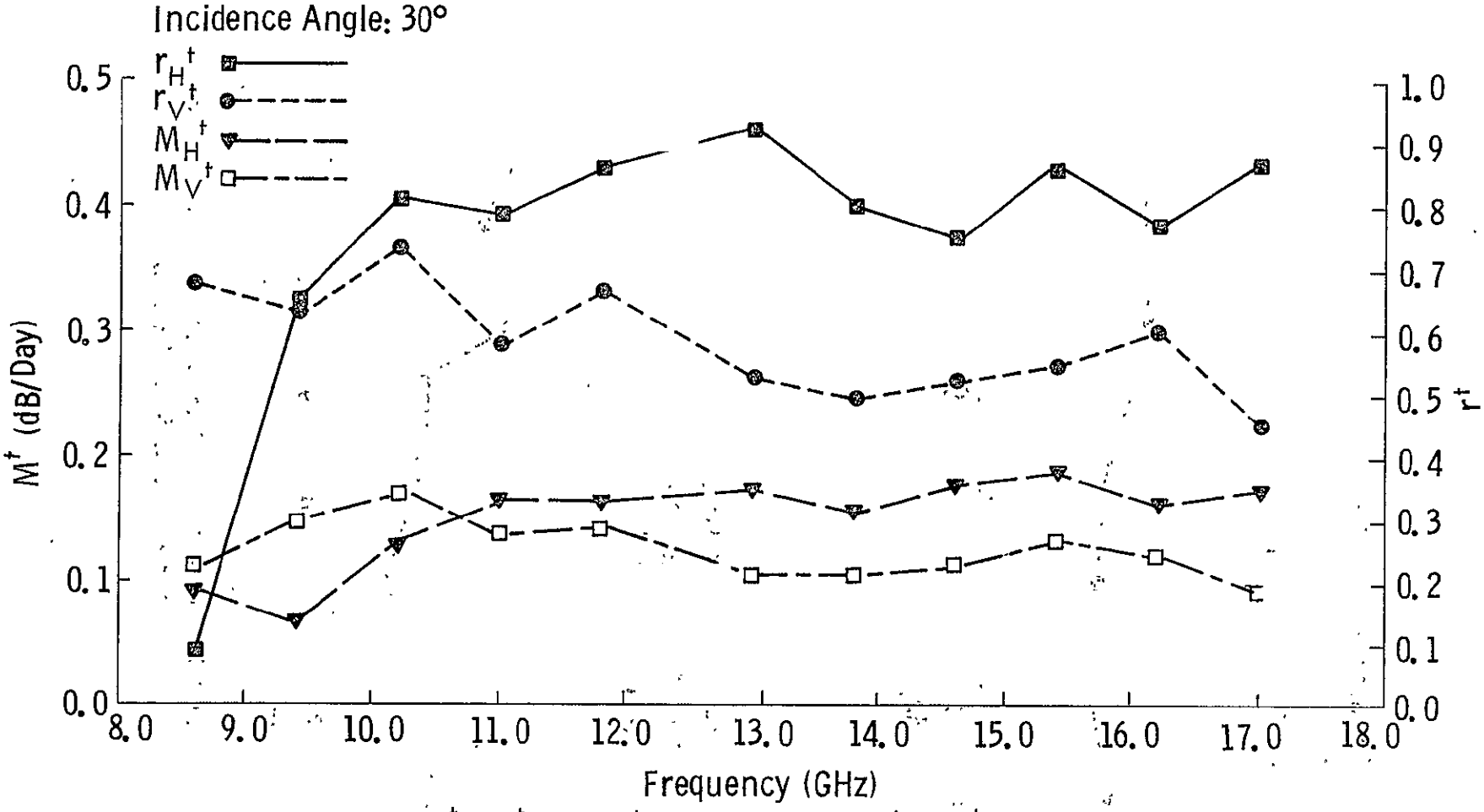

Figure 5e. Variations of M_H^t, M_V^t, r_H^t, and r_V^t with frequency. M_H^t, M_V^t, r_H^t, and r_V^t are the slopes (dB/day) and estimated correlation coefficients respectively, obtained by a linear regression of σ^o (dB) on time (days). The incidence angle is 30°.

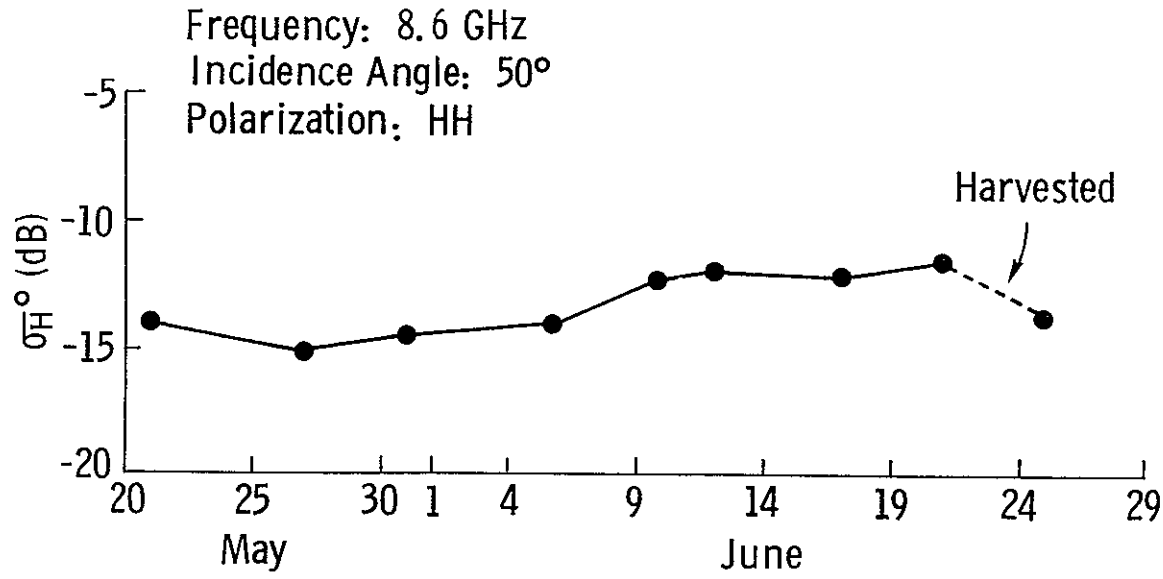

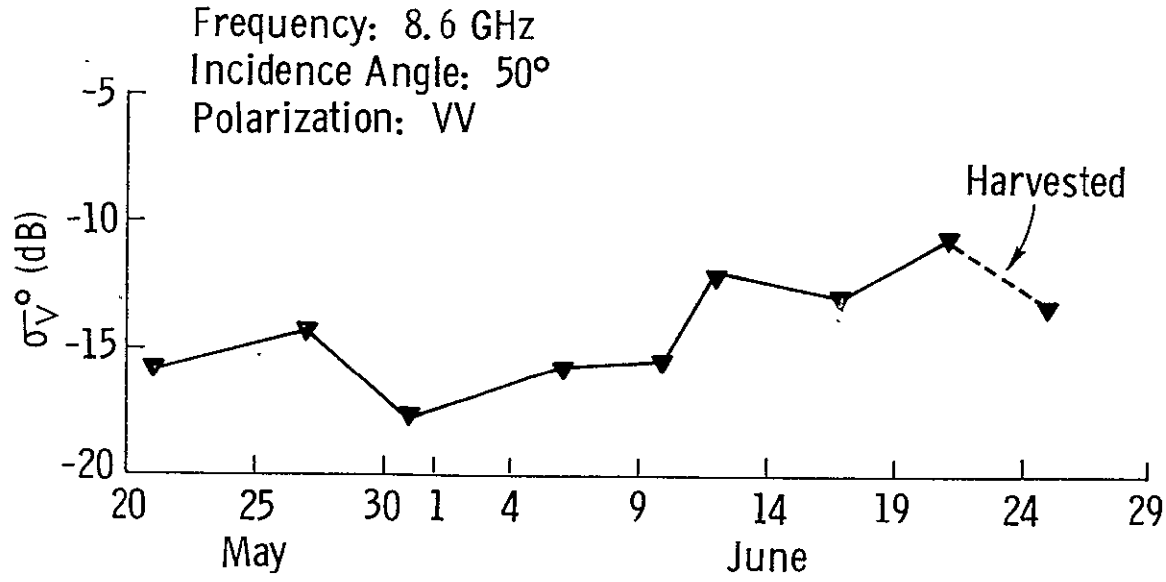

Figure 6a. Temporal variations of $\overline{\sigma_H}^\circ$ (dB) and $\overline{\sigma_V}^\circ$ (dB) as measured at 50°, 8.6 GHz.

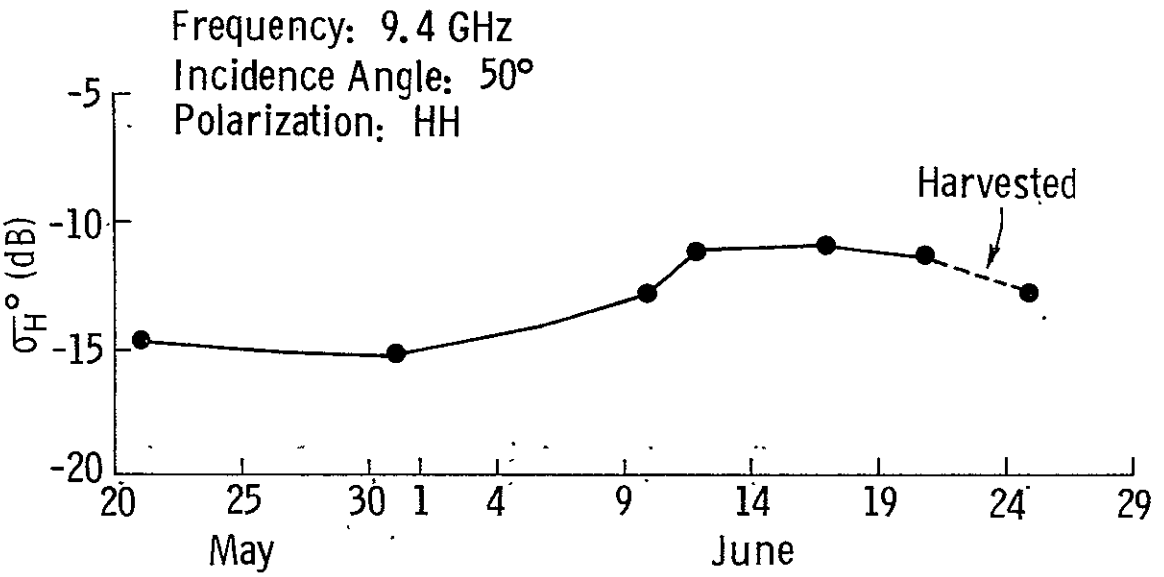

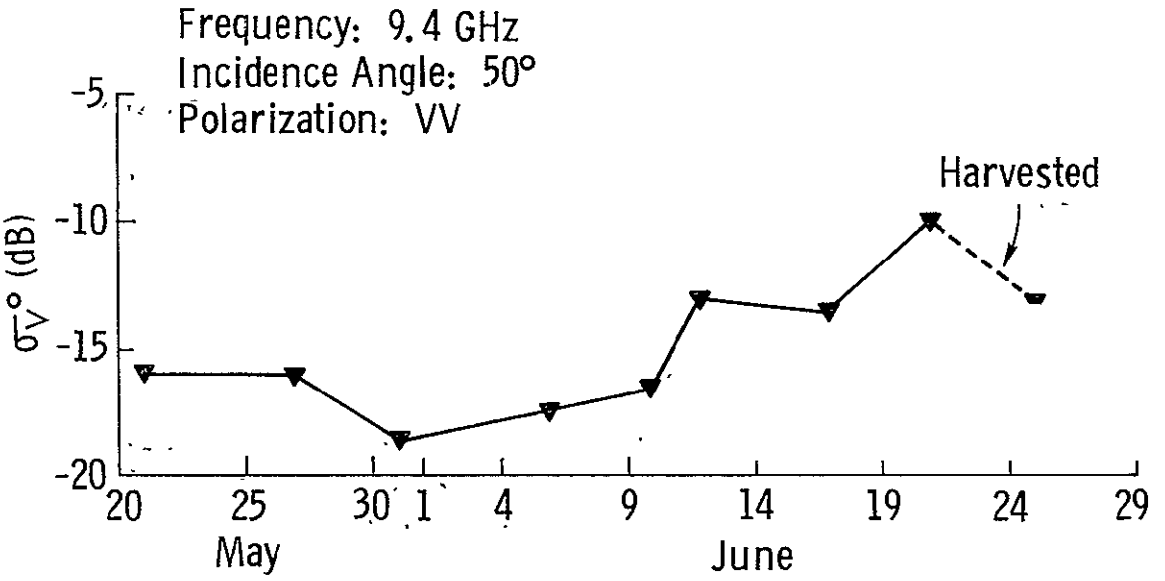

Figure 6b. Temporal variations of σ_H° (dB) and σ_V° (dB) as measured at 50°, 9.4 GHz.

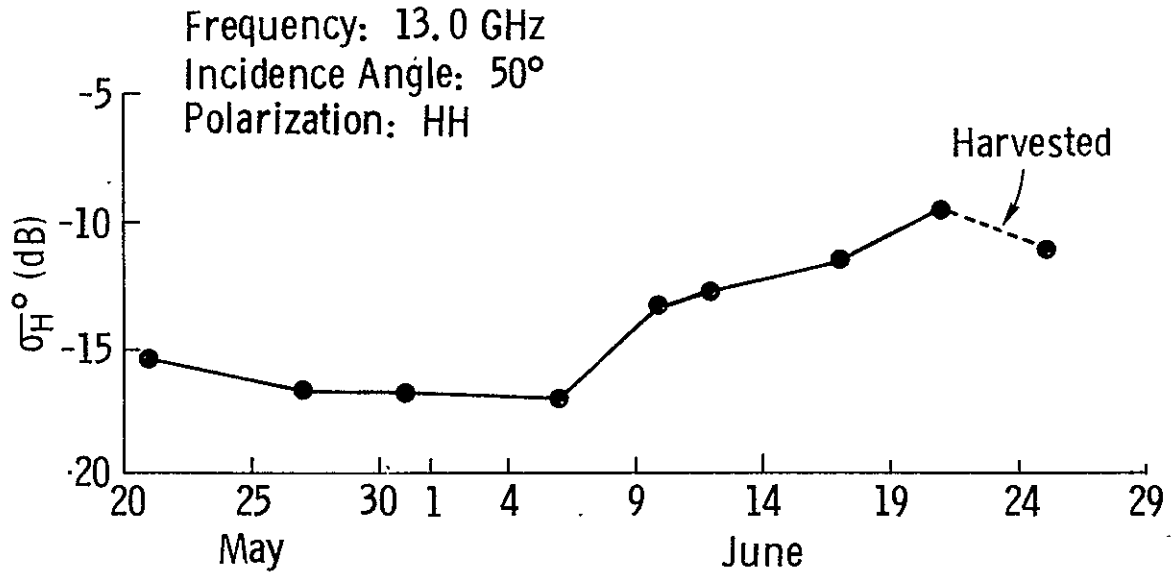

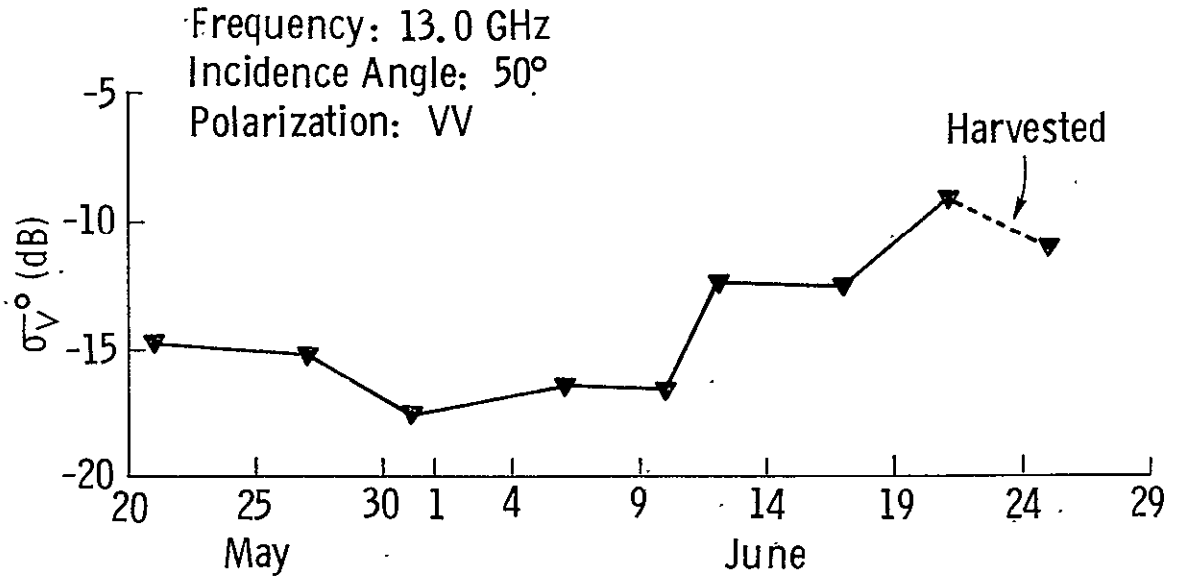

Figure 6c. Temporal variations of σ_H° (dB) and σ_V° (dB) as measured at 50°, 13.0 GHz.

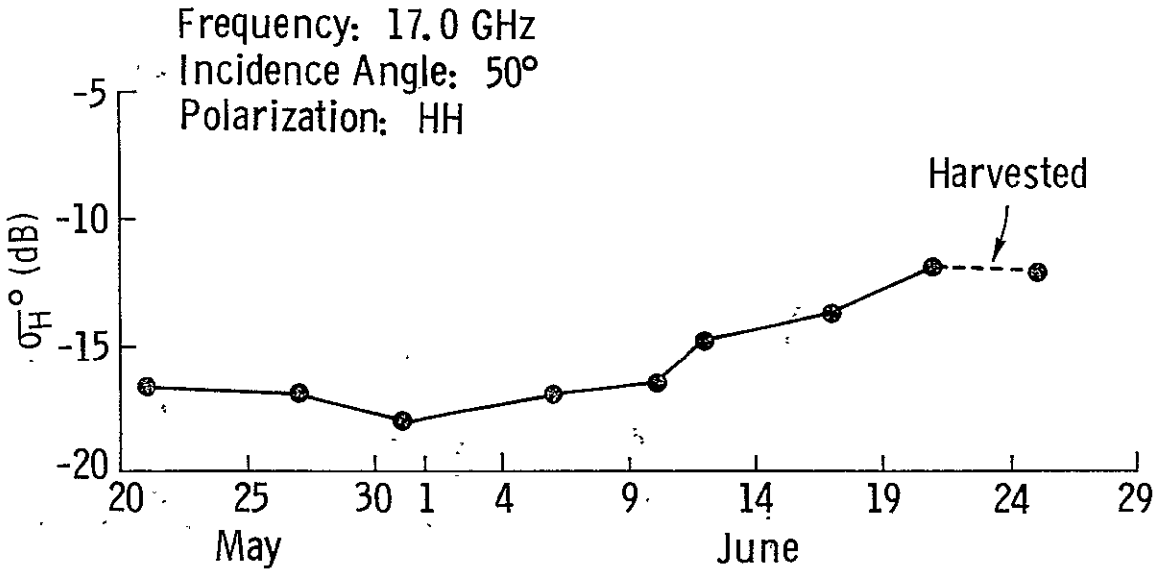

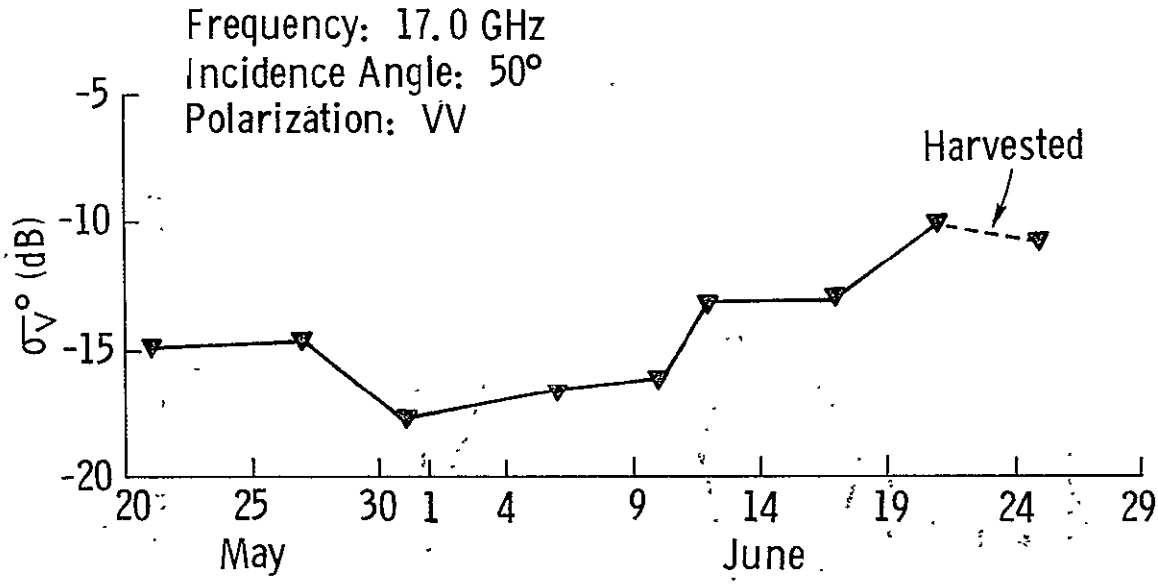

Figure 6d. Temporal variations of σ_H° (dB) and σ_V° (dB) as measured at 50°, 17.0 GHz.

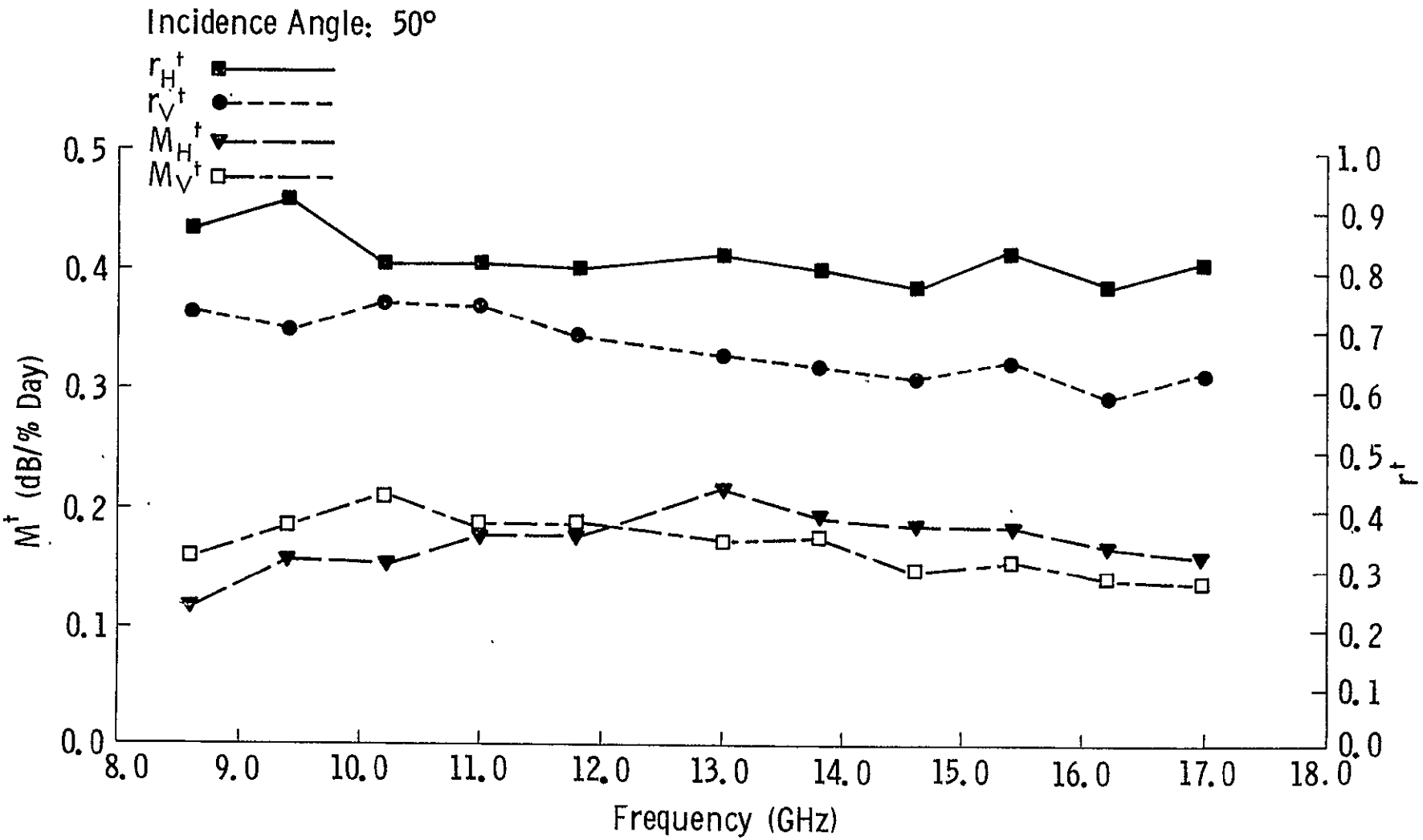

Figure 6e. Variations of M_H^t, M_V^t, r_H^t, and r_V^t with frequency. M_H^t, M_V^t, r_H^t, and r_V^t are the slopes (dB/day) and estimated correlation coefficients respectively, obtained by a linear regression of σ^o (dB) on time (days). The incidence angle is 50°.

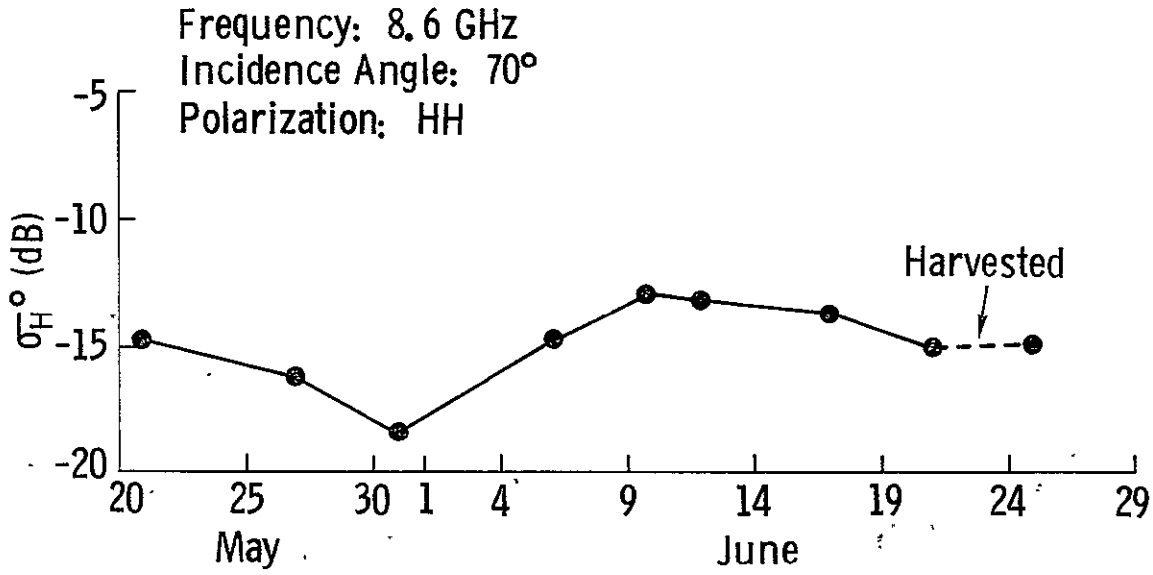

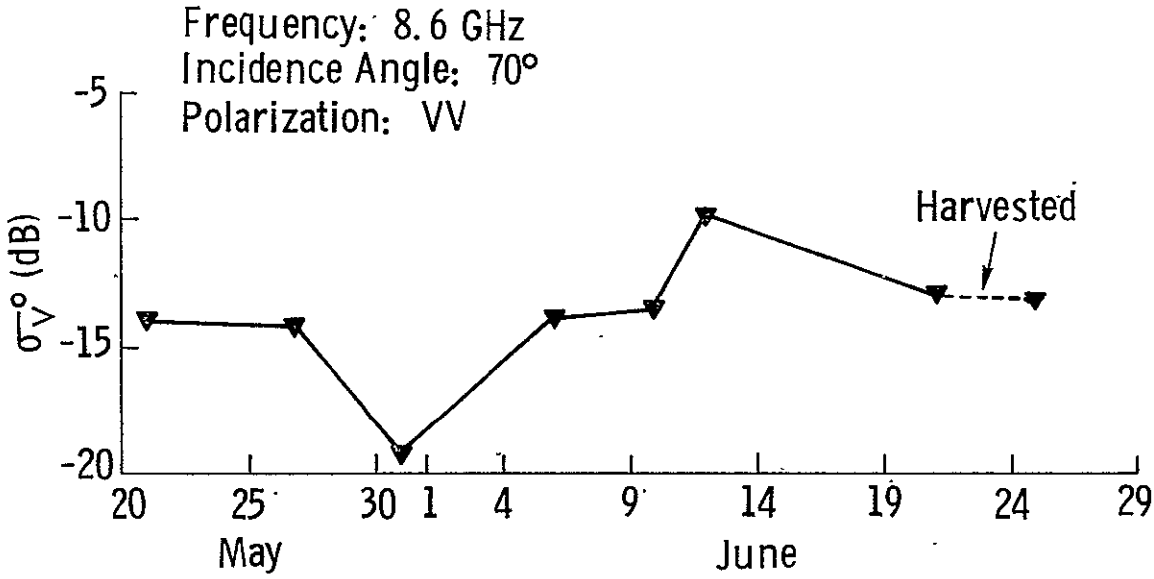

Figure 7a. Temporal variations of σ°_H (dB) and σ°_V (dB) as measured at 70°, 8.6 GHz.

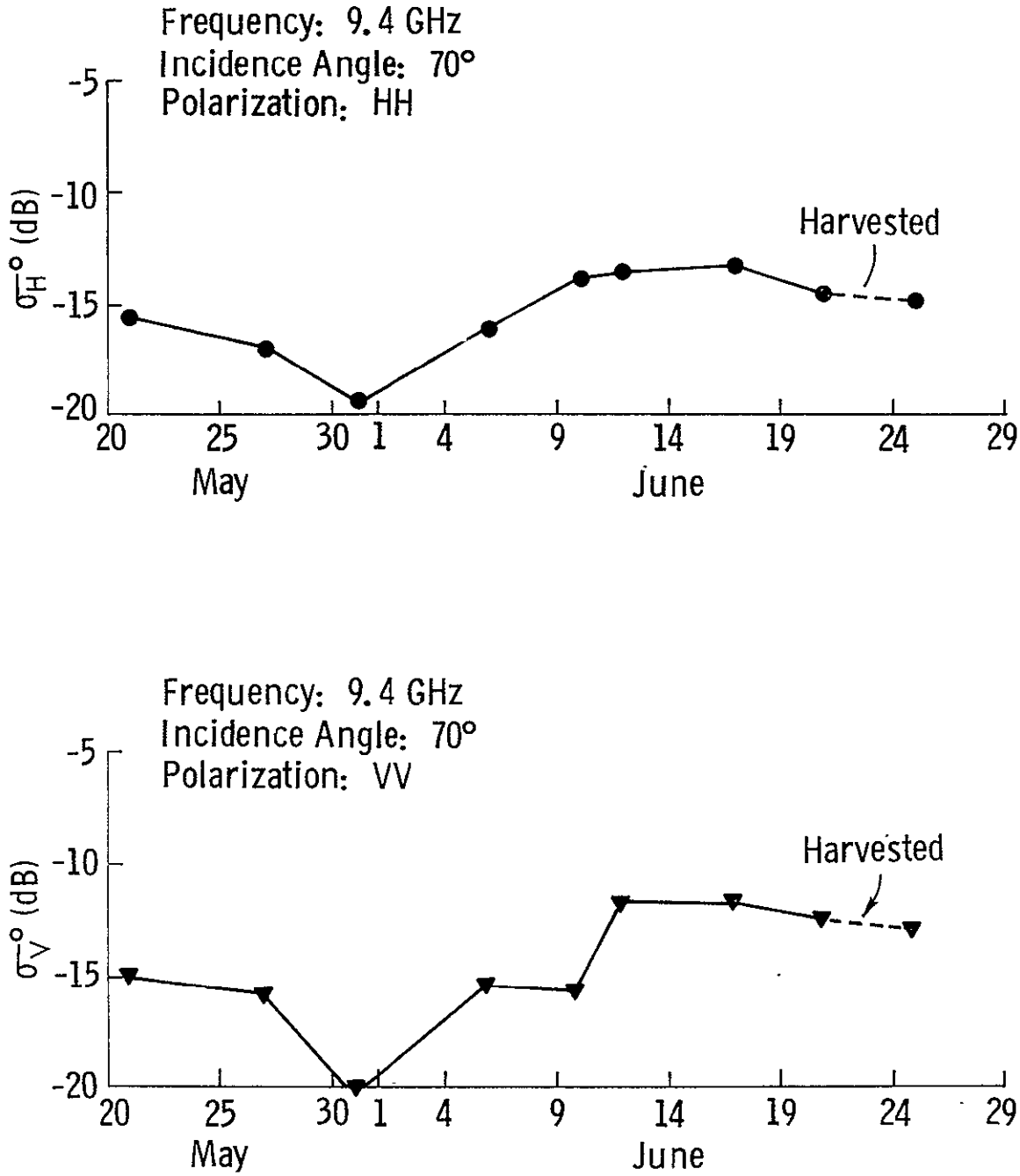

Figure 7b. Temporal variations of σ_H° (dB) and σ_V° (dB) as measured at 70°, 9.4 GHz.

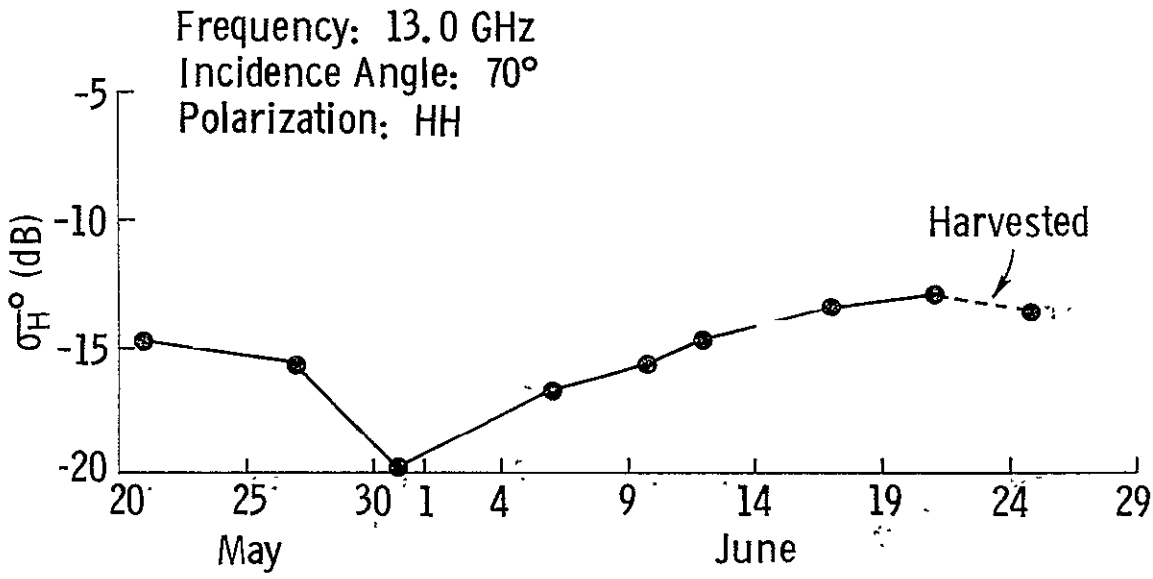

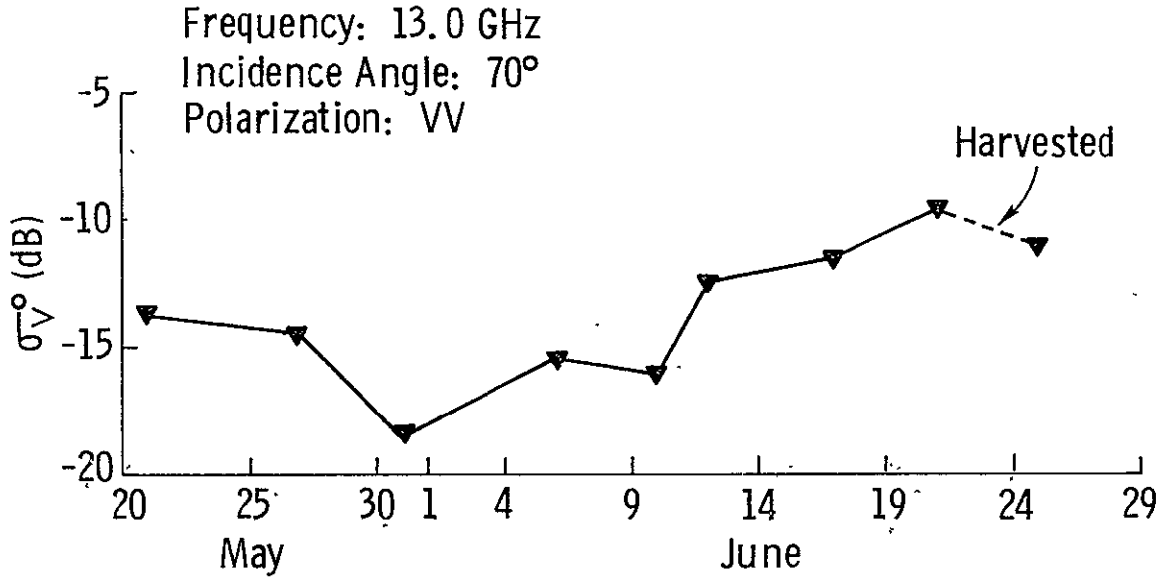

Figure 7c. Temporal variations of σ_H° (dB) and σ_V° (dB) as measured at 70°, 13.0 GHz.

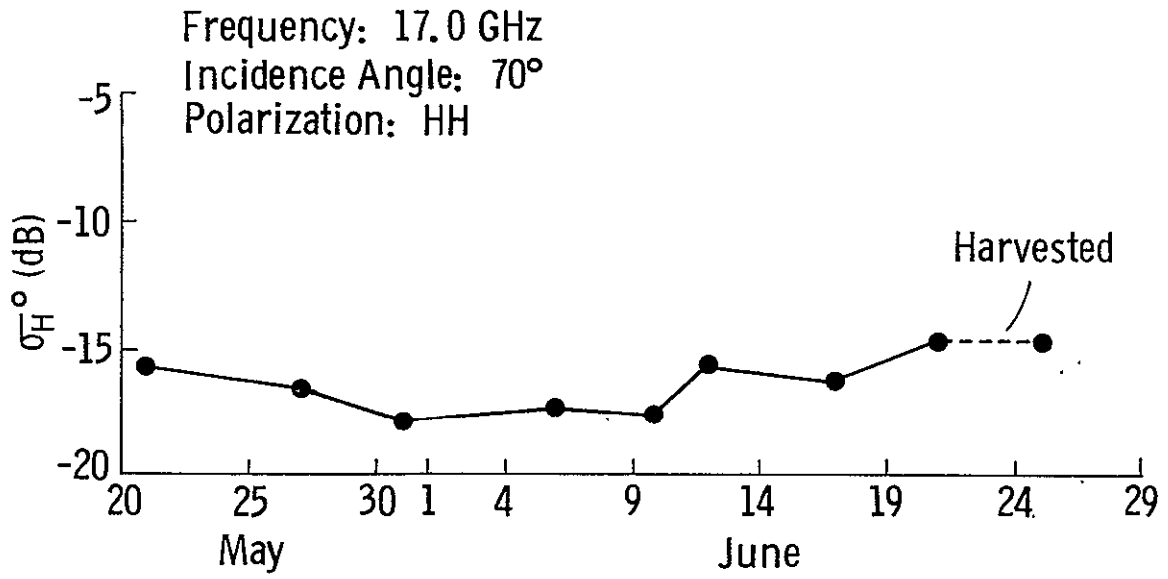

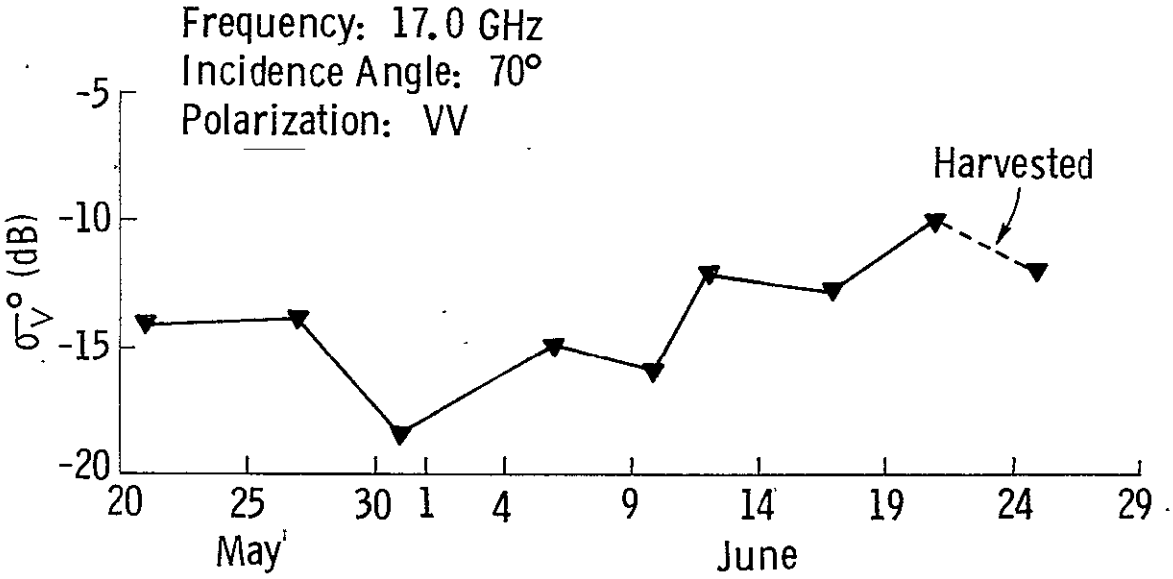

Figure 7d. Temporal variations of σ_H° (dB) and σ_V° (dB) as measured at 70°, 17.0 GHz.

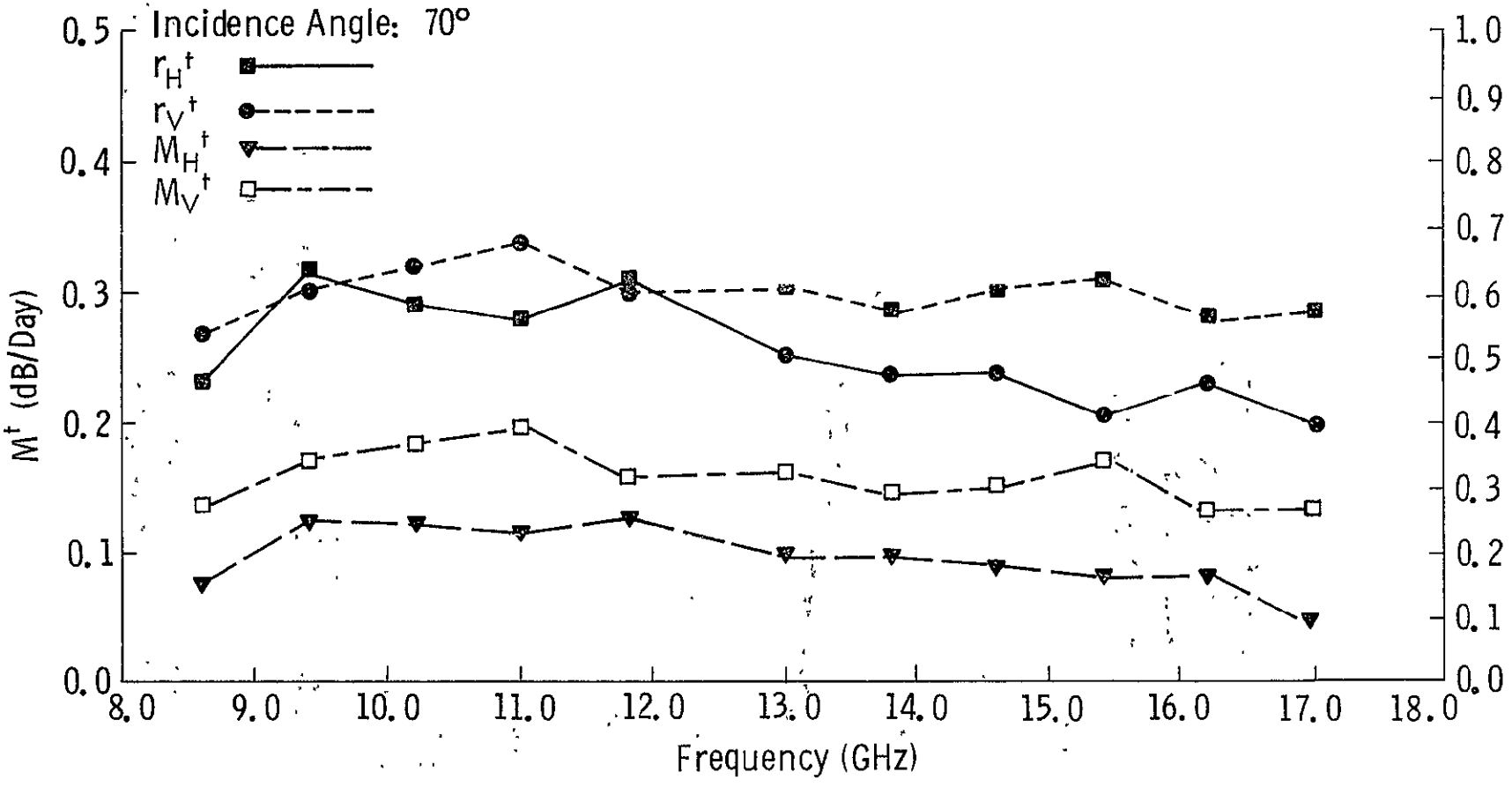

Figure 7e. Variations of $M_H{}^t$, $M_V{}^t$, $r_H{}^t$, and $r_V{}^t$ with frequency. $M_H{}^t$, $M_V{}^t$, $r_H{}^t$, and $r_V{}^t$ are the slopes (dB/day) and estimated correlation coefficients respectively, obtained by a linear regression of σ^o (dB) on time (days). The incidence angle is 70°.

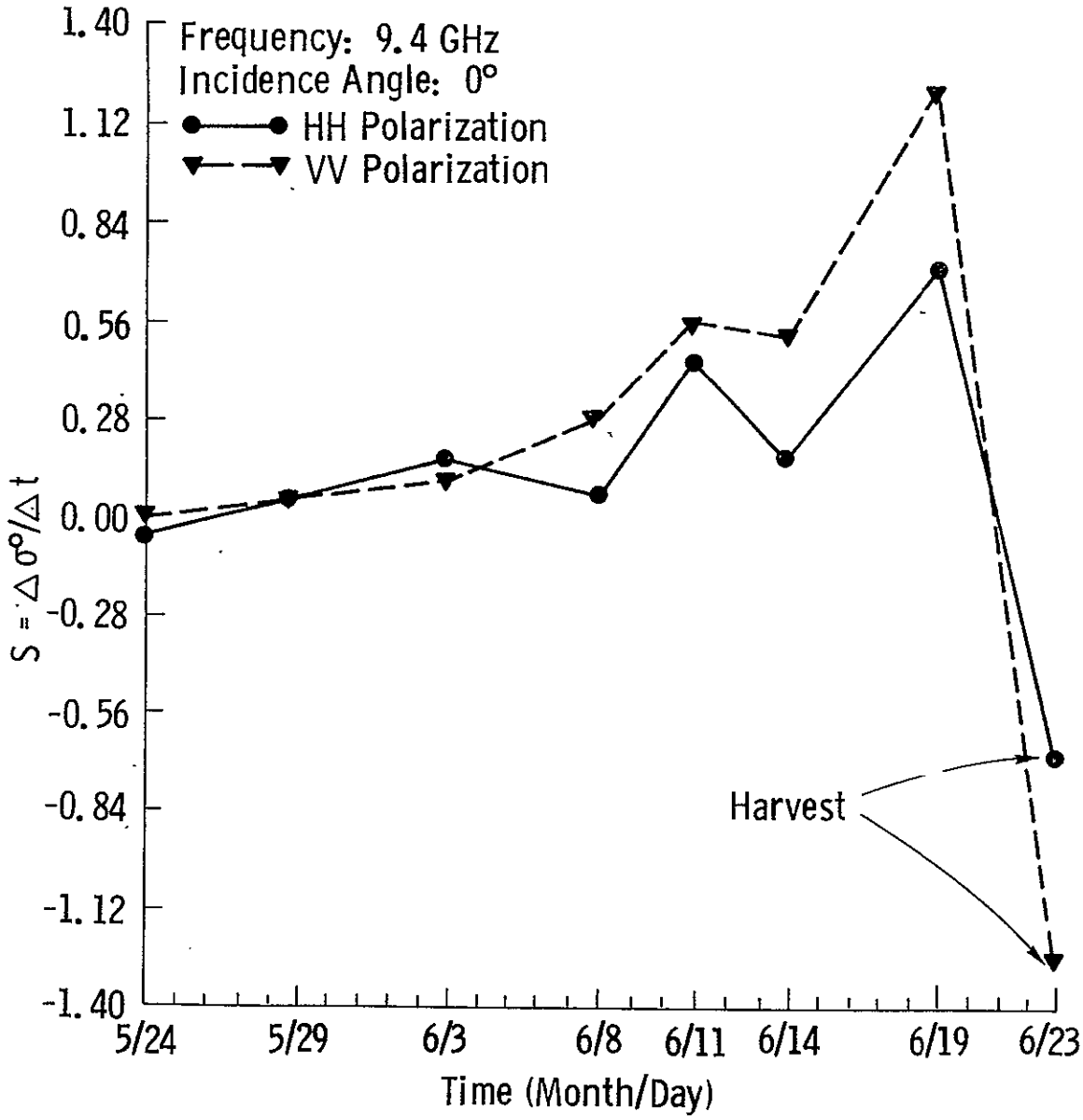

Figure 8a. Variations of S (defined in section 4.2) with time. Frequency = 9.4 GHz, incidence angle = 0°.

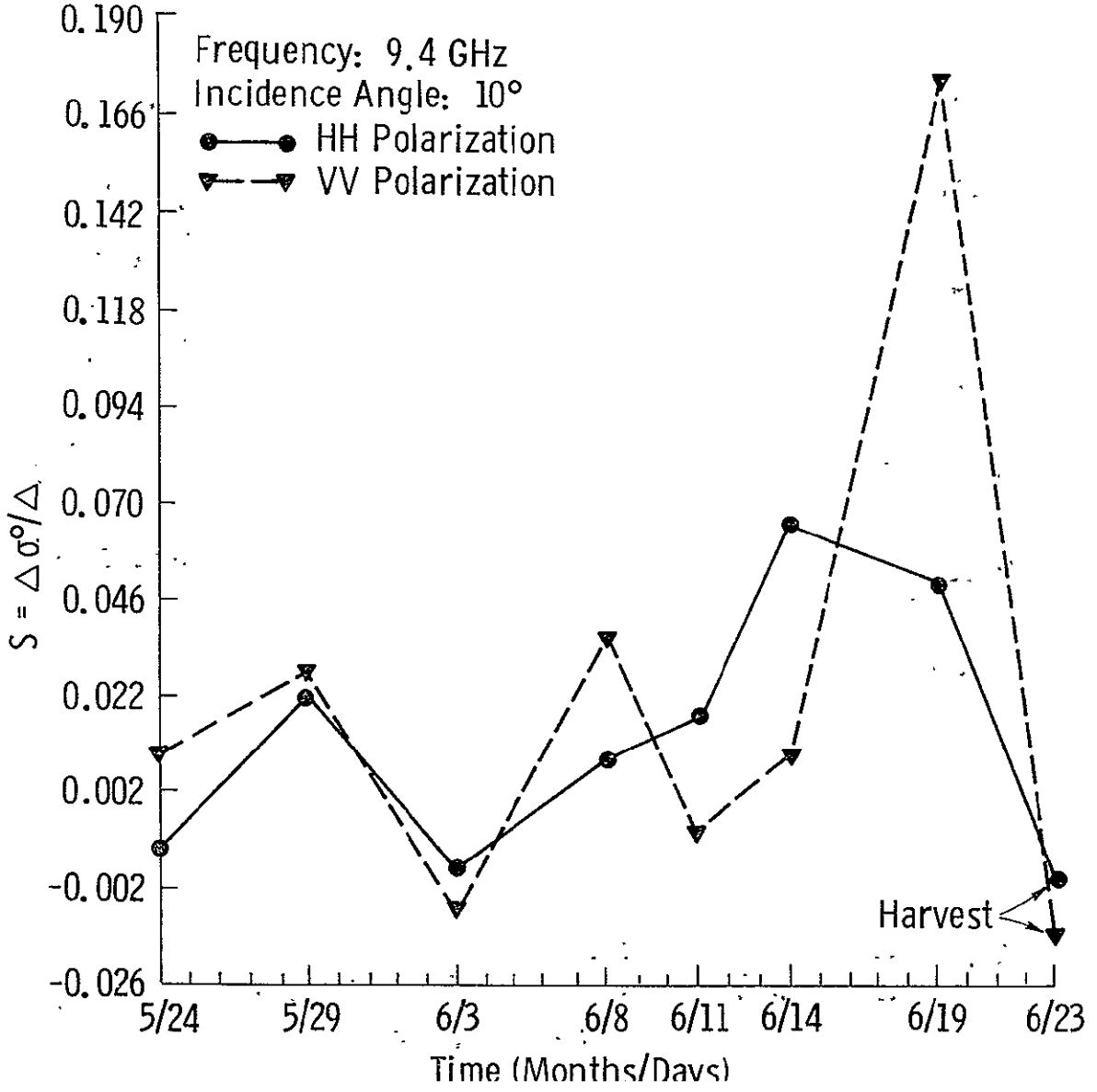

Figure 8b. Variations of S (defined in section 4.2) with time. Frequency = 9.4 GHz, incidence angle = 10°

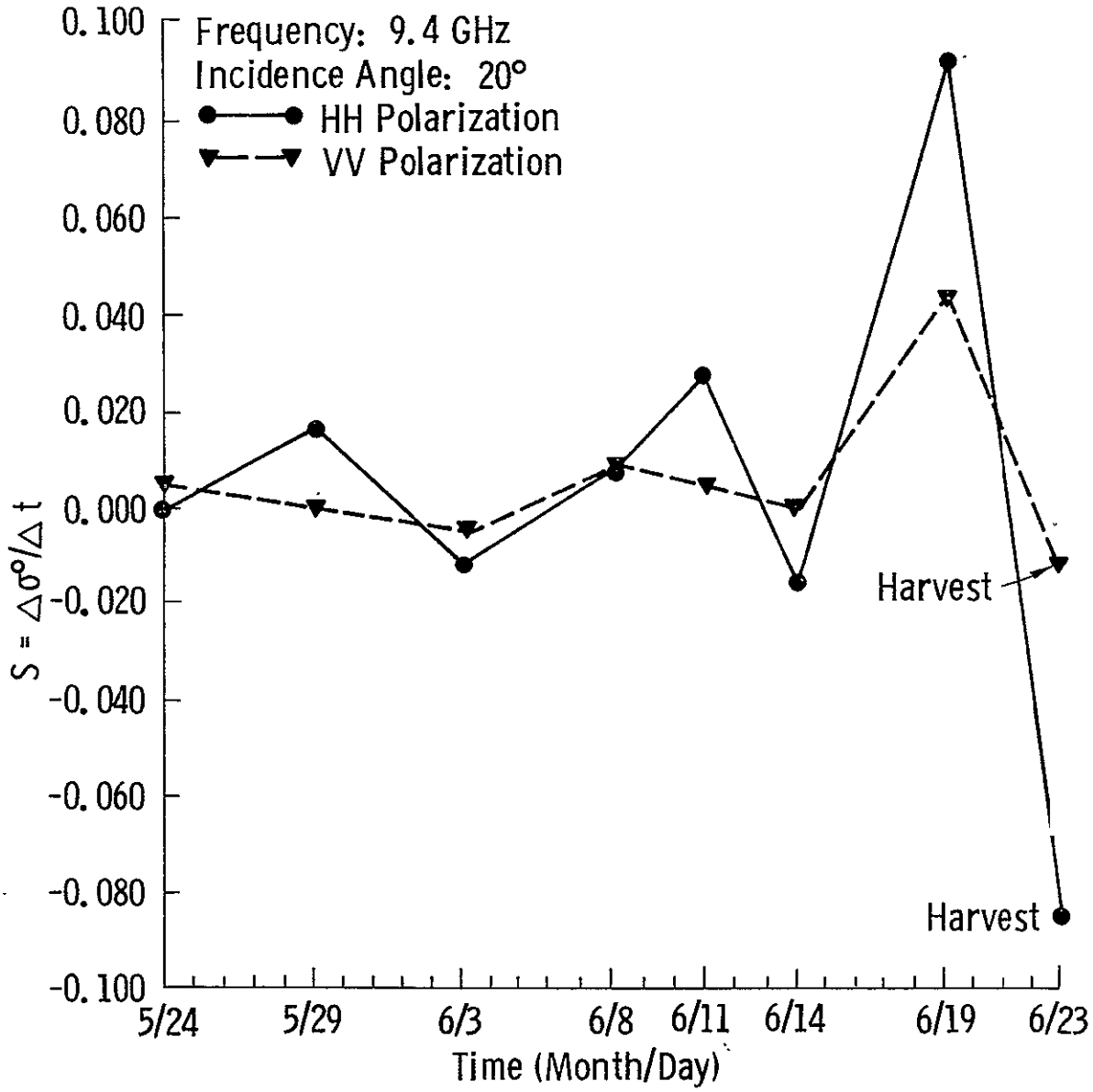

Figure 8c. Variations of S (defined in section 4.2) with time. Frequency = 9.4 GHz, incidence angle = 20°.

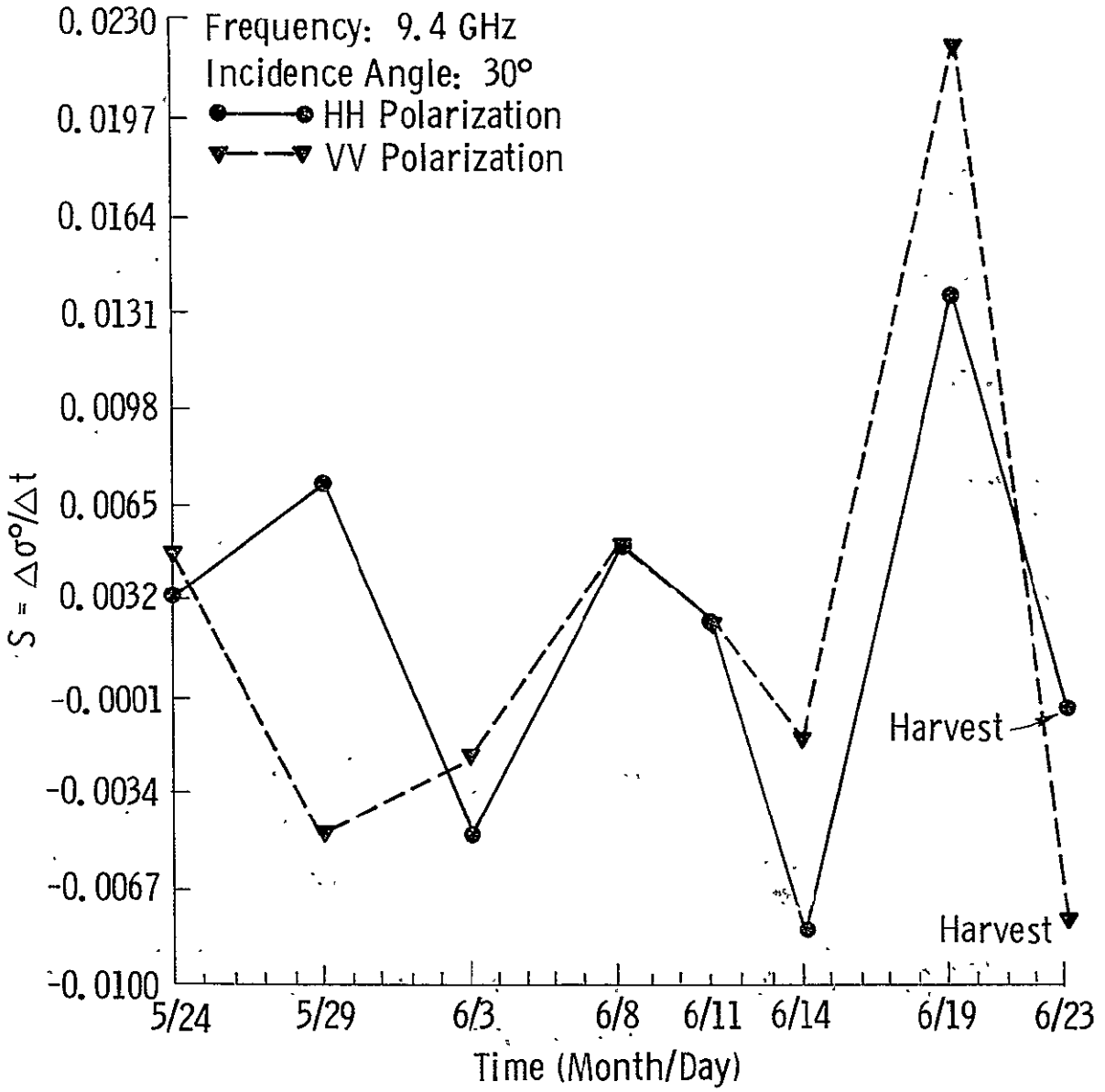

Figure 8d. Variations of S (defined in section 4.2) with time. Frequency = 9.4 GHz, incidence angle = 30°.

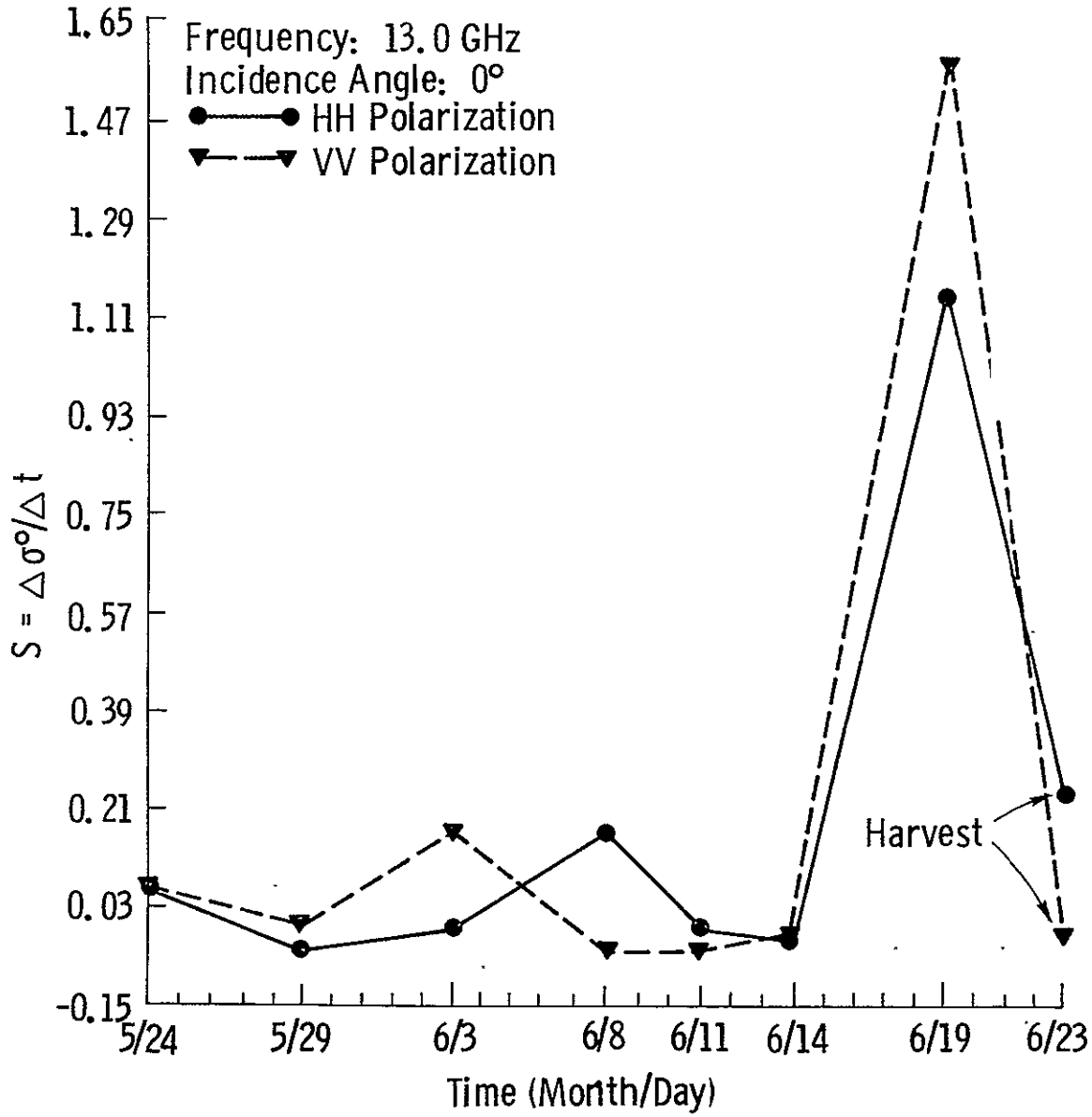

Figure 8e. Variations of S (defined in section 4.2) with time. Frequency = 13.0 GHz, incidence angle = 0°.

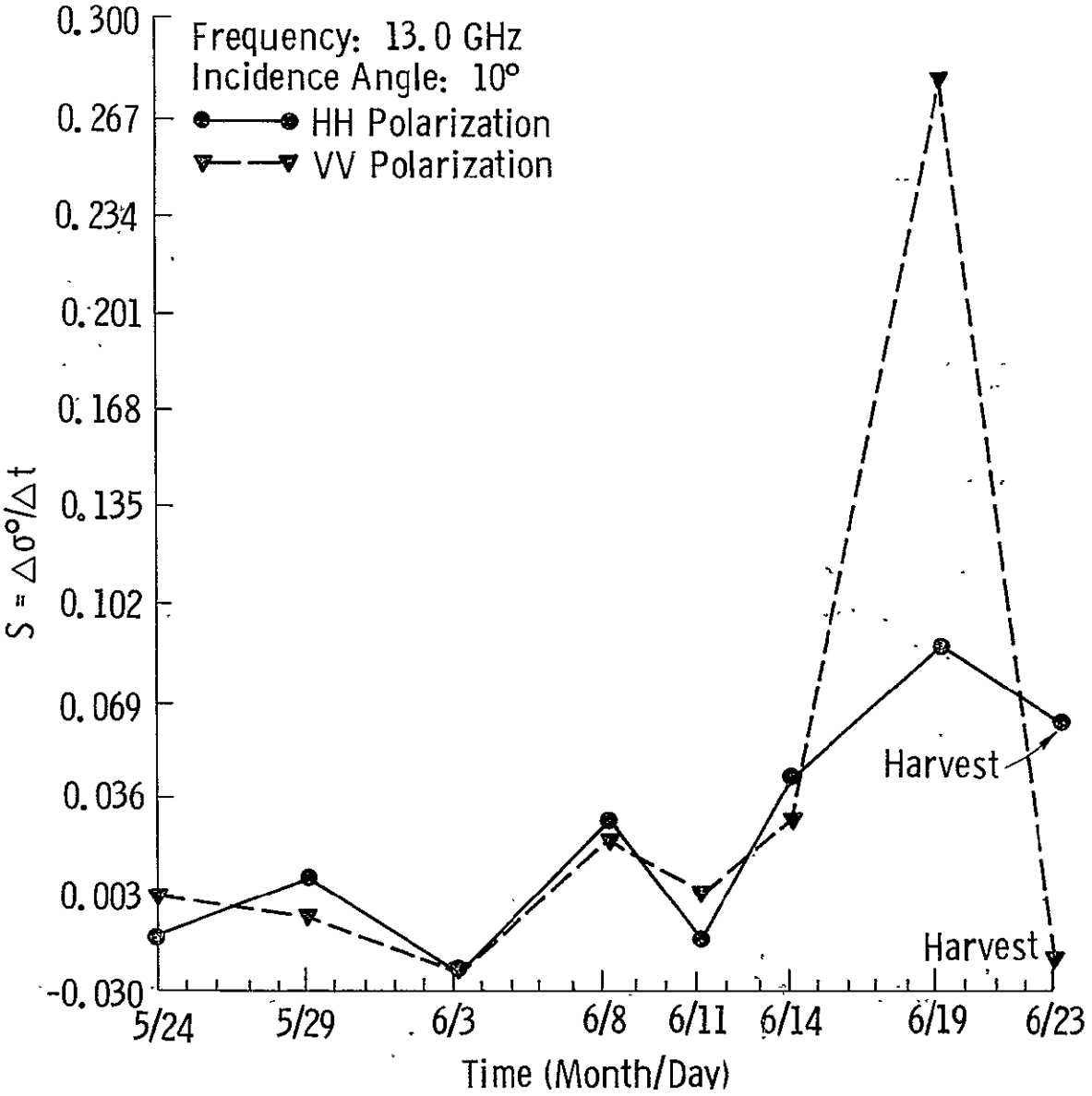

Figure 37. Variations of S (defined in section 4.2) with time. Frequency = 13.0 GHz, incidence angle = 10°.

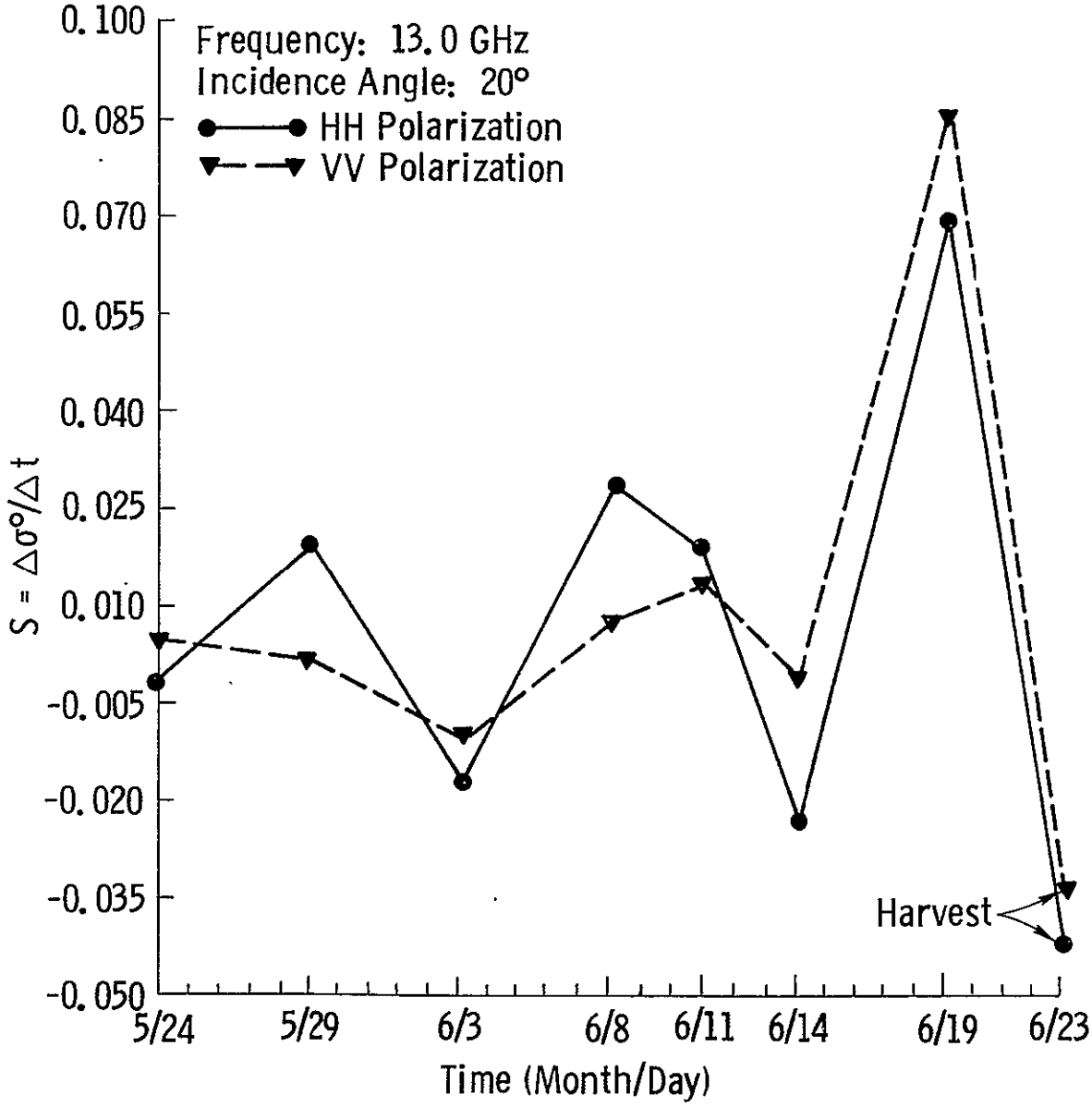

Figure 8g. Variations of S (defined in section 4.2) with time. Frequency = 13.0 GHz, incidence angle = 20°.

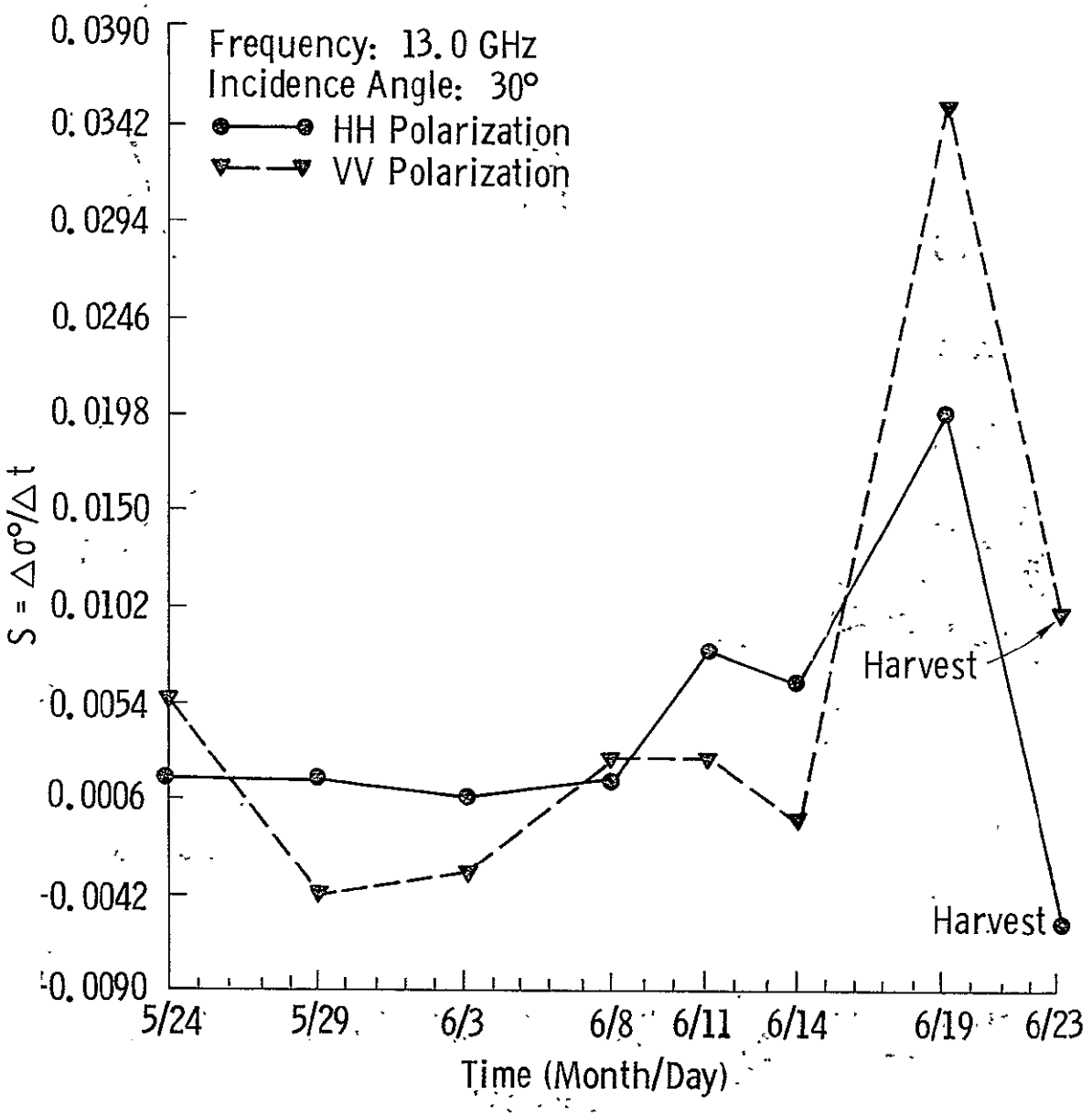

Figure 8h. Variations of S (defined in section 4.2) with time. Frequency = 13.0 GHz, incidence angle = 30°.

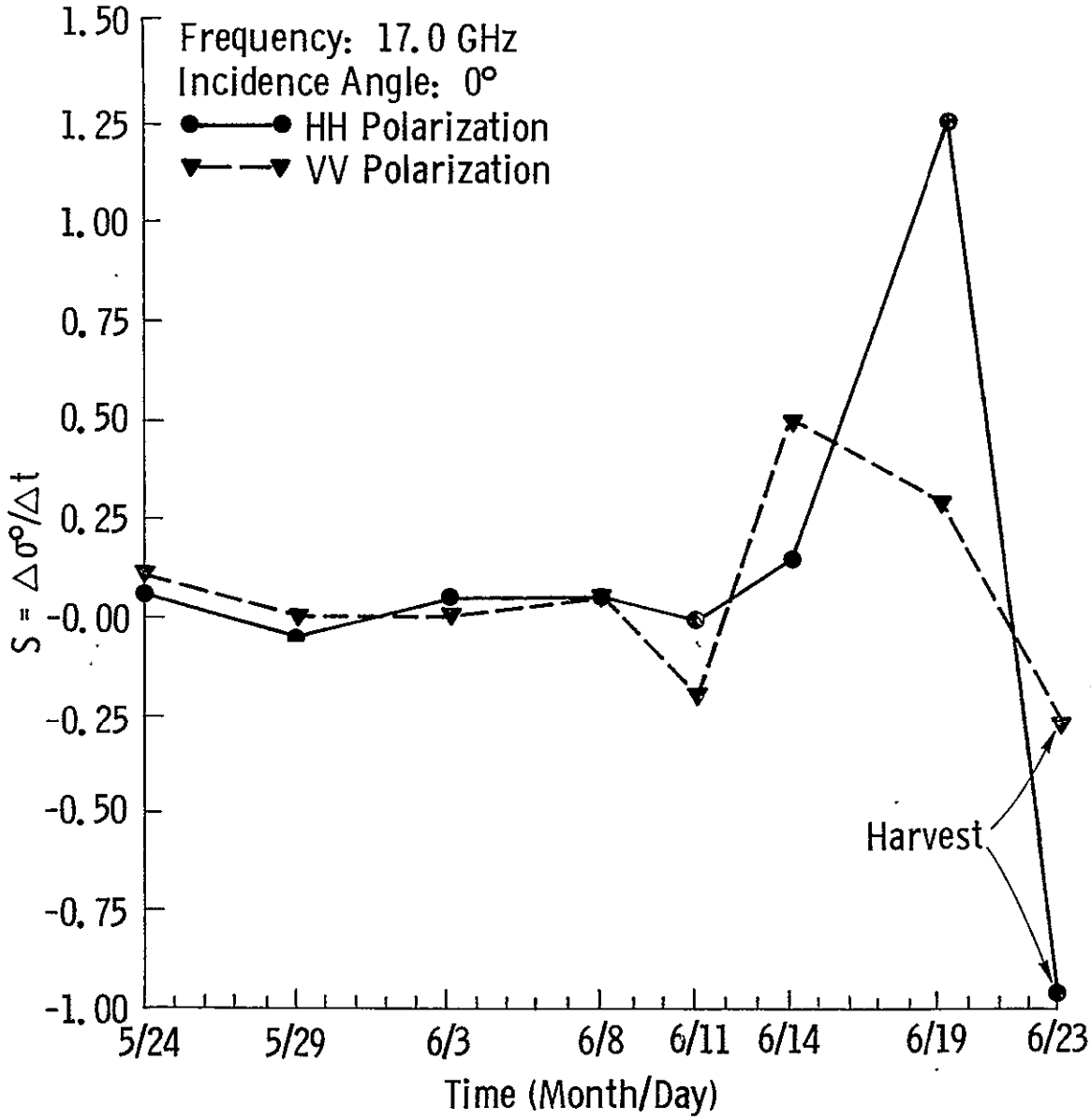

Figure 8i. Variations of S (defined in section 4.2) with time. Frequency = 17.0 GHz, incidence angle = 0°.

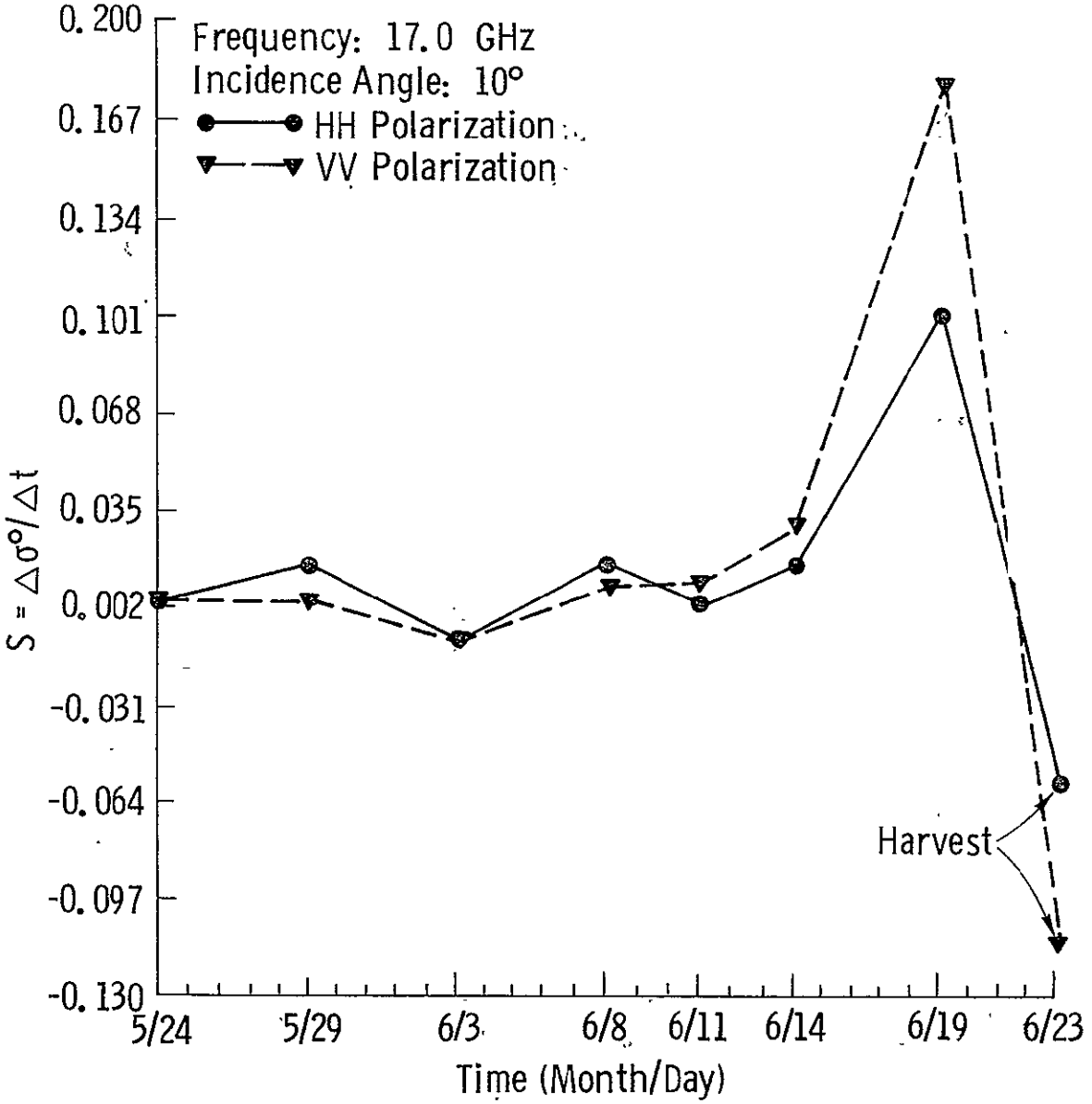

Figure 8j. Variations of S (defined in section 4.2) with time. Frequency = 17.0 GHz, incidence angle = 10°.

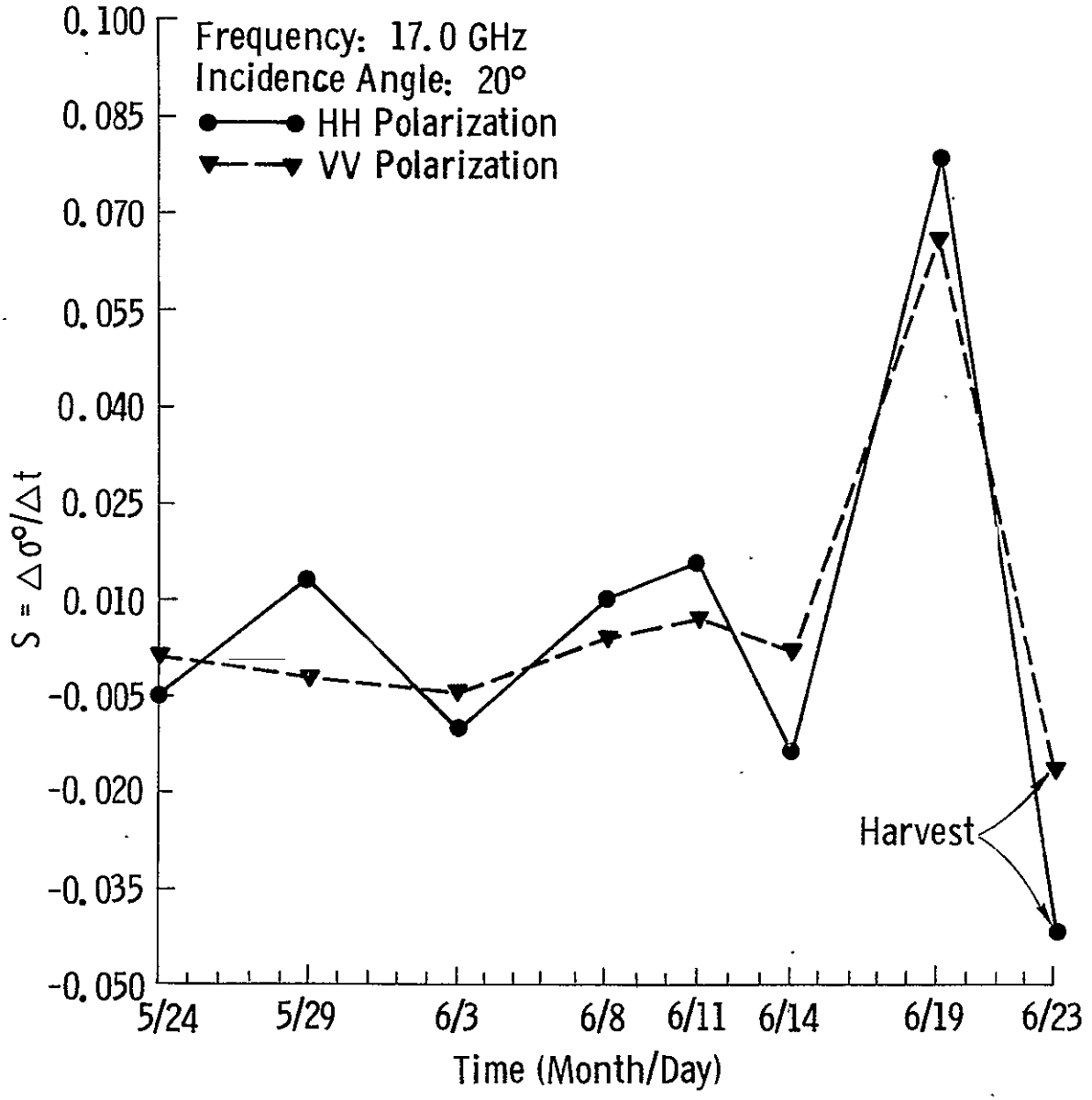

Figure 8k. Variations of S (defined in section 4.2) with time. Frequency = 17.0 GHz, incidence angle = 20°.

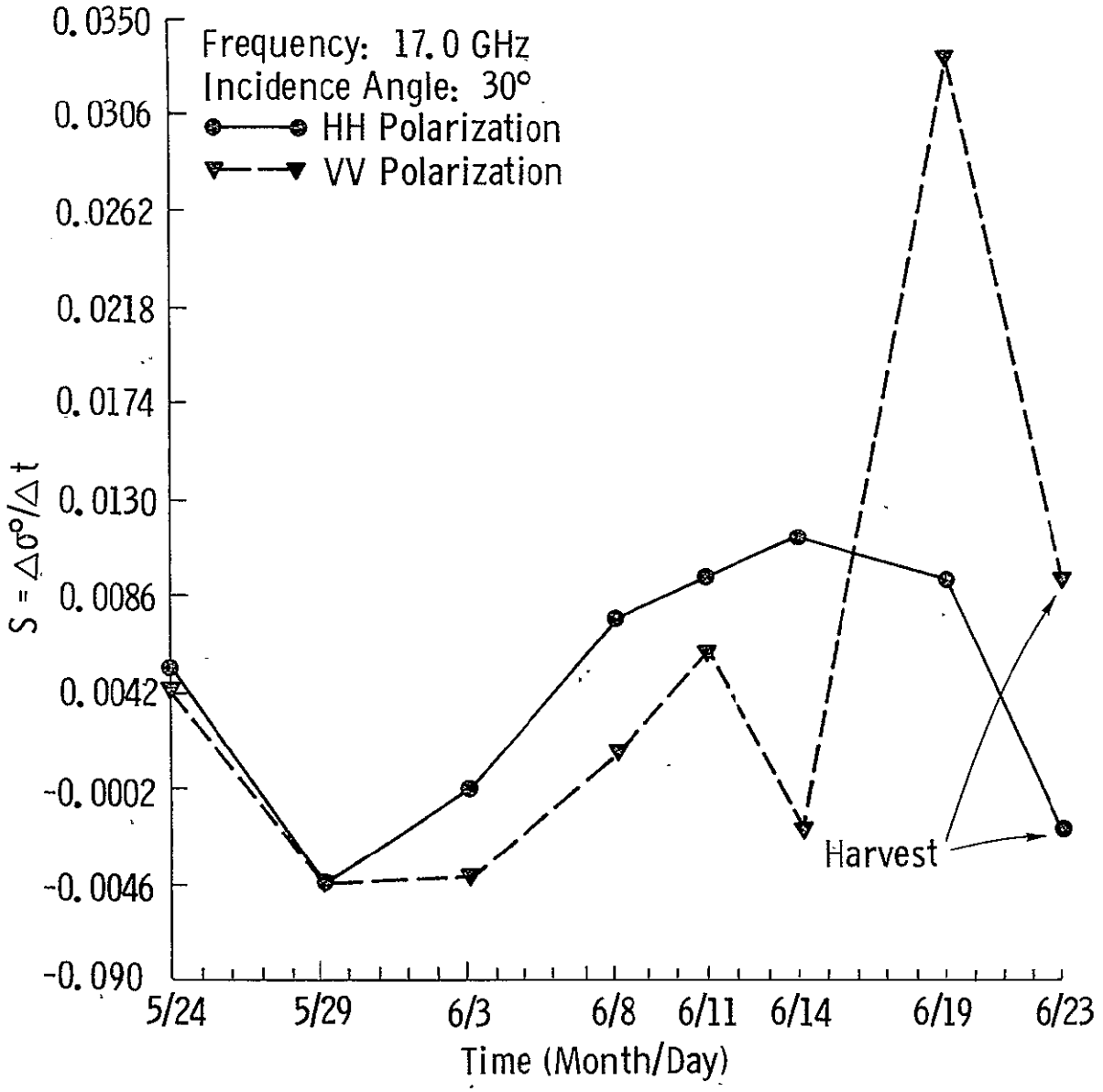

Figure 81. Variations of S (defined in section 4.2) with time. Frequency = 17.0 GHz, incidence angle = 30°.

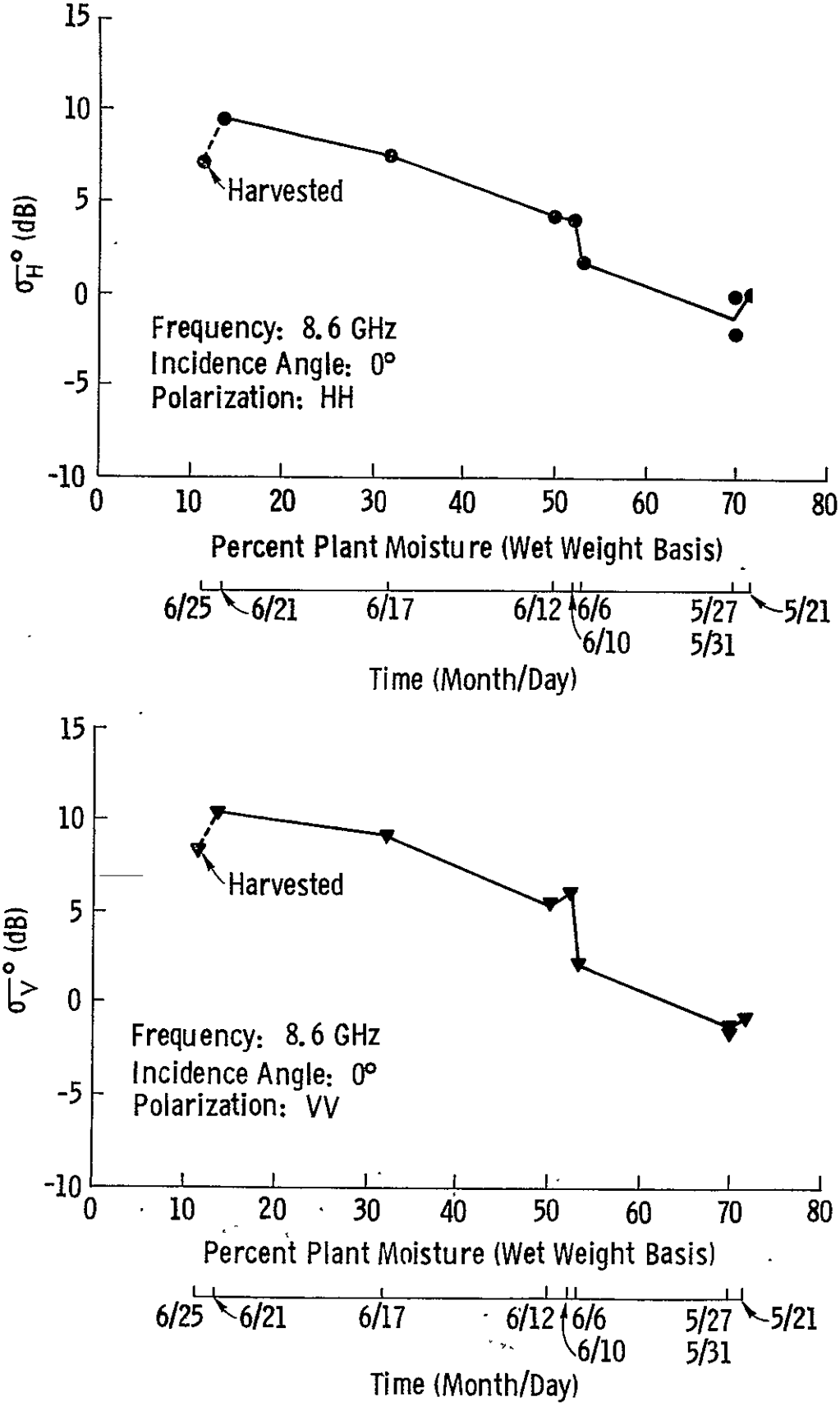

Figure 9a. Variations of σ_H° (dB) and σ_V° (dB) with plant moisture. Frequency = 8.6 GHz, incidence angle = 0°.

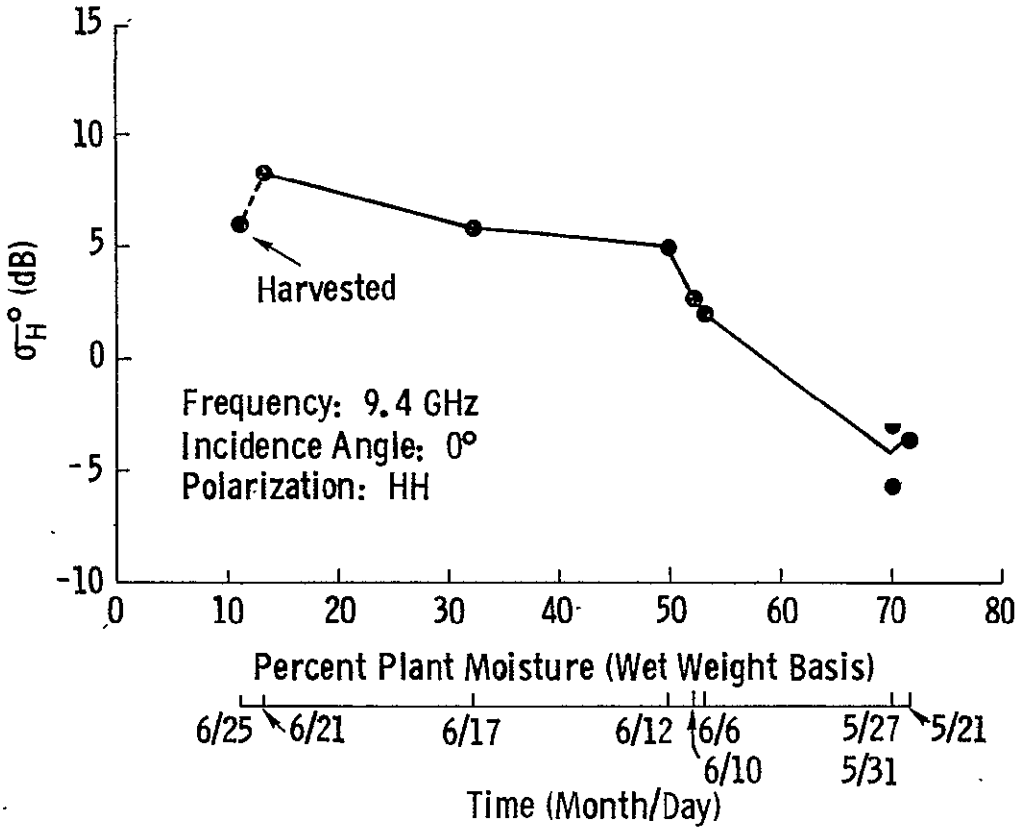

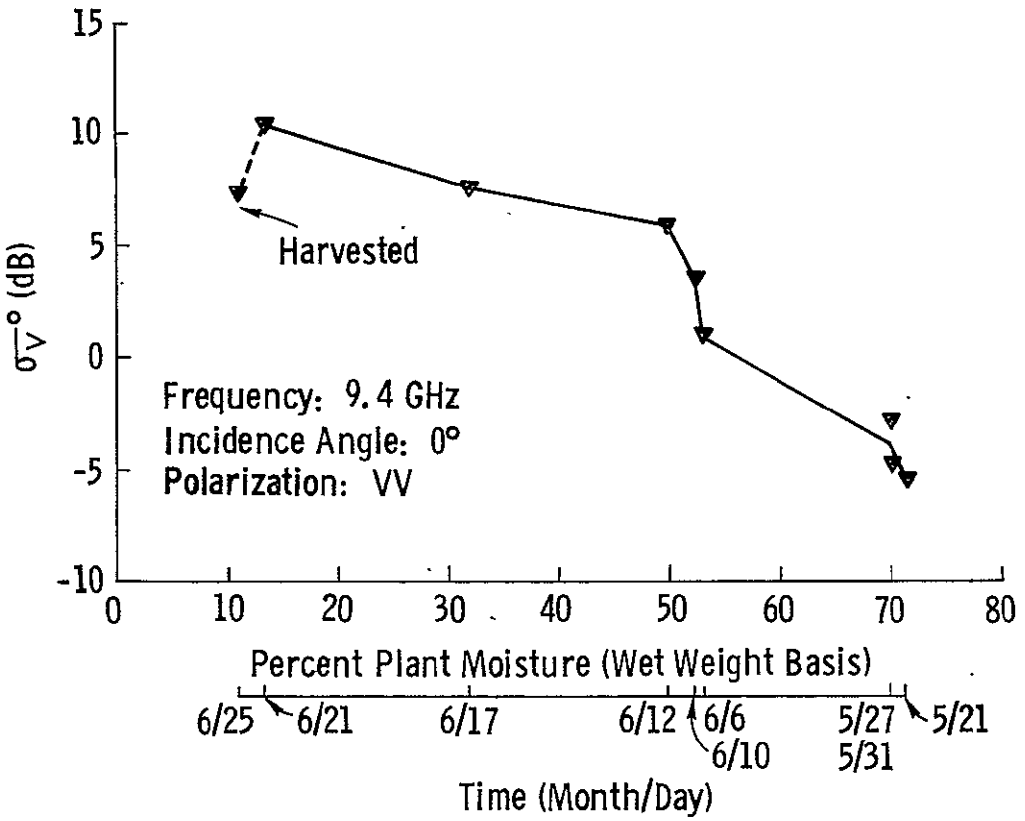

Figure 9b. Variations of σ_H° (dB) and σ_V° (dB) with plant moisture. Frequency = 9.4 GHz, incidence angle = 0°.

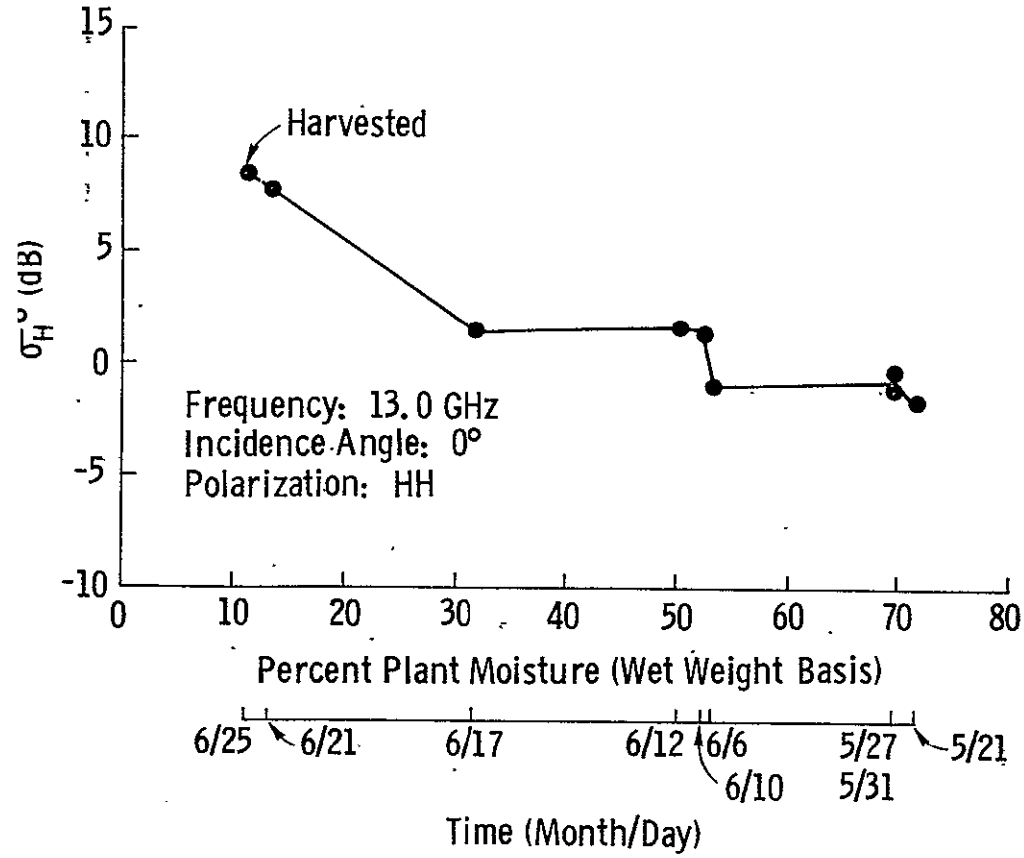

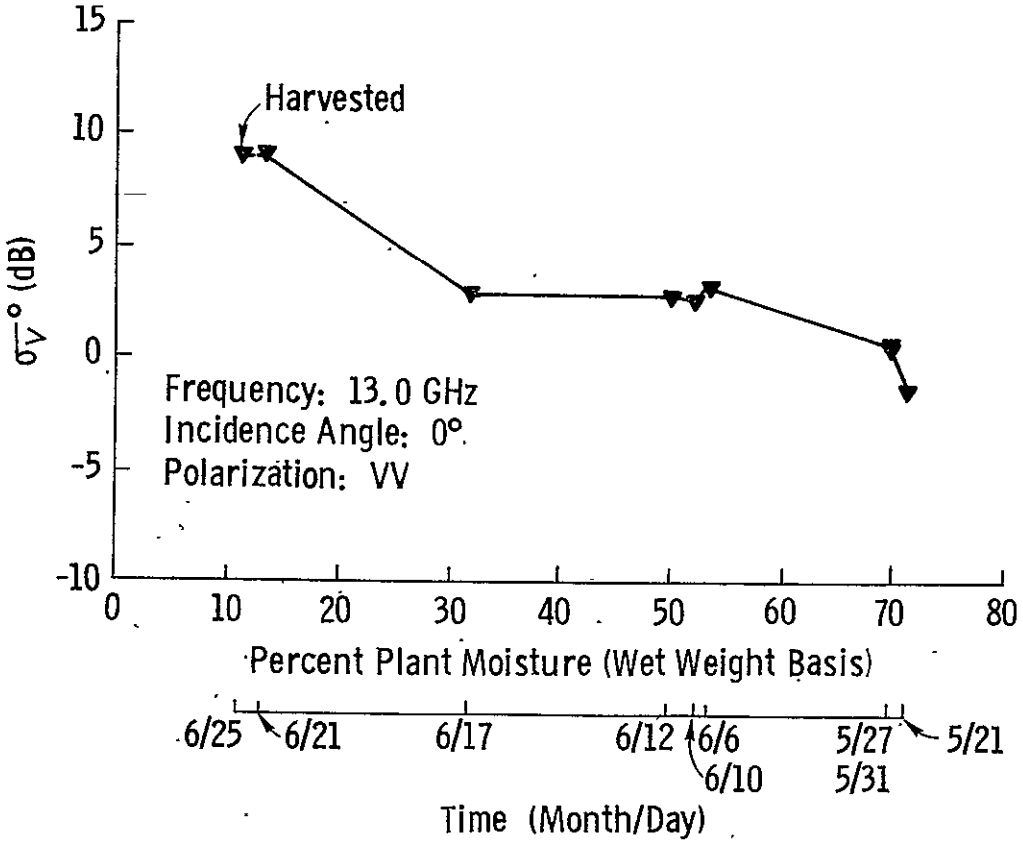

Figure 9c. Variations of σ_H° (dB) and σ_V° (dB) with plant moisture. Frequency = 13.0 GHz, incidence angle = 0°.

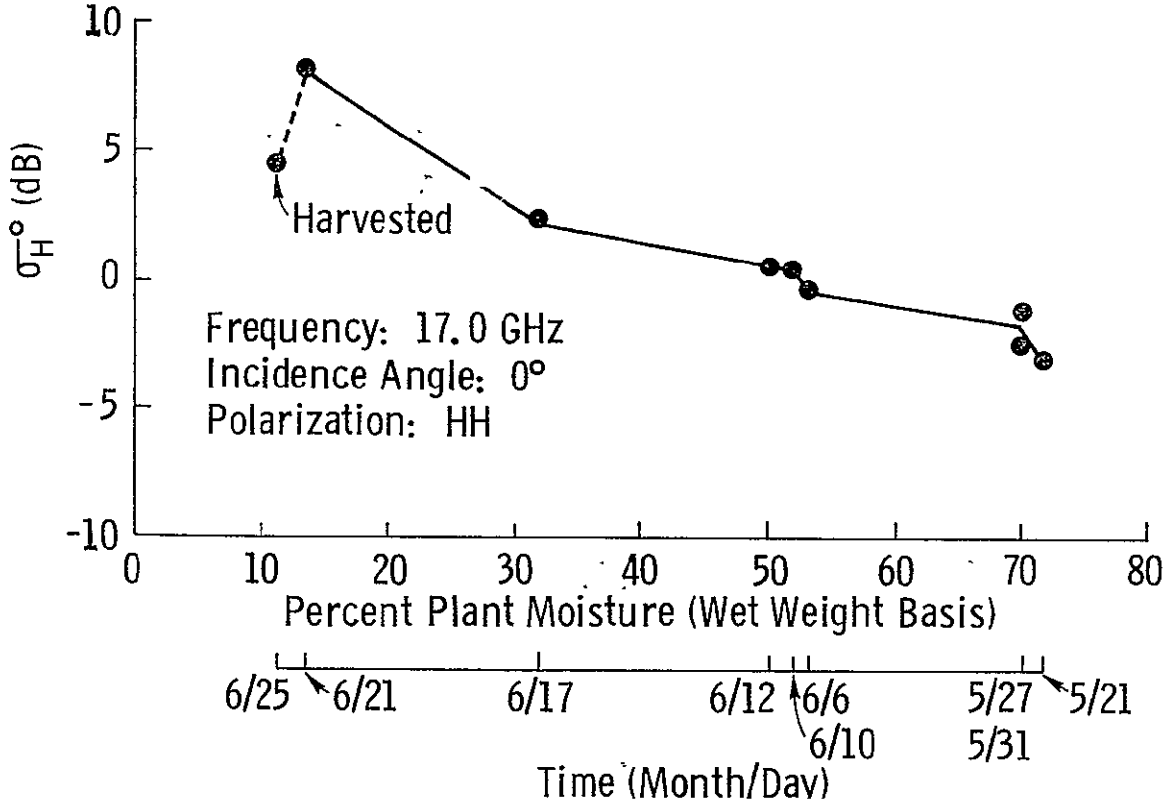

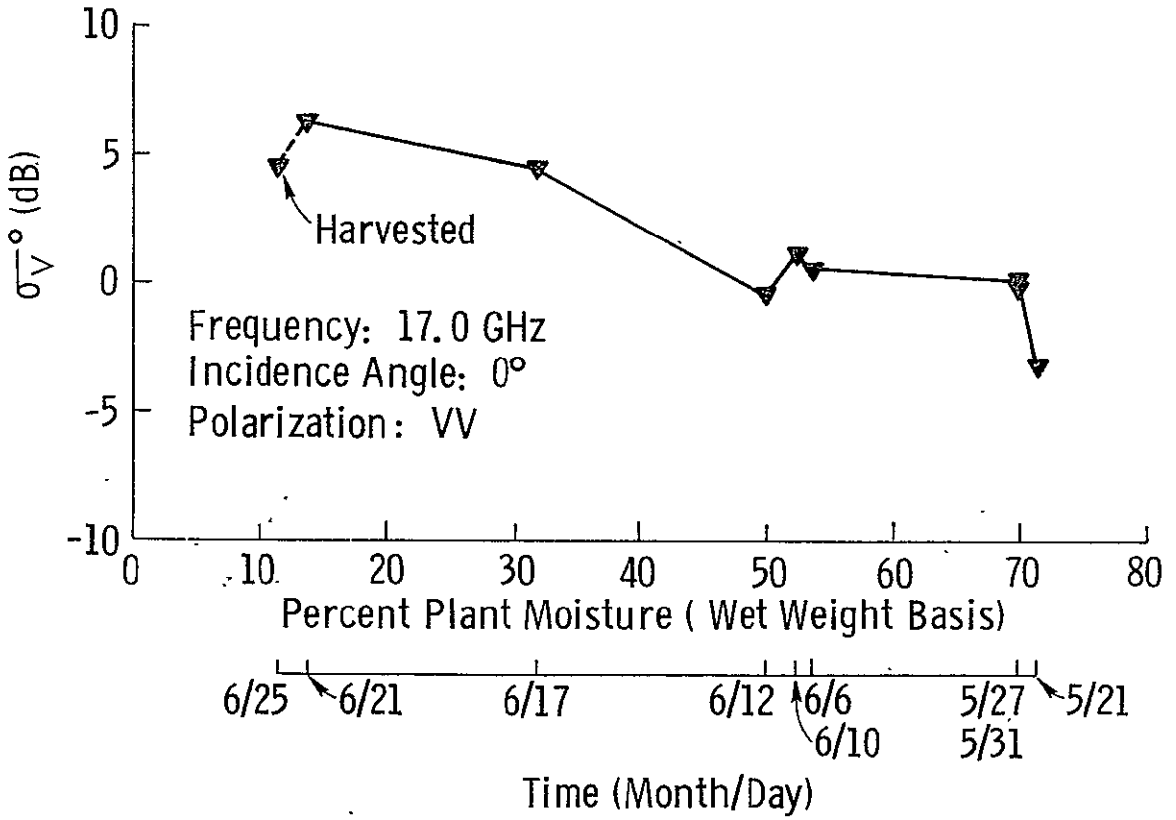

Figure 9d. Variations of σ_H° (dB) and σ_V° (dB) with plant moisture. Frequency = 17.0 GHz, incidence angle = 0°.

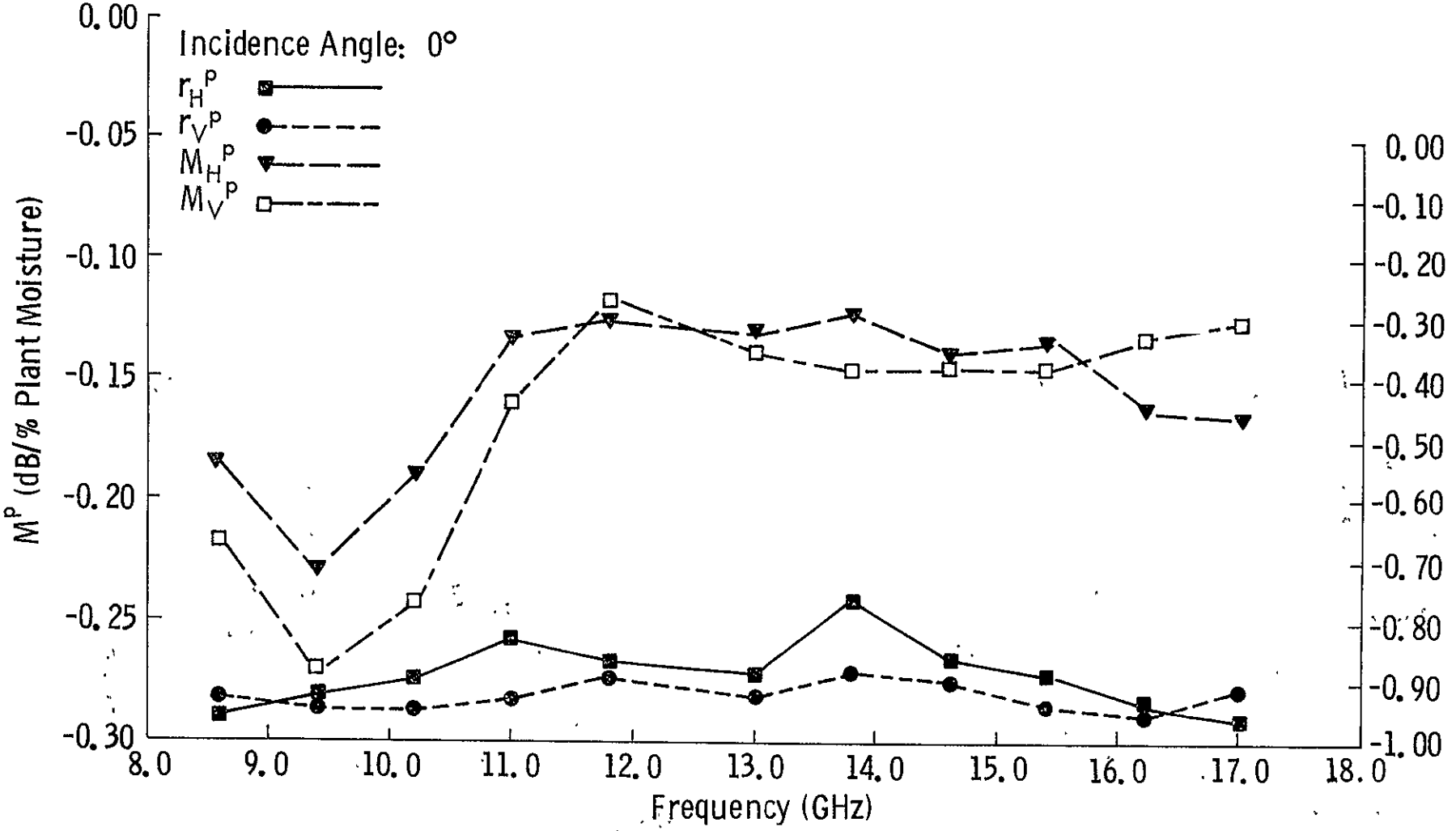

Figure 9e. Variations of M_H^p, M_V^p, r_H^p, and r_V^p with frequency. M_H^p, M_V^p, r_H^p, and r_V^p are the slopes (dB/percent plant moisture) and estimated correlation coefficients respectively, obtained by a linear regression of σ^o(dB) on plant moisture. The incidence angle is 0°.

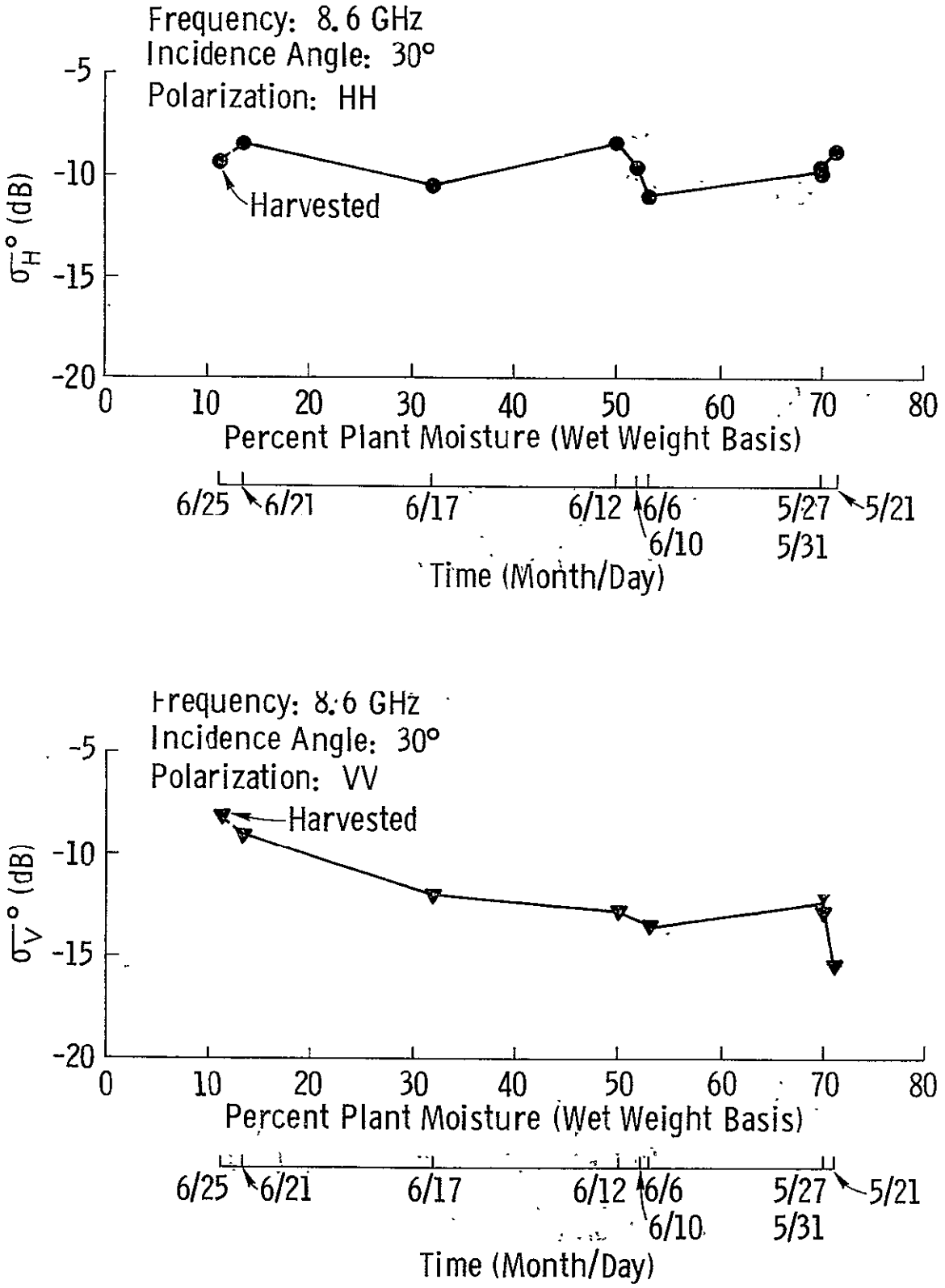

Figure 10a. Variations of σ_H° (dB) and σ_V° (dB) with plant moisture. Frequency = 8.6 GHz, Incidence angle = 30°.

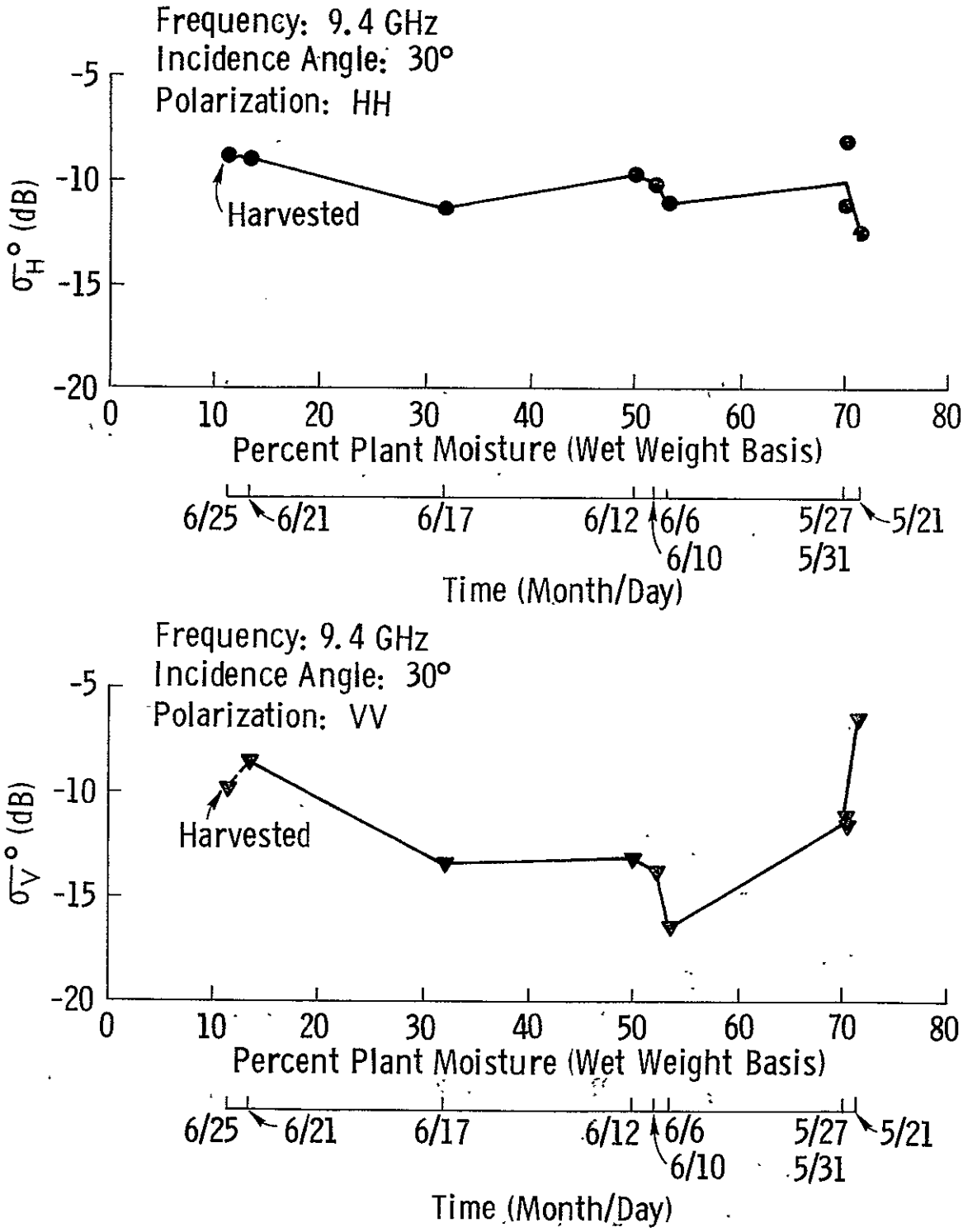

Figure 10b. Variations of σ°_H (dB) and σ°_V (dB) with plant moisture. Frequency = 9.4 GHz, incidence angle = 30°.

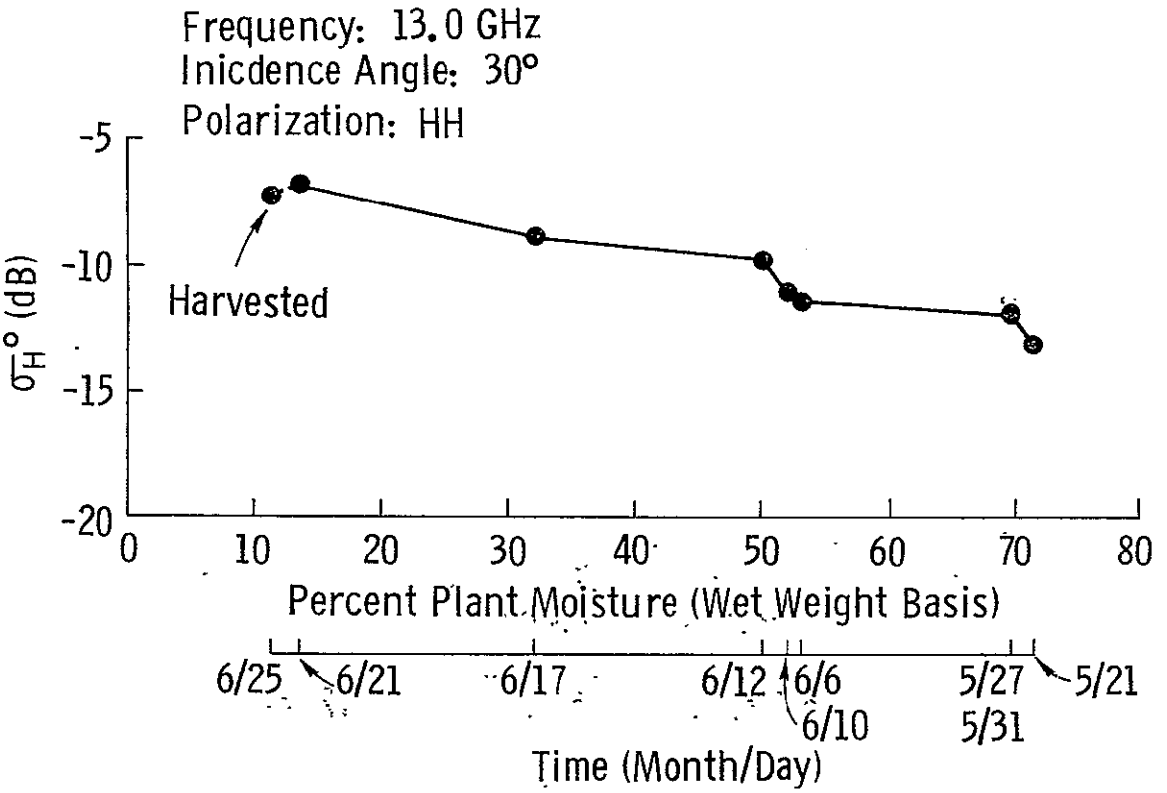

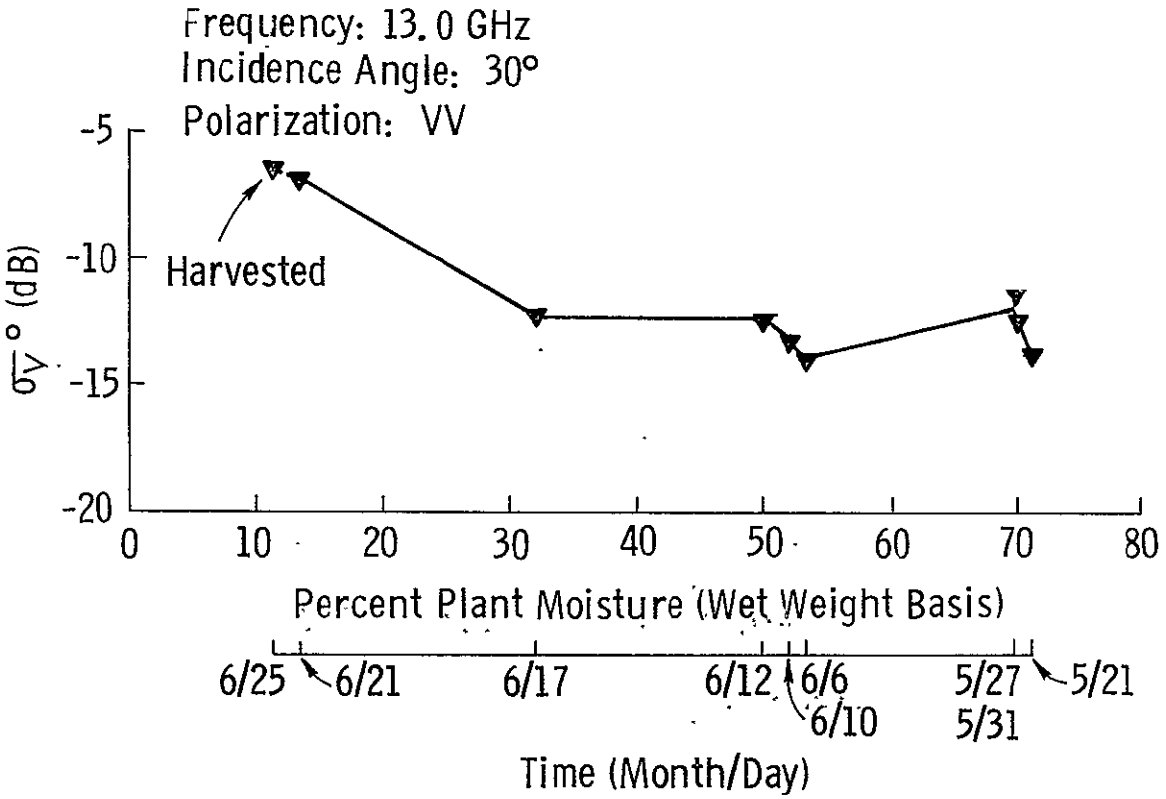

Figure 10c. Variations of σ_H° (dB) and σ_V° (dB) with plant moisture. Frequency = 13.0 GHz, incidence angle = 30°.

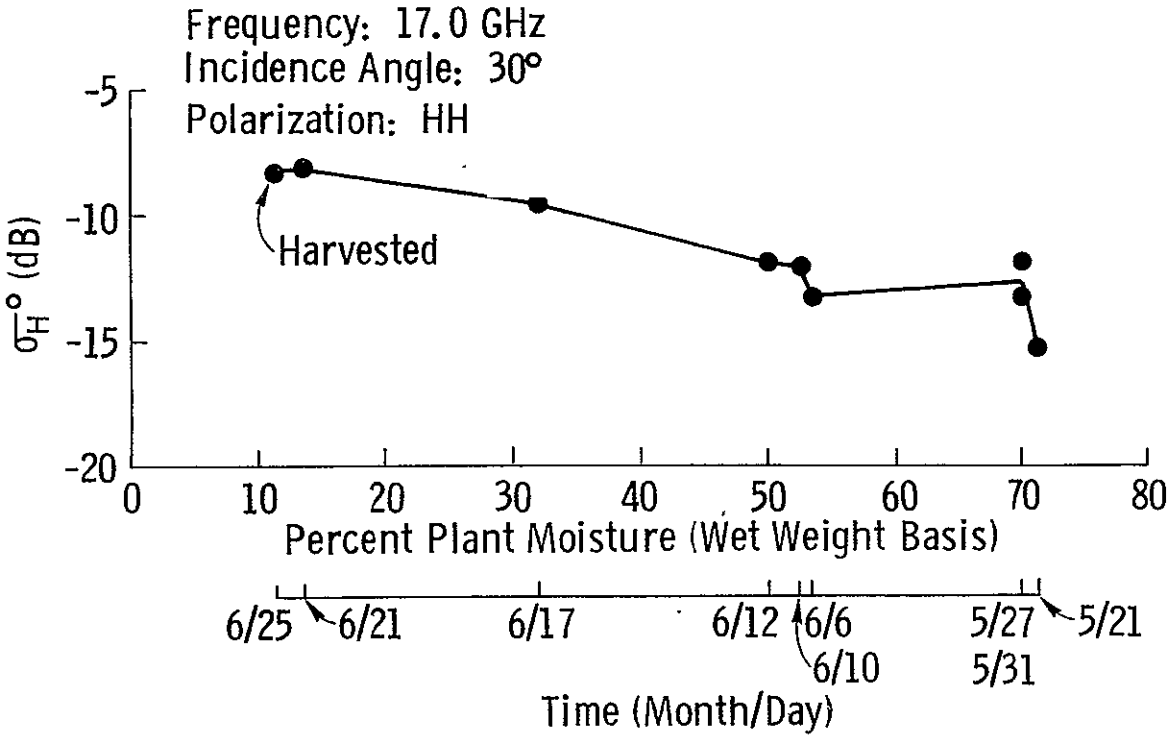

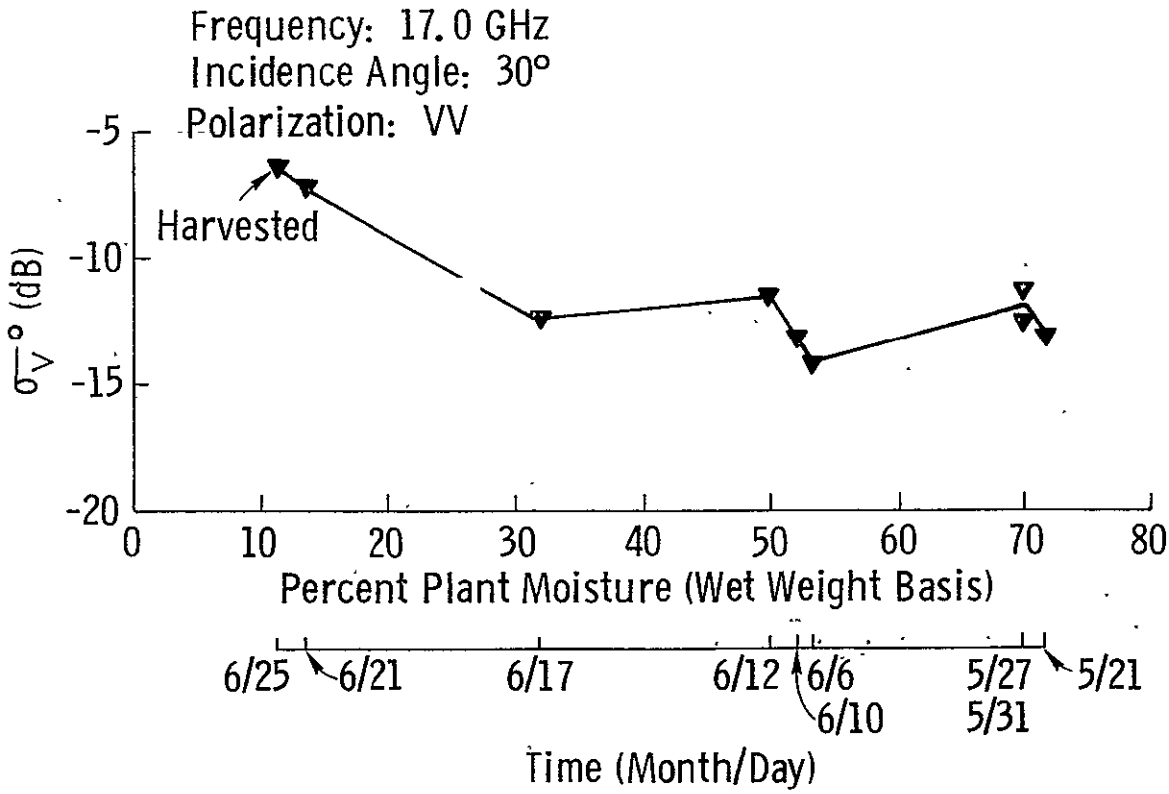

Figure 10d. Variations of σ_H° (dB) and σ_V° (dB) with plant moisture. Frequency = 17.0 GHz, incidence angle = 30°.

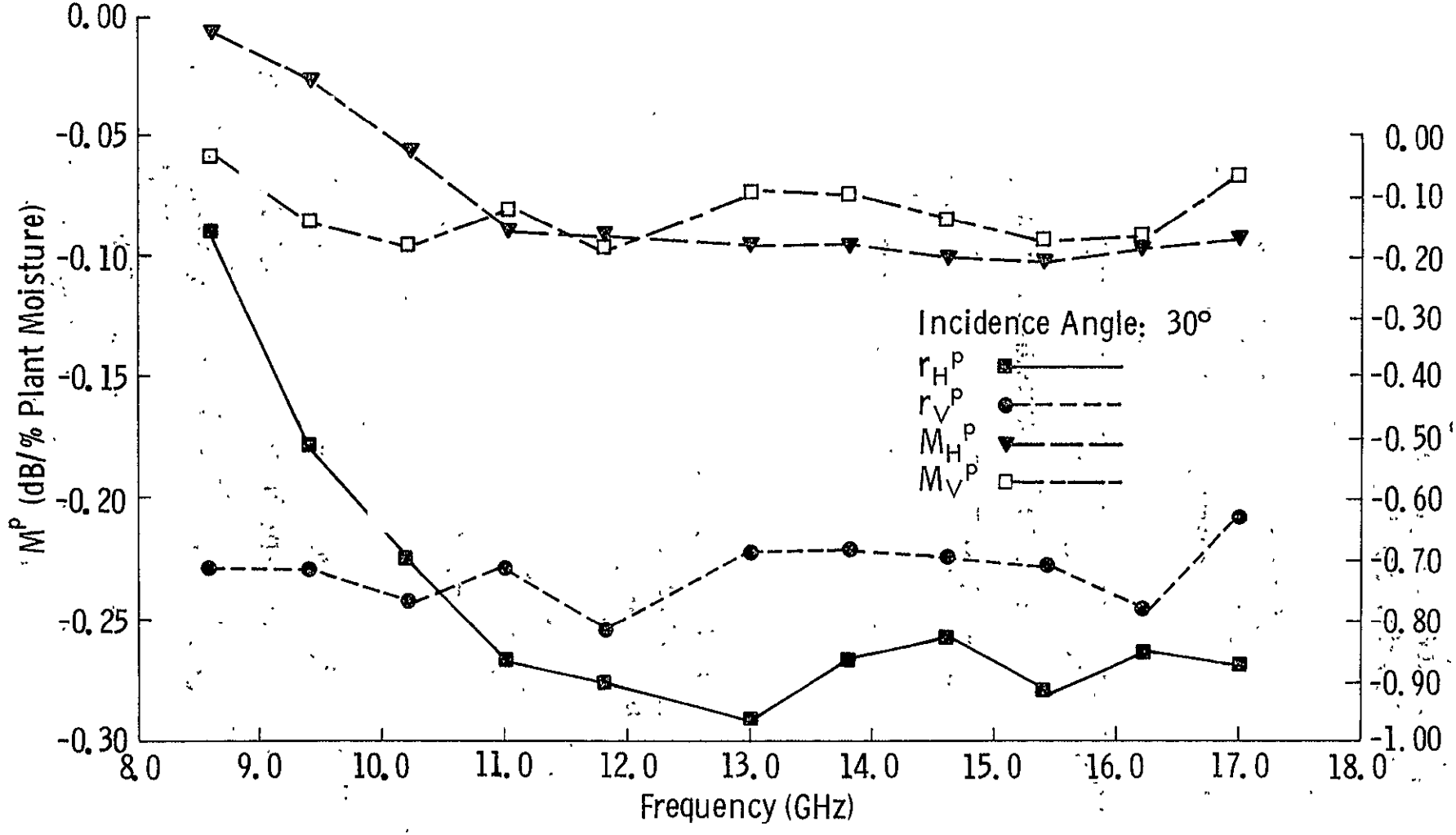

Figure 10e. Variations of M_H^P, M_V^P, r_H^P, and r_V^P with frequency. M_H^P, M_V^P, r_H^P, and r_V^P are the slopes (dB/percent plant moisture) and estimated correlation coefficients respectively, obtained by a linear regression of σ^o(dB) on plant moisture. The incidence angle is 30°.

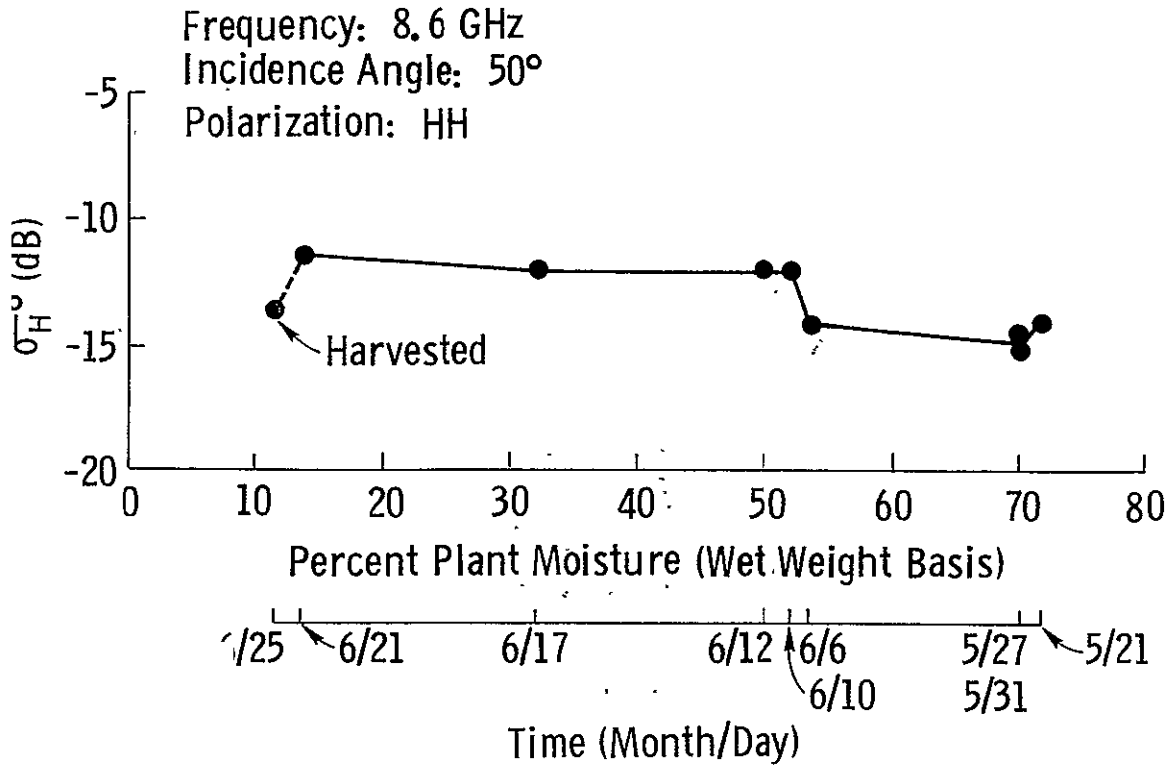

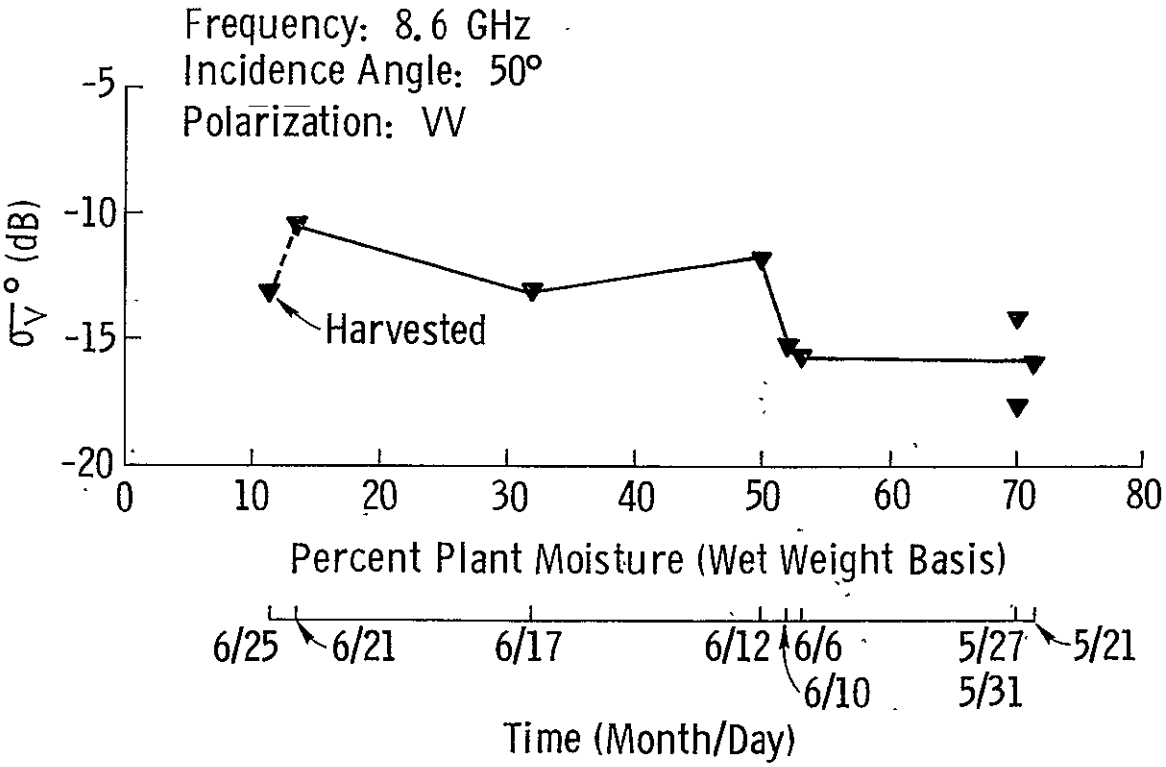

Figure 11a. Variations of $\bar{\sigma}^{\circ}_{H}$ (dB) and $\bar{\sigma}^{\circ}_{V}$ (dB) with plant moisture. Frequency = 8.6 GHz, incidence angle = 50°.

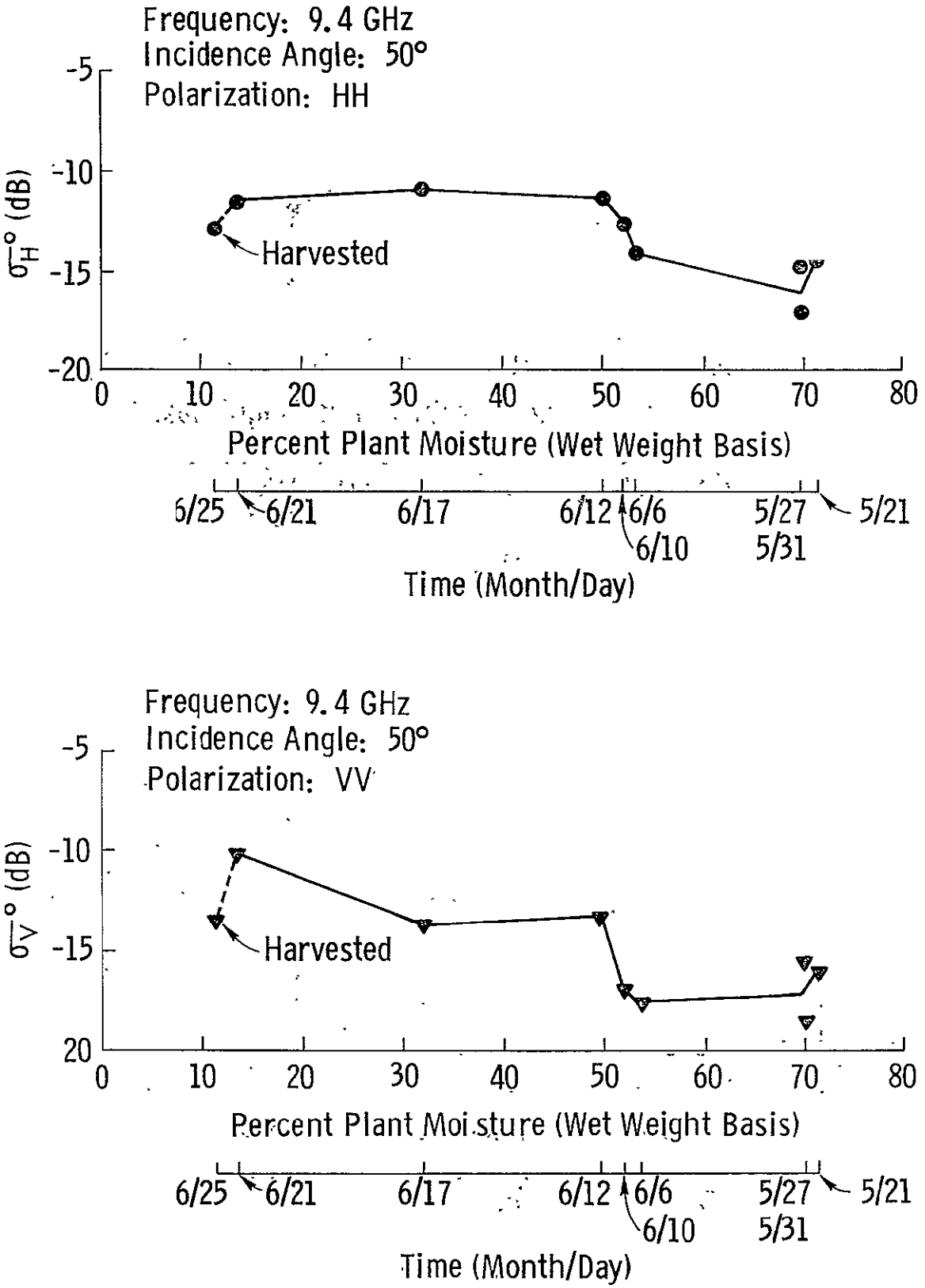

Figure 11b. Variations of σ_H° (dB) and σ_V° (dB) with plant moisture. Frequency = 9.4 GHz, incidence angle = 50°.

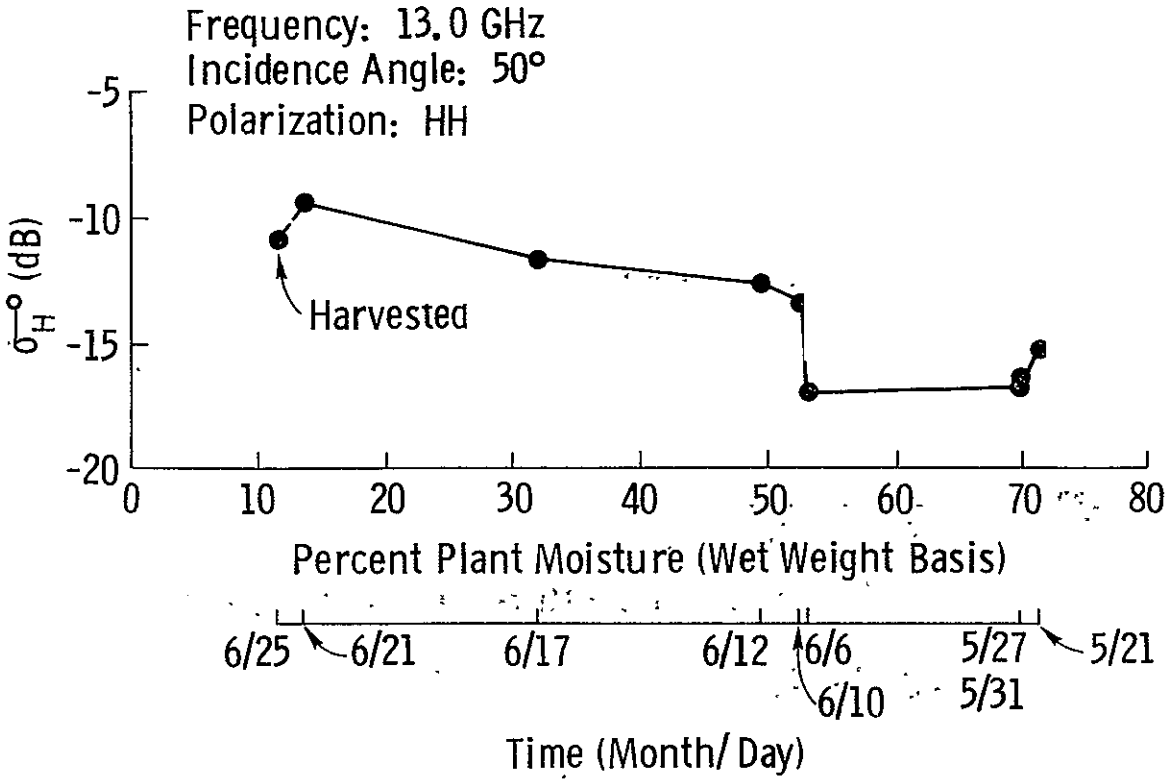

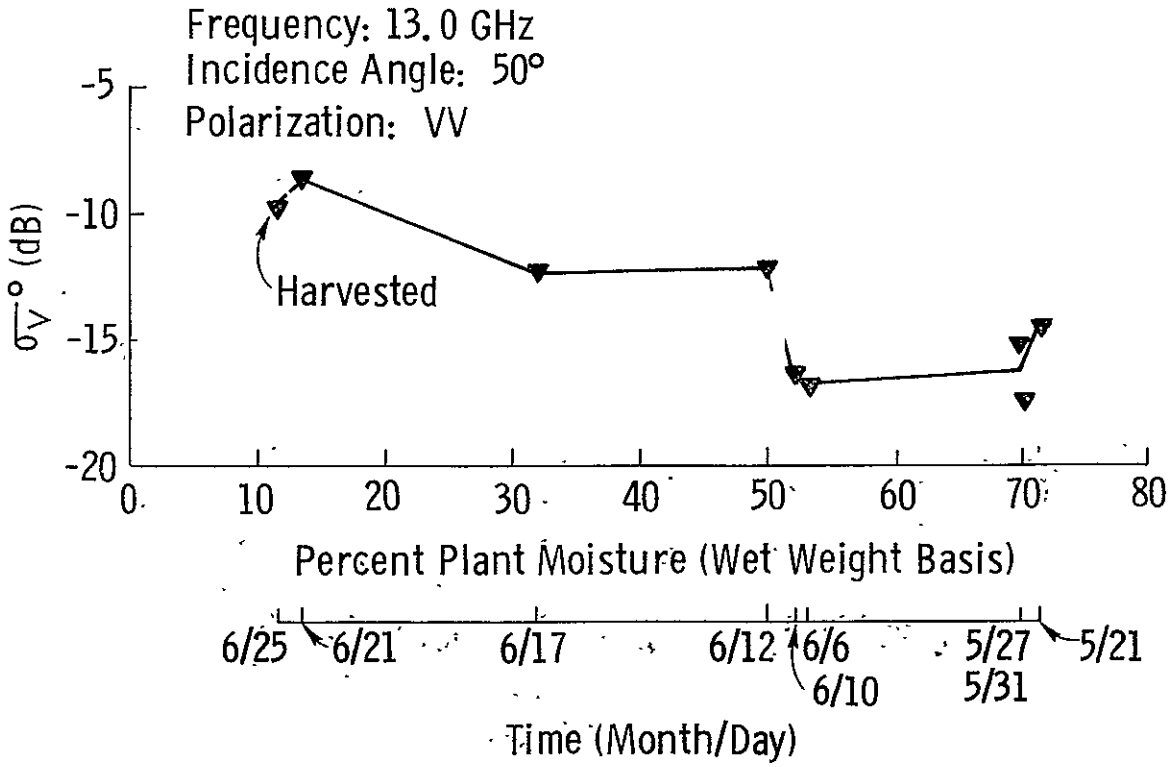

Figure 11c. Variations of σ°_H (dB) and σ°_V (dB) with plant moisture. Frequency = 13.0 GHz, incidence angle = 50°.

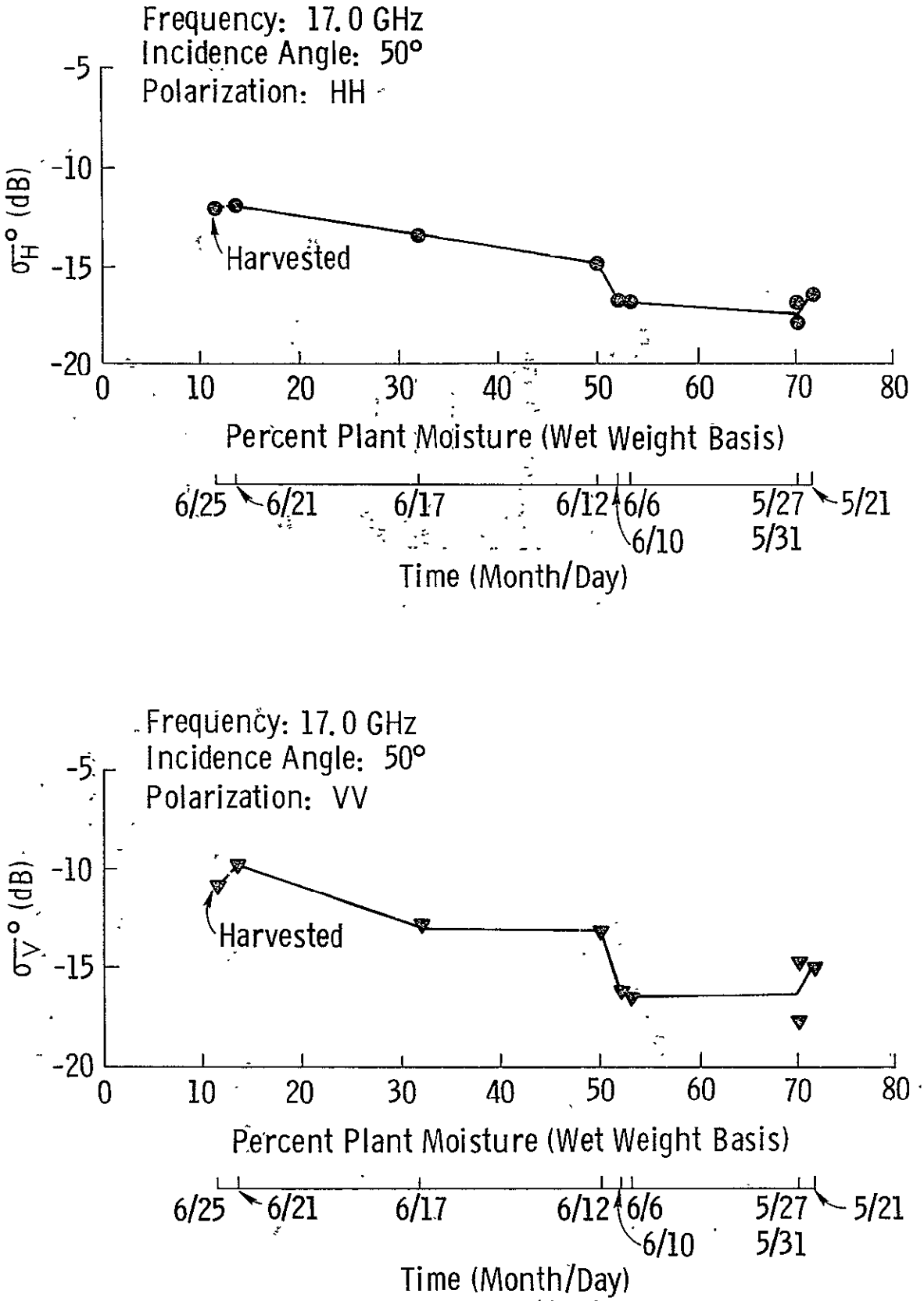

Figure 11d. Variations of σ_H° (dB) and σ_V° (dB) with plant moisture. Frequency = 17.0 GHz, incidence angle = 50°.

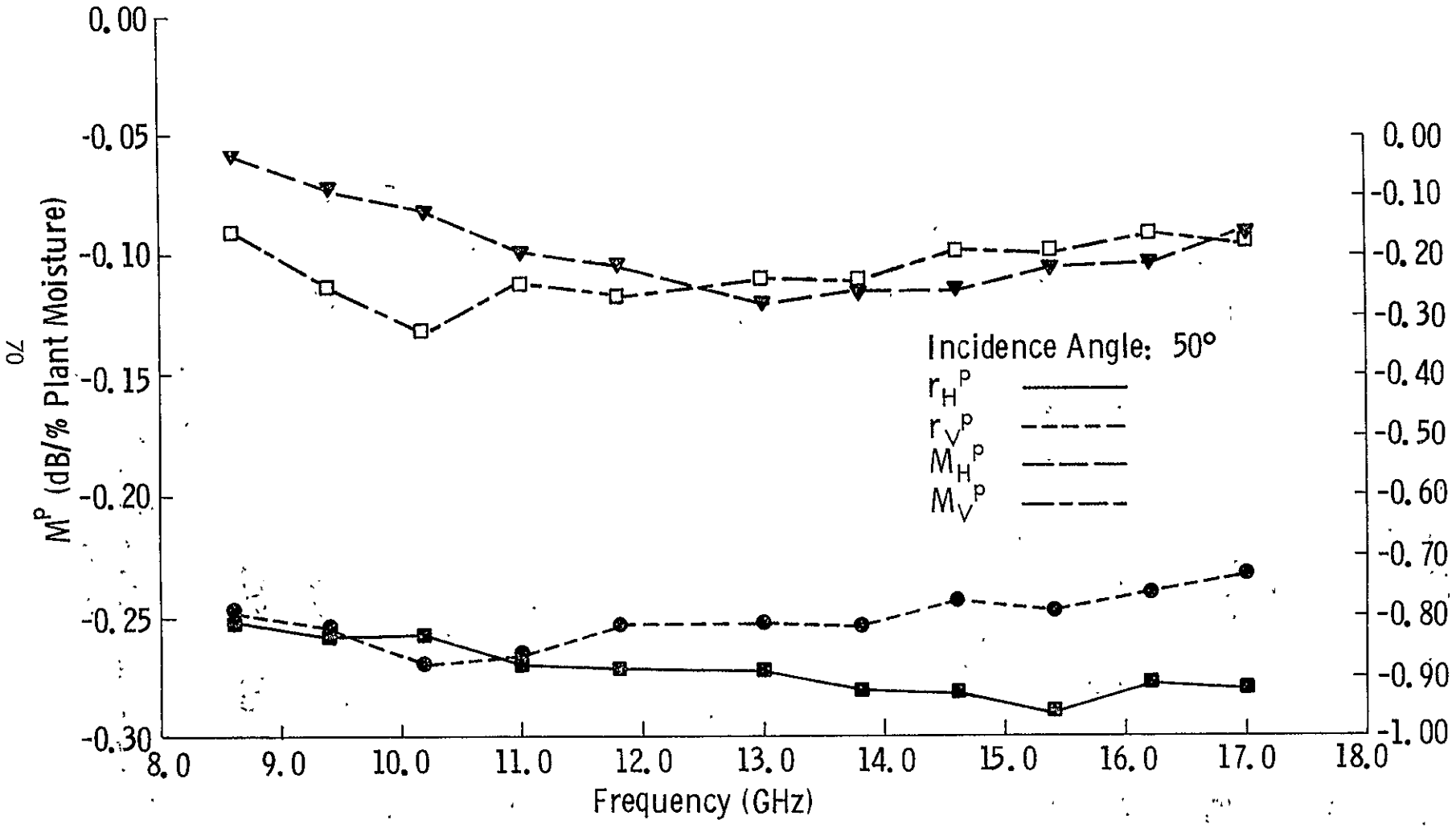

Figure 11e. Variations of M_H^P, M_V^P, r_H^P, and r_V^P with frequency. M_H^P, M_V^P, r_H^P, and r_V^P are the slopes (dB/percent plant moisture) and estimated correlation coefficients respectively, obtained by a linear regression of σ^o (dB) on plant moisture. The incidence angle is 50°.

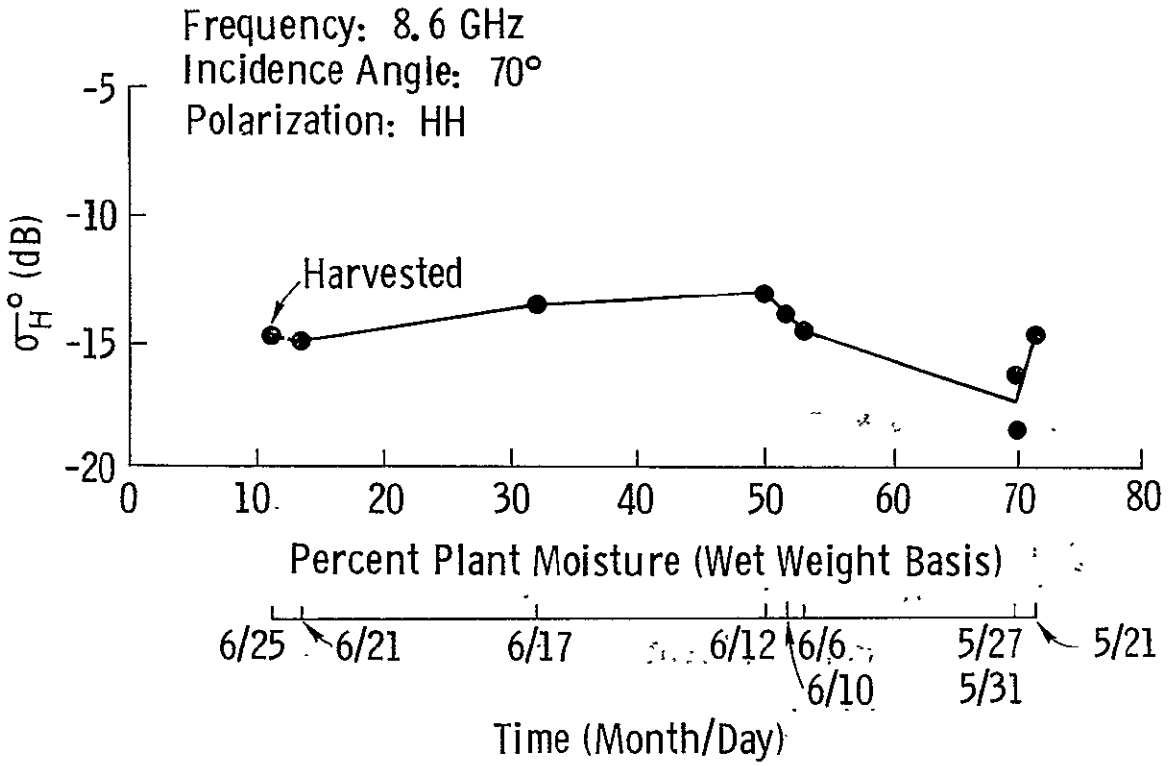

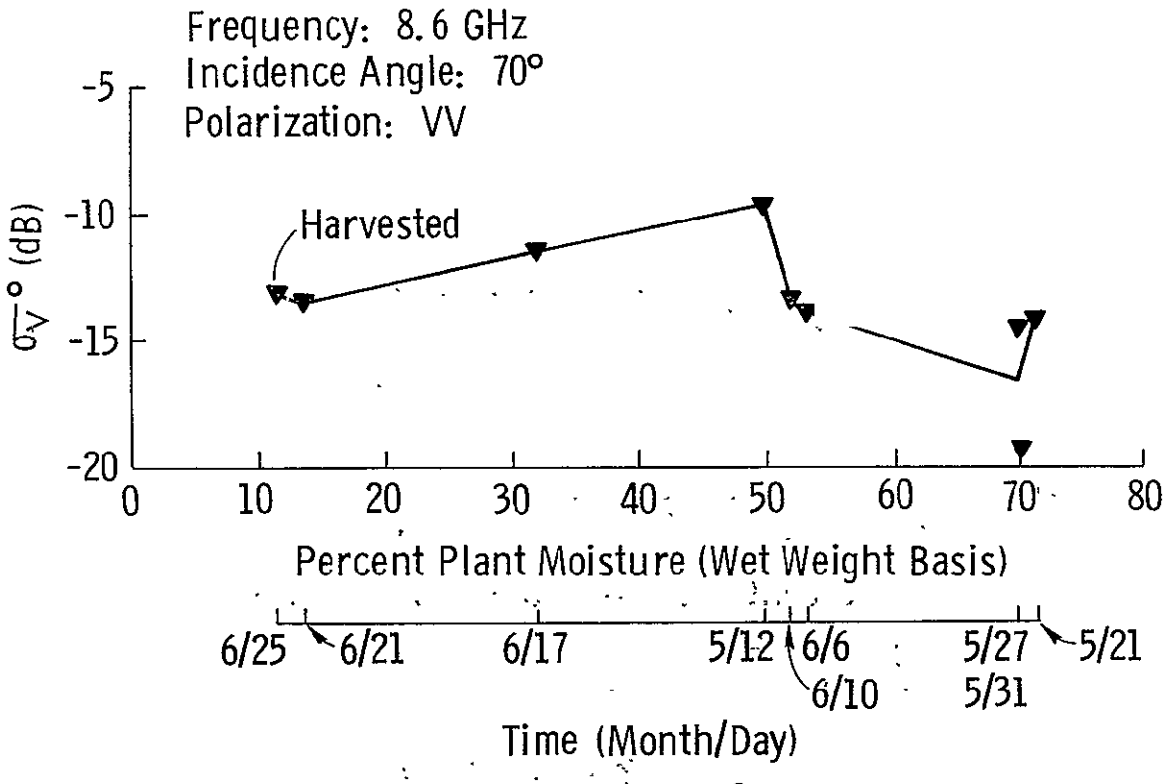

Figure 12a. Variations of σ_H° (dB) and σ_V° (dB) with plant moisture. Frequency = 8.6 GHz, incidence angle = 70°.

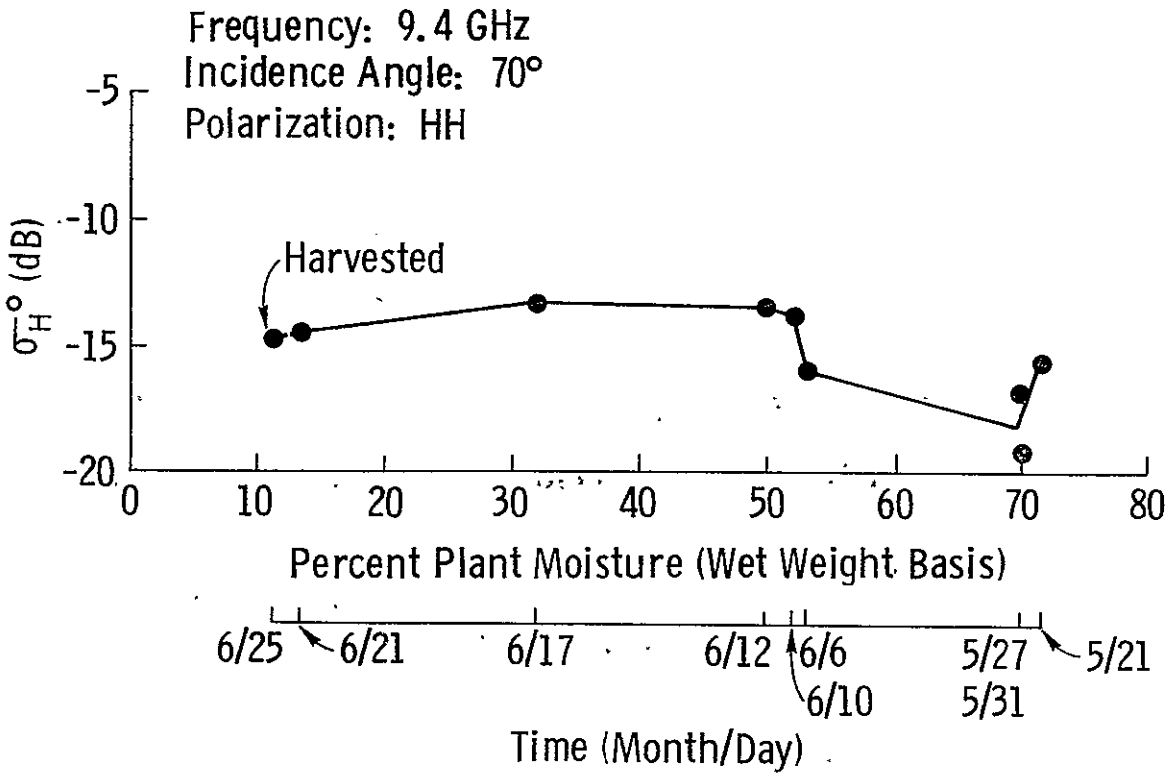

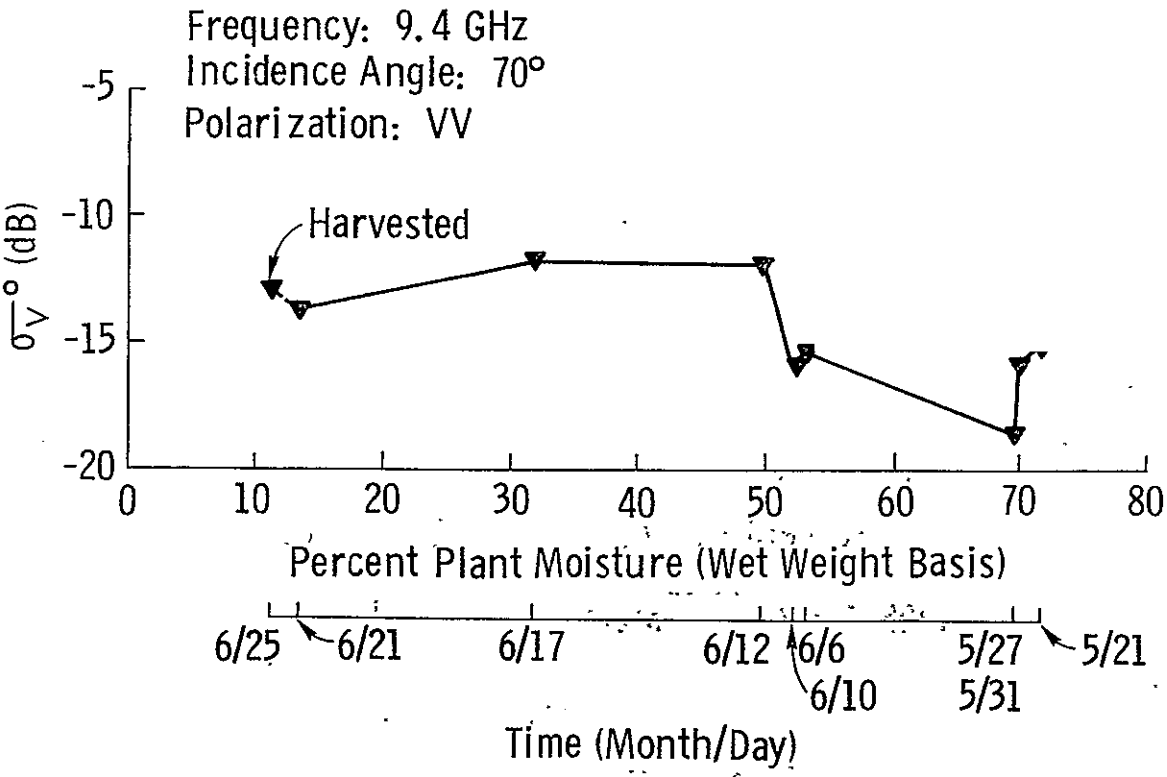

Figure 12b. Variations of σ_H° (dB) and σ_V° (dB) with plant moisture. Frequency = 9.4 GHz, incidence angle = 70°.

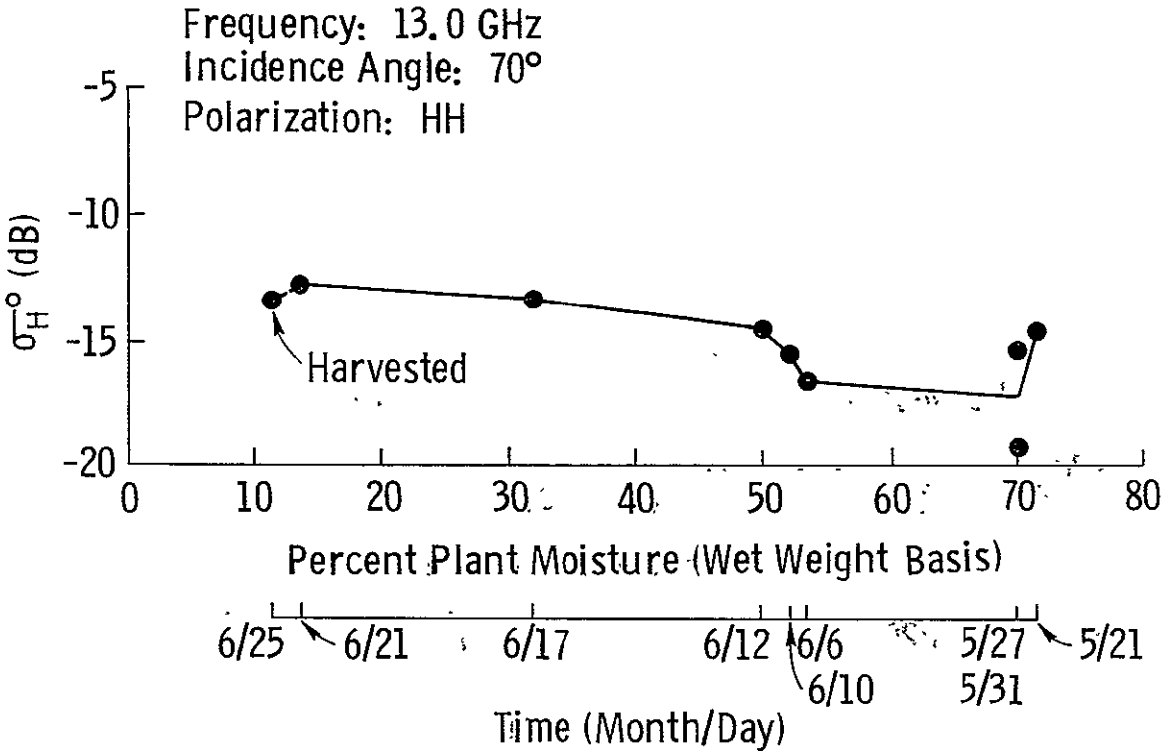

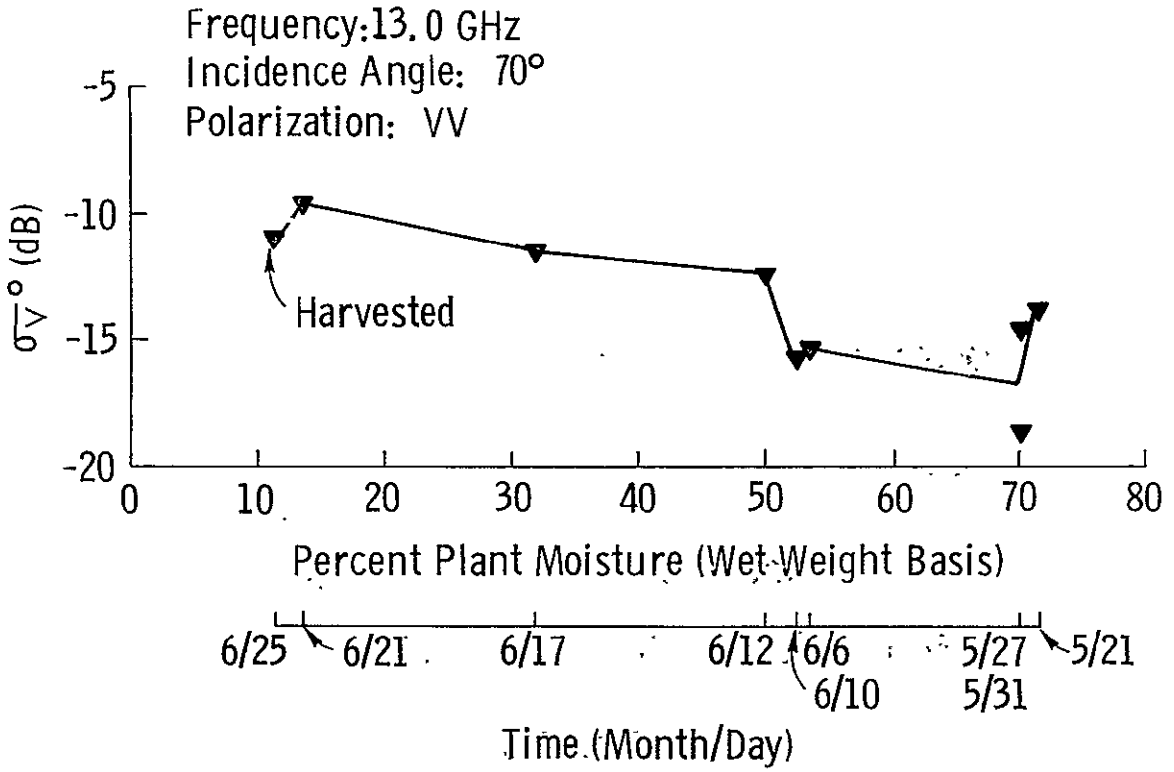

Figure 12c. Variations of σ_H° (dB) and σ_V° (dB) with plant moisture. Frequency = 13.0 GHz, incidence angle = 70°.

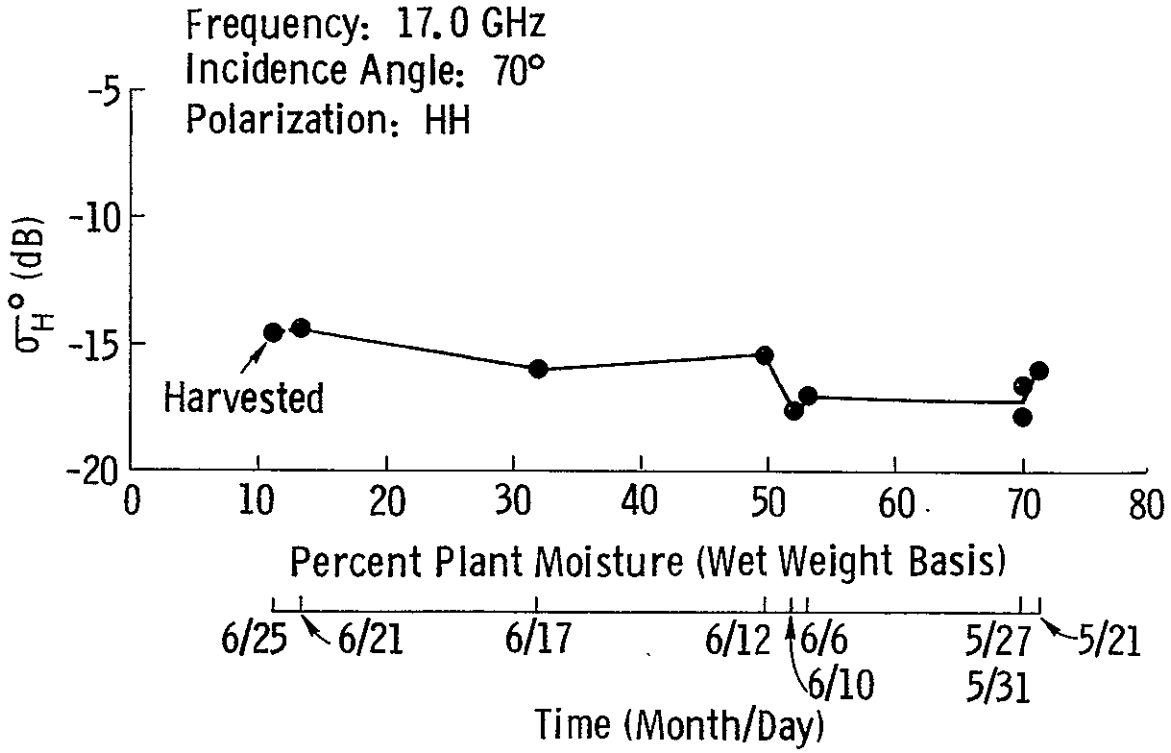

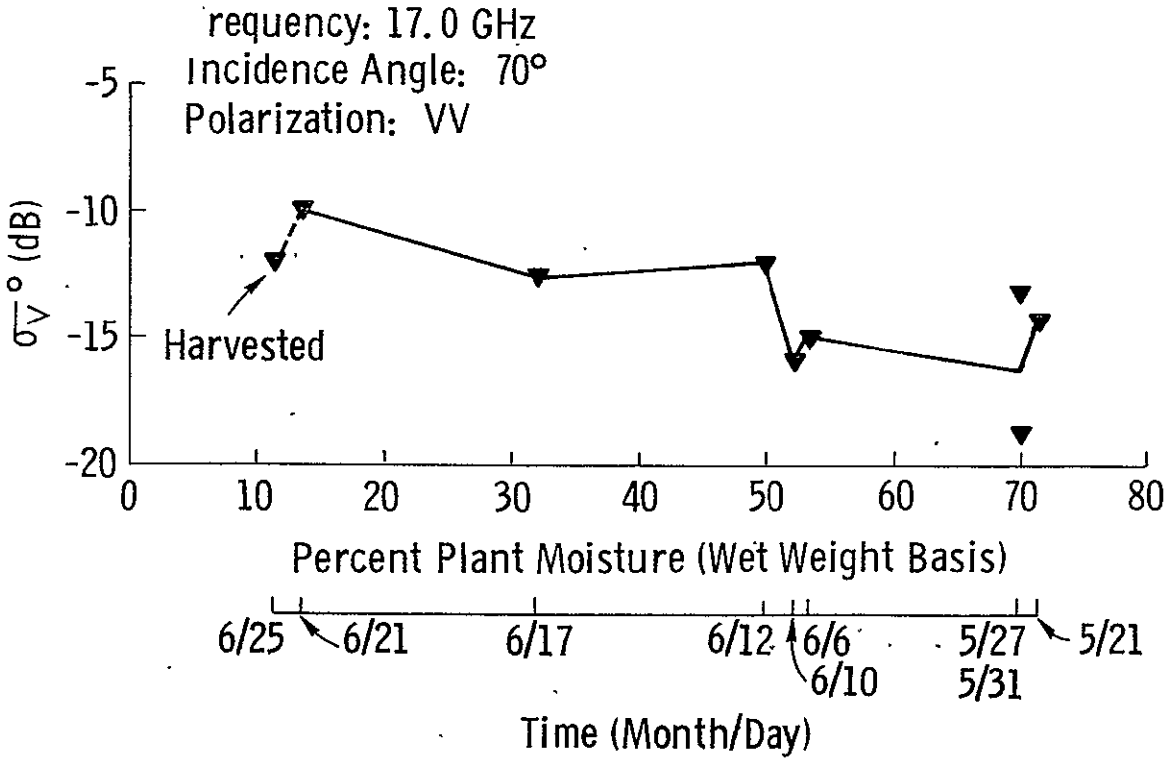

Figure 12d. Variations of σ_H° (dB) and σ_V° (dB) with plant moisture. Frequency = 17.0 GHz, incidence angle = 70°.

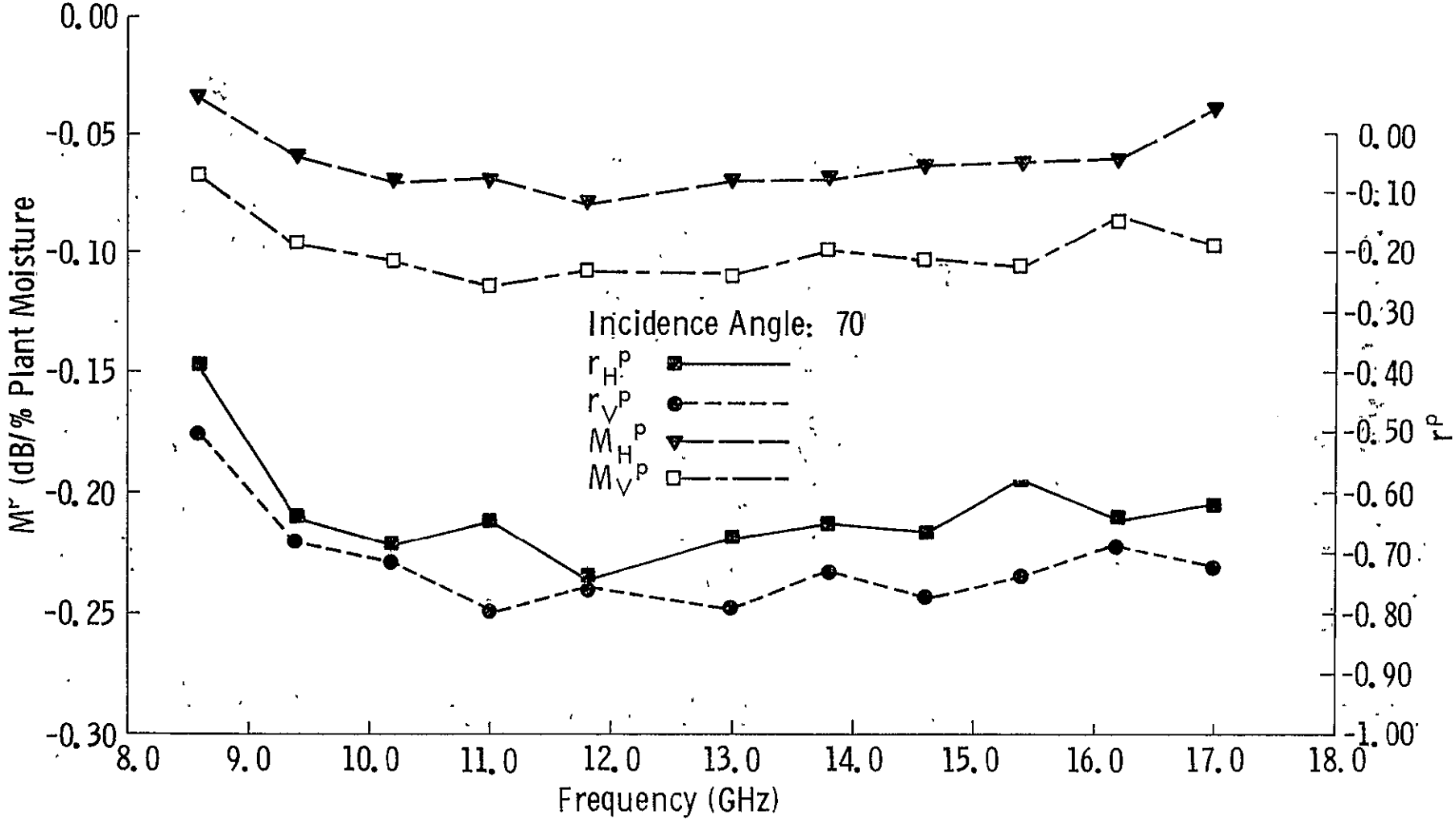

Figure 12e. Variations of M_H^p, M_V^p, r_H^p, and r_V^p with frequency. M_H^p, M_V^p, r_H^p, and r_V^p are the slopes (dB/percent plant moisture) and estimated correlation coefficients respectively, obtained by a linear regression of σ^o (dB) on plant moisture. The incidence angle is 70°.

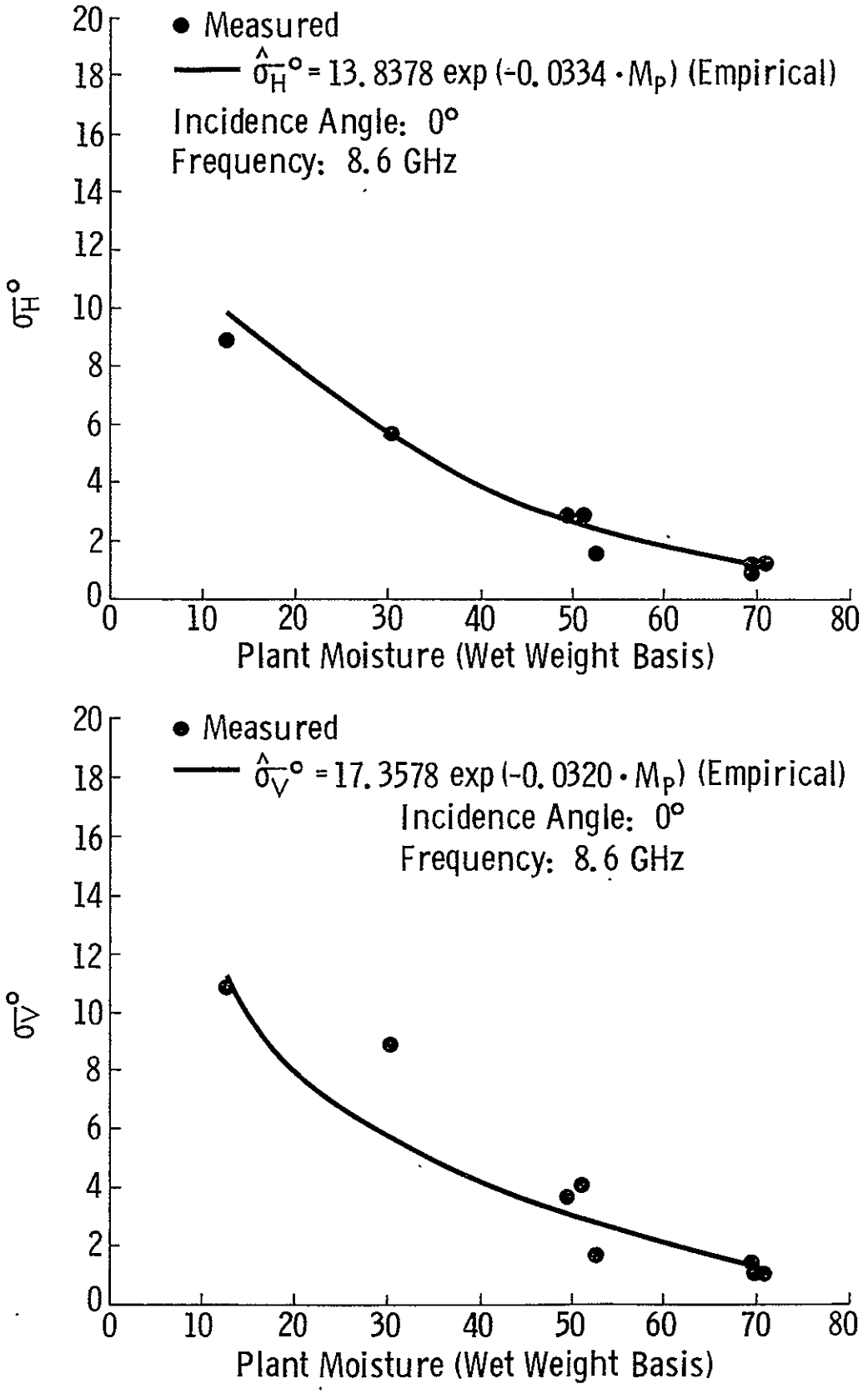

Figure 13a. Variations of σ_H° and σ_V° (real units) with plant moisture. The solid lines represent the nonlinear regression curve corresponding to the equation shown with the figure. The frequency is 8.6 GHz and the incidence angle is 0°.

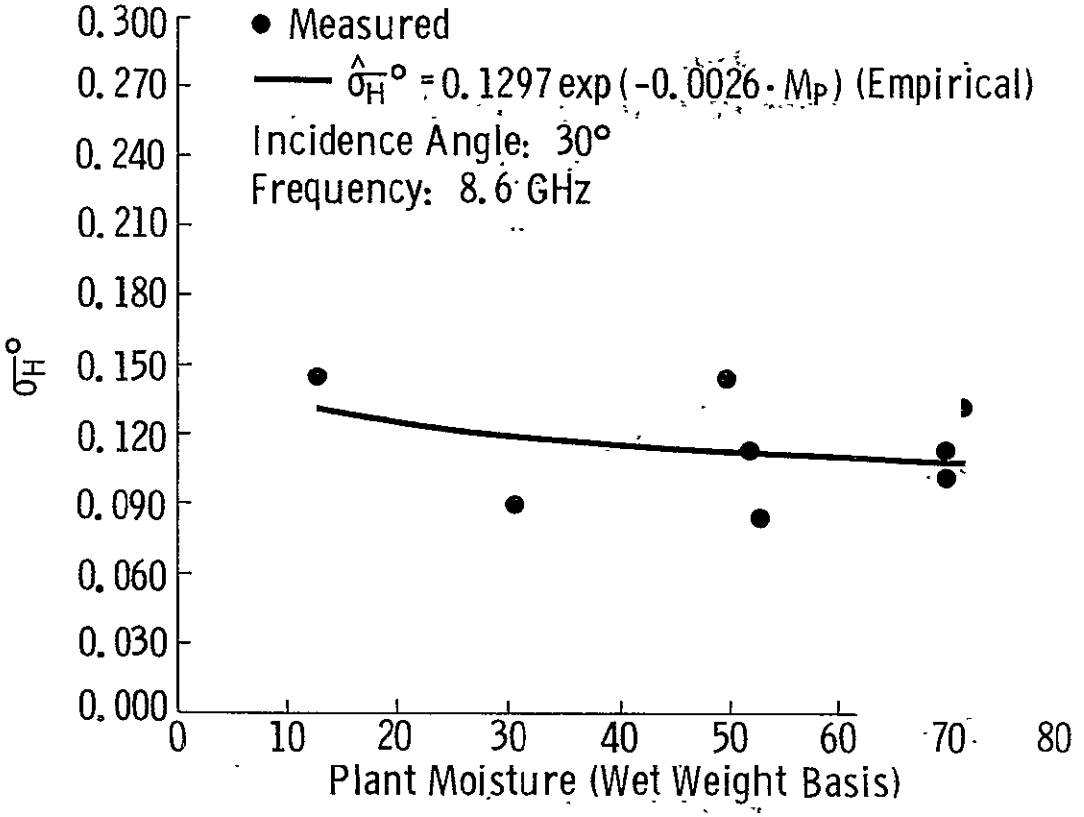

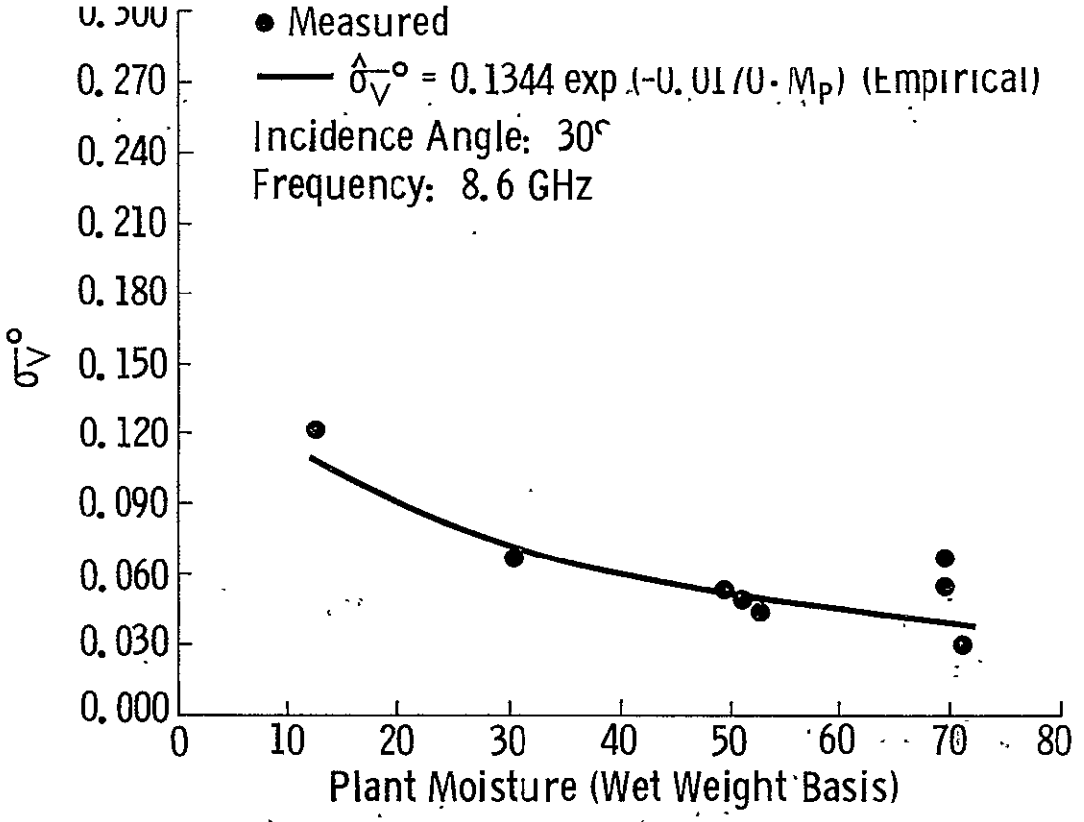

Figure 13b. Variations of σ_H° and σ_V° (real units) with plant moisture. The solid lines represent the nonlinear regression curve corresponding to the equation shown with the figure. The frequency is 8.6 GHz and the incidence angle is 30°.

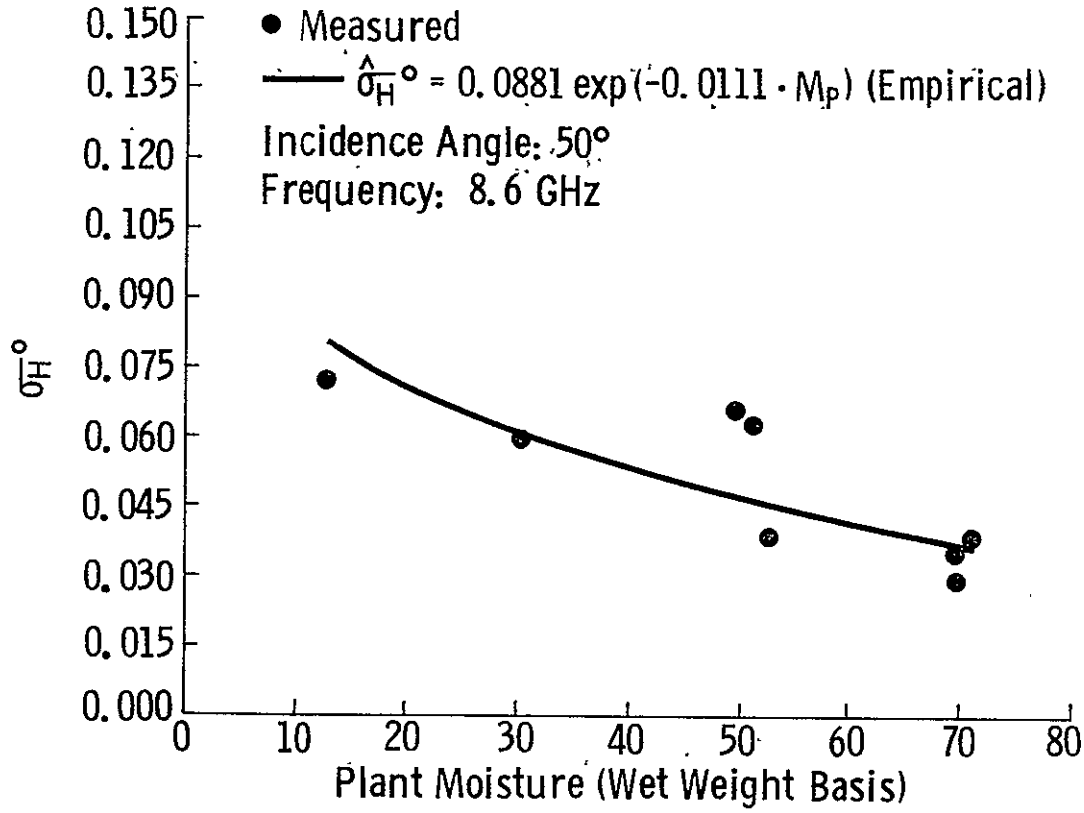

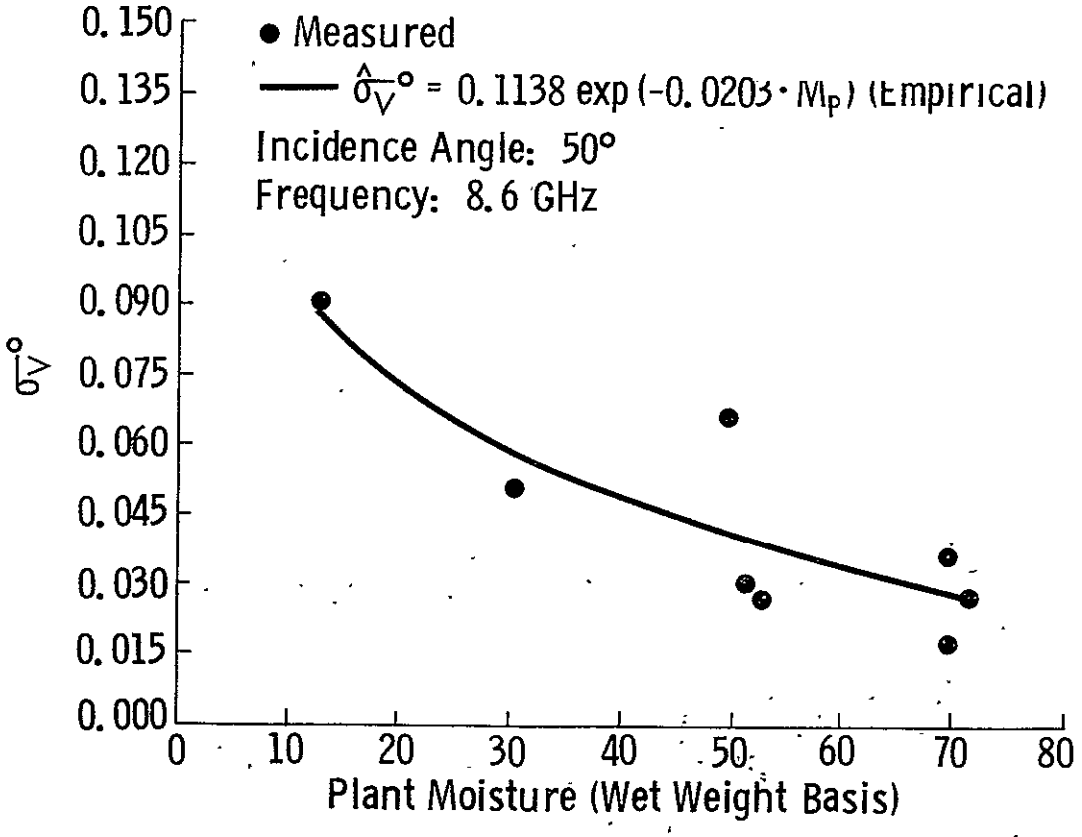

Figure 13c. Variations of σ_H° and σ_V° (real units) with plant moisture. The solid lines represent the nonlinear regression curve corresponding to the equation shown with the figure. The frequency is 8.6 GHz and the incidence angle is 50°.

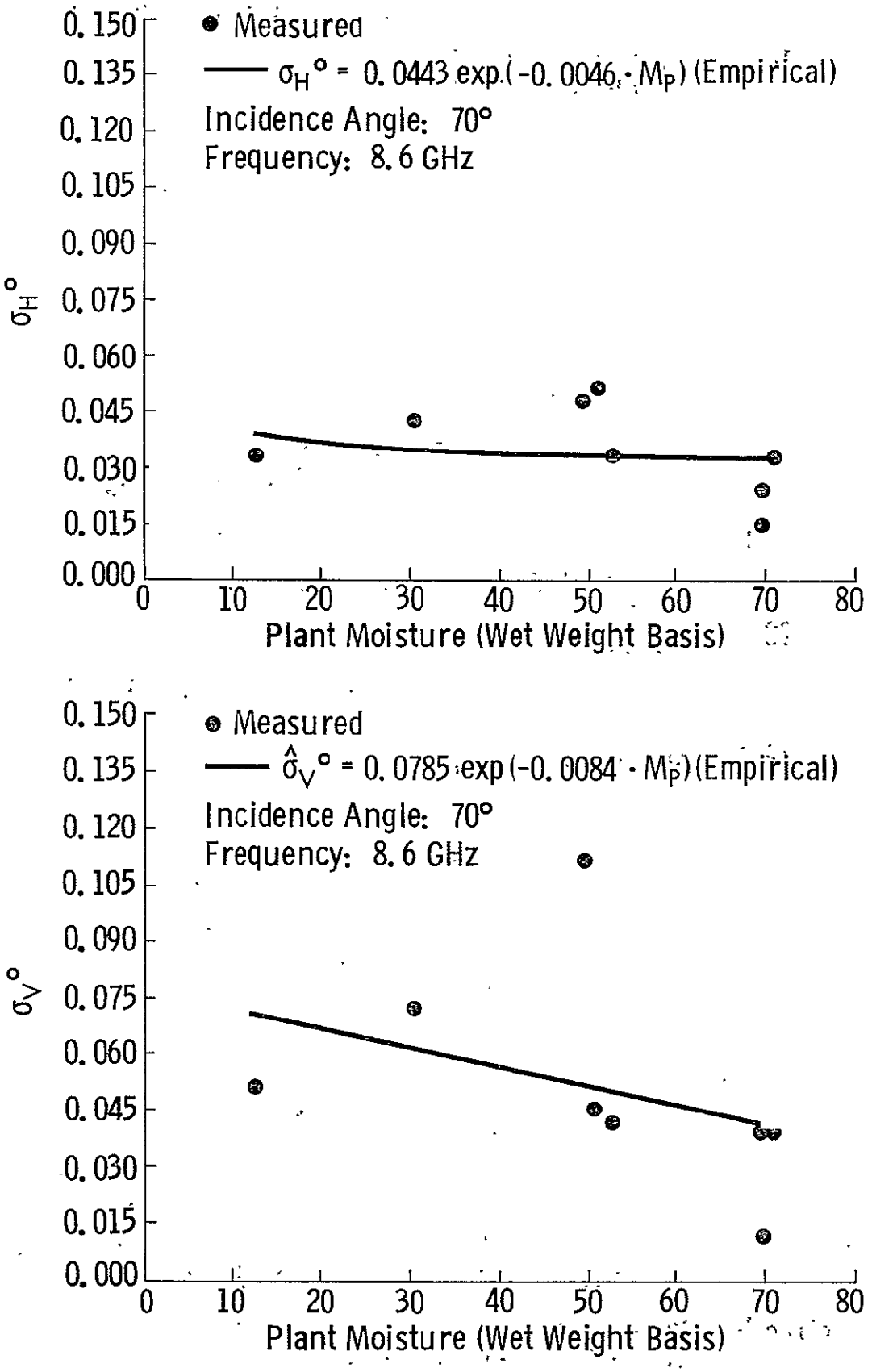

Figure 13d. Variations of σ_H° and σ_V° (real units) with plant moisture. The solid lines represent the nonlinear regression curve corresponding to the equation shown with the figure. The frequency is 8.6 GHz and the incidence angle is 70°.

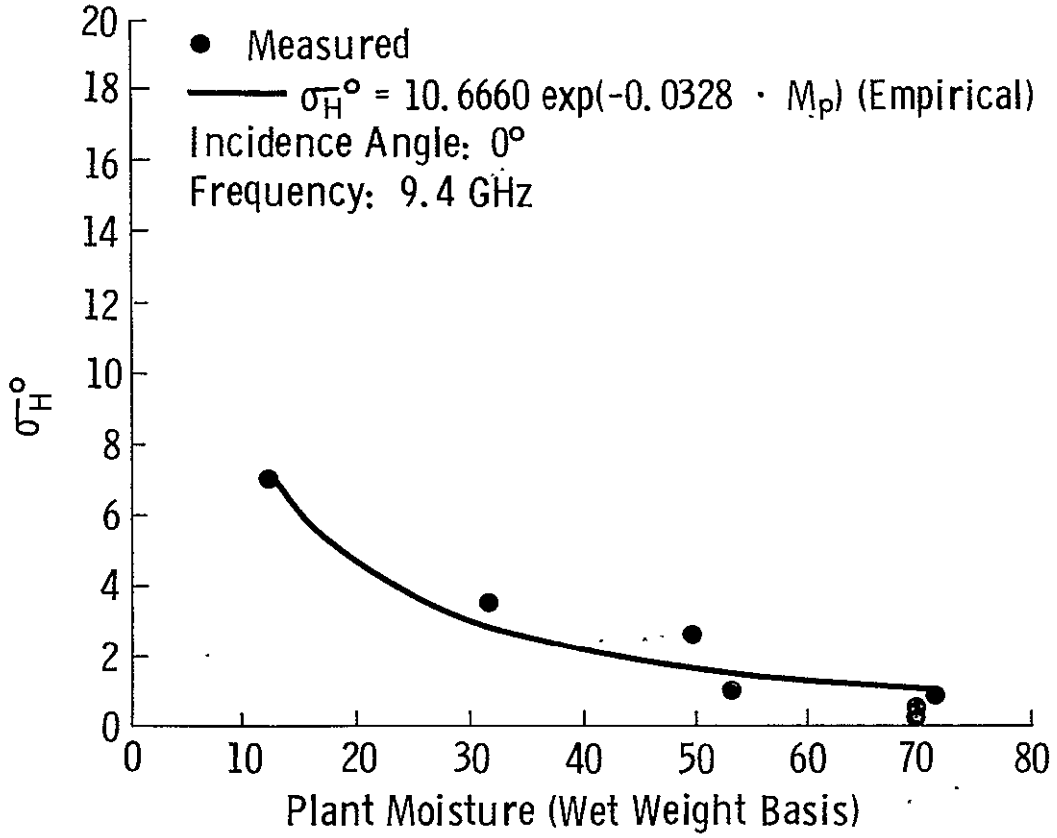

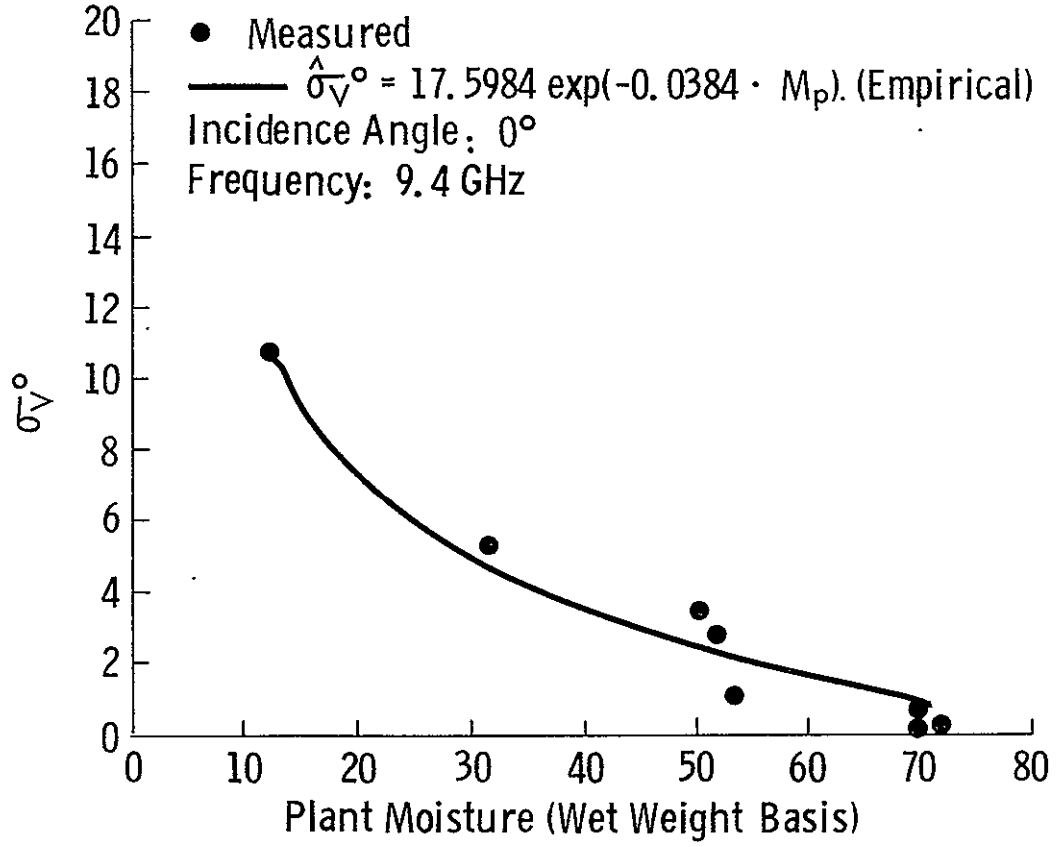

Figure 14a. Variations of $\overline{\sigma_H}^\circ$ and $\overline{\sigma_V}^\circ$ (real units) with plant moisture. The solid lines represent the nonlinear regression curve corresponding to the equation shown with the figure. The frequency is 9.4 GHz and the incidence angle is 0°.

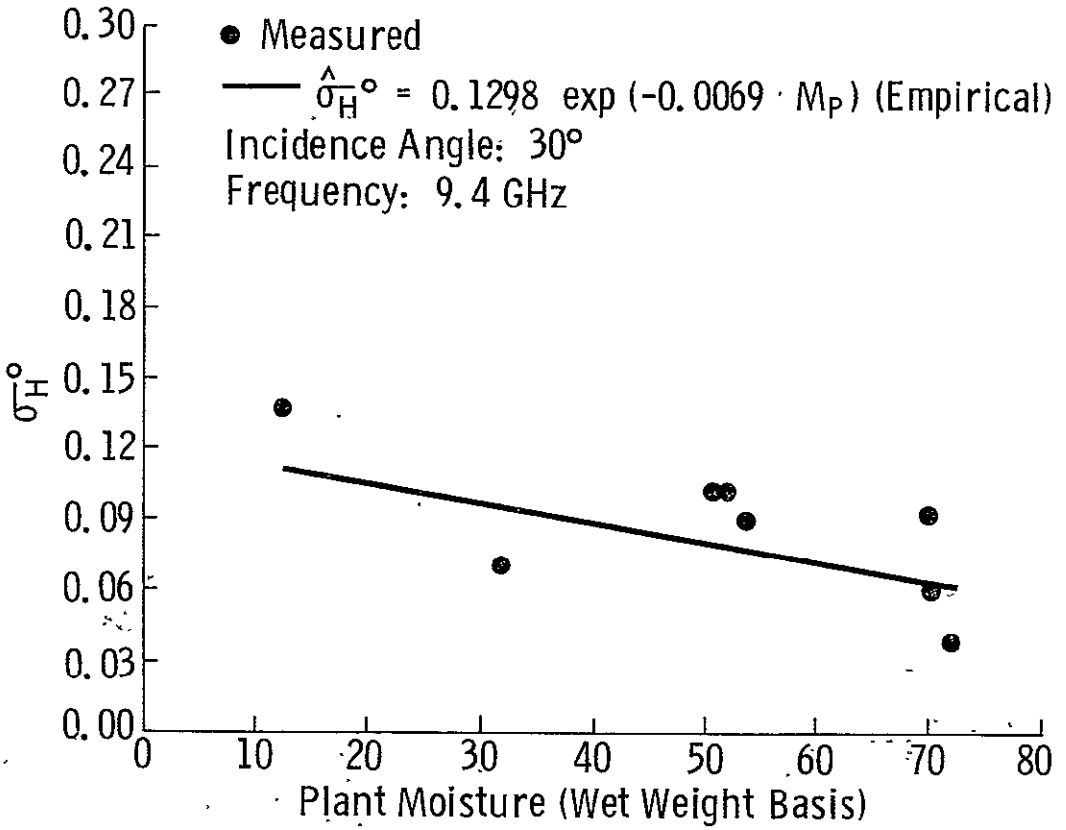

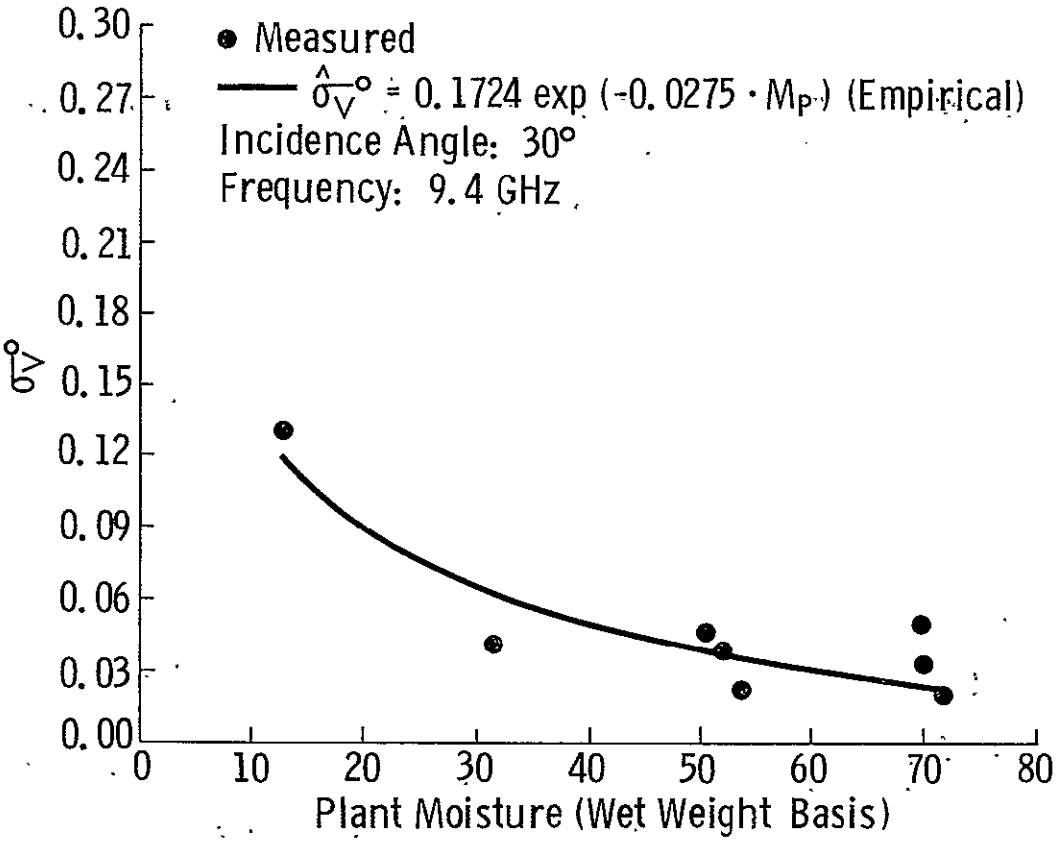

Figure 14b. Variations of σ°_H and σ°_V (real units) with plant moisture. The solid lines represent the nonlinear regression curve corresponding to the equation shown with the figure. The frequency is 9.4 GHz and the incidence angle is 30°.

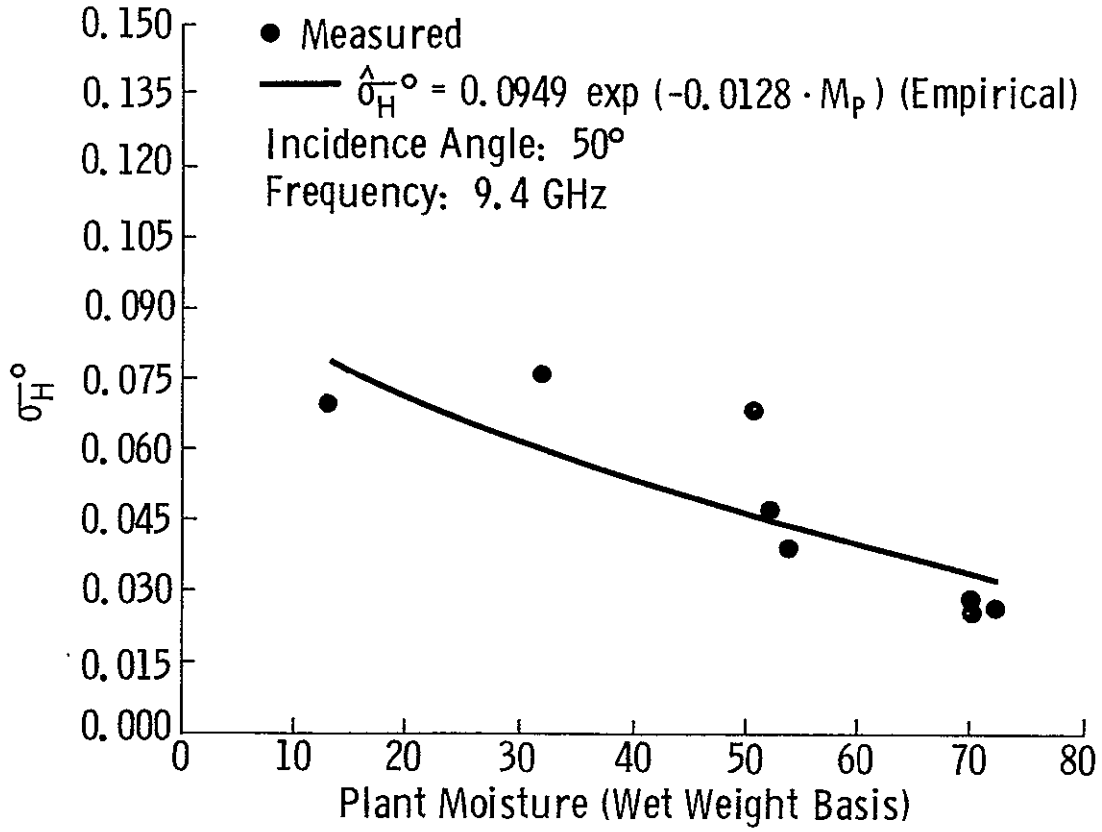

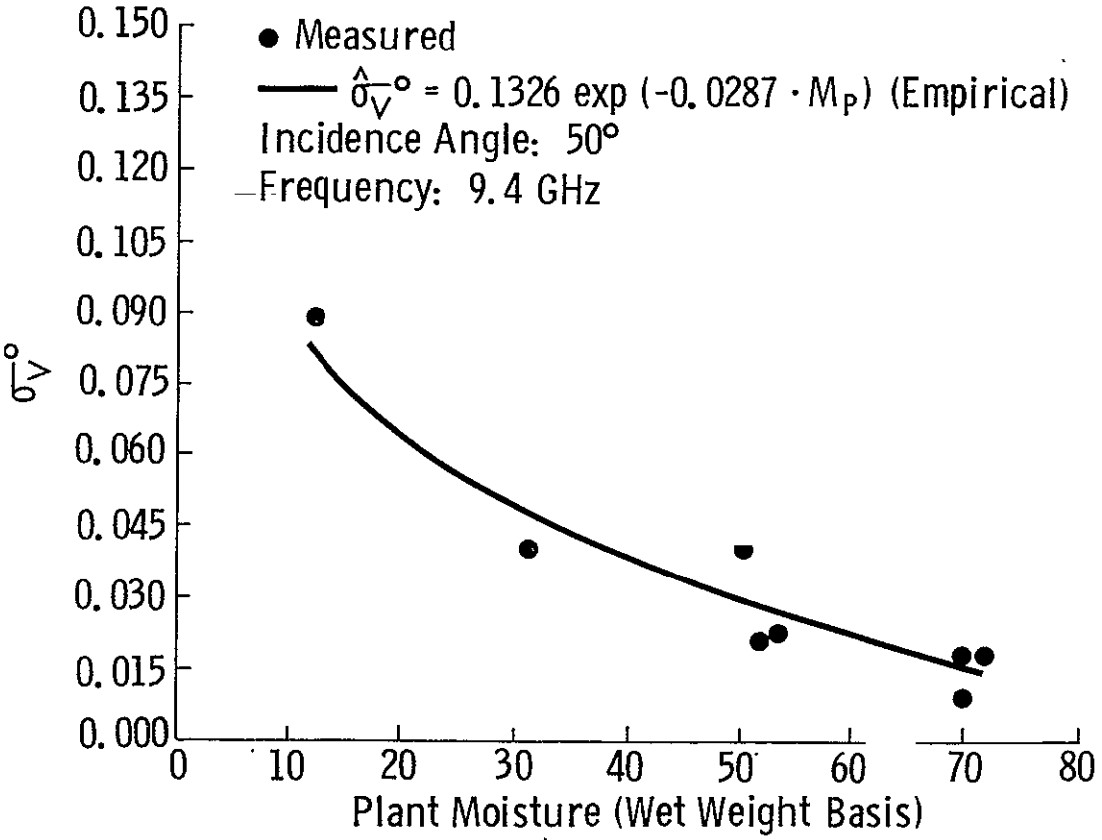

Figure 14c. Variations of σ°_H and σ°_V (real units) with plant moisture. The solid lines represent the nonlinear regression curve corresponding to the equation shown with the figure. The frequency is 9.4 GHz and the incidence angle is 50°.

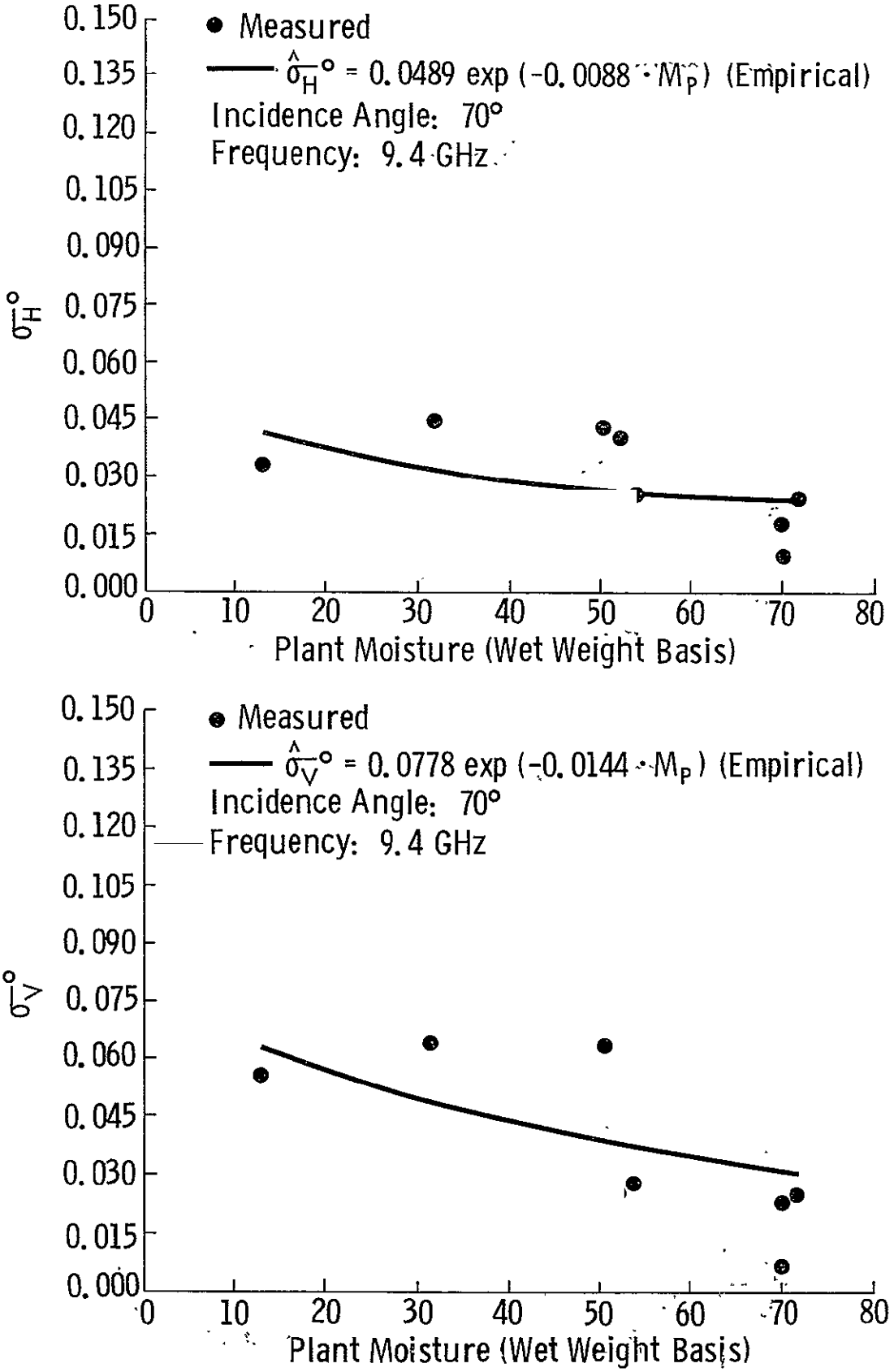

Figure 14d. Variations of σ_H° and σ_V° (real units) with plant moisture. The solid lines represent the nonlinear regression curve corresponding to the equation shown with the figure. The frequency is 9.4 GHz and the incidence angle is 70°.

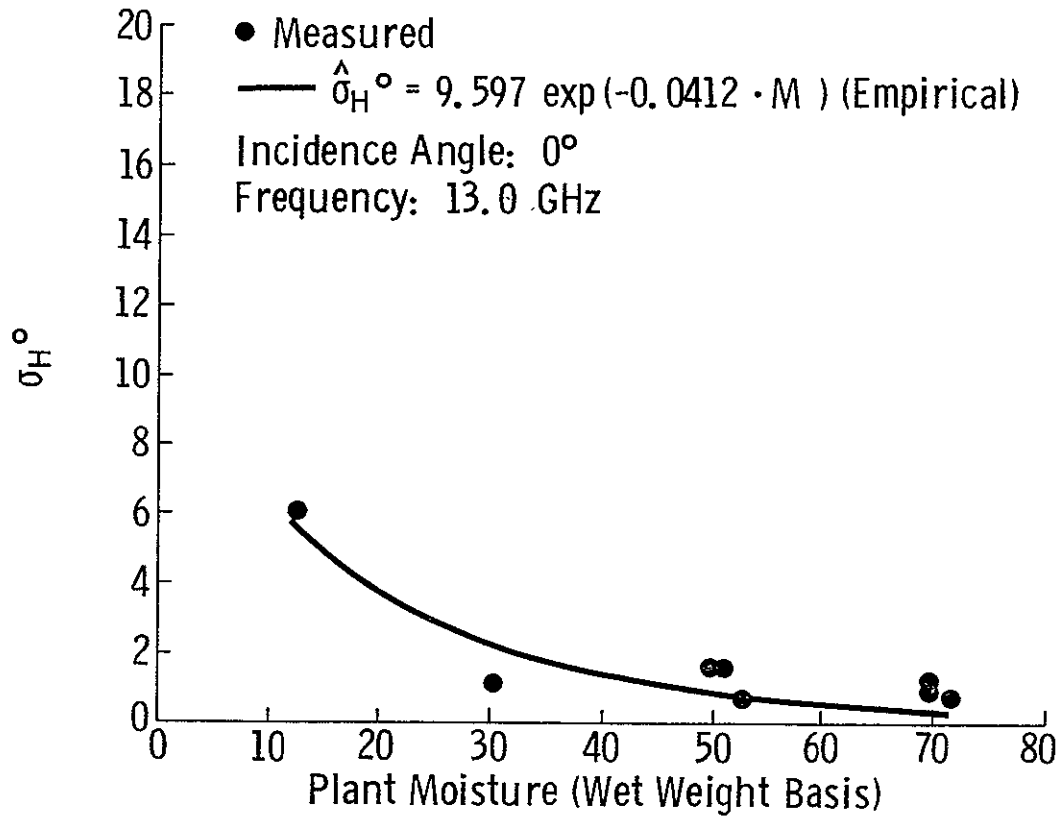

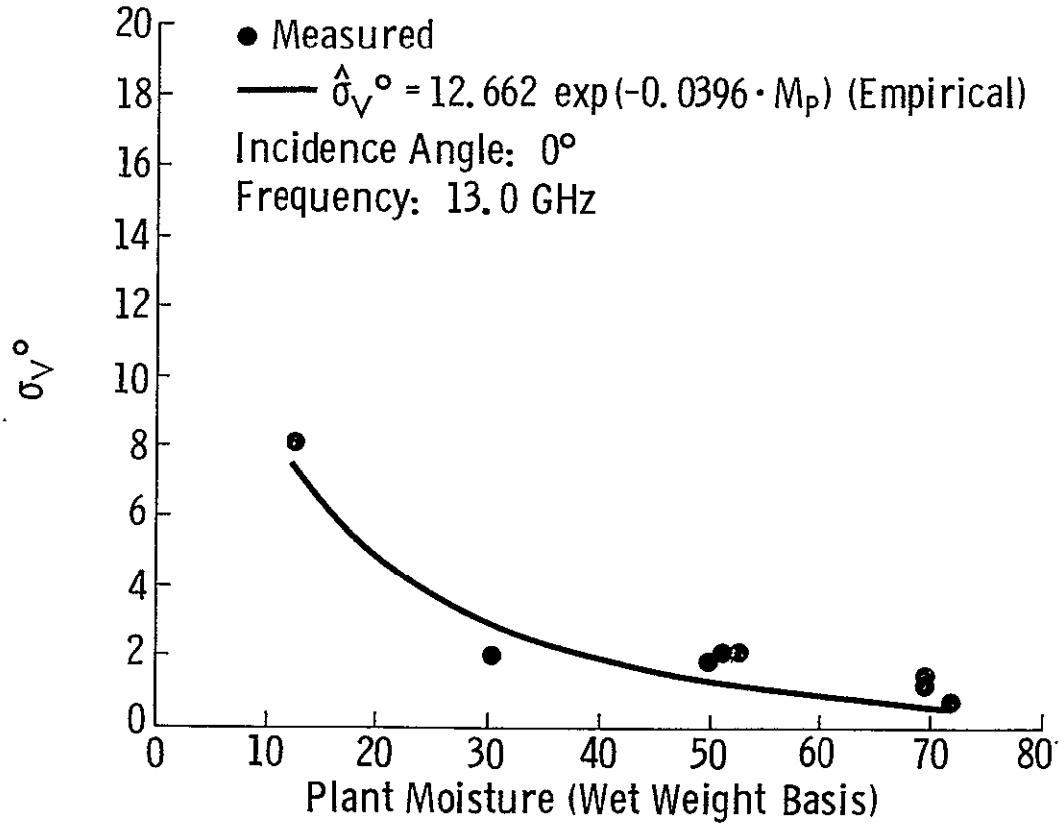

Figure 15a. Variations of σ_H° and σ_V° (real units) with plant moisture. The solid lines represent the nonlinear regression curve corresponding to the equation shown with the figure. The frequency is 13.0 GHz and the incidence angle is 0°.

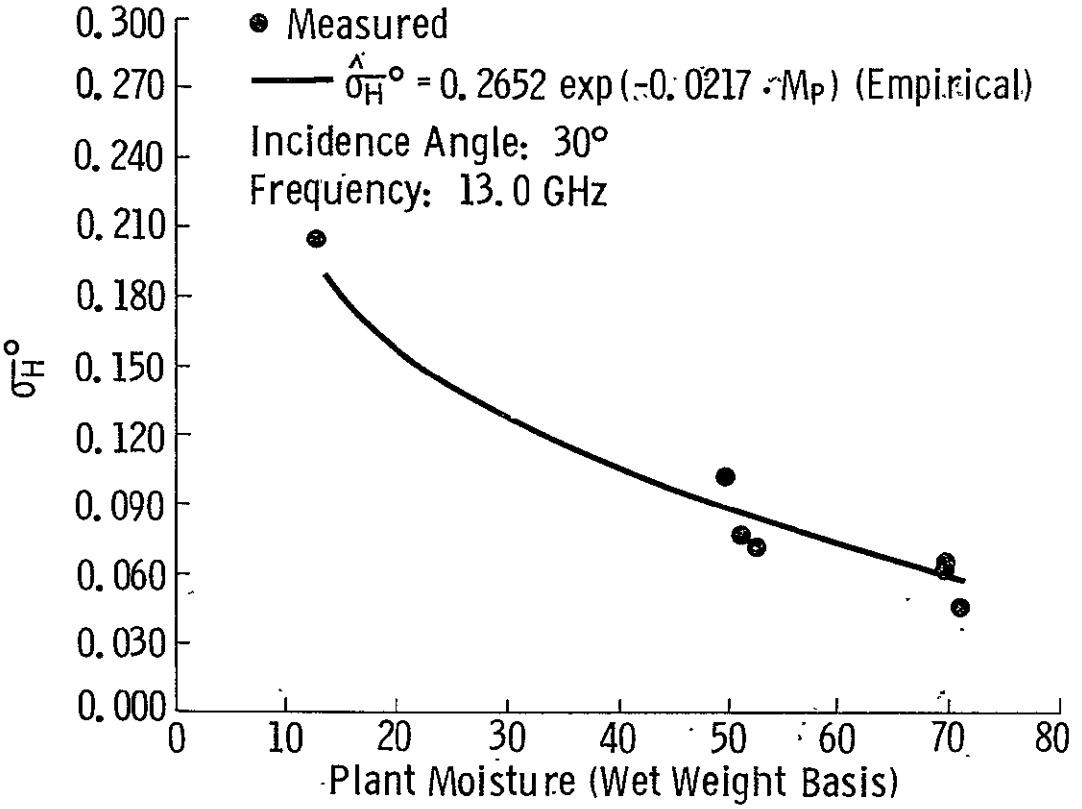

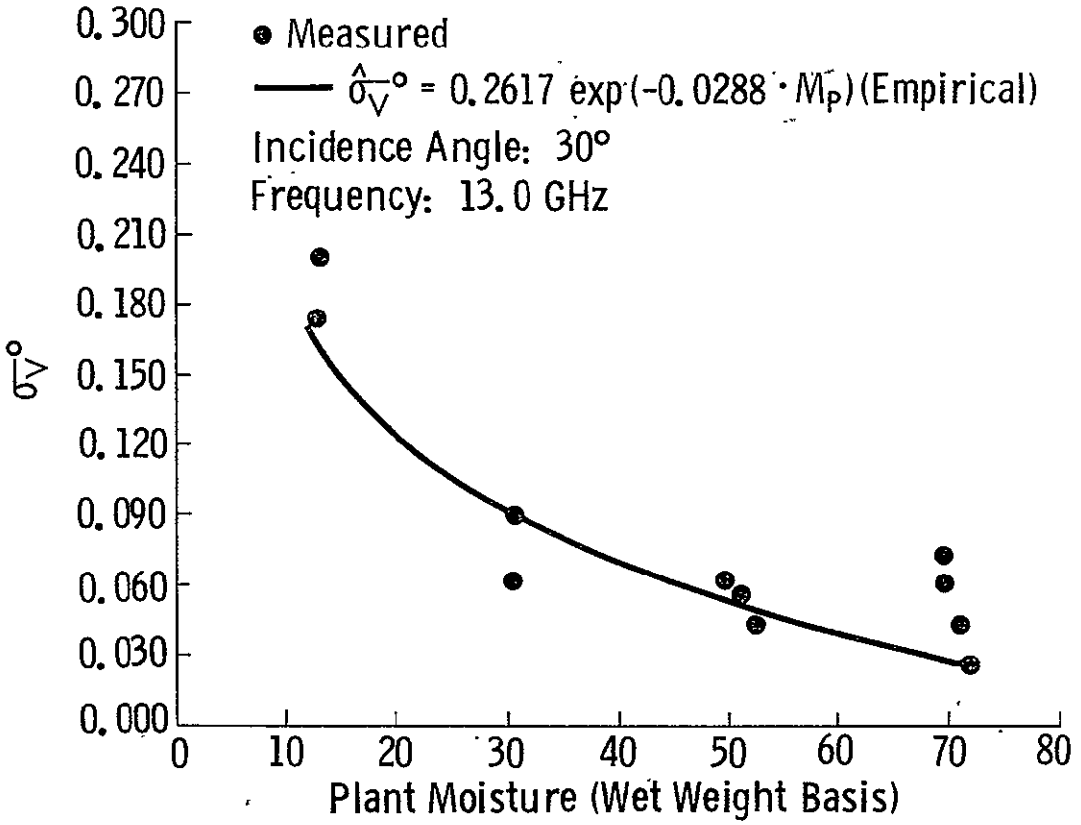

Figure 15b. Variations of σ°_H and σ°_V (real units) with plant moisture. The solid lines represent the nonlinear regression curve corresponding to the equation shown with the figure. The frequency is 13.0 GHz and the incidence angle is 30°.

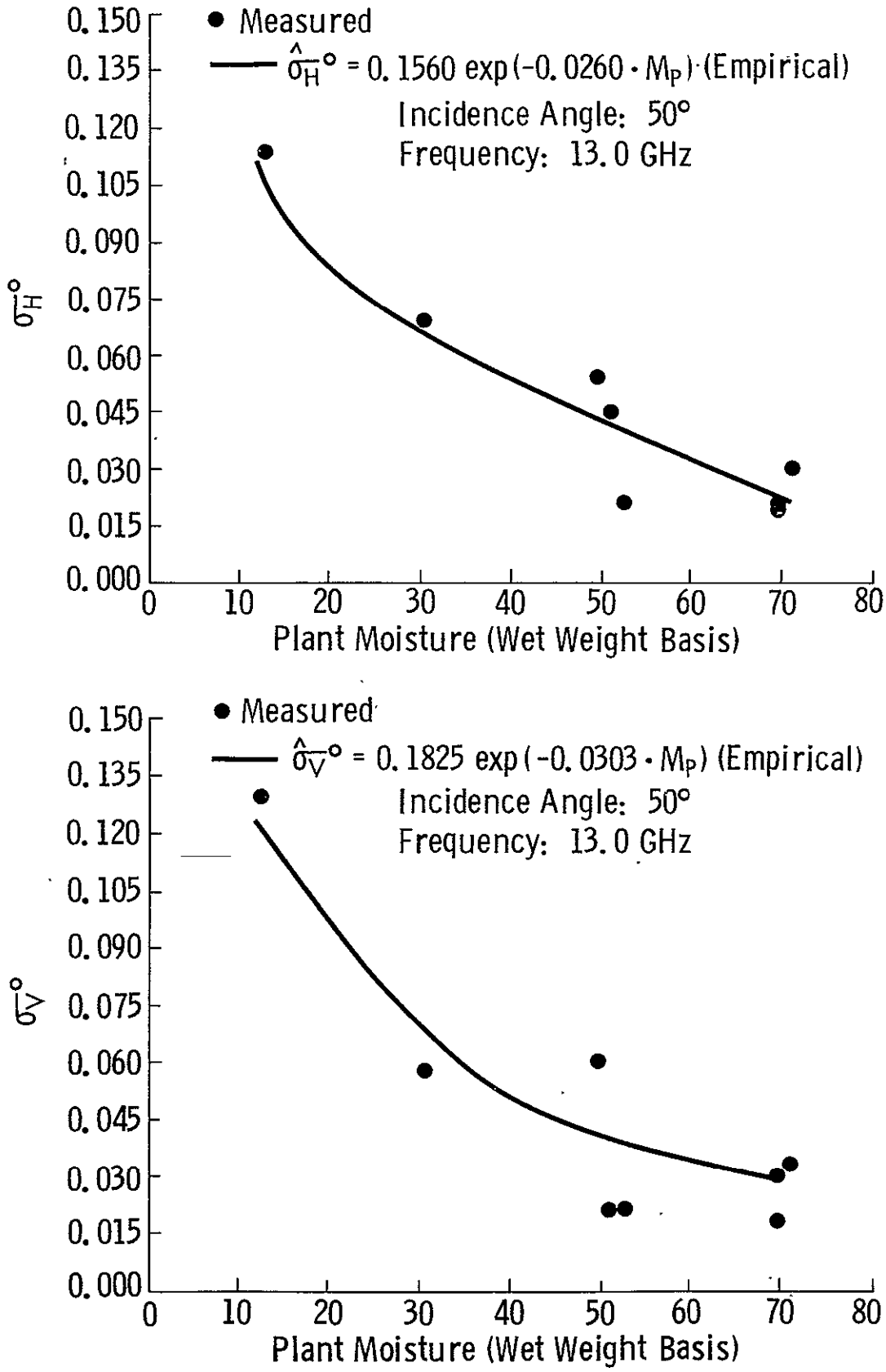

Figure 15c. Variations of σ_H° and σ_V° (real units) with plant moisture. The solid lines represent the nonlinear regression curve corresponding to the equation shown with the figure. The frequency is 13.0 GHz and the incidence angle is 50°.

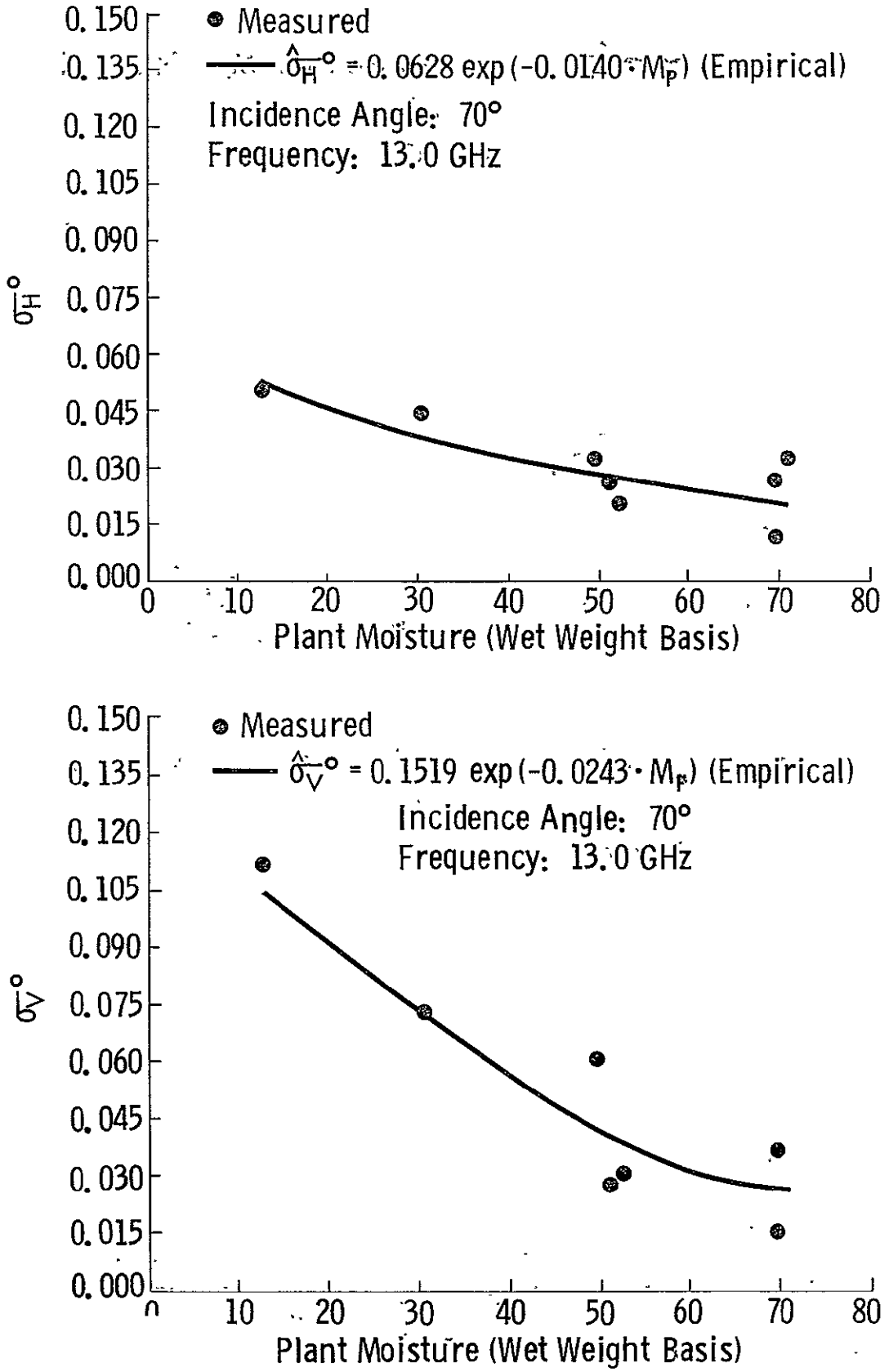

Figure 15d. Variations of σ_H° and σ_V° (real units) with plant moisture. The solid lines represent the nonlinear regression curve corresponding to the equation shown with the figure. The frequency is 13.0 GHz and the incidence angle is 70°.

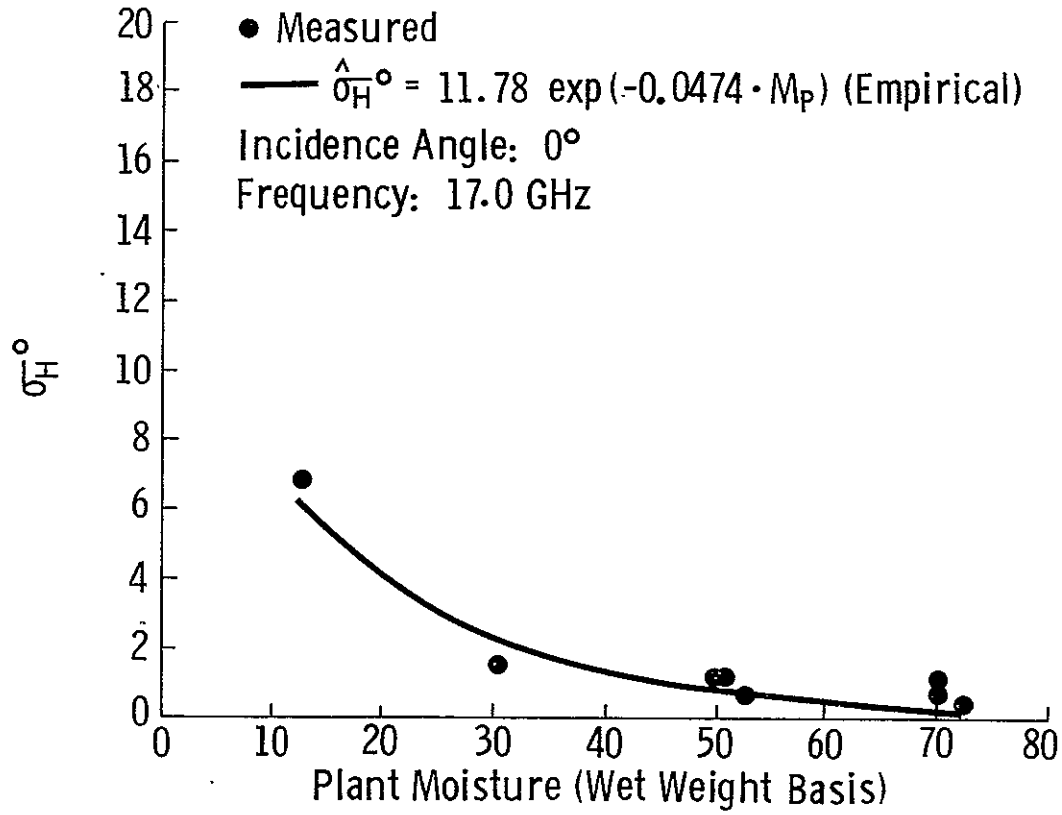

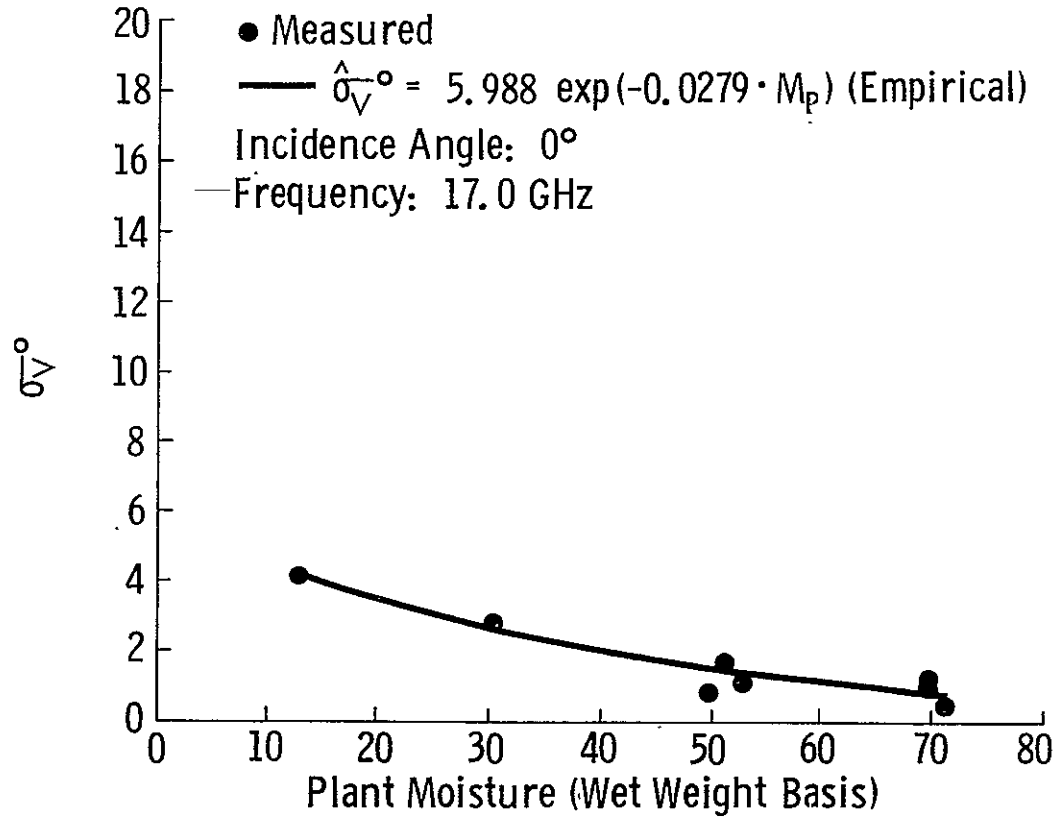

Figure 16a. Variations of σ_H° and σ_V° (real units) with plant moisture. The solid lines represent the nonlinear regression curve corresponding to the equation shown with the figure. The frequency is 17.0 GHz and the incidence angle is 0°.

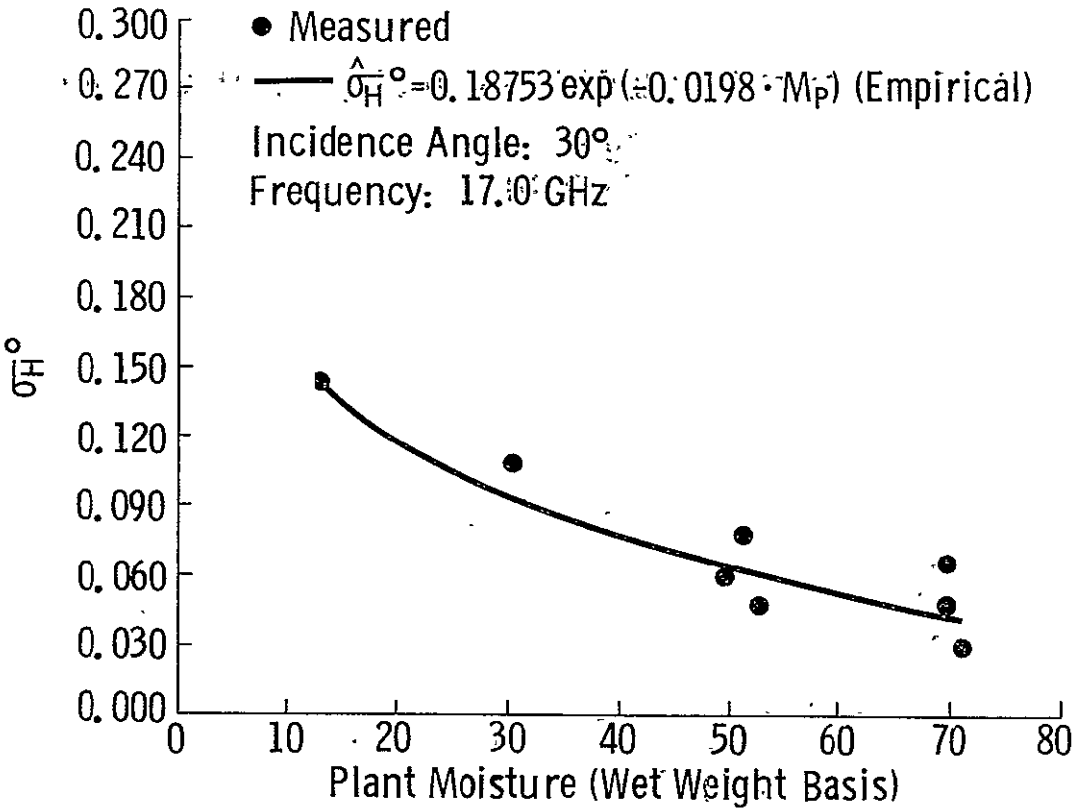

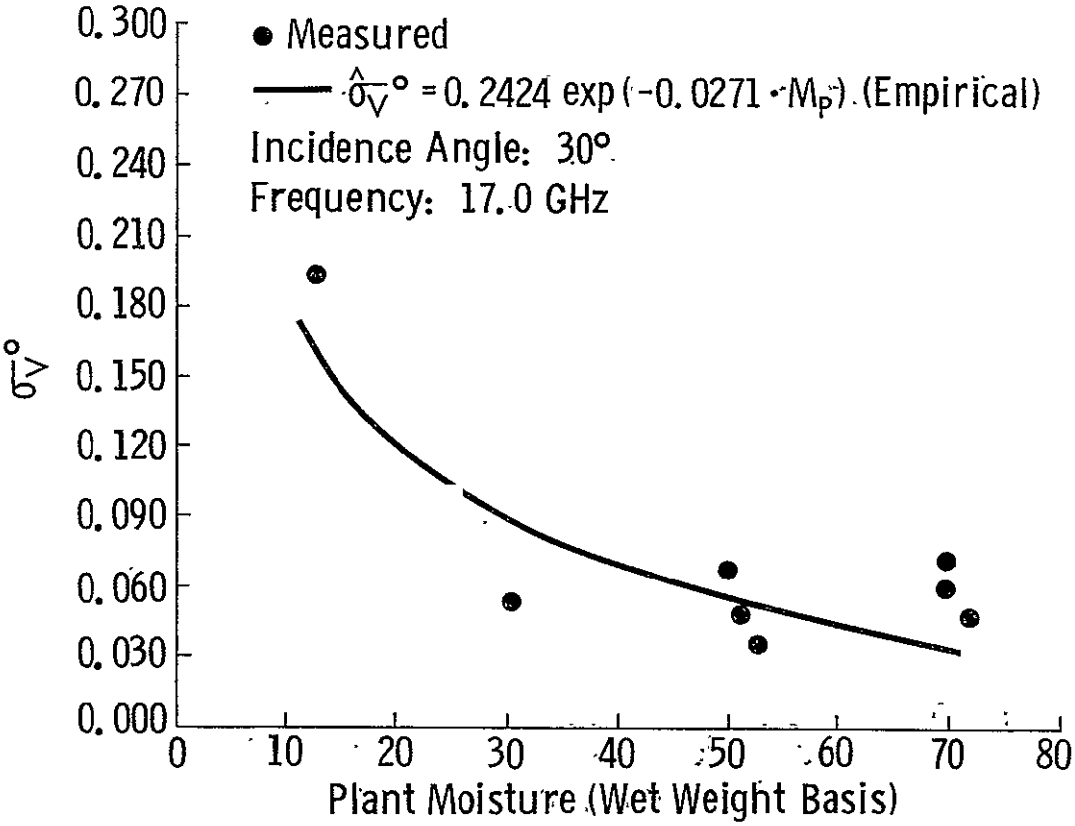

Figure 16b. Variations of σ_H° and σ_V° (real units) with plant moisture. The solid lines represent the nonlinear regression curve corresponding to the equation shown with the figure. The frequency is 17.0 GHz and the incidence angle is 30°.

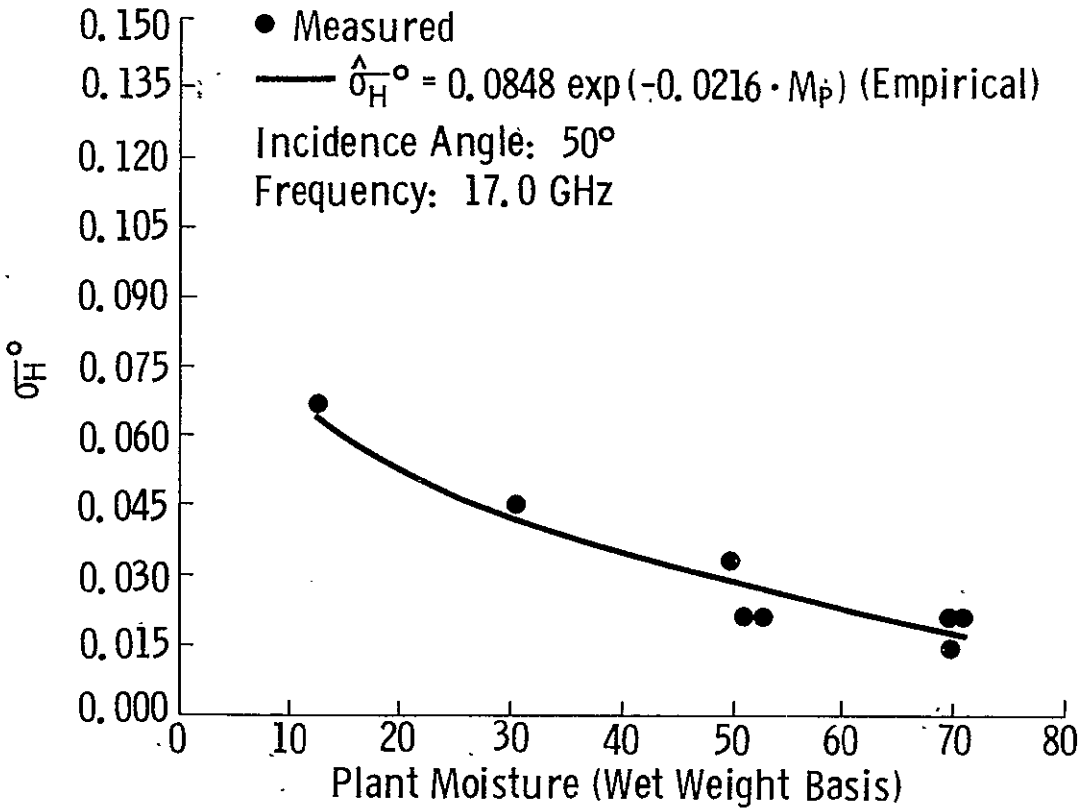

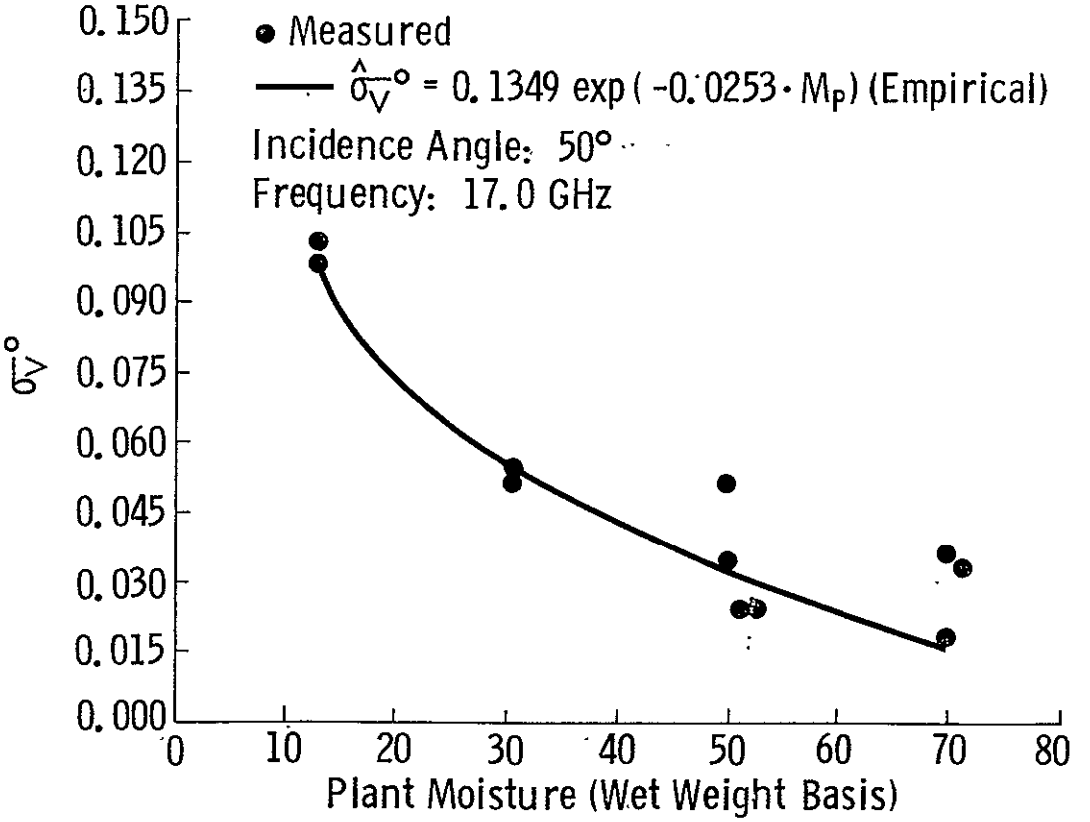

Figure 16c. Variations of σ_H° and σ_V° (real units) with plant moisture. The solid lines represent the nonlinear regression curve corresponding to the equation shown with the figure. The frequency is 17.0 GHz and the incidence angle is 50°.

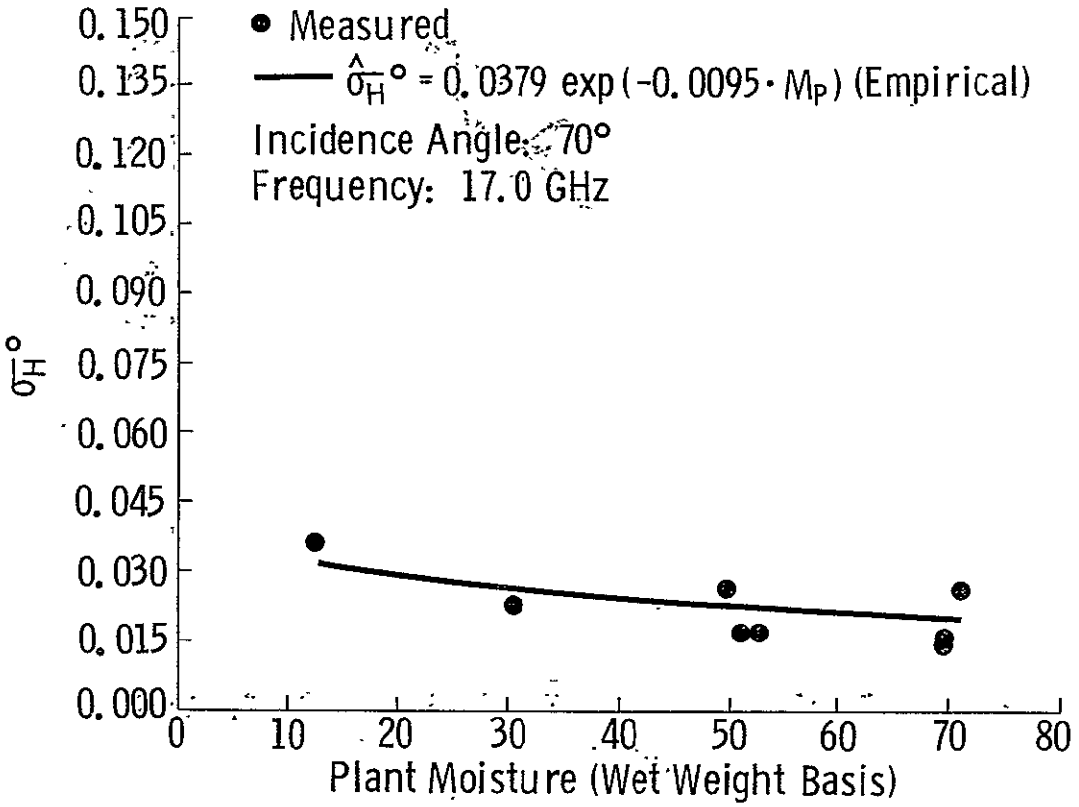

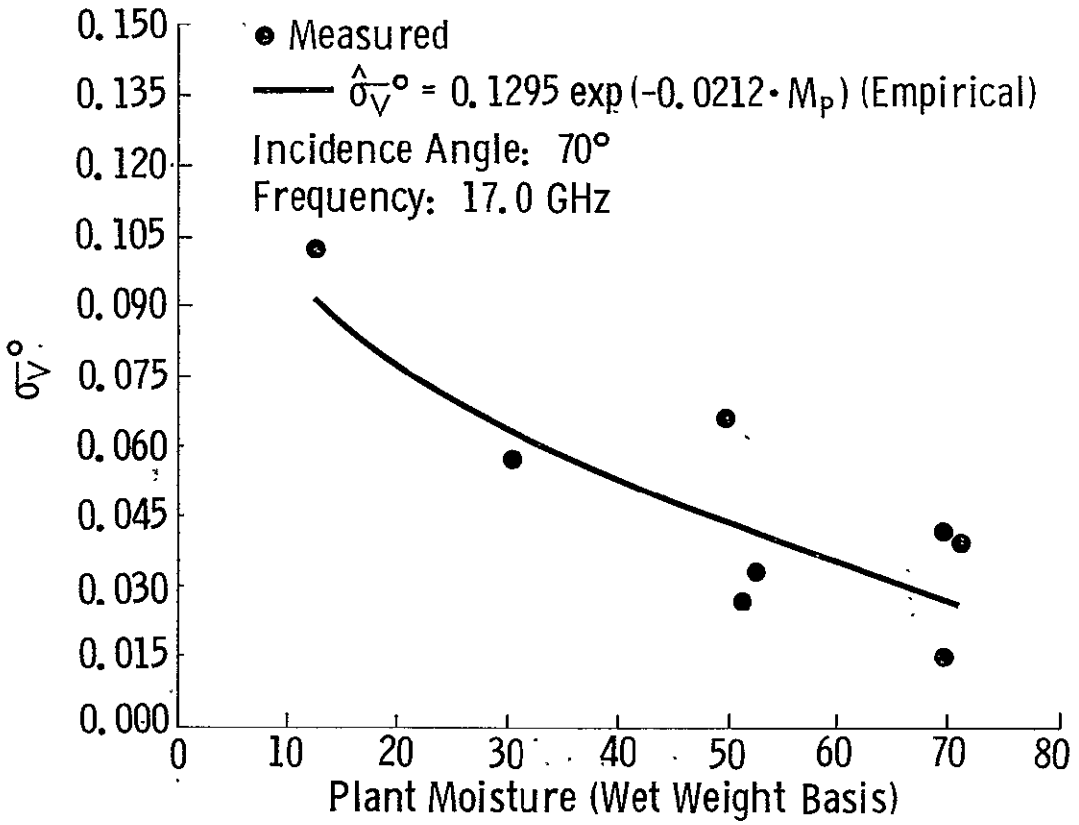

Figure 16d. Variations of σ_H° and σ_V° (real units) with plant moisture. The solid lines represent the nonlinear regression curve corresponding to the equation shown with the figure. The frequency is 17.0 GHz and the incidence angle is 70°.

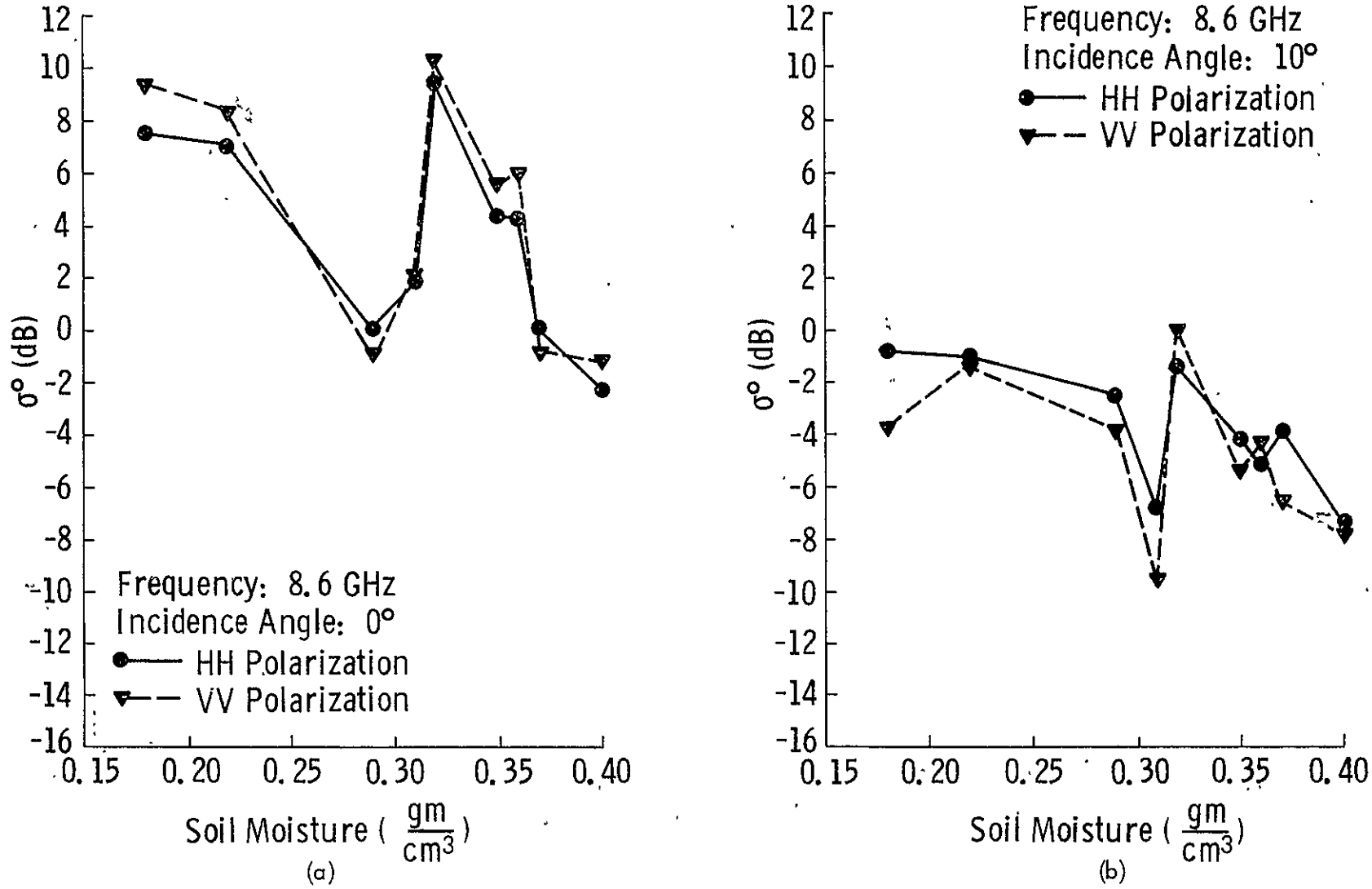

Figure 17. Measured scattering coefficient, σ° (dB), as a function of soil moisture content by volume at 8.6 GHz for angles of (a) 0°, (b) 10°, and (c) 20°.

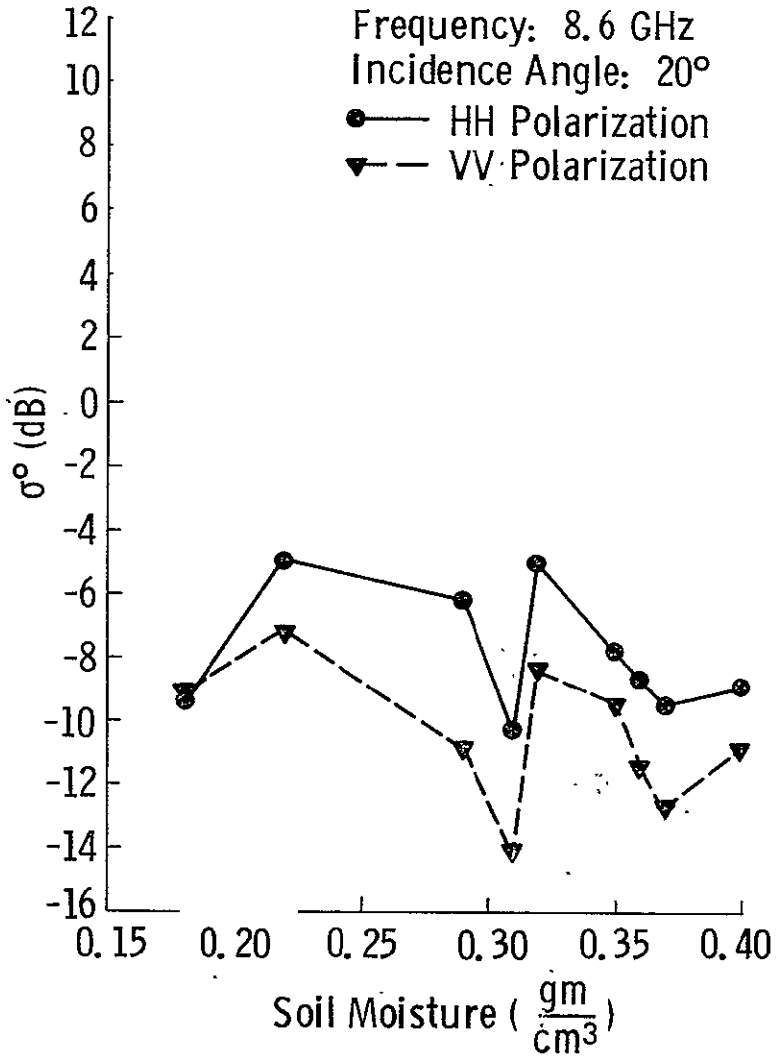
Frequency: 8.6 GHz
Incidence Angle: 20°
HH Polarization
VV Polarization
σ° (dB)
12
10
8
6
4
2
0
-2
-4
-6
-8
-10
-12
-14
-16
0.15
0.20
0.25
0.30
0.35
0.40
Soil Moisture (gm/cm3)

(17c)

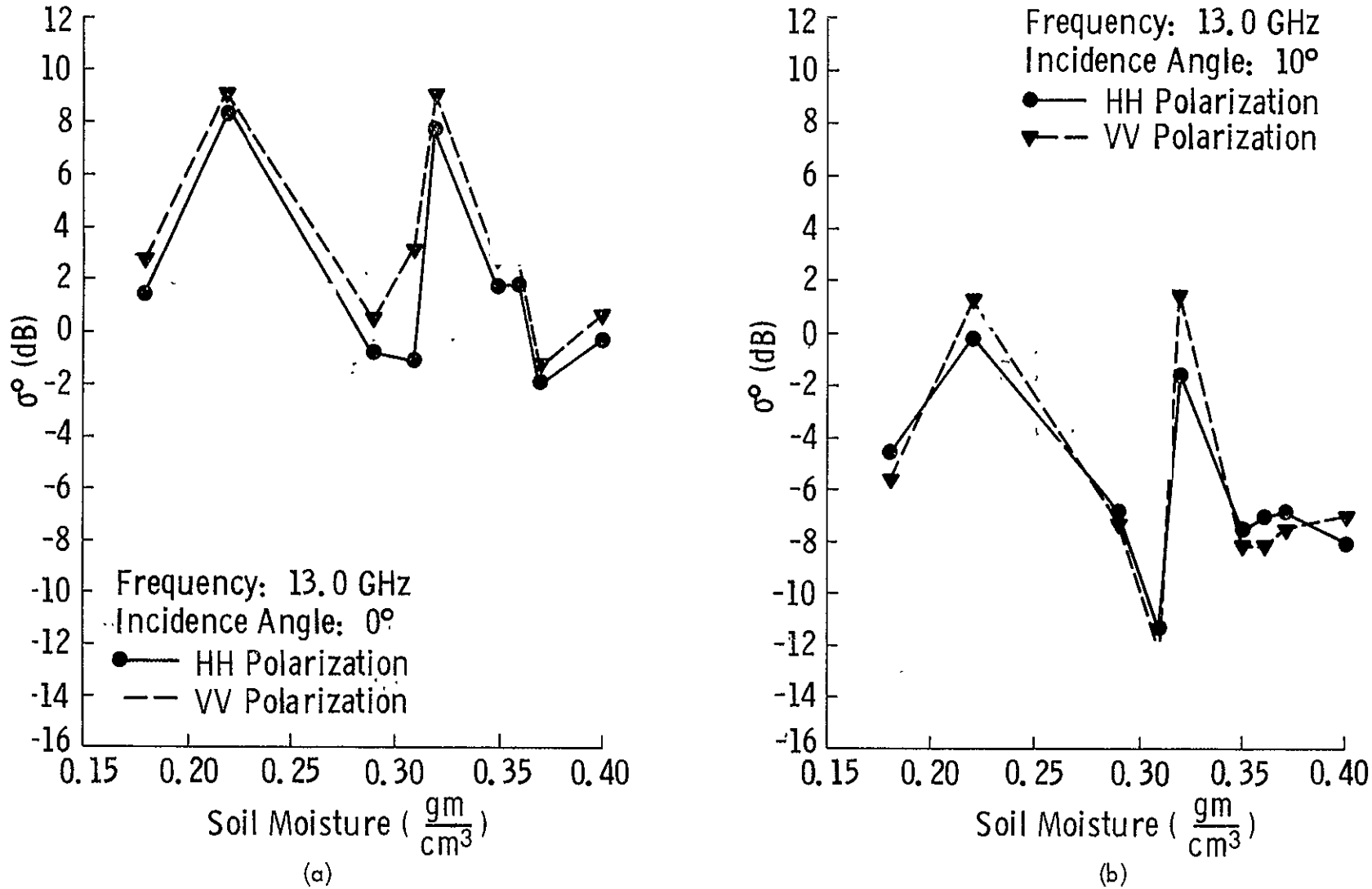

Figure 18. Measured scattering coefficient, σ° (dB), as a function of soil moisture content by volume at 13.0 GHz for angles of (a) 0°, (b) 10°, and (c) 20°

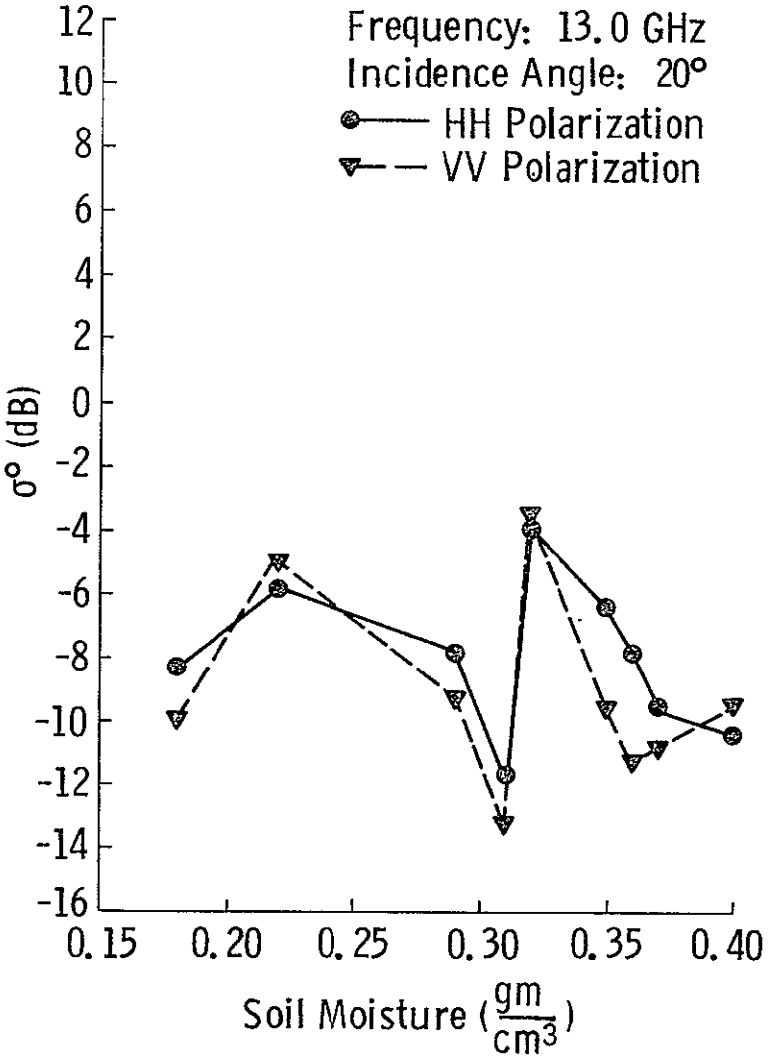
Frequency: 13.0 GHz
Incidence Angle: 20°
HH Polarization
VV Polarization
σ° (dB)
12
10
8
6
4
2
0
-2
-4
-6
-8
-10
-12
-14
-16
0.15
0.20
0.25
0.30
0.35
0.40
Soil Moisture (gm/cm3)

(18c)

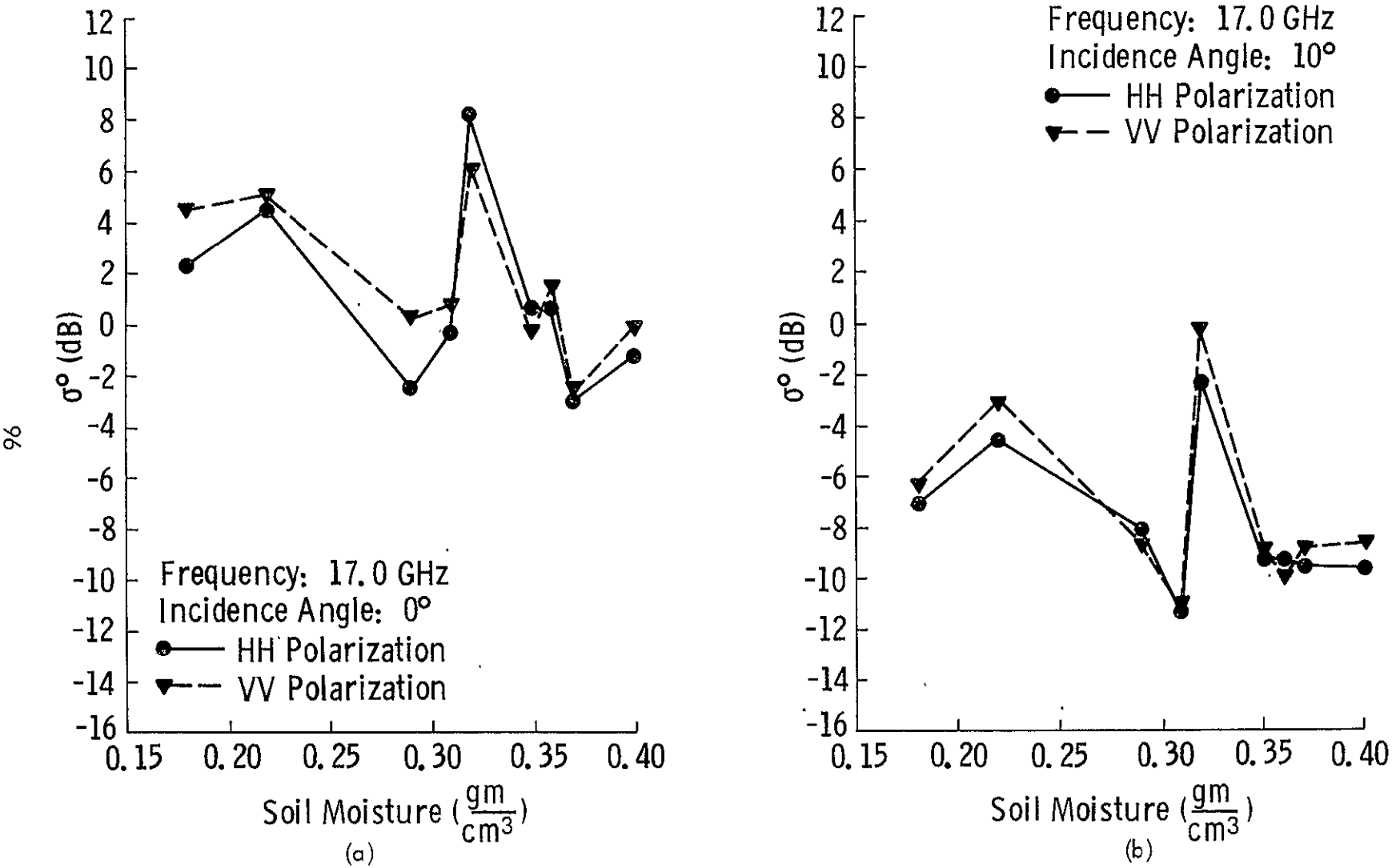

Figure 19. Measured scattering coefficient, σ^{o} (dB), as a function of soil moisture content by volume at 17.0 GHz for angles of (a) 0°, (b) 10°, (and (c) 20°.

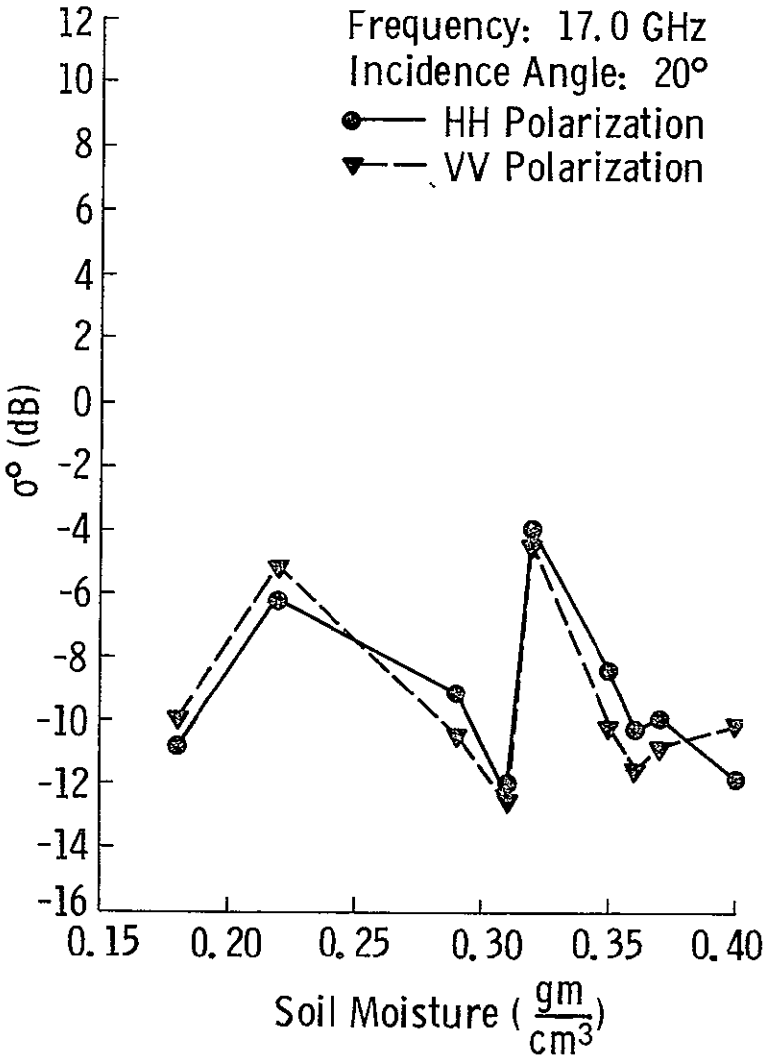
Frequency: 17.0 GHz
Incidence Angle: 20°
HH Polarization
VV Polarization
σ° (dB)
12
10
8
6
4
2
0
-2
-4
-6
-8
-10
-12
-14
-16
0.15
0.20
0.25
0.30
0.35
0.40
Soil Moisture (gm/cm3)

(19c)

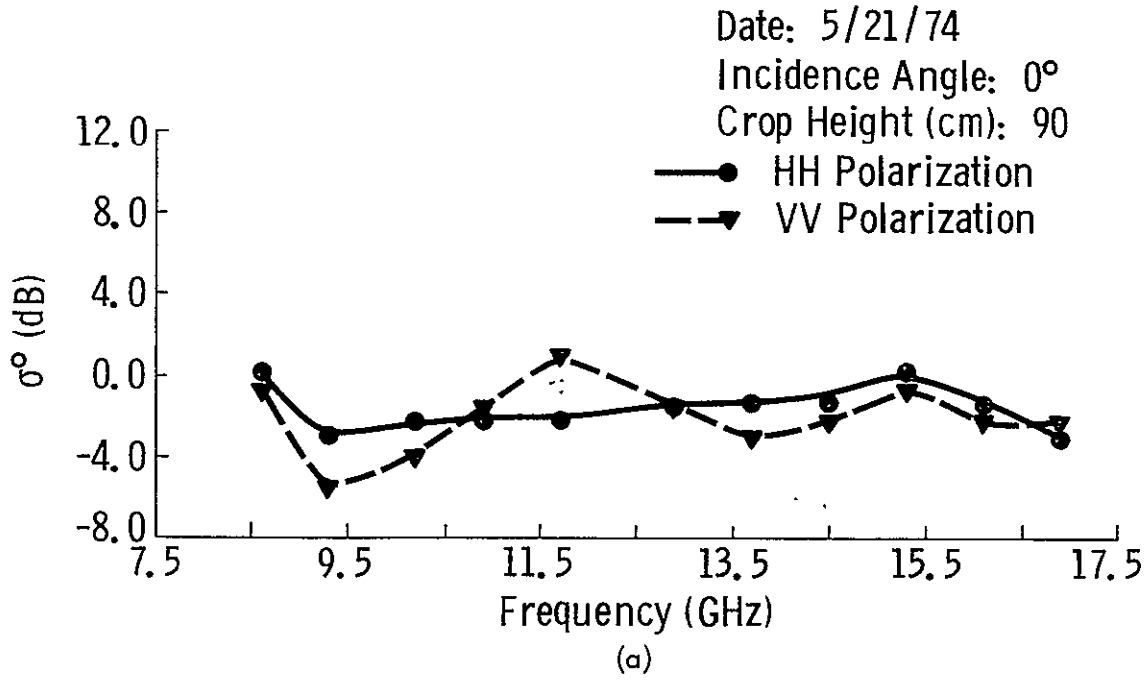

(a)

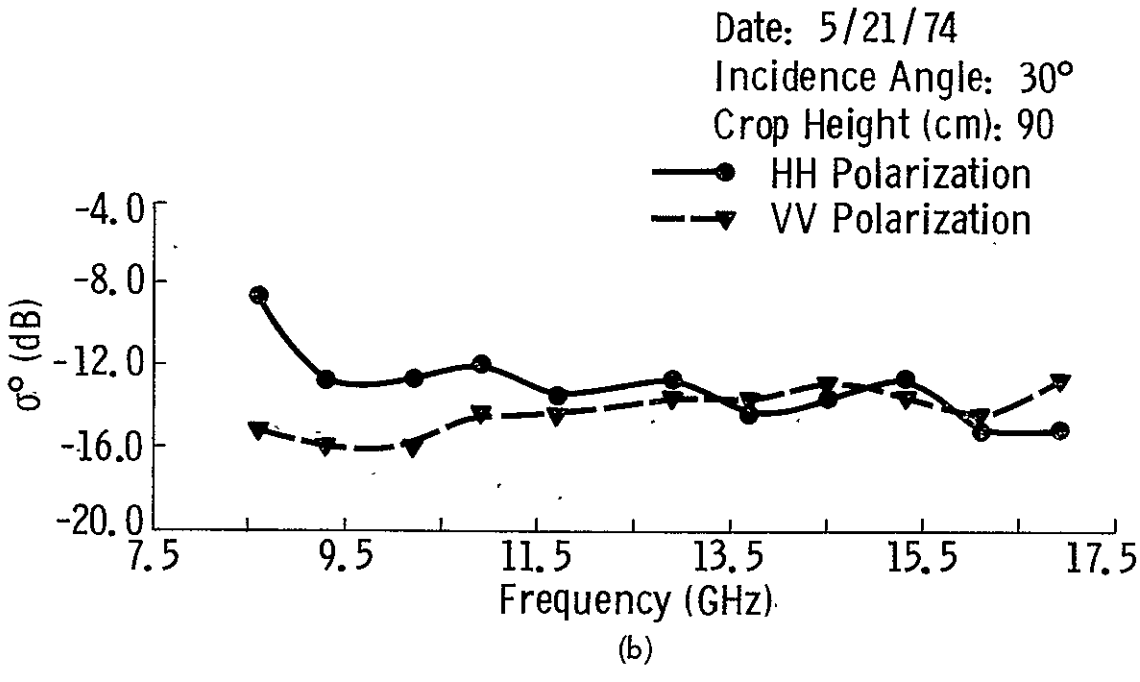

(b)

Figure 20. 8 - 18 GHz spectral response of σ_H° and σ_V° (dB) for May 21, 1974 at angles of (a) 0°, (b) 30°, (c) 50°, and (d) 70°.

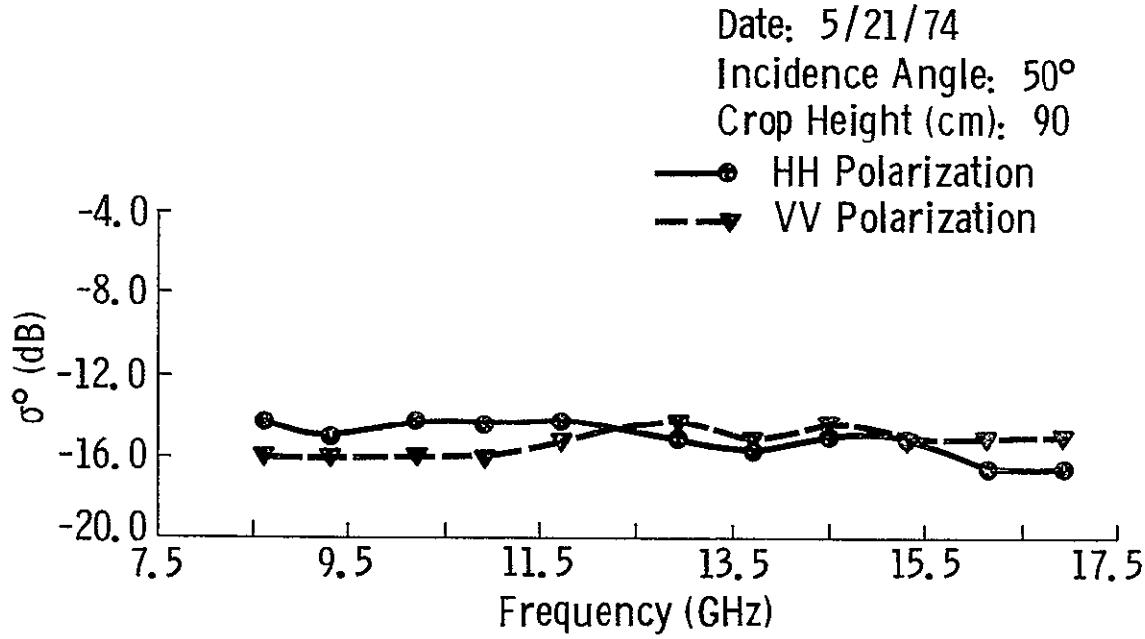
Date: 5/21/74
Incidence Angle: 50°
Crop Height (cm): 90
HH Polarization
VV Polarization
σ° (dB)
-4.0
-8.0
-12.0
-16.0
-20.0
7.5
9.5
11.5
13.5
15.5
17.5
Frequency (GHz)

(20c)

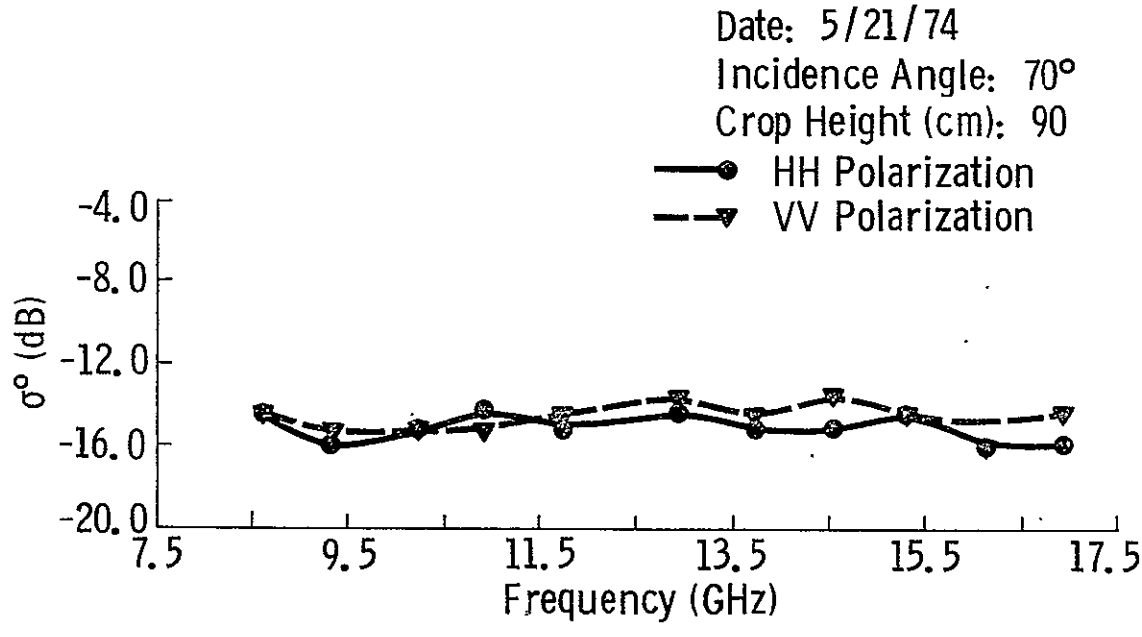
Date: 5/21/74
Incidence Angle: 70°
Crop Height (cm): 90
HH Polarization
VV Polarization
σ° (dB)
-4.0
-8.0
-12.0
-16.0
-20.0
7.5
9.5
11.5
13.5
15.5
17.5
Frequency (GHz)

(20d)

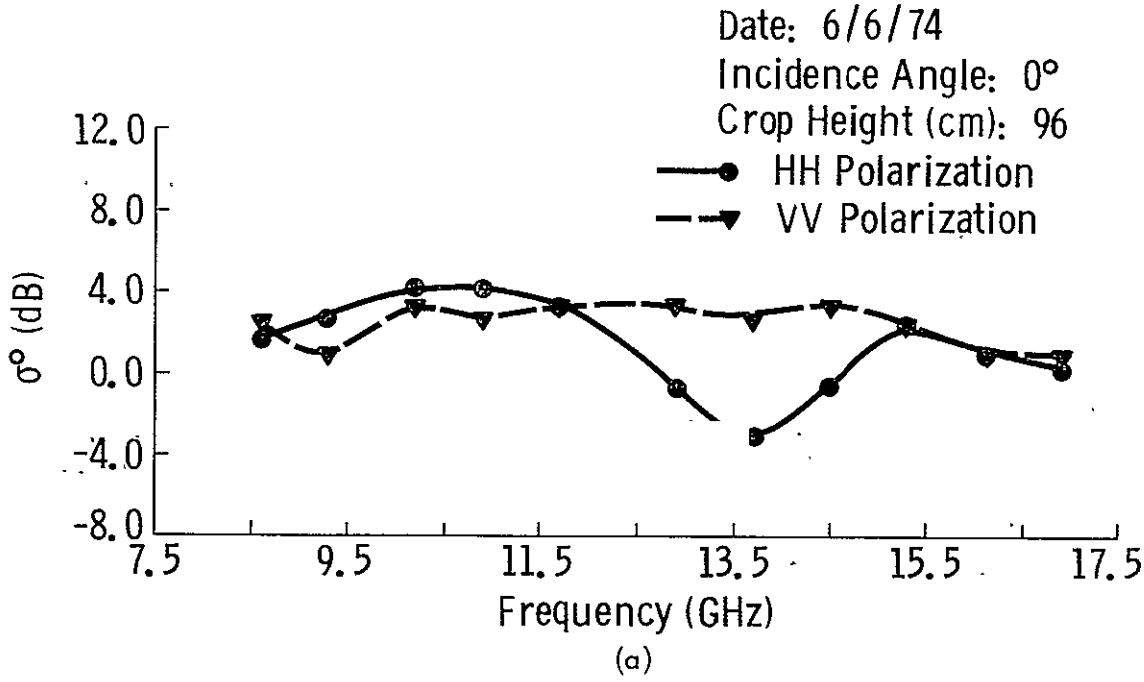

(a)

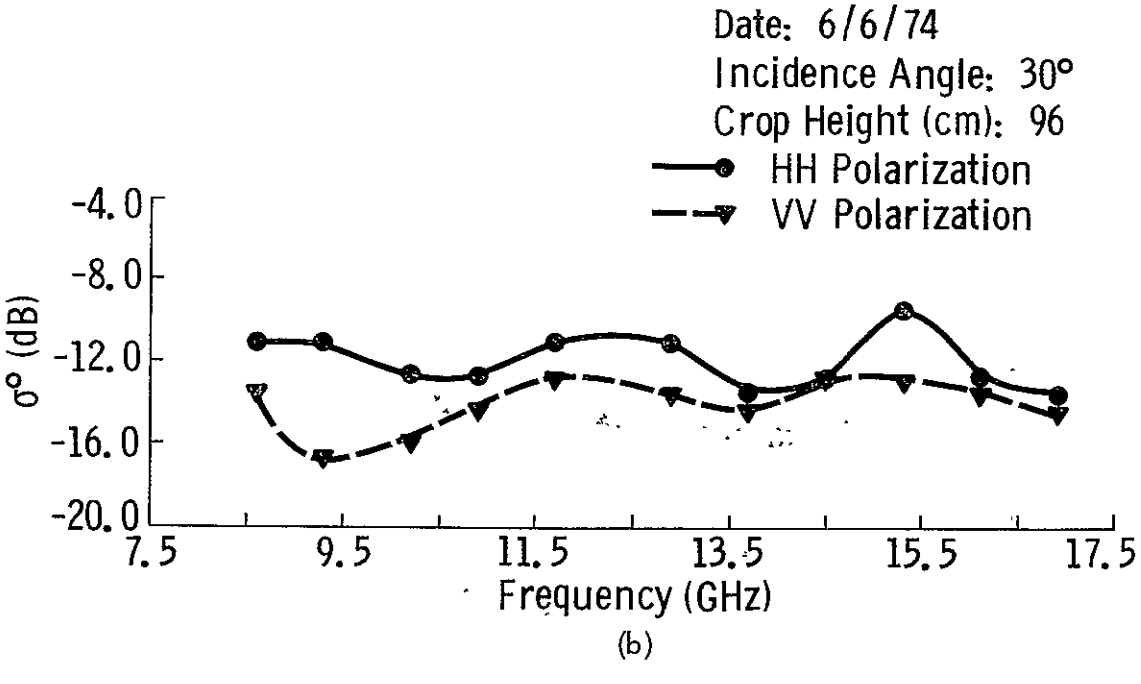

(b)

Figure 21. 8 - 18 GHz spectral response of σ_H° and σ_V° (dB) for June 6, 1974 at angles of (a) 0°, (b) 30°, (c) 50°, and (d) 70°

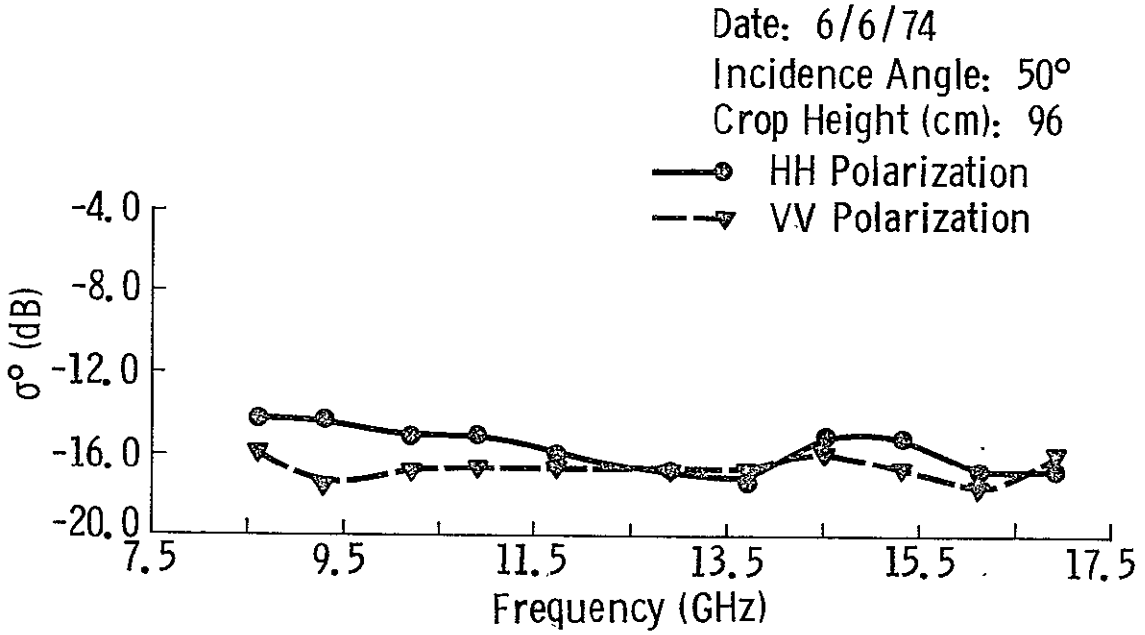
Date: 6/6/74
Incidence Angle: 50°
Crop Height (cm): 96
HH Polarization
VV Polarization
σ° (dB)
-4.0
-8.0
-12.0
-16.0
-20.0
7.5
9.5
11.5
13.5
15.5
17.5
Frequency (GHz)

(21c)

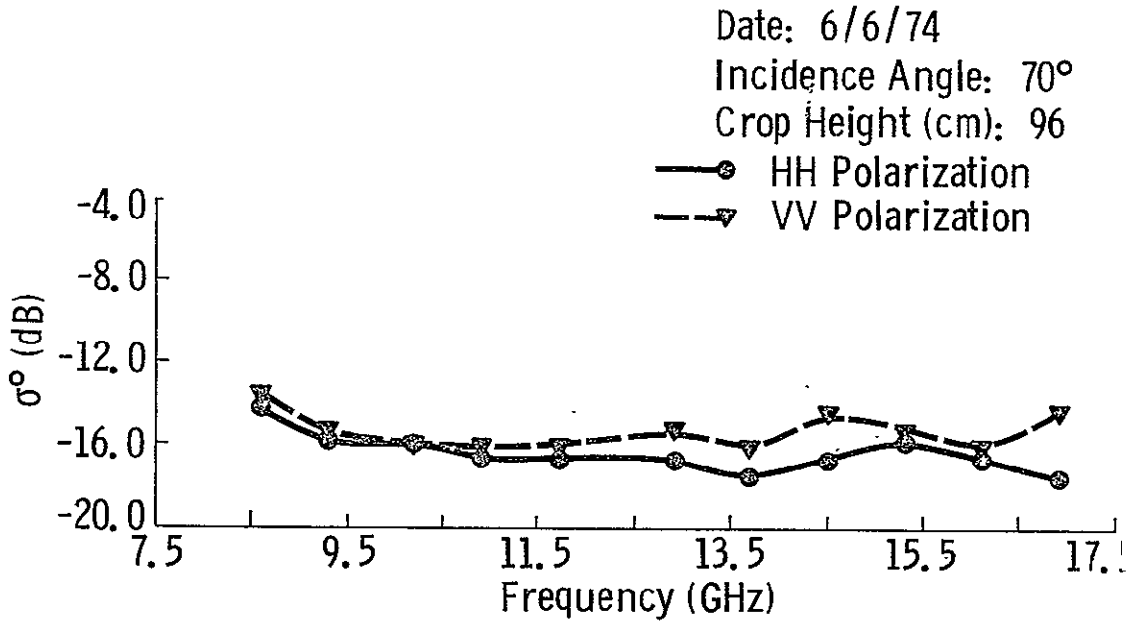
Date: 6/6/74
Incidence Angle: 70°
Crop Height (cm): 96
HH Polarization
VV Polarization
σ° (dB)
-4.0
-8.0
-12.0
-16.0
-20.0
7.5
9.5
11.5
13.5
15.5
Frequency (GHz)

(21d)

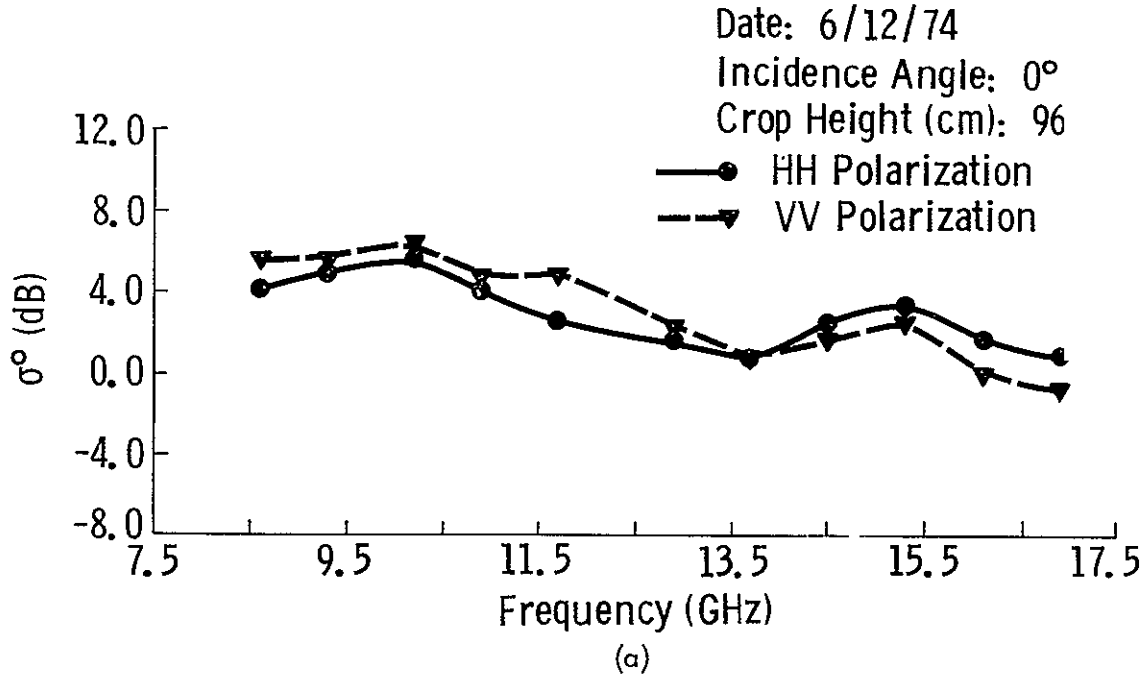

(a)

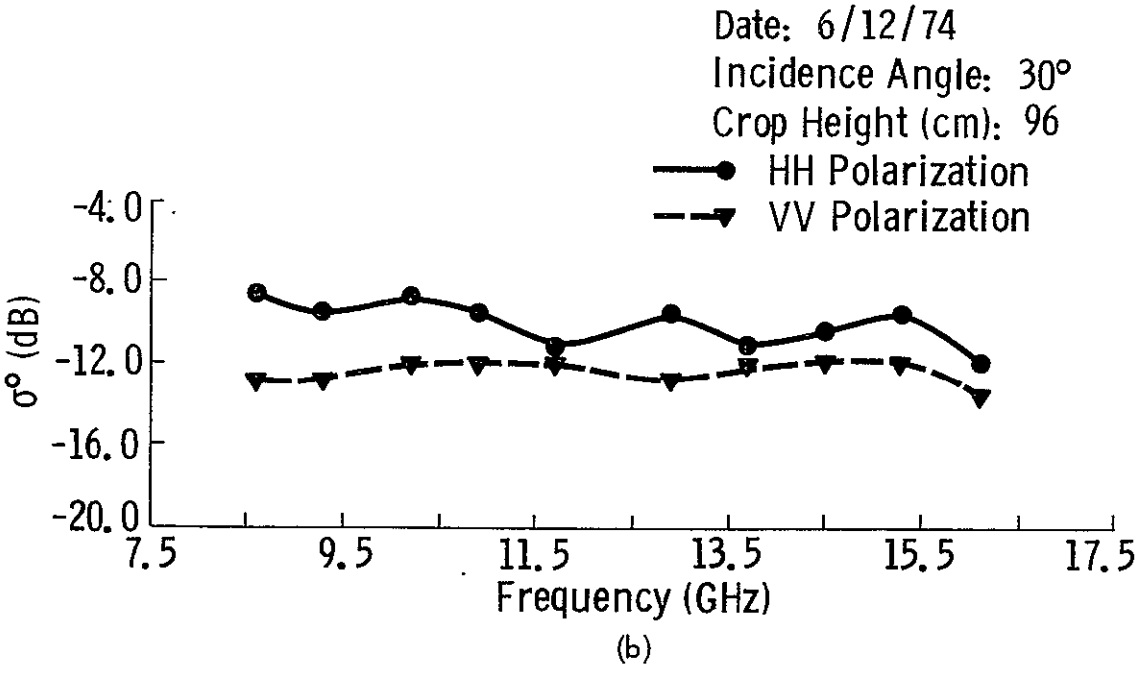

(b)

Figure 22. 8 - 18 GHz spectral response of σ_H° and σ_V° (dB) for June 12, 1974 at angles of (a) 0°, (b) 30°, (c) 50°, and (d) 70°.

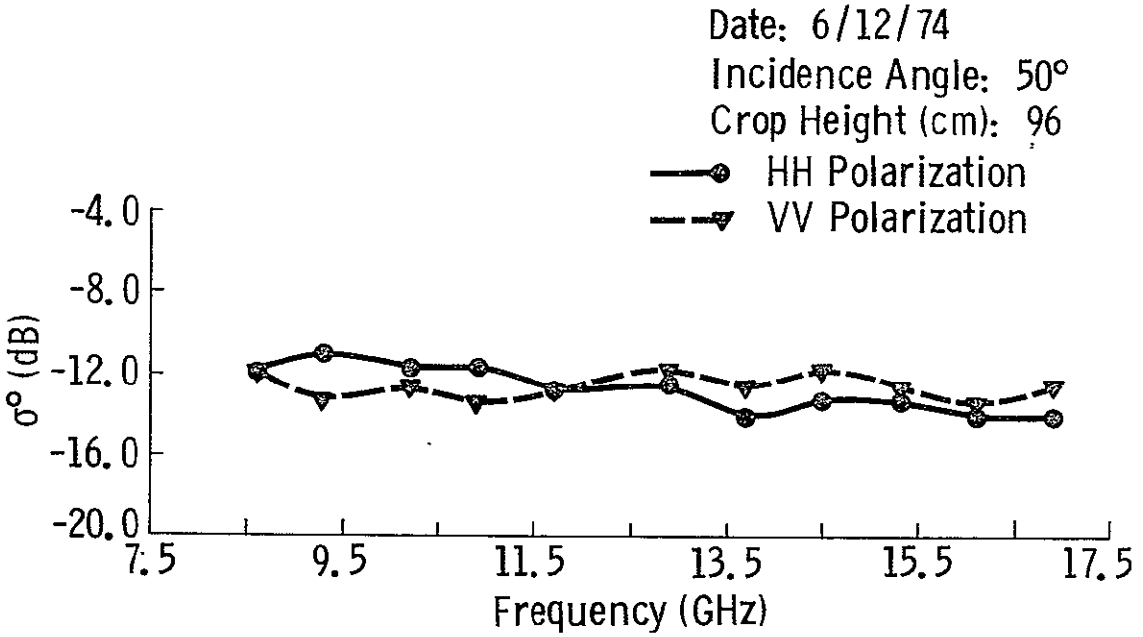
Date: 6/12/74
Incidence Angle: 50°
Crop Height (cm): 96
HH Polarization
VV Polarization
-4.0
-8.0
-12.0
-16.0
-20.0
σ° (dB)
7.5
9.5
11.5
13.5
15.5
17.5
Frequency (GHz)

(22c)

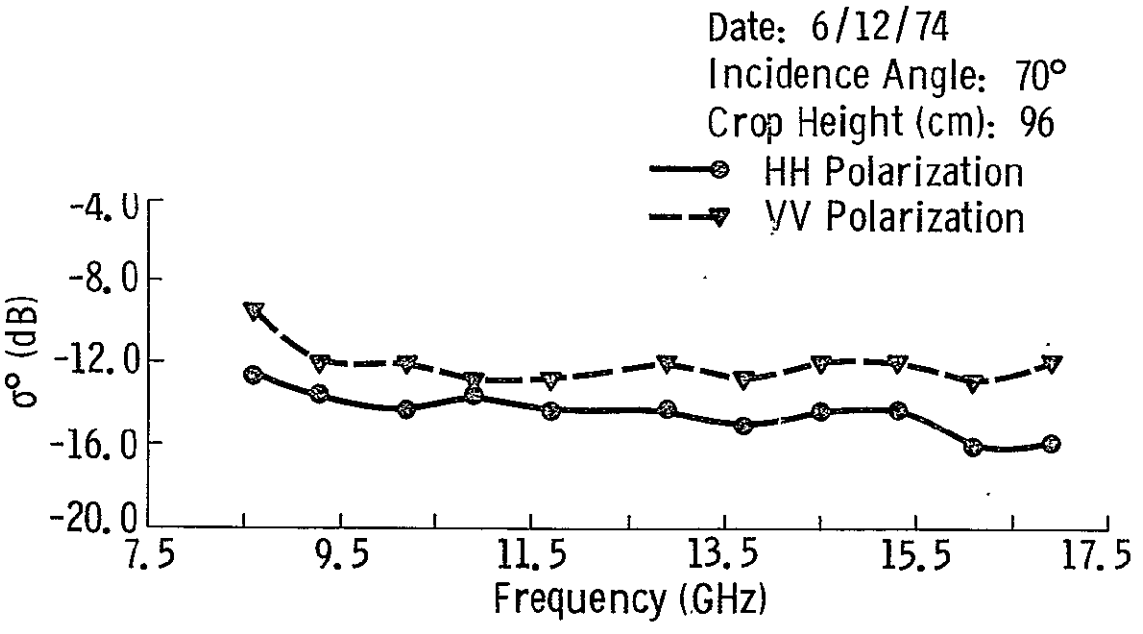
Date: 6/12/74
Incidence Angle: 70°
Crop Height (cm): 96
HH Polarization
VV Polarization
-4.0
-8.0
-12.0
-16.0
-20.0
σ° (dB)
7.5
9.5
11.5
13.5
15.5
17.5
Frequency (GHz)

(22d)

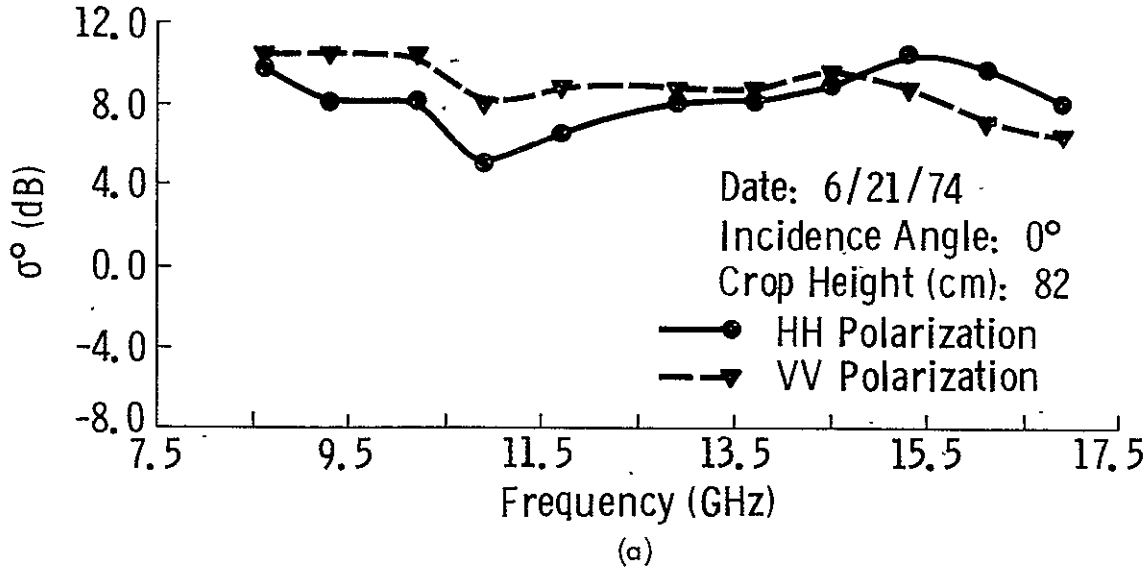

(a)

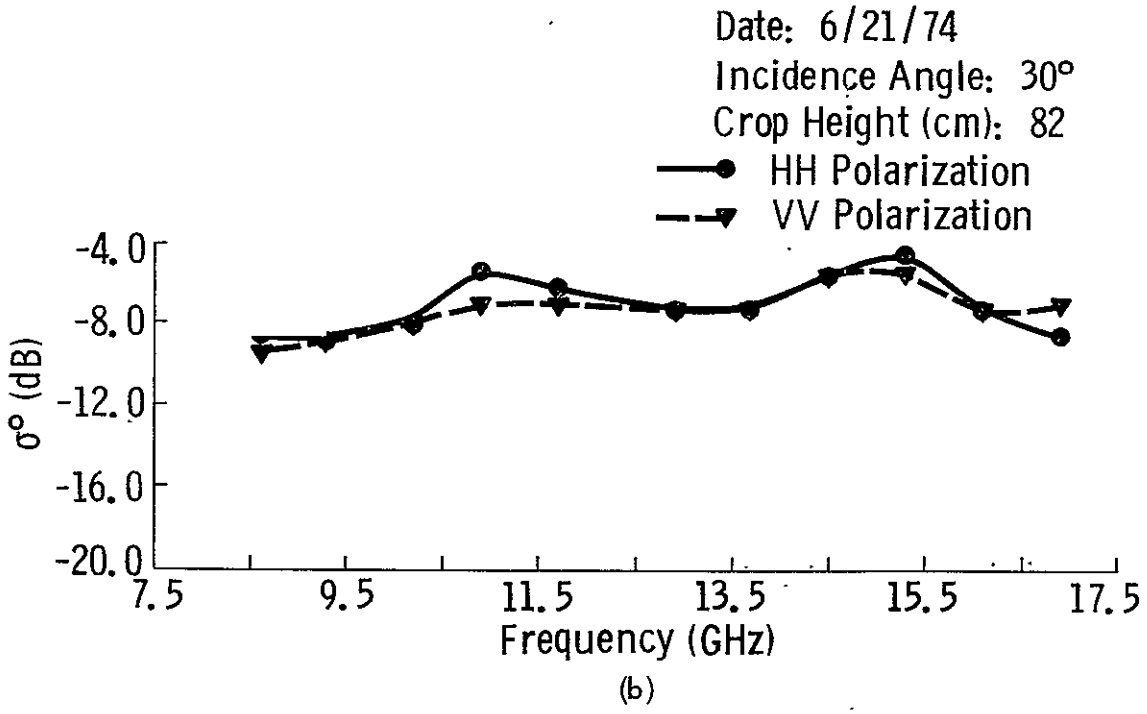

(b)

Figure 23. 8 - 18 GHz spectral response of σ_H° and σ_V° (dB) for June 21, 1974 at angles of (a) 0°, (b) 30°, (c) 50°, and (d) 70°.

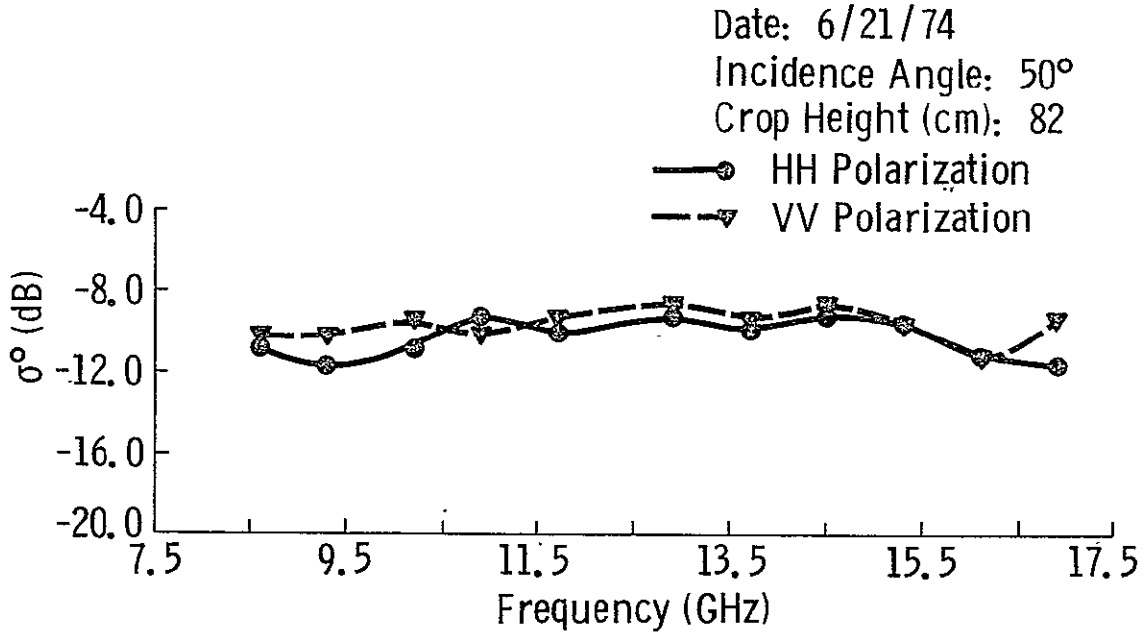
Date: 6/21/74
Incidence Angle: 50°
Crop Height (cm): 82
HH Polarization
VV Polarization
σ° (dB)
-4.0
-8.0
-12.0
-16.0
-20.0
7.5
9.5
11.5
13.5
15.5
17.5
Frequency (GHz)

(23c)

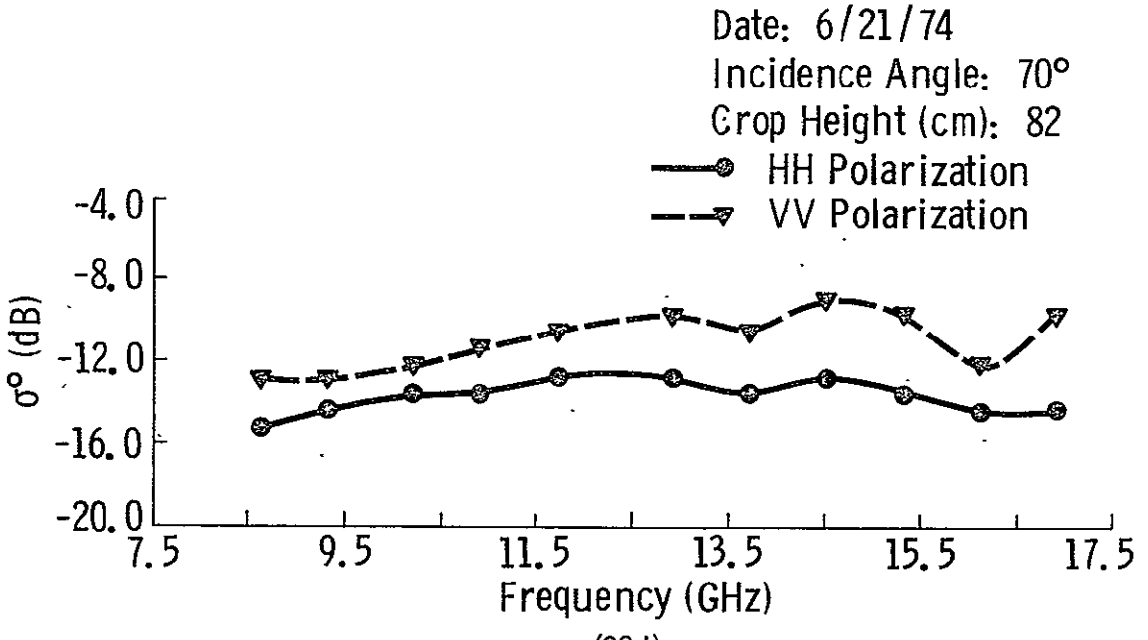
Date: 6/21/74
Incidence Angle: 70°
Crop Height (cm): 82
HH Polarization
VV Polarization
σ° (dB)
-4.0
-8.0
-12.0
-16.0
-20.0
7.5
9.5
11.5
13.5
15.5
17.5
Frequency (GHz)

(23d)

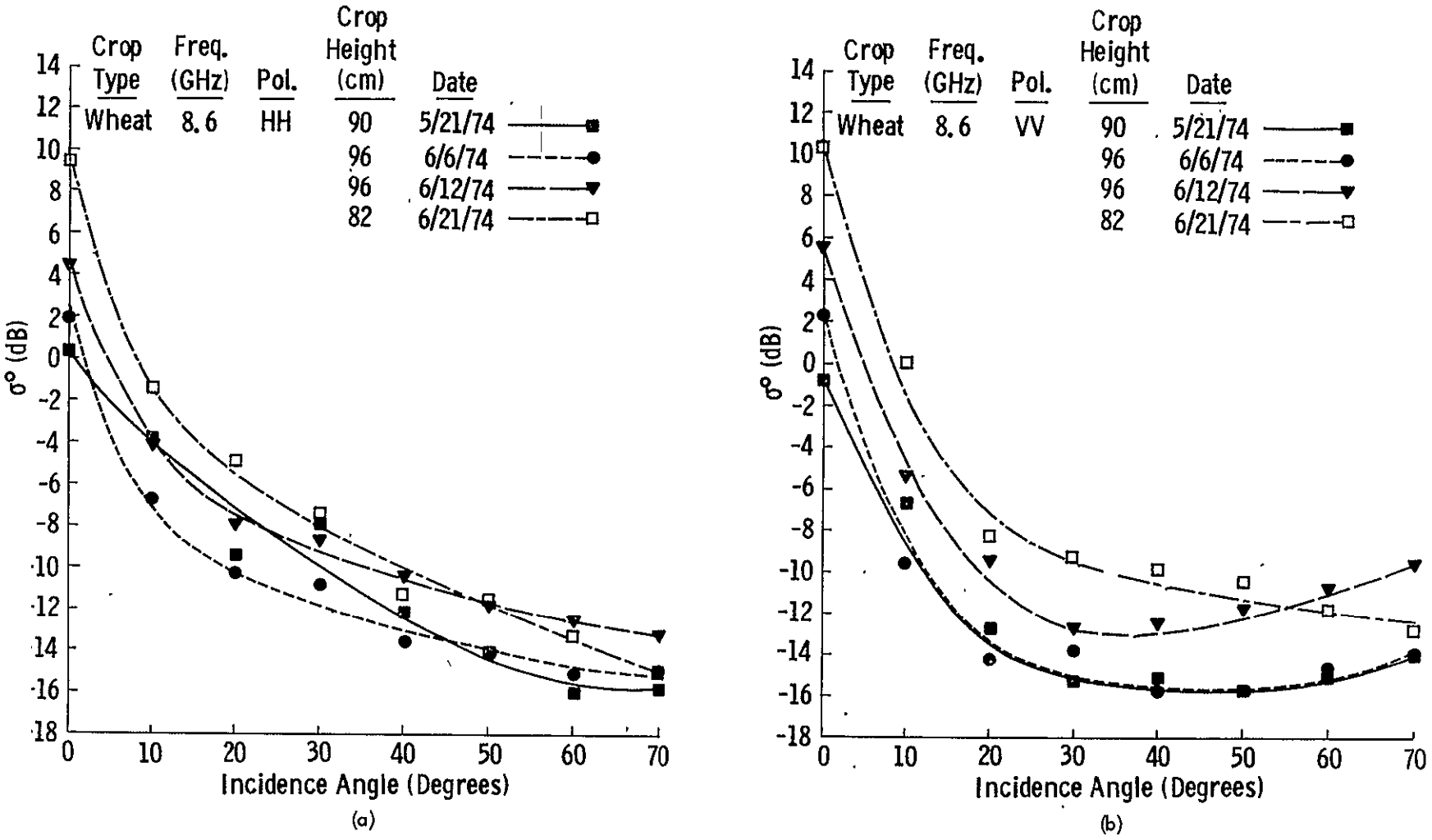

Figure 24. Angular response of (a) σ°_{H} and (b) σ°_{V} at 8.6 GHz at various stages of development.

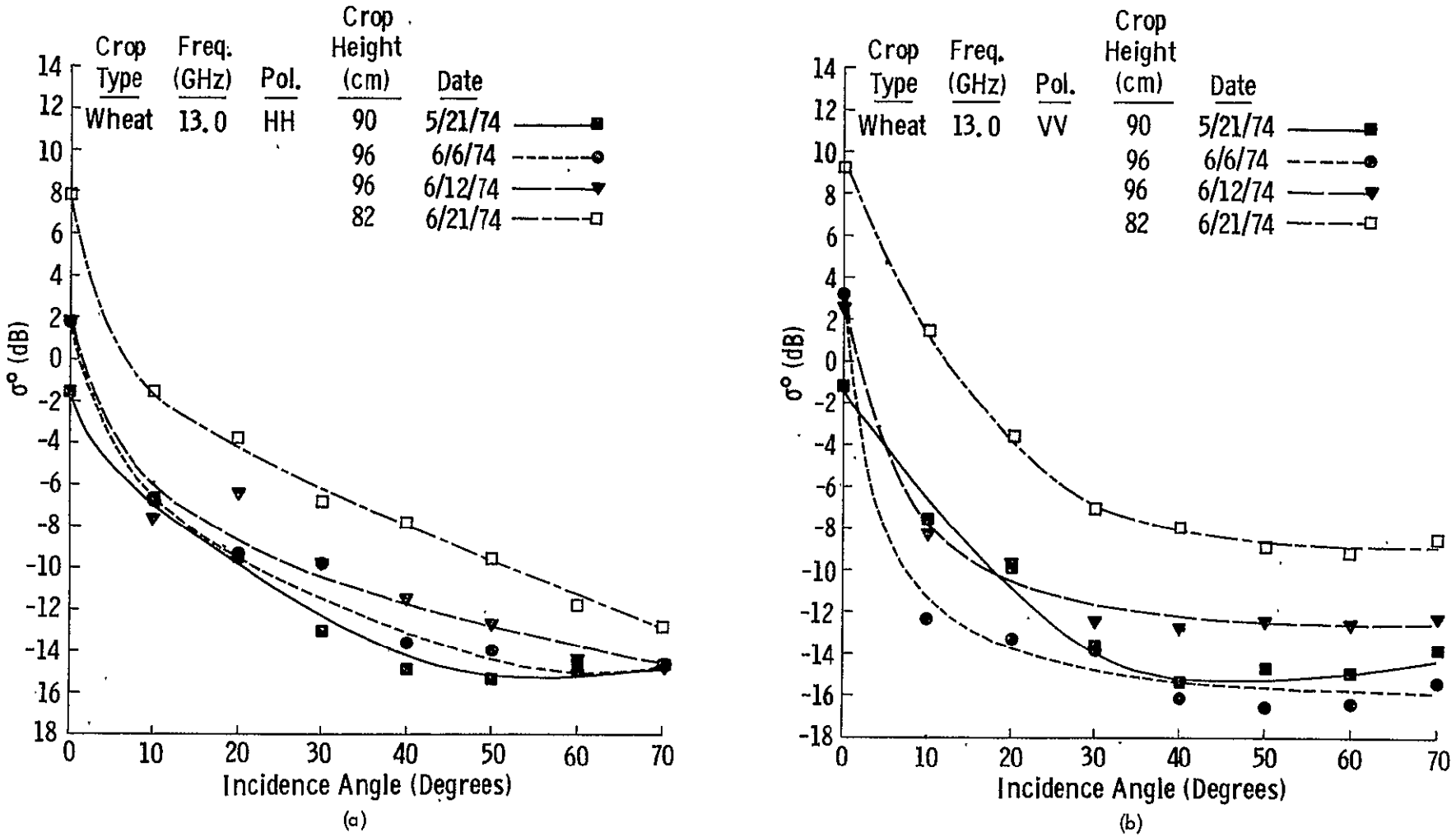

Figure 25. Angular response of (a) σ_H° and (b) σ_V° at 13.0 GHz at various stages of development.

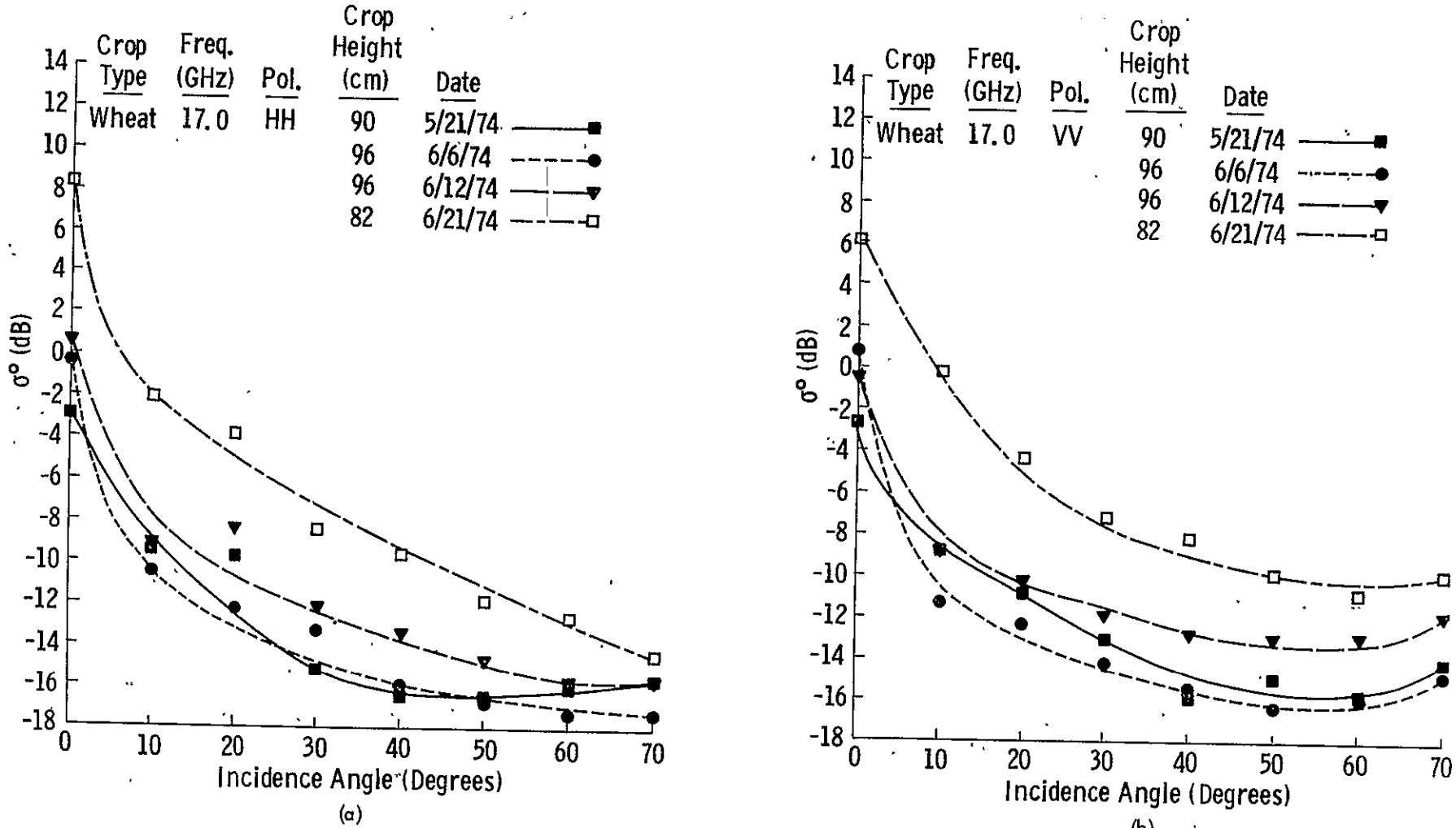

Figure 26. Angular response of (a) σ_H° and (b) σ_V° at 17.0 GHz at various stages of development.

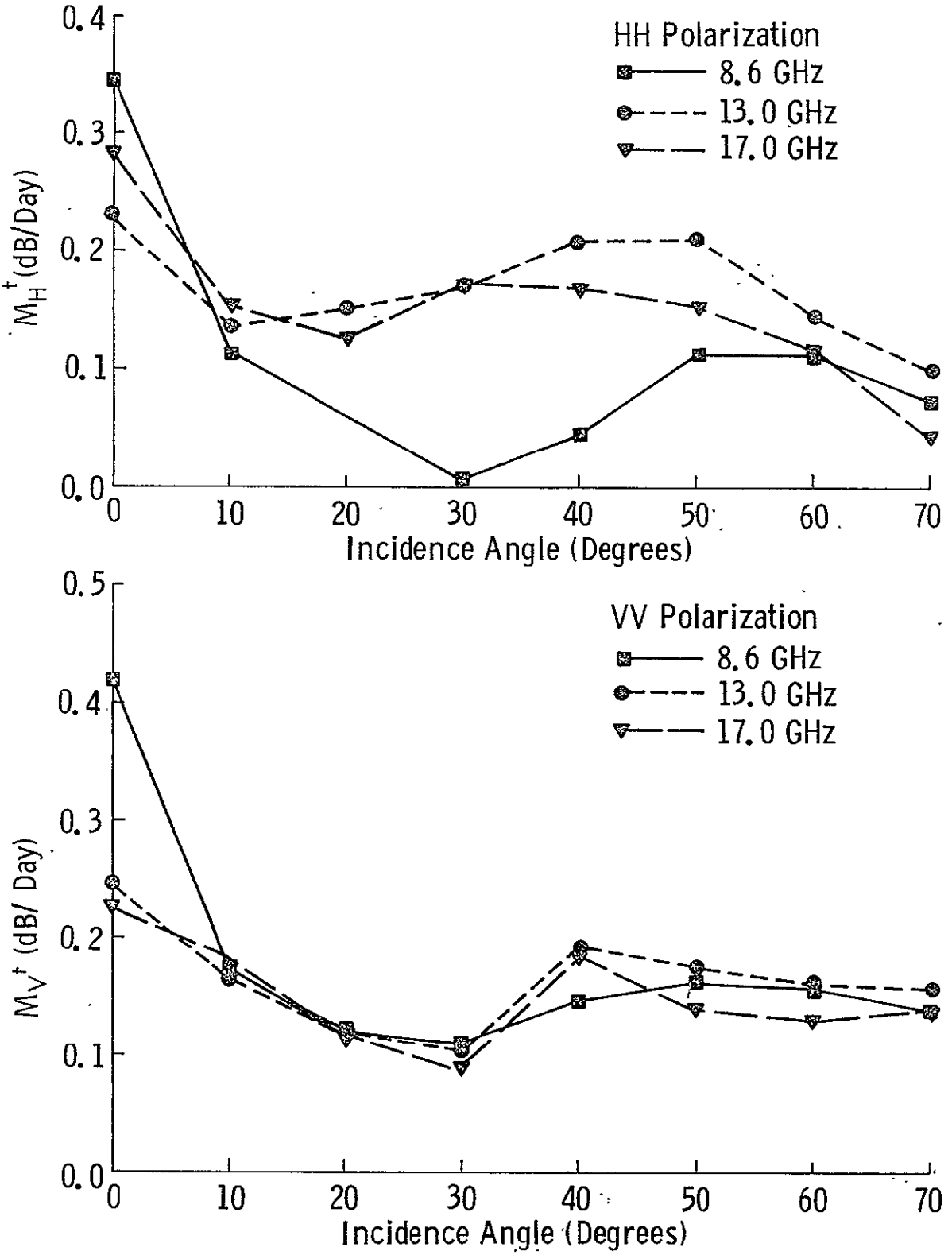

Figure 27a. Variations of M_H^t and M_V^t with angle for three frequencies. M_H^t and M_V^t are the slopes (dB/day) of regression lines obtained by regressing σ^o (dB) on time (days).

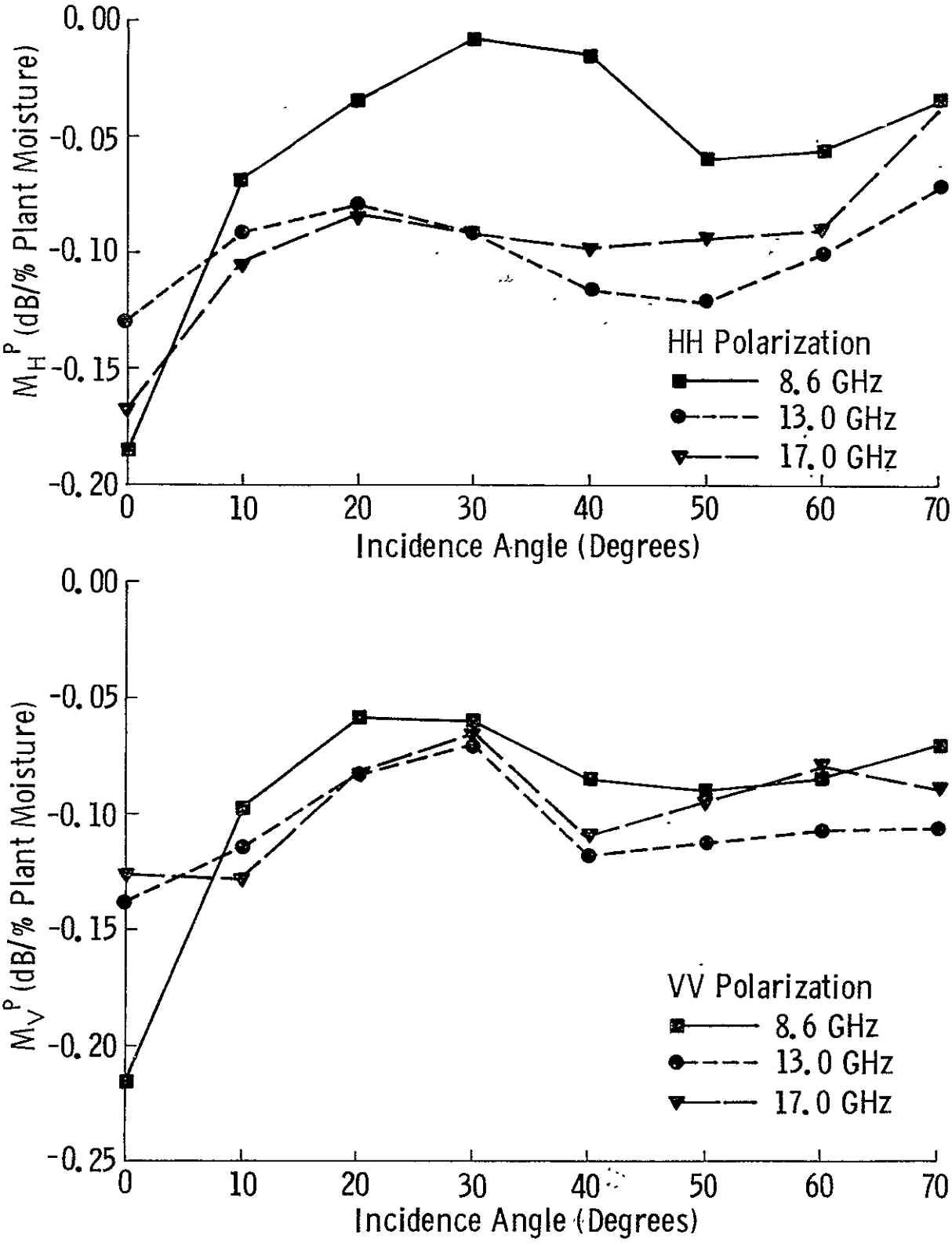

Figure 27b. Variations of M_H^P and M_V^P with angle for three frequencies. M_H^P and M_V^P are the slopes (dB/percent plant moisture) of regression lines obtained by regressing σ^o (dB) on plant moisture (wet weight basis).

APPENDIX A: Ground Truth Summary for 1974 Wheat Scattering Experiment.

WHEAT GROUND TRUTH 1974

	Soil Moisture (g/cm^3)			% Plant Moisture	Plant Height (m)
Date	N	M	F		
May 21	0.37	0.37	0.36	72	0.90
May 27	0.40	0.40	0.40	70	0.96
May 31	0.29	0.31	0.31	69	0.96
June 6	0.31	0.32	0.35	53	0.96
June 10	0.36	0.36	0.36	52	0.96
June 12	0.35	0.35	0.35	50	0.96
June 17	0.18	0.19	0.20	32	0.96
June 21	0.32	0.33	0.31	13	0.84*
June 25	0.22	0.21	0.21	11	0.32

* = wheat heads nodded

N = near range sample

M = medium range sample

F = far range sample

APPENDIX B: Wheat Scattering Coefficients, 1974.

Averaged Sigma0 Wheat, May 21, 1974

ANTENNA ANGLE 0

FREQ	8.6	9.4	10.2	11.0	11.8	13.0	13.8	14.6	15.4	16.2	17.0
POL HH	0.1	-3.3	-2.4	-2.3	-2.2	-1.9	-1.7	-1.9	0.3	-1.5	-2.9
POL VV	-0.8	-5.2	-3.6	-1.2	0.7	-1.3	-3.0	-2.2	-0.7	-2.5	-2.7

ANTENNA ANGLE 10

FREQ	8.6	9.4	10.2	11.0	11.8	13.0	13.8	14.6	15.4	16.2	17.0
POL HH	-3.9	-5.4	-6.0	-7.1	-7.6	-6.7	-7.1	-7.9	-4.8	-7.3	-9.5
POL VV	-6.7	-10.0	-10.3	-8.1	-9.0	-7.5	-8.0	-7.5	-5.6	-9.3	-8.8

ANTENNA ANGLE 20

FREQ	8.6	9.4	10.2	11.0	11.8	13.0	13.8	14.6	15.4	16.2	17.0
POL HH	-9.4	-10.5	-10.8	-8.1	-8.9	-9.5	-9.6	-10.4	-8.5	-11.1	-9.8
POL VV	-12.7	-13.6	-11.2	-12.1	-12.1	-10.7	-11.3	-11.5	-13.4	-12.4	-10.7

ANTENNA ANGLE 30

FREQ	8.6	9.4	10.2	11.0	11.8	13.0	13.8	14.6	15.4	16.2	17.0
POL HH	-8.8	-12.4	-12.4	-11.6	-13.5	-13.0	-14.1	-13.5	-12.5	-14.8	-15.2
POL VV	-15.3	-16.3	-15.7	-14.1	-14.5	-13.6	-13.4	-12.9	-13.4	-14.3	-13.0

ANTENNA ANGLE 40

FREQ	8.6	9.4	10.2	11.0	11.8	13.0	13.8	14.6	15.4	16.2	17.0
POL HH	-12.2	-13.8	-14.1	-13.9	-14.5	-14.9	-15.6	-14.6	-14.4	-16.7	-16.5
POL VV	-15.1	-17.0	-16.0	-16.1	-15.7	-15.4	-15.2	-14.8	-15.4	-16.8	-15.8

ANTENNA ANGLE 50

FREQ	8.6	9.4	10.2	11.0	11.8	13.0	13.8	14.6	15.4	16.2	17.0
POL HH	-14.0	-14.9	-14.1	-14.2	-14.5	-15.3	-16.1	-14.8	-15.3	-16.7	-16.6
POL VV	-15.7	-16.1	-15.9	-15.9	-15.2	-14.7	-15.0	-14.0	-15.1	-15.5	-14.9

ANTENNA ANGLE 60

FREQ	8.6	9.4	10.2	11.0	11.8	13.0	13.8	14.6	15.4	16.2	17.0
POL HH	-14.9	-16.0	-15.4	-15.3	-15.4	-14.6	-15.3	-14.2	-14.3	-15.9	-16.0
POL VV	-14.9	-16.1	-15.9	-15.4	-15.7	-14.9	-15.2	-13.9	-15.1	-16.4	-15.7

ANTENNA ANGLE 70

FREQ	8.6	9.4	10.2	11.0	11.8	13.0	13.8	14.6	15.4	16.2	17.0
POL HH	-14.7	-15.6	-14.9	-14.5	-15.4	-14.7	-15.5	-15.0	-14.6	-16.1	-15.7
POL VV	-14.1	-15.2	-15.0	-15.2	-14.6	-13.9	-14.1	-13.3	-14.5	-15.9	-14.1

Averaged Sigma0 Wheat, May 27, 1974

ANTENNA ANGLE 0

FREQ	8.6	9.4	10.2	11.0	11.8	13.0	13.8	14.6	15.4	16.2	17.0
POL HH	-2.1	-5.7	-2.9	-1.2	0.4	-0.2	1.1	1.1	0.4	-0.7	-1.1
POL VV	-1.1	-4.9	-1.8	-1.9	0.3	0.6	1.2	2.0	0.6	-0.2	0.1

ANTENNA ANGLE 10

FREQ	8.6	9.4	10.2	11.0	11.8	13.0	13.8	14.6	15.4	16.2	17.0
POL HH	-7.3	-7.1	-7.7	-7.5	-8.3	-8.0	-9.5	-8.2	-7.4	-9.9	-9.6
POL VV	-7.6	-8.2	-8.4	-10.1	-8.9	-7.0	-7.2	-8.8	-7.6	-8.0	-8.6

ANTENNA ANGLE 20

FREQ	8.6	9.4	10.2	11.0	11.8	13.0	13.8	14.6	15.4	16.2	17.0
POL HH	-8.9	-11.1	-10.3	-9.7	-10.4	-10.3	-10.3	-9.4	-9.6	-11.4	-11.7
POL VV	-10.8	-11.3	-12.1	-10.7	-10.8	-9.4	-8.7	-8.0	-9.9	-9.8	-10.0

ANTENNA ANGLE 30

FREQ	8.6	9.4	10.2	11.0	11.8	13.0	13.8	14.6	15.4	16.2	17.0
POL HH	-10.0	-11.1	-11.5	-11.7	-12.3	-12.2	-12.7	-11.3	-11.0	-12.1	-12.0
POL VV	-11.7	-12.8	-11.9	-11.2	-11.4	-11.3	-11.1	-10.2	-10.3	-12.3	-11.3

ANTENNA ANGLE 40

FREQ	8.6	9.4	10.2	11.0	11.8	13.0	13.8	14.6	15.4	16.2	17.0
POL HH	-12.2	-13.2	-12.7	-14.6	-15.0	-14.5	-14.8	-14.2	-12.9	-15.4	-14.7
POL VV	-13.5	-13.9	-13.5	-14.2	-13.3	-13.6	-14.0	-12.7	-13.3	-15.2	-14.0

ANTENNA ANGLE 50

FREQ	8.6	9.4	10.2	11.0	11.8	13.0	13.8	14.6	15.4	16.2	17.0
POL HH	-15.2	-15.2	-15.6	-15.7	-16.5	-16.7	-17.6	-15.8	-15.9	-16.8	-15.9
POL VV	-14.3	-16.1	-16.3	-16.2	-15.5	-15.1	-15.2	-14.3	-14.7	-15.7	-14.4

ANTENNA ANGLE 60

FREQ	8.6	9.4	10.2	11.0	11.8	13.0	13.8	14.6	15.4	16.2	17.0
POL HH	-15.9	-17.1	-17.1	-16.5	-16.7	-17.1	-17.3	-15.7	-15.6	-17.0	-17.2
POL VV	-15.0	-16.0	-15.4	-15.8	-15.4	-14.4	-15.9	-14.9	-15.7	-16.4	-14.9

ANTENNA ANGLE 70

FREQ	8.6	9.4	10.2	11.0	11.8	13.0	13.8	14.6	15.4	16.2	17.0
POL HH	-16.1	-16.9	-16.6	-16.2	-16.0	-15.5	-16.5	-15.1	-15.1	-16.2	-16.7
POL VV	-14.2	-15.8	-15.3	-15.2	-15.0	-14.4	-14.7	-13.6	-13.6	-14.6	-13.7

Averaged Sigma0 Wheat, May 31, 1974

ANTENNA ANGLE 0

FREQ	8.6	9.4	10.2	11.0	11.8	13.0	13.8	14.6	15.4	16.2	17.0
POL HH	0.	-3.2	-3.9	-3.9	-2.5	-0.7	-0.4	-0.4	1.2	-1.0	-2.4
POL VV	-1.0	-2.9	-3.3	-2.4	-1.3	0.5	-0.6	1.0	-0.5	-0.5	0.3

ANTENNA ANGLE 10

FREQ	8.6	9.4	10.2	11.0	11.8	13.0	13.8	14.6	15.4	16.2	17.0
POL HH	-2.4	-5.5	-6.3	-4.1	-5.6	-6.8	-7.9	-6.3	-6.3	-8.6	-8.0
POL VV	-3.8	-5.9	-6.9	-6.0	-7.8	-7.2	-6.7	-5.7	-6.5	-8.6	-8.6

ANTENNA ANGLE 20

FREQ	8.6	9.4	10.2	11.0	11.8	13.0	13.8	14.6	15.4	16.2	17.0
POL HH	-6.1	-8.3	-8.0	-9.0	-8.2	-7.7	-9.2	-8.2	-6.6	-8.9	-9.1
POL VV	-10.8	-11.7	-10.8	-11.6	-9.0	-9.2	-9.8	-9.4	-9.5	-11.1	-10.4

ANTENNA ANGLE 30

FREQ	8.6	9.4	10.2	11.0	11.8	13.0	13.8	14.6	15.4	16.2	17.0
POL HH	-9.7	-9.7	-10.2	-10.8	-11.3	-11.7	-12.7	-12.2	-10.4	-12.2	-13.1
POL VV	-12.7	-14.6	-13.5	-13.9	-12.8	-12.4	-13.5	-12.4	-12.2	-13.7	-12.4

ANTENNA ANGLE 40

FREQ	8.6	9.4	10.2	11.0	11.8	13.0	13.8	14.6	15.4	16.2	17.0
POL HH	-11.2	-12.8	-12.6	-12.7	-13.2	-14.1	-15.1	-14.1	-13.7	-15.7	-15.3
POL VV	-15.2	-16.3	-16.6	-16.6	-16.5	-15.8	-15.7	-13.1	-15.1	-16.5	-14.3

ANTENNA ANGLE 50

FREQ	8.6	9.4	10.2	11.0	11.8	13.0	13.8	14.6	15.4	16.2	17.0
POL HH	-14.5	-15.3	-15.2	-16.2	-17.0	-16.8	-18.0	-17.0	-16.2	-18.8	-18.0
POL VV	-17.6	-18.9	-18.8	-18.6	-18.3	-17.4	-18.6	-17.2	-18.0	-19.0	-17.6

ANTENNA ANGLE 60

FREQ	8.6	9.4	10.2	11.0	11.8	13.0	13.8	14.6	15.4	16.2	17.0
POL HH	-17.1	-19.1	-19.3	-19.4	-20.2	-19.7	-20.9	-19.4	-19.9	-21.0	-20.7
POL VV	-19.0	-20.3	-20.3	-19.8	-19.6	-19.1	-16.6	-18.6	-19.8	-20.8	-16.0

ANTENNA ANGLE 70

FREQ	8.6	9.4	10.2	11.0	11.8	13.0	13.8	14.6	15.4	16.2	17.0
POL HH	-18.4	-19.4	-19.9	-19.6	-19.9	-19.7	-21.0	-19.7	-20.3	-20.6	-17.9
POL VV	-19.1	-20.7	-20.3	-19.5	-19.6	-18.4	-19.4	-18.1	-19.3	-19.9	-18.4

Averaged Sigma0 Wheat, June 6, 1974

ANTENNA ANGLE 0

FREQ	8.6	9.4	10.2	11.0	11.8	13.0	13.8	14.6	15.4	16.2	17.0
POL HH	1.9	2.1	4.0	3.7	3.0	-1.0	-2.8	-0.7	2.7	0.9	-0.2
POL VV	2.2	0.9	3.2	2.3	3.1	3.2	2.1	3.4	2.7	0.6	0.8

ANTENNA ANGLE 10

FREQ	8.6	9.4	10.2	11.0	11.8	13.0	13.8	14.6	15.4	16.2	17.0
POL HH	-6.9	-8.0	-6.5	-6.0	-10.1	-11.5	-9.9	-8.5	-10.3	-11.1	-11.4
POL VV	-9.6	-11.5	-12.7	-9.3	-13.4	-12.3	-12.1	-10.6	-11.2	-12.9	-11.2

ANTENNA ANGLE 20

FREQ	8.6	9.4	10.2	11.0	11.8	13.0	13.8	14.6	15.4	16.2	17.0
POL HH	-10.3	-10.8	-8.3	-9.3	-8.7	-11.7	-12.5	-9.1	-9.4	-11.0	-12.2
POL VV	-14.3	-14.7	-13.0	-13.7	-12.9	-13.3	-13.9	-11.5	-12.3	-12.6	-12.3

ANTENNA ANGLE 30

FREQ	8.6	9.4	10.2	11.0	11.8	13.0	13.8	14.6	15.4	16.2	17.0
POL HH	-10.9	-11.0	-12.6	-12.4	-10.9	-11.4	-13.3	-12.4	-9.9	-13.0	-13.2
POL VV	-13.8	-16.6	-15.6	-14.4	-12.7	-13.5	-14.4	-12.7	-13.1	-13.8	-14.2

ANTENNA ANGLE 40

FREQ	8.6	9.4	10.2	11.0	11.8	13.0	13.8	14.6	15.4	16.2	17.0
POL HH	-13.5	-14.7	-14.5	-14.6	-15.6	-15.5	-15.2	-14.5	-14.1	-15.5	-16.0
POL VV	-15.8	-17.2	-17.4	-17.5	-17.1	-16.2	-17.3	-14.5	-15.6	-17.3	-15.5

ANTENNA ANGLE 50

FREQ	8.6	9.4	10.2	11.0	11.8	13.0	13.8	14.6	15.4	16.2	17.0
POL HH	-14.9	-14.2	-15.5	-15.5	-15.6	-16.9	-17.2	-15.4	-15.4	-16.9	-16.8
POL VV	-15.6	-17.5	-17.0	-16.9	-16.9	-16.5	-17.0	-15.6	-16.7	-17.5	-16.2

ANTENNA ANGLE 60

FREQ	8.6	9.4	10.2	11.0	11.8	13.0	13.8	14.6	15.4	16.2	17.0
POL HH	-15.1	-15.7	-15.2	-16.7	-15.9	-17.3	-18.0	-17.0	-16.1	-17.9	-17.3
POL VV	-14.6	-16.7	-16.3	-16.9	-16.7	-16.3	-14.0	-12.7	-13.2	-17.3	-16.1

ANTENNA ANGLE 70

FREQ	8.6	9.4	10.2	11.0	11.8	13.0	13.8	14.6	15.4	16.2	17.0
POL HH	-14.7	-16.0	-15.8	-16.4	-16.5	-16.6	-17.9	-16.4	-16.3	-16.9	-17.3
POL VV	-13.9	-15.5	-16.1	-16.2	-15.9	-15.3	-15.9	-14.3	-14.9	-15.9	-14.7

Averaged Sigma0 Wheat, June 10, 1974

ANTENNA ANGLE 0

FREQ	8.6	9.4	10.2	11.0	11.8	13.0	13.8	14.6	15.4	16.2	17.0
POL HH	4.4	2.9	2.4	1.6	2.6	1.9	1.0	1.3	3.6	2.4	0.8
POL VV	6.1	3.6	3.1	2.7	1.9	2.9	3.3	3.8	4.7	2.2	1.6

ANTENNA ANGLE 10

FREQ	8.6	9.4	10.2	11.0	11.8	13.0	13.8	14.6	15.4	16.2	17.0
POL HH	-5.1	-7.1	-7.7	-8.0	-7.8	-7.0	-9.4	-8.1	-6.5	-7.6	-9.1
POL VV	-4.3	-6.5	-8.1	-8.5	-8.8	-8.3	-8.4	-8.1	-8.2	-9.3	-9.9

ANTENNA ANGLE 20

FREQ	8.6	9.4	10.2	11.0	11.8	13.0	13.8	14.6	15.4	16.2	17.0
POL HH	-8.6	-9.5	-9.0	-8.2	-8.8	-7.6	-8.2	-8.5	-7.6	-9.2	-10.1
POL VV	-11.4	-11.8	-10.9	-11.9	-11.3	-11.3	-10.6	-10.7	-10.4	-10.5	-11.4

ANTENNA ANGLE 30

FREQ	8.6	9.4	10.2	11.0	11.8	13.0	13.8	14.6	15.4	16.2	17.0
POL HH	-9.4	-10.0	-9.1	-9.4	-10.8	-11.1	-11.1	-10.2	-10.2	-11.7	-11.1
POL VV	-13.1	-13.8	-12.9	-12.9	-13.5	-12.9	-13.0	-12.4	-12.3	-13.2	-13.4

ANTENNA ANGLE 40

FREQ	8.6	9.4	10.2	11.0	11.8	13.0	13.8	14.6	15.4	16.2	17.0
POL HH	-11.0	-12.8	-12.6	-12.0	-13.1	-12.7	-13.2	-12.3	-12.0	-14.4	-14.6
POL VV	-14.3	-15.8	-15.1	-16.3	-15.6	-14.8	-15.4	-14.0	-15.1	-16.0	-15.0

ANTENNA ANGLE 50

FREQ	8.6	9.4	10.2	11.0	11.8	13.0	13.8	14.6	15.4	16.2	17.0
POL HH	-12.0	-12.8	-12.7	-12.9	-14.2	-13.4	-15.6	-14.6	-14.6	-16.4	-16.5
POL VV	-15.3	-16.7	-16.5	-16.4	-16.7	-16.5	-16.5	-15.6	-16.1	-17.4	-16.3

ANTENNA ANGLE 60

FREQ	8.6	9.4	10.2	11.0	11.8	13.0	13.8	14.6	15.4	16.2	17.0
POL HH	-13.1	-14.0	-14.5	-14.3	-15.3	-15.6	-16.6	-16.0	-14.8	-17.1	-17.6
POL VV	-15.2	-17.7	-17.3	-17.4	-17.2	-16.9	-17.1	-16.2	-16.5	-18.2	-17.5

ANTENNA ANGLE 70

FREQ	8.6	9.4	10.2	11.0	11.8	13.0	13.8	14.6	15.4	16.2	17.0
POL HH	-12.9	-13.8	-14.5	-14.7	-15.5	-15.6	-16.8	-15.7	-15.6	-17.1	-17.6
POL VV	-13.4	-15.9	-15.7	-16.1	-16.5	-15.9	-15.8	-15.0	-15.5	-17.1	-15.7

Averaged Sigma0 Wheat, June 12, 1974

ANTENNA ANGLE 0

FREQ	8.6	9.4	10.2	11.0	11.8	13.0	13.8	14.6	15.4	16.2	17.0
POL HH	4.4	5.1	5.3	4.2	2.8	1.7	1.2	2.1	3.0	1.7	0.7
POL VV	5.6	5.9	6.6	4.5	4.5	2.7	1.1	1.6	2.3	0.2	-0.4

ANTENNA ANGLE 10

FREQ	8.6	9.4	10.2	11.0	11.8	13.0	13.8	14.6	15.4	16.2	17.0
POL HH	-4.1	-6.0	-4.6	-5.8	-7.1	-7.6	-8.7	-7.4	-3.7	-7.6	-9.1
POL VV	-5.4	-7.1	-7.3	-7.5	-6.7	-8.2	-8.2	-7.9	-6.9	-7.7	-8.8

ANTENNA ANGLE 20

FREQ	8.6	9.4	10.2	11.0	11.8	13.0	13.8	14.6	15.4	16.2	17.0
POL HH	-7.8	-7.0	-7.4	-7.6	-7.9	-6.3	-7.8	-8.3	-6.8	-8.3	-8.4
POL VV	-9.4	-11.4	-10.1	-11.6	-8.9	-9.5	-9.0	-9.9	-9.4	-9.3	-10.1

ANTENNA ANGLE 30

FREQ	8.6	9.4	10.2	11.0	11.8	13.0	13.8	14.6	15.4	16.2	17.0
POL HH	-8.5	-9.7	-9.1	-9.7	-10.9	-9.9	-11.2	-10.1	-9.3	-12.3	-12.1
POL VV	-12.7	-13.1	-11.7	-11.9	-12.3	-12.4	-12.3	-11.6	-11.8	-13.3	-11.9

ANTENNA ANGLE 40

FREQ	8.6	9.4	10.2	11.0	11.8	13.0	13.8	14.6	15.4	16.2	17.0
POL HH	-10.4	-9.9	-10.4	-10.8	-11.4	-11.5	-12.1	-12.0	-10.9	-13.8	-13.3
POL VV	-12.4	-13.8	-13.6	-12.8	-12.5	-12.7	-12.9	-12.6	-12.4	-14.5	-12.8

ANTENNA ANGLE 50

FREQ	8.6	9.4	10.2	11.0	11.8	13.0	13.8	14.6	15.4	16.2	17.0
POL HH	-11.9	-11.5	-12.1	-12.3	-13.0	-12.7	-14.6	-13.3	-13.4	-14.6	-14.7
POL VV	-11.8	-13.2	-13.1	-13.7	-12.7	-12.3	-12.8	-11.8	-12.6	-13.8	-13.0

ANTENNA ANGLE 60

FREQ	8.6	9.4	10.2	11.0	11.8	13.0	13.8	14.6	15.4	16.2	17.0
POL HH	-12.5	-13.4	-13.7	-13.9	-14.6	-15.0	-15.9	-14.6	-14.4	-15.6	-15.9
POL VV	-10.9	-12.5	-12.7	-13.5	-13.5	-12.6	-12.9	-12.0	-12.7	-14.0	-12.9

ANTENNA ANGLE 70

FREQ	8.6	9.4	10.2	11.0	11.8	13.0	13.8	14.6	15.4	16.2	17.0
POL HH	-13.1	-13.6	-14.5	-13.9	-14.5	-14.7	-15.3	-14.6	-14.3	-15.6	-15.6
POL VV	-9.6	-11.8	-12.2	-12.7	-12.7	-12.3	-12.5	-11.7	-11.6	-13.1	-11.9

Averaged Sigma0 · Wheat, June 17, 1974

ANTENNA ANGLE 0

FREQ	8.6	9.4	10.2	11.0	11.8	13.0	13.8	14.6	15.4	16.2	17.0
FOL HH	7.5	6.0	4.4	2.8	2.5	1.4	1.1	2.0	2.6	2.5	2.4
FOL VV	9.4	7.7	6.7	3.8	2.7	2.7	2.7	4.3	4.2	3.9	4.6

ANTENNA ANGLE 10

FREQ	8.6	9.4	10.2	11.0	11.8	13.0	13.8	14.6	15.4	16.2	17.0
FOL HH	-0.8	-2.9	-3.9	-2.1	-4.4	-4.6	-5.8	-6.8	-5.9	-6.8	-7.2
FOL VV	-3.7	-5.6	-5.6	-5.2	-4.3	-5.5	-4.8	-7.0	-6.2	-7.8	-6.3

ANTENNA ANGLE 20

FREQ	8.6	9.4	10.2	11.0	11.8	13.0	13.8	14.6	15.4	16.2	17.0
FOL HH	-9.4	-8.8	-6.5	-9.1	-9.9	-8.3	-8.1	-9.5	-8.5	-9.6	-10.5
FOL VV	-9.2	-11.5	-10.4	-11.4	-10.6	-9.9	-9.4	-10.0	-9.1	-10.3	-10.0

ANTENNA ANGLE 30

FREQ	8.6	9.4	10.2	11.0	11.8	13.0	13.8	14.6	15.4	16.2	17.0
FOL HH	-10.5	-11.3	-9.4	-9.2	-10.4	-9.0	-11.8	-11.2	-9.0	-11.2	-9.7
FOL VV	-12.0	-13.6	-11.1	-12.7	-11.2	-12.4	-12.4	-11.9	-11.8	-12.9	-12.5

ANTENNA ANGLE 40

FREQ	8.6	9.4	10.2	11.0	11.8	13.0	13.8	14.6	15.4	16.2	17.0
FOL HH	-10.8	-11.7	-10.8	-10.3	-10.2	-10.5	-11.8	-10.1	-10.7	-12.9	-12.8
FOL VV	-11.4	-12.9	-12.0	-12.0	-11.3	-11.2	-11.9	-11.2	-11.5	-12.4	-11.4

ANTENNA ANGLE 50

FREQ	8.6	9.4	10.2	11.0	11.8	13.0	13.8	14.6	15.4	16.2	17.0
FOL HH	-12.2	-11.0	-10.9	-11.2	-10.8	-11.7	-13.1	-12.2	-12.1	-14.1	-13.6
FOL VV	-12.8	-13.7	-12.8	-12.8	-12.2	-12.4	-12.7	-12.6	-12.7	-14.0	-13.0

ANTENNA ANGLE 60

FREQ	8.6	9.4	10.2	11.0	11.8	13.0	13.8	14.6	15.4	16.2	17.0
FOL HH	-12.9	-12.5	-12.4	-12.1	-12.0	-12.8	-14.0	-12.9	-12.9	-14.2	-15.0
FOL VV	-12.4	-13.4	-12.3	-12.6	-12.3	-11.8	-12.1	-12.4	-12.8	-14.2	-13.0

ANTENNA ANGLE 70

FREQ	8.6	9.4	10.2	11.0	11.8	13.0	13.8	14.6	15.4	16.2	17.0
FOL HH	-13.8	-13.4	-13.1	-12.7	-13.1	-13.4	-14.9	-14.2	-14.1	-15.2	-16.1
FOL VV	-11.4	-11.9	-11.2	-10.9	-11.4	-11.4	-11.9	-11.4	-11.4	-13.5	-12.5

Averaged Sigma0 Wheat, June 21, 1974

ANTENNA ANGLE 0

FREQ	8.6	9.4	10.2	11.0	11.8	13.0	13.8	14.6	15.4	16.2	17.0
POL HH	9.5	8.4	8.0	5.1	6.1	7.8	8.1	9.0	10.1	9.7	8.3
POL VV	10.4	10.3	10.8	7.7	8.9	9.1	8.5	9.3	9.0	7.1	6.2

ANTENNA ANGLE 10

FREQ	8.6	9.4	10.2	11.0	11.8	13.0	13.8	14.6	15.4	16.2	17.0
POL HH	-1.4	-1.4	0.3	-1.8	-1.1	-1.5	0.2	-2.9	1.4	-1.1	-2.2
POL VV	0.	-0.4	-1.1	-0.8	0.	1.5	2.3	-0.2	0.6	-0.1	-0.2

ANTENNA ANGLE 20

FREQ	8.6	9.4	10.2	11.0	11.8	13.0	13.8	14.6	15.4	16.2	17.0
POL HH	-4.9	-3.0	-3.1	-2.3	-2.5	-3.7	-3.6	-3.0	-0.7	-5.5	-3.9
POL VV	-8.3	-6.2	-3.5	-3.2	-3.5	-3.5	-3.1	-2.4	-2.3	-3.8	-4.3

ANTENNA ANGLE 30

FREQ	8.6	9.4	10.2	11.0	11.8	13.0	13.8	14.6	15.4	16.2	17.0
POL HH	-8.5	-8.9	-7.9	-5.6	-6.4	-6.9	-7.0	-5.3	-4.7	-6.9	-8.4
POL VV	-9.3	-8.8	-8.1	-7.2	-6.8	-7.0	-7.2	-5.4	-5.2	-7.4	-7.2

ANTENNA ANGLE 40

FREQ	8.6	9.4	10.2	11.0	11.8	13.0	13.8	14.6	15.4	16.2	17.0
POL HH	-11.3	-9.4	-9.4	-8.8	-8.7	-7.8	-8.1	-7.3	-7.0	-9.3	-9.6
POL VV	-9.8	-9.9	-8.8	-8.9	-7.8	-8.0	-7.2	-7.6	-6.5	-9.1	-8.1

ANTENNA ANGLE 50

FREQ	8.6	9.4	10.2	11.0	11.8	13.0	13.8	14.6	15.4	16.2	17.0
POL HH	-11.4	-11.6	-10.9	-9.9	-10.5	-9.5	-10.5	-9.2	-9.6	-11.1	-11.9
POL VV	-10.5	-10.2	-9.3	-10.4	-9.6	-8.9	-9.4	-8.9	-9.9	-10.8	-9.9

ANTENNA ANGLE 60

FREQ	8.6	9.4	10.2	11.0	11.8	13.0	13.8	14.6	15.4	16.2	17.0
POL HH	-13.3	-13.0	-11.8	-12.0	-11.2	-11.8	-12.0	-10.9	-11.4	-13.0	-12.6
POL VV	-11.8	-11.8	-11.9	-11.4	-11.2	-10.2	-10.6	-10.2	-10.4	-12.7	-10.8

ANTENNA ANGLE 70

FREQ	8.6	9.4	10.2	11.0	11.8	13.0	13.8	14.6	15.4	16.2	17.0
POL HH	-15.0	-14.6	-13.6	-13.5	-13.0	-12.9	-13.6	-12.8	-13.3	-14.4	-14.4
POL VV	-12.9	-12.6	-11.8	-10.8	-10.7	-9.5	-10.7	-8.9	-9.9	-12.1	-9.9

Averaged Sigma0 Wheat Stubble, June 25, 1974

ANTENNA ANGLE 0

FREQ	8.6	9.4	10.2	11.0	11.8	13.0	13.8	14.6	15.4	16.2	17.0
FOL HH	7.2	6.2	6.7	6.5	7.9	8.5	7.5	6.4	6.8	5.3	4.6
FOL VV	8.5	7.6	7.5	7.3	8.6	9.1	8.5	7.1	6.3	4.8	5.0

ANTENNA ANGLE 10

FREQ	8.6	9.4	10.2	11.0	11.8	13.0	13.8	14.6	15.4	16.2	17.0
FOL HH	-1.0	-2.0	-1.9	-0.9	-0.1	-0.2	-2.4	-0.7	-1.1	-3.6	-4.4
FOL VV	1.3	-1.1	-0.4	-1.2	0.2	1.3	0.1	1.0	-0.5	-3.1	-3.0

ANTENNA ANGLE 20

FREQ	8.6	9.4	10.2	11.0	11.8	13.0	13.8	14.6	15.4	16.2	17.0
FOL HH	-4.8	-8.0	-6.0	-6.0	-6.7	-5.8	-6.9	-6.1	-5.0	-5.0	-6.1
FOL VV	-7.1	-7.1	-6.6	-6.9	-6.4	-4.9	-5.5	-5.7	-4.7	-6.3	-5.1

ANTENNA ANGLE 30

FREQ	8.6	9.4	10.2	11.0	11.8	13.0	13.8	14.6	15.4	16.2	17.0
FOL HH	-9.4	-8.9	-8.7	-7.8	-7.7	-7.4	-7.0	-6.6	-7.7	-7.1	-8.6
FOL VV	-8.4	-9.9	-9.3	-8.1	-7.1	-6.2	-4.9	-5.4	-6.4	-8.0	-6.4

ANTENNA ANGLE 40

FREQ	8.6	9.4	10.2	11.0	11.8	13.0	13.8	14.6	15.4	16.2	17.0
FOL HH	-11.0	-9.7	-10.0	-9.7	-9.7	-8.2	-8.8	-7.5	-7.8	-9.6	-9.1
FOL VV	-11.3	-10.3	-9.3	-9.6	-9.2	-8.1	-8.4	-7.2	-7.6	-9.3	-8.2

ANTENNA ANGLE 50

FREQ	8.6	9.4	10.2	11.0	11.8	13.0	13.8	14.6	15.4	16.2	17.0
FOL HH	-13.6	-12.9	-12.3	-10.9	-10.8	-11.0	-11.3	-10.6	-10.0	-11.3	-12.0
FOL VV	-13.1	-13.4	-11.8	-11.0	-10.4	-9.8	-9.9	-9.4	-9.7	-11.1	-10.8

ANTENNA ANGLE 60

FREQ	8.6	9.4	10.2	11.0	11.8	13.0	13.8	14.6	15.4	16.2	17.0
FOL HH	-12.8	-13.1	-12.4	-11.6	-11.6	-11.5	-12.6	-12.1	-11.4	-13.2	-13.1
FOL VV	-12.8	-13.6	-11.8	-11.4	-10.7	-10.5	-10.2	-10.3	-10.3	-11.5	-10.7

ANTENNA ANGLE 70

FREQ	8.6	9.4	10.2	11.0	11.8	13.0	13.8	14.6	15.4	16.2	17.0
FOL HH	-14.9	-14.9	-14.1	-13.4	-13.2	-13.5	-14.5	-13.1	-12.6	-14.8	-14.5
FOL VV	-13.1	-13.2	-12.7	-12.2	-10.8	-10.9	-10.8	-10.2	-11.9	-12.4	-12.0

CRINC LABORATORIES

Chemical Engineering Low Temperature Laboratory

Remote Sensing Laboratory

Flight Research Laboratory

Chemical Engineering Heat Transfer Laboratory

Nuclear Engineering Laboratory

Environmental Health Engineering Laboratory

Information Processing Laboratory

Water Resources Institute

Technical Transfer Laboratory

Air Pollution Laboratory

Satellite Applications Laboratory

CRINC